Experimental investigation of intensity measures for probabilistic structural fire engineering

MEFE Thesis

Tony Park

Hsp24

14283613

Submission Date: 13 July 2020

UNIVERSITY OF CANTERBURY
Te Whare Wānanga o Waitaha
CHRISTCHURCH NEW ZEALAND

Deputy Vice-Chancellor's Office
Postgraduate Research Office

Co-Authorship Form - Masters

This form is to accompany the submission of any thesis that contains research reported in co-authored work that has been published, accepted for publication, or submitted for publication. A copy of this form should be included for each co-authored work that is included in the thesis. Completed forms should be included at the front (after the thesis abstract) of each copy of the thesis submitted for examination and library deposit.

Please indicate the chapter/section/pages of this thesis that are extracted from co-authored work and provide details of the publication or submission from the extract comes:

This paper is a summary of the major parts of the thesis

Park H., Abu A. and Moss P., 2019. Severity measures in probabilistic structural fire design. Proceedings of the 10th International Symposium on Steel Structures, November 13-16, 2019, Jeju, Korea, 24 - 27

Please detail the nature and extent (%) of contribution by the candidate:

Hyunseok Park did 80% of the work under our supervision.

Certification by Co-authors:

If there is more than one co-author then a single co-author can sign on behalf of all

The undersigned certifies that:

- The above statement correctly reflects the nature and extent of the Masters candidate's contribution to this co-authored work
- In cases where the candidate was the lead author of the co-authored work he or she wrote the text

Name: *Associate Professor Anthony Abu* Signature: ***Anthony K. Abu*** Date: *13/07/2020*

ABSTRACT

There are a number of limitations in current design methods for structural fire engineering. The biggest concern is that a worst-case fire is assumed - which means that there may be a fire that is worse than what the structure may be designed for which may lead to structural failure. Thus it is important to accurately quantify fire in order to design structures for realistic scenarios they may be exposed to. In order to develop a method to quantify fire appropriately, Probabilistic Structural Fire Engineering (PSFE) has been introduced, following PBEE.

The Pacific Earthquake Engineering Research (PEER) Centre has developed a Performance Based Earthquake Engineering (PBEE) method. It is a probabilistic method to quantify earthquakes and design structures considering the likelihood of earthquakes and the importance of the structure. PBEE's four analytical methods find the relationship between the hazard and the associated structural response. PSFE has implemented the same PBEE framework in order to develop relationships between fires and structure to help meet primary stakeholder goals of life safety of occupants and protection of property.

This study is a first step to help provide experimental data to help verify numerical models that have been proposed in probabilistic studies as PSFE relied on the use of numerical models to obtain large number of data to analyse for structural fire engineering.

The experiments involved a pin ended single steel I-beam under pre-flashover fire with two point loads acting on the beam. In total, 102 different results were obtained: thermal and structural response of the beam under different design fires were recorded. Fire characteristics, Fire Severity Measures (FSM), structural response and Engineering Demand Parameters (EDP) were analysed to find the FSM with the strongest relationship with EDPs. Having FSMs that have strong correlations with EDP indicate that fires can be more easily quantified and corresponding structural response may be more accurately predicted.

In total, five FSMs (duration, peak HRR, TER, average HRR, growth rate) and two EDPs (maximum beam temperature, peak axial force) were investigated with the test results. Cloud Analysis was used as the analytical method to investigate the relationship between fire exposure and structural response, as it requires no scaling and uses the raw data obtained from experiments. The results show that the most efficient FSM for both EDPs was Total Energy Released with R^2 value of 0.8908 and 0.8959 for thermal and structural responses respectively. There are further studies to be done on PSFE to develop the method for eventual use in real structural fire engineering designs in future.

ACKNOWLEDGEMENTS

I would like to thank my supervisors, Associate Professor Anthony Abu and Professor Peter Moss for all the knowledge and support they have given me throughout my time as an MEFE student. I would not have been able to finish my thesis without their guidance and the weekly meetings we had. It was not just about the research but all the valuable discussions we had and their valuable life experiences they shared with me, which will surely help me after I graduate.

I would also like to thank Mayank Shrivastava and Jono Macintyre who were there to help whenever I needed feedback. Their advice and experience as postgraduate students helped significantly.

I would like to thank Grant Dunlop and Logan Cooper who helped me carry out a large number of experiments in the fire lab. My experimental based research would never have been possible if they have not spent the time to set up the experiments as well as provide me with their practical knowledge for the experiments. Their help and support was amazing and it is greatly appreciated.

Special thanks to ARUP and SFPE for their respective scholarships in the MEFE programme, which helped to support my studies.

I would like to thank my parents, Umma Abba, Lucy, Ki for all the support and encouragement during my university life. Lastly, I would like to thank my wife Hazel for the continuous support and care during my research. You all gave me the motivation to finish this work.

CONTENTS

LIST OF FIGURES

LIST OF TABLES

Nomenclature

a	Regression coefficients in Cloud Analysis
b	Regression coefficients in Cloud Analysis
A	Distance from the load to the end of beam
A_m/V	Section factor for unprotected steel member
c_a	Specific heat of steel
D	Diameter of burner
E	Modulus of Elasticity
ḣ	Heat flux to unit surface area
h_{net}	Net heat flux per unit area
H_f	Flame height
I	Second moment of area
k_{sh}	Correction factor for the shadow effect
L	Length of the beam
P	Load
$\dot{Q}$	Heat Release Rate
Δt	Time interval
α_c	Coefficient of heat transfer by convection
Φ	Configuration factor
$\Delta\theta_{a,t}$	Temperature increase in unprotected steel member
Θ_m	Temperature of the member surface
ρ_a	Unit mass of steel
ε_m	Surface emissivity of the member

ε_f	Emissivity of the flames, of the fire
σ	Stefan Boltzmann constant (=5.67 . 10^{-8} [W/m^{2}K^4])

LIST OF ABBREVIATIONS

CA	Cloud Analysis
CIR	Cumulative Incident Radiation
EDP	Engineering Demand Parameter
FSA	Fire Stripe Analysis
FSM	Fire Severity Measure
HRR	Heat Release Rate
IDA	Incremental Dynamic Analysis
IFA	Incremental Fire Analysis
IM	Intensity Measure
MSA	Multi Stripe Analysis
PBEE	Performance Based Earthquake Engineering
PEER	Pacific Earthquake Engineering Research
PSFE	Probabilistic Structural Fire Engineering
SSA	Single Stripe Analysis
TER	Total Energy Released

1. INTRODUCTION

1.1 Structural Fire Design

Structural fires are significantly large fires which threaten structures. These fires are typically quantified by a number of variables such as fuel load and ventilation factors which all have uncertainties (Gernay *et al.* 2016). This makes it difficult to accurately predict the behaviour of fire and hence their likelihood to endanger building occupants and affect the structural stability of a building. Our awareness of fire safety typically arises whenever there is a fire incident that results in fatalities. In 2018, there were 45,894 structure-related fires reported in the UK. This is more than 25% of the total number of fires reported (Home Office, 2019). In New Zealand 5,033 incidents of structural fires were reported in 2018, more than 27% of the total number of fires (Fire and Emergency New Zealand, 2019). It shows that structural fires or large fires inside buildings make a large proportion of the total number of fires reported each year. A number of studies have been carried out to develop methods to design structures in order to provide resilience against fire (Devaney, 2014; Hamilton, 2011; Lange *et al.* 2014; Moss *et al.* 2014; Shirvastava, 2019). The primary purpose of structural fire design is to safeguard occupants by providing structural stability. However, these studies have aimed at providing the original intent of life safety and protecting property to meet additional needs of stakeholders, such as business continuity. There are methods to assess the required level of protection for buildings under fire exposure. Depending on the building's characteristics such as its height, occupant type and occupant load, the fire resistance rating of the structure or part of the structure is determined accordingly. Fire safety measures, including both active and passive systems (e.g. sprinklers and fire resistant walls), are introduced to provide appropriate fire resistance to the structure. This provides resilience against fire to meet the design purposes as stated previously.

Currently, the assessment is done in one of two different ways – by using prescriptive or performance-based design approaches. The prescriptive design approach is the conventional method that is used when the requirements and design options have been pre-defined based on simple rules from experience of historic fires and tests (Buchanan, 1994). These rules are prescribed specifications that meet design codes. As a result, they limit engineers from taking proactive actions to increase safety beyond compliance, as the building must comply with the specified technical and procedural requirements set by the regulator. On the other hand, the performance-based approach is where engineers have flexibility in determining the technical and procedural approach to control and design for fire safety subject to meeting a range of performance criteria (Hadjisophocleous, 1998). It is important to show the regulatory authority

that safety measures have been applied in order to deliver a safe building. Although the performance-based approach is flexible, it has general guidance of steps to be followed.

The first step to Performance Based Design (PBD) is setting the fire safety objectives. This varies depending on the structure's use, importance level and many other factors. For example, a structure's objective may be to only ensure it withstands a fire long enough for the occupants to evacuate safely or it may be to control the fire in the room of origin to minimize the impact on business continuity of the overall structure. Once the objectives are defined, the required structural performance during exposure to fire may be assessed based on agreed design acceptance criteria. The assessment of the structure requires that appropriate design fires are considered. These are selected by taking into account factors like the fuel load, the compartment size and location of the fire, to typically find the expected worst fire scenario the structure could experience. A structural-fire analysis is then carried out using the defined design fire to estimate member temperatures. The analysis can be done in three ways: using tabulated data, simple theoretical calculation methods or advanced calculation methods, by the use of finite element modelling (Buchanan and Abu, 2017). Once the thermal response of the structural elements are obtained, the structural response of the elements can be calculated. This process may be iterated to verify member sizes to satisfy the design acceptance criteria. This is now what is known as Structural Fire Engineering (SFE) design. Although this process has been found to be robust, PBD of structures under fire conditions has its limitations.

The biggest drawback is that the worst possible fire scenarios are assumed. There is currently no established method that accurately predicts the worst fire exposure to a structure. As such the assumed worst fire may actually not be the worst for the chosen structure. One example of this would be an assumption of all windows breaking simultaneously (100% glazing failure) when the compartment reaches a certain temperature. This is not true in real fire conditions as windows may break at different stages. This may result in changes in the temperature of the compartment throughout the fire. This suggests that slight changes in the assumptions can have greater impact on structural resistance and result in structural failure. These worst possible fires in the design are not guaranteed to occur and in fact, they may never occur during the lifetime of a structure. Hence, there is uncertainty about the probable fire that may occur. Another example would be the location of the fire in relation to critical structural elements in a given building. A chosen design fire may have no impact on the overall structural stability when exposed to beams or columns, whereas it can have a significant impact if a critical connection is exposed. There are other scenarios where a better performance of the overall structure may be obtained by the loss of some elements. With all these different considerations and scenarios, a

better method is required to accurately and simply predict and quantify multiple fire exposures so multiple structural responses can be investigated for more realistic building design.

In order to mitigate such limitations in current performance-based design in structural fire engineering, a probabilistic based design approach has been introduced. By using probability, the randomness in fire exposure and furthermore the structural response can be more reasonably accounted for. Probabilistic engineering design is not being proposed just in fire engineering but other engineering disciplines have adopted some principles in dealing with hazards with random intensities as well. They include earthquakes (Cornell and Krawinkler, 2000), tsunamis (Riggs *et al*. 2008), hurricanes (Barbato *et al*. 2011) and wind (Petrini and Ciampoli, 2012).

Probabilistic methods are being used in current fire engineering designs. Probabilistic Risk Assessment (PRA) (Van Coile *et al.* 2018) is being used in fire engineering to identify hazards associated with particular designs and quantify their risk probabilities and the associated impact. By weighing the level of risk and impact a certain hazard poses, appropriate mitigation measures are proposed to reduce the overall risk to the project. Another method that has been developed recently is Probabilistic Structural Fire Engineering (PSFE), based on the Pacific Earthquake Engineering Research (PEER) Centre's existing Performance Based Earthquake Engineering (PBEE) method. This method quantifies fires and finds the response of the impacted structure due to the chosen fire. These methods all have the same limitation – lack of real data. These data can be obtained by real structural fire events or through experiments. The limitations in these methods are explained in the next section. That is why these methods are based on numerical analysis and software simulations such as SAFIR (Franssen, 2005), VULCAN (Bailey, 1995) and OPENSEES (Ribeiro *et al. 2016).* Although these methods are used widely, they are only as good as the simplifications that were used in their development and the limited test data which were used in their calibration. This is shown from a number of studies where different results were obtained from various fire models which proved that there are uncertainties in each of the models (Pope and Bailey, 2006).

Both structural fires and earthquakes are a low probability-high consequence hazard. However, there is a clear difference in the amounts of recorded data available between the two disciplines: earthquake engineering and structural fire engineering. For earthquakes, it is relatively simple to measure even the smallest motions as it only requires sensors to be installed in buildings to collect data. On the other hand for a structural fire, a number of conditions have to be met to sufficiently record and measure the fire. Firstly, a fire has to develop to be large enough to actually threaten the structure as it will have no significant effect

on structural stability if the fire is controlled in advance. Other important parts of data collection would be having the right kind and number of sensors installed in the building which then must be able to withstand high temperatures in order to record the compartment temperature from the beginning to the end of the fire as well as sensors to record the structure's response. Since fire is a rare event, most structures will not experience a significant fire during their lifetimes and the sensors will be of no use if they are never used. This is the biggest problem of structural fire engineering, in particular since only the final outcome of structural fires can be obtained without the information during the fire as it develops. As structural fire cannot be easily predicted, there is currently no way to accurately record how the structure and its elements behave inside the building during a fire unless it was planned as part of an experiment. It is also highly unusual for manufacturers to burn their own products or structures for experimental research and development only, unless the product is specifically designed to provide fire protection. The products do not require fire tests to be carried out as they do not require fire resistance. Therefore, the amount of data available for real structural response of buildings is extremely limited. There have been structural fire studies involving full scale experiments such as the Cardington fire test (Lennon and Moore, 2003; Sanad *et al. 2000;* Wang *et al.* 1995). They were conducted in the mid-1990s and is still being used today in research, which proves the importance of experiments but also addresses the ongoing lack of availability of full scale experiments. Although there has been full scale experiments done for structural fire studies, they only involve a small number of tests, producing deterministic based studies rather than probabilistic based results. This further limits data for the successful development of a probabilistic design assessment approach.

As observed above, the most important factor in developing a probabilistic based method is having a large dataset containing a broad range of different fire severities. It is crucial to have a wide spectrum of data in order to reasonably quantify the fire and the associated structural response. This must be first done with real experimental data as analytical data lacks in reliability due to its embedded limitations. Once a method to quantify fire using probabilistic approach is developed, analytical models can then be modified and verified as appropriate. However, there are a number of reasons why there have not been many probabilistic driven structural fire tests. The main issue is the costs involved in setting up and running large experimental programmes.

Firstly, a full-scale structural fire test is very costly. As the probabilistic approach is based on a large dataset, experiments must be carried out multiple times with the same or similar setup. It is almost impossible to carry out full scale experiments involving an entire structure as it will be

immensely costly. Another issue is the amount of resources it will require. Large amount of resources will be needed to run multiple number of full scale structural tests and this can be in material and workforce. Lastly, the experiments must be consistent in order to have reliability and confidence. However in fire, there are countless number of variables that are uncontrollable which may affect the overall outcome. These uncontrollable variables include the ambient temperature, weather and even the season of the year. It can be the temperature of the material before the experiment or the laboratory environment. All of these variables can have an effect on the development of a fire that leads to a change in the overall outcome of the structural response. For example, if the first experiment was carried out on a cold morning and the next test was done around noon, the ambient temperature would have changed and may not produce the same result as the morning experiment. Since it is evident that there will be a number of uncertainties in different variables in structural fire experiments, the importance of large dataset is emphasized. It is essential to provide as much data as possible in order to address these uncertainties through analysis by using different methods in probabilistic approach. Therefore, initial studies to obtain probabilistic fire data must be within a reasonable cost and be easily tested multiple times to minimize resource with minimum variables while obtaining as much data as possible. A simple structure that responds to fire to best describe the structural response would be ideal to produce large number of tests to obtain a large dataset.

Probabilistic structural fire studies by a number of researchers implemented a probabilistic method developed in earthquake engineering (Devaney, 2014; Hamilton, 2011; Lange *et al.* 2014; Moss *et al.* 2014). These studies identified different fire parameters and investigate the relationship between fire parameters and the structural response. This study aims to implement the same method through structural fire experiments to find the best fire parameter that can quantify the structure's response.

1.2 Aims and Objectives

The aim of the study is to validate numerical models of probabilistic structural fire design with experimental data. A simple experiment that can be repeated easily to provide reliable data can be used to further develop PSFE. This will be the foundation work to quantify fire and its associated structural response. With real structural fire data, studies involving numerical analysis can be verified. Improvements that could be made to the numerical models can also be identified.

The specific objectives are

- To develop a simple structural fire experiment to be used for a probabilistic based experimental study
- To evaluate the validity of current probabilistic structural fire engineering design approach based on the proposed experimental data
- To investigate relationships between pre-flashover fire parameters and structural response
- To identify the best pre-flashover fire parameter that can suitably predict structural response.

1.3 Report Outline

Chapter 1 has provided a brief overview of what structural fire design is and the foundation of what this study will focus on. Chapter 2 describes the literature used to gain background knowledge for the thesis. The past studies that have built up to help carry out this project and the reasoning behind the methodologies used in this research are described in this chapter. Chapter 3 describes the process taken to carry out the experiments. A simple pre-flashover fire experiment is carried out to acquire structural fire data. The description includes information on procedures and instrumentation. Chapter 4 shows the results of thermal and structural experiments. It provides information on how the structure performs under different fire severity levels. Chapter 5 uses the experimental data from Chapter 4 to find the best fire parameter candidate using different analytical methods. It also discusses about the comparison between the expected and actual results. Chapter 6 is an overall summary of the entire work that has been done to further develop PSFE. It identifies the main conclusions of the study as well as recommendations for future studies.

2. LITERATURE REVIEW

This chapter expands on the background in Chapter 1. It provides an overview of current probabilistic based methods in structural fire engineering. It explains the framework developed by the Pacific Earthquake Engineering Research (PEER) Centre's work and how it has been adapted for use in Probabilistic Structural Fire Engineering (PSFE). The chapter also identifies the gaps in PSFE studies and what is required to further develop PSFE. The study's area of focus is determined as a result of the findings from the literature review.

2.1 Probabilistic based design methods in Structural Fire Engineering

The objective of structural fire design is to determine the amount of fire protection (if required) for the design and to provide safety features accordingly to meet the building regulations. This allows the designer to increase the level of reliability of the design for the overall structure. It is beneficial especially for structural fire design as the level of a structure's importance and its business continuity varies depending on the use of the structure. There are different types of buildings depending on the building characteristics such as fuel load and occupant type. For example, structures such as airports or shopping malls will have bigger impact on their business if there is a fire compared to a small retail shop if they were to evacuate due to fire. By having a control on the overall design system, designers can provide adequate robustness and reliability to the structure. Since fire is a phenomenon with countless number of variables with uncertainties, a certain outcome can never be guaranteed. This is why a probabilistic approach will be more beneficial compared to a deterministic approach in structural fire engineering since it can quantify the level of confidence against the uncertainties in each of the variables. It will give engineers freedom to design structures to different level of protection with a clear indication of the level of safety of the structure.

Probabilistic based methods have already been developed. Some have been implemented in building designs, while others are continuously undergoing further development. Some examples are the Probabilistic Risk Analysis (PRA) (Van Coile *et al.* 2018) and PEER Centre's Performance Based Earthquake Engineering (PBEE) based PSFE (Cornell and Kawinkler, 2000). Each of the methods provide engineers a way for an assessment of risk for the structure and design the structure appropriately. PRA is being used in the current fire engineering field to control the level of risk in a structure and to design to a standard where the risks can be managed to meet building regulations. The PSFE is an extension of the PEER Centre's PBEE method to structural fire engineering. It was developed by using numerical analysis to find the best relationship between fire and structure to be able to quantify fire and therefore its

structural response. The PSFE method has never been studied using real experimental data and was based only on numerical analysis. The method would be able to gain more confidence if it was able to be further developed using real data as there are clear limitations in numerical models during its development stages as explained in chapter 1.

2.2 Pacific Earthquake Engineering Research Centre

The PEER Centre (Cornell and Kawinkler, 2000) is a consortium of different institutions including eleven main institutions that are involved heavily in the PEER work. The goal of the PEER Centre is to develop seismic design technologies for economic and safety needs of owners and society. By specifying performance goals and improving seismic risk assessments, they have gained worldwide attention. They have provided society with quantitative methods for characterizing earthquakes and being able to manage the risks related to the hazards. This quantitative method is called the Performance-Based Earthquake Engineering (PBEE) and is being used in today's earthquake engineering designs.

2.2.1 PBEE Framework

The PBEE framework provides a method to accurately quantify the intensity of earthquakes and therefore assess structures due to ground excitation from the earthquake. The research has developed a framework to achieve the performance objective of calculating the mean annual frequency exceeding a building's specified limit state. The specified limit state is a pre-defined design criteria and the building is considered to have failed when it exceeds that specified limit state. The framework is a linear methodology characterized by three domains: a hazard domain, a structural domain and a loss domain and these can be further divided into four stages. PBEE is divided into four stages which are: hazard analysis, structural analysis, damage analysis and loss analysis (Jayaler, 2003) as shown in Figure 2.1. The objective of the PEER Centre was to find relationships between each of these domains and to develop analytical methods to quantify the effects of probable earthquakes and hence design buildings as appropriate.

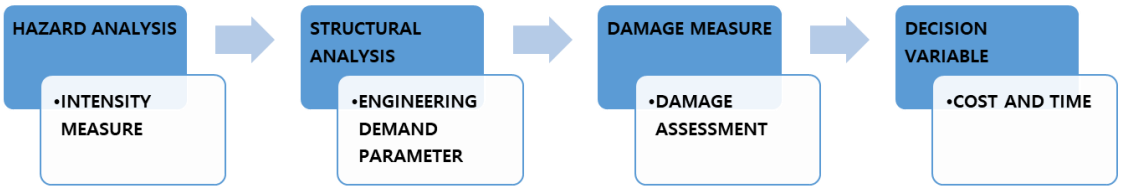

Figure 2.1: Four stages of PBEE framework (Jayaler, 2003)

The framework covers the entire timeline of a structure from the beginning of the earthquake through to the repair of the structure. The four stages are expressed and quantified with pinch variables for each analysis: Intensity Measure (IM), Engineering Demand Parameter (EDP), Damage Measure (DM) and Decision Variable (DV) respectively. IM describes the characteristics of the earthquake, EDP describes the responsive structural characteristics from the earthquake. DM and DV describe the results and consequences of the earthquake. The DM and DV are the final outcome of the earthquake and describe the primary and secondary objectives such as the life safety of occupants as well as time and cost to repair the building which may be important to the stakeholders (Moehle and Deierlein, 2004; Porter, 2003). In earthquake engineering, an example of an IM would be peak ground acceleration; EDP includes variables such as maximum inter-story drift ratios; DM assesses the level of damage on the structure and DV is an indication of cost or time to repair the structure. Each of these variables is related to each other and each of the analysis stages.

By using the relationships between the hazard domain and the structural domain, structural response and related loss due to the earthquakes have been found. These relationships were found using past earthquake data and determining ideal intensity measures for the earthquake that were able to quantify the structural response of buildings. From this, the structural response could be calculated for different seismic actions. This then led on to designing buildings with a chosen probability of exceeding a specified limit state. The overall process can be briefly shown in following steps,

1. Firstly, find the importance level of a building.
2. The importance level is then converted into an equivalent return period of a certain sized earthquake. A building with higher importance level will be designed to withstand an earthquake with longer return period since longer return period means higher magnitude for an earthquake.
3. By using the probability of occurrence for an earthquake with a defined magnitude, the building can be designed accordingly to prevent structural failure for earthquakes with less magnitude.

The key to this relationship is identifying the ideal IM that best describes the EDP. As IM is used as a tool to quantify the structural response, it is important to find an IM that has a strong relationship with a number of different structural variables. In order to identify such IM, there are four criteria to be met. They are efficiency, sufficiency, scaling robustness, hazard computability and predictability (Luco and Cornell, 2007; Moss *et al*. 2014; Tothong and Luco, 2007; Giovenale *et al.* 2004). Efficiency in general terms is the ability to accomplish something

with the least amount of resources, whatever it may require. In PEER, it is measured as the dispersion of the EDP which is determined by the overall distribution of the data points. A sufficient IM will be efficient enough to predict structural response independently of other IMs or earthquake characteristics. The scaling robustness means a good IM should have unbiased results even after being scaled. The hazard computability represents how hard it is to calculate the IM. A good IM must be easily attainable. The predictability of an IM shows how accurately the EDPs can be calculated.

PBEE provides accurate prediction of a building's response to earthquakes at any intensity level. The PBEE framework allows engineers to determine the level of safety a building design will have following the Building Regulations. For example, business continuity will be critical for a hospital. A hospital in an area with a probability of high intensity earthquake occurring will be designed to withstand such earthquake with a chosen level of safety to comply with the building code. Since a hospital is a high importance level structure, it is important that the design has an adequate safety factor. Designers have the freedom to choose the level of safety they can provide to ensure the hospital will be able to be used straight after an earthquake. PBEE is useful in earthquake engineering since there are a number of variables that may affect the structural response of the structure such as building height and geological characteristic of the region. A number of studies have been carried out to validate the PEER Centre's framework for the use of a similar approach in PSFE, and they are discussed in the next section (Devaney, 2014; Hamilton, 2011; Lange *et al.* 2014; Moss *et al.* 2014; Shrivastava, 2018).

2.2.2 Implementation of peer framework in PSFE

A number of studies used the framework developed by PEER to implement PSFE (Devaney, 2014; Hamilton, 2011; Lange *et al.* 2014; Moss *et al.* 2014; Shrivastava 2018). These studies indicate that there are a lot of similarities, but also fundamental differences between earthquake and fire. Earthquakes occur outside the structure and the seismic action affects the entire structure. This means that the entire structure is affected as a whole whereas for a fire, it starts in one compartment of the building and may spread on to other areas. This shows that the structure cannot be treated as one system as it occurs under earthquakes. Also for earthquakes, structural response is at room temperature only. On the other hand, fires occur inside or outside the building and affect both thermal and mechanical characteristics in the structure. Earthquake engineering only involves mechanical analysis whereas fire engineering involves thermo-mechanical analysis resulting in more complexity. There have been changes in some of the terms used such as the Fire Severity Measure (FSM) that has been introduced to replace PBEE's

IM (Intensity Measure). An example of FSM would be compartment temperature, fuel load, heat release rate and other fire parameters in structural fire.

Lange *et al.* (2014) focused on the evaluation of the PEER Centre's PBEE method in order to apply each of the four stages on to the analysis for structures in fire. The four stages of the PBEE method were thoroughly investigated. The study illustrated how the four stages, hazard analysis, structural analysis, damage analysis and loss analysis could be used in PSFE. Limitations of implementation of PBEE into PSFE were also identified such as using a number of different numerical models to analyse structural fire through the framework. These included the repairability and cost of fire damaged composite structures, consideration of other fire profiles as the study only covered parametric fires, and lastly the use of advanced models to explore various engineering demand parameters and damage measures.

The study by Moss *et al.* (2014) was carried out to investigate a two bay continuous reinforced concrete beam under a four hour parametric fire using SAFIR. The purpose of this study was to implement the PBEE method on to PSFE. Various fuel loads, lining factors and ventilation factors were used to produce a series of 102 parametric fires. By implementing one of the analytical methods from PBEE, i.e Incremental Dynamic Analysis, Incremental Fire Analysis (IFA) was developed to find the best relationship between the fire characteristics and the structural response. It showed that the total heat energy and the reinforcement temperature resulted in the least variation of the predicted maximum vertical displacement of the beam. The study involved use of only one numerical model. As stated previously, different models have shown to provide different results and this may affect the reliability of the study's conclusions.

Shrivastava et al. (2018) investigated the current state of the art of probabilistic performance based structural fire engineering. The research focused on reviewing different studies done on probabilistic structural fire engineering. This included the Probabilistic Risk Analysis method (Van Coile *et al.* 2018) which compares various design solutions with certain acceptable risk allocated by the stakeholder. The main focus of Shrivastava et al. (2018) was on the PBEE based probabilistic structural fire engineering. The implementation of the four main stages of PBEE and the limitations and improvements that must be made for PSFE. This included the number of different variables involved in post-flashover compartment fires, providing an appropriate intensity measure selection procedure and scaling of fire curves resulting in unrealistic characteristics. It showed that PSFE still required work such as further investigation of the PBEE's analytical methods to apply in PSFE.

Another study by Shrivastava (2019) further develops the PBEE implemented in PSFE by introducing a new analytical method specifically for fire engineering. The previous study by Shrivastava et al. (2018) identified the clear limitations of the state of the art of PSFE. As stated before, one of the limitations was the impracticality of scaling fires. This is due to fire having too many variables to control and scale. Excessive scaling of fire will affect various fire parameters which will change the overall fire profile. For example, if the duration of a fire profile is scaled, the related fire parameters such as total heat released and average heat release rate will also be affected. The conclusion was to avoid excessive scaling of the fire profiles in PSFE. This resulted in developing a new method called Fire Stripe Analysis (FSA). This method provided a way to minimize the scaling error by using a number of narrow bands to avoid extensive scaling of fire profiles. The method was then used to analyse the relationship between the fire variables and structural characteristic of a composite beam in a typical office building. The study showed that the Cumulative Incident Radiation, which is the total incident radiant heat flux the element is exposed to, was the most efficient Intensity Measure. However, further work is required to investigate other criteria for choosing an ideal FSM such as computability and predictability. The study also researched the uncertainties involved in the structural finite element modelling for different structural configurations using 2D and 3D models. It showed that an isolated member produces more conservative results than the structural response of a beam which is a part of a larger structure. The research would require further investigation on other material structures such as concrete structures or steel structures as the research only focused on the steel-concrete framed structure using finite element models without carrying out experiments.

In previous research, numerical analysis and modelling was used to carry out thermo-mechanical analysis on the structure in PSFE. This is due to the excessive amount of cost and time required to carry out large number of experiments to develop a probabilistic approach. Even though numerical analysis is reliable, limitations still exist with advanced modelling due to mathematical simplifications in the development stages of the models. Advanced thermal and structural analysis programs such as SAFIR, VULCAN and OPENSEES (Franssen, 2005; Bailey, 1995; Ribeiro *et al. 2016)* require more analysis runtime as the accuracy of the models increase. Other limitations include the models not being able to consider mass transfer or shrinkage of the material such as timber and concrete. Although the advanced models are close to experimental results, it is still not the same as it cannot be highly reliable. For example, assuming an identical set up with the same variables, numerical models will produce an identical set of results independent of how many runs they undergo. However, this is not the case in experiments. Since fire is a phenomenon with countless number of variables and uncertainties, even if the test was carried out in a same set up, it is very unlikely for the test to

produce identical results. It may have a slight or a large difference and this can be used to further study probabilistic approach for a PSFE. Through experiments, the uncertainty of different variables in structural fire can be investigated by obtaining large dataset which then can be applied to develop the numerical models.

2.2.3 Fire Severity Measure – Engineering Demand Parameter

There are variables related to each of these stages and this study expands on the first two stages: Hazard analysis and structural analysis are the two stages that concentrate on the fire-structure relationship. This is directly related to the main goal of the study which is to find the relationship between different fire parameters (FSM) and structural responses (EDP). Hazard analysis is simply quantifying the characteristics of the hazard itself. This is expressed with FSMs where each FSMs will provide different aspects of the fire and have different meanings. For example, the duration of the fire will explain how long the fire was but it will not show how much energy was released from the fire. On the other hand, total heat released for that fire will explain the total heat energy released but not on how long the structure was exposed to the fire or its maximum temperature. The next stage is the structural analysis which is how a structure responds to the hazard. This is expressed by using a structural response called an EDP. Again, this can be any variable that explains how a structure has responded to fire. Different variables measure a particular aspect of the structures reaction to a fire. For example, a structural connection which has weaker strength and loadbearing capacity will be more affected by the temperature profile than a main column of the structure when exposed to same amount of heat, and the same structural beam will have higher deflection when the fire is right below the beam compared to when the fire is 10 m away from the beam. This interaction between fire and structural response shows the importance of FSM-EDP relationship as different severity of fire will have varying impact on to different parts of the structure during fire depending on a number of variables.

The FSM-EDP relationship should allow accurate prediction of the response of the structure at a chosen Fire Severity level. It is important for FSM candidates to provide adequate information on the effect of the fire on the structural characteristics. For example, a 60 minute fire does not provide any information on the characteristics of the fire other than its duration and exposure to the standard fire. It is important to find a FSM that has a clear relationship with the structure to be able to accurately predict the structural response.

2.2.4 Fire Severity Measure

One of the main objective of these studies to develop PSFE is to identify an ideal FSM. As explained for PBEE's IMs, there are criteria to be met to be an ideal FSM.. An efficient FSM will

require only a small number of analyses to achieve the level of confidence for the structural response. A sufficient FSM is independent of fire characteristics. For example, a sufficient FSM will not distinguish between short-duration high-temperature fire and long-duration low-temperature fire if the structural responses are identical. The scaling robustness means that a good FSM should have unbiased results compared to an unscaled fire. The hazard computability represents how hard it is to calculate the FSM and how easily the data can be obtained. The predictability of an FSM shows how accurately the structural response can be calculated.

2.2.5 Engineering Demand Parameter

EDPs are variables that describe the behaviour of a structure due to the hazard. EDP can be divided into two groups, local and global EDP. The local EDPs will describe the structure at a component level whereas global EDPs will describe the structure as a whole. An example of a local EDP will be the mid span deflection of a beam whereas a global EDP will be inter-story drift of a building. The relationship between FSM and EDP can be analysed through a number of methods.

2.3 Analytical methods

There are a number of analytical methods to investigate the FSM-EDP relationship. The PEER Centre has developed four different methods to find the relationship between the hazard and the structure. These methods are used to find an IM-EDP relationship to best describe the structural response for the given hazard. The methods are called Single Stripe Analysis (SSA), Cloud Analysis (CA), Multi Stripe Analysis (MSA) and Incremental Dynamic Analysis (IDA) (Jayaler, 2003). These methods use a large number of data of earthquakes and structural response to find the median and the standard deviation to find correlation between different IMs and EDPs. Each method has its own advantages and disadvantages in terms of calculation efficiency and accuracy. The methods can be classified into two groups: Narrow range methods and wide range methods. There are also Incremental Fire Analysis and Fire Stripe Analysis which was developed specifically for PSFE (Moss *et al.* 2014; Shrivastava, 2019).

2.3.1 Narrow Range Methods

Narrow range methods include Single Stripe Analysis (SSA) and Cloud Analysis (CA). They estimate the dispersion, which is the level of overall distribution of data over a comparatively small range of IM. They require low computational effort. This means that they require small number of analysis runs compared to the wide range methods. However, they are not as accurate as the wide range methods.

2.3.1.1 Single Stripe Analysis

SSA involves structural dynamic analyses for a set of data that have been scaled to a chosen IM level. The plot of SSA on to a single IM level will provide a scatter of data in a stripe-like shape. It is then applied to the structure which will then provide the necessary EDP. The EDP is plotted against IM on the logarithmic scale. This plot is then used to find the median and the dispersion of the EDP on the level of IM chosen. The most important decision in SSA is to determine the level of IM to investigate. The result from the study by PEER showed that the estimated result was significantly greater than the true result (Jayaler, 2003).

2.3.1.2 Cloud Analysis

CA gathers data from a set of different IM levels on a structure. This method results in a cloud-like plot over the entire IM-EDP range unlike the SSA. Once an IM is chosen, various EDP values are recorded based on different exposures levels of IMs. This is then plotted on to an IM-EDP graph. Once the plot is obtained, linear regression is applied to the cloud response on the natural logarithmic scale. Statistical properties of the cloud response such as the median EDP for a chosen level of IM is found using this natural logarithmic scale. The result from the study by PEER showed that the estimated result using the CA resulted in underestimating the actual behaviour (Jayaler, 2003).

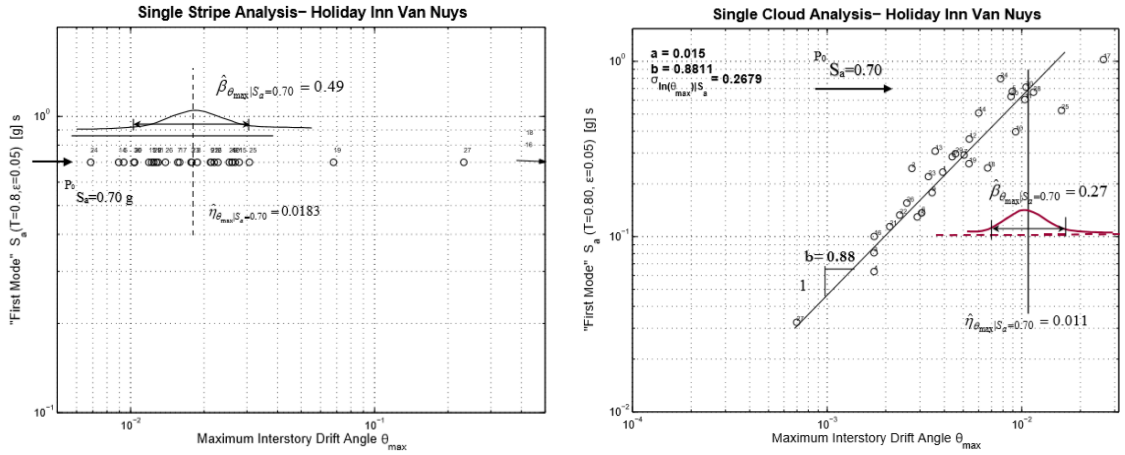

Figure 2.2: Narrow range methods, SSA (left) and CA (right) (Jayaler, 2003)

2.3.2 Wide Range Methods

Wide range methods include Multi Stripe Analysis (MSA) and Incremental Dynamic Analysis (IDA). These methods require more computationally intensive analysis efforts as they cover wider range of parameters. The two methods have a larger scope of application and can have a

better view on the overall response compared to the narrow range methods. They can also be used to calculate the probability of failure of the structure.

2.3.2.1 Multiple Stripe Analysis

MSA is a collection of single stripe analyses at multiple levels of IM. MSA can estimate the statistical properties over a wide range of IM values. They are carried out by scaling a set of data at different levels of IM. The statistical properties for each stripe are calculated as in SSA. The results over the entire spectrum of levels are plotted on the logarithmic scale. The median of the plot is estimated by the 50th percentile curve. The dispersion of the plot is obtained by the average width of the band from 16th, 50th and 84th percentiles in the logarithmic scale. A study by Jayaler (2003) showed that the result from MSA approximated the actual behaviour better than CA.

2.3.3 Incremental Dynamic Analysis

An IDA curve is created by scaling a single sample to multiple IM levels and recording the EDP of each of the scaled IMs. This is repeated to create a multiple number of curves. The IDA method is capable of finding the likelihood of global limit state of the structure. The IDA curve provides a broader view of how the structure responds to different severity levels. The difference to the MSA curve is that IDA results in a single continuous curve whereas the MSA results in a set of curves where the 50th percentile curve is obtained.

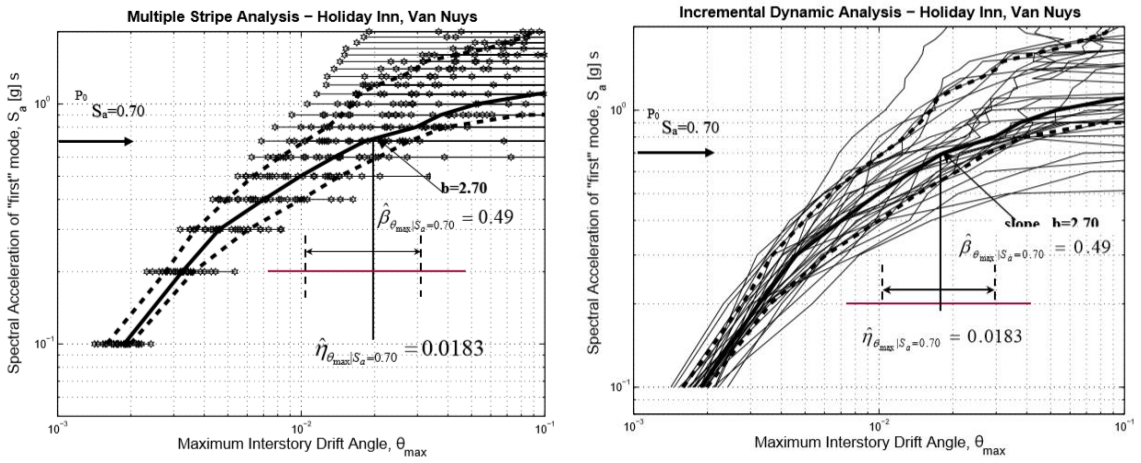

Figure 2.3: Wide range methods, MSA (left) and IDA (right) (Jayaler, 2003)

2.3.4 Incremental Fire Analysis

IDA which was developed for earthquakes was further developed as Incremental Fire Analysis (IFA) to be specifically used for PSFE (Moss *et al.* 2014). IFA is used to find the capacity of a structure by using a range of fires with increasing values of a chosen fire severity from the

minimum severity to the structure's failure level. The median points for each of the IM levels result in the IFA curve. As the number of fire profiles increase for IFA plot, the bias of the database decreased.

2.3.1 Fire Stripe Analysis

The analytical methods developed by PEER such as SSA, MSA and IDA have clear limitations to be directly applied to PSFE. This is due to the extensive scaling required to carry out the analysis. Unlike earthquakes, scaling a fire results in significant changes in fire characteristics. In order to mitigate these negative scaling effects, an analysis method called Fire Stripe Analysis (FSA) has been developed specifically for PSFE (Shrivastava, 2019). A number of narrow bands are created along the entire FSM level. The fire profiles within each of the bands are scaled to allocated bands resulting in very restricted amount of scaling which is considered reasonable to neglect the scaling error as shown in Figure 2.5. Further study was done to generate multiple number of parametric fires (Johnstone et al. 2019). The fires were then analysed with the five analysis methods to find the most accurate method. It showed that FSA was the most accurate way to analyse the data in PSFE. However, it is important to note that these were done through numerical analysis only.

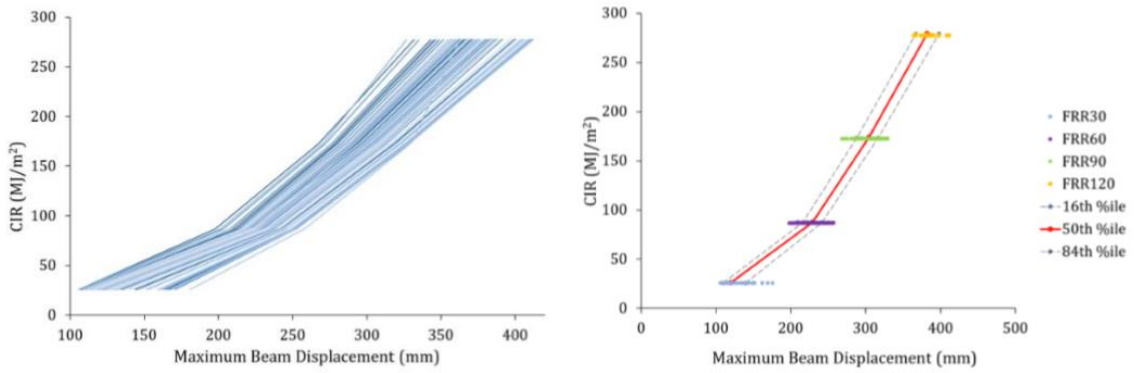

Figure 2.4: PSFE IFA (left) and FSA (right) (Johnstone et al. 2019)

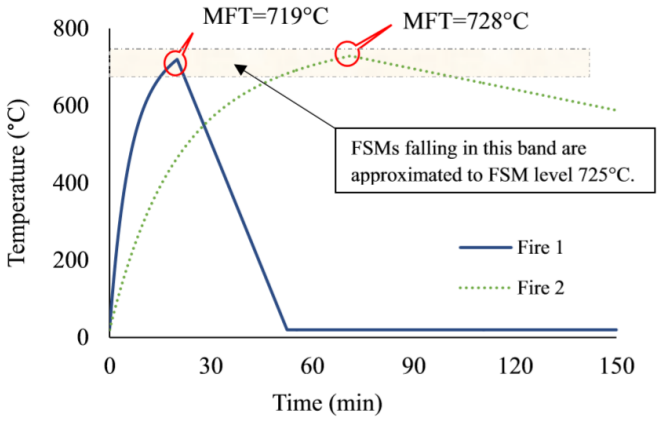

Figure 2.5: FSA scaling method using small bands (Shrivastava et al., 2018)

2.4 Experimental data in PSFE

The lack of experimental data in probabilistic structural fire engineering was identified through literature review as majority of the studies provided structural fire results using numerical analysis (Devaney, 2014; Hamilton, 2011; Lange *et al.* 2014; Moss *et al.* 2014; Shirvastava, 2019). This is due to a number of reasons. The main reason is the cost. In order to carry out a fully developed structural fire test, compartment fires are needed to assess the post-flashover behaviour of a structure. Compartment fires are governed by a number of factors. The compartment ventilation factor will vary depending on the size of open area. The amount of fuel load within the compartment will impact the growth of fire and its duration, the type of material of the structure that is to be tested may have an impact in the development of the fire. Whether an entire structure is to be tested or a part of a structure is tested, it will require significant amount of building material as well as the sensors that is required to withstand heat and measure the structural response throughout the entire experiment. On top of this, it is a probabilistic based study and therefore the experiment must be carried out a number of times which will result in substantial amount of resources and time to conduct. These are only some of the complexities in compartment fire experiments and this is why there has not been many experiments and hence the reason behind why the current probabilistic based studies in structural fire is mostly based on finite element modelling. Experiments are needed to support the development of the mathematical simplifications for the growth of probabilistic methods.

This study will conduct an experiment involving a single element under a pre-flashover fire and set a foundation to the overall experimental based PSFE. The larger goal of this study is to provide a wide range of understanding of experimental based PSFE. This will then become a stepping stone which allows further studies to be conducted involving large scale testing for

PSFE. In this study pre-flashover will be more beneficial. Compared to post-flashover fire, experiments with pre-flashover fires are considerably simpler to carry out and the set up does not require a compartment. The number of variables that must be controlled are less and the time taken for a test can be reduced. A single element is tested rather than an entire structure or multiple elements of a structure. By using a single element, it will reduce time and amount of resources required to carry out this study. It also will provide data on the most basic structural response of the element to a fire and will be the first step to finding a relationship between fire and the structure through experimental data. By reducing the complexity of the experiment, it provides time to carry out greater number of experiments to have more reliable data and basis for the study. Building material that responds quickly to heat will be beneficial for this study and something that can be measured with simple measurement tools will be ideal.

2.5 Conclusions

The literature review has shown a number of studies done to develop PSFE by implementing the PEER Centre's PBEE framework. However, it can be seen that there is no data available on PSFE through experiments. The studies have heavily involved numerical modelling instead of experiments and this also has limitations within the model itself and there were still a number of differences between reality and numerical models due to assumptions made. For such reasons, there is not enough evidence or proof to support the studies that have used numerical models are reliable or reflect full scale structures in real life. This limits the development of probabilistic structural fire design methods. Experiments will help to validate the results of numerical models. Hence the need for experimental data is crucial in structural fire engineering and especially for PSFE and therefore this study will focus on providing as much experimental data as possible to obtain a large experimental dataset.

3. EXPERIMENTAL SET UP

It has been identified in Chapter 2 that the experiment must be of a simple set up and provide as much experimental data as possible for analysis of the structure-fire relationship. This chapter explains the background and the reasoning behind the decisions made for the experiment set up and execution. This includes the set up itself as well as the variables that are recorded and varied throughout the tests. It also describes equipment instrumentation.

3.1 Background

Structural fire studies have focused on obtaining data from numerical models such as SAFIR and VULCAN (Franssen, 2005; Bailey, 1995). It has been identified that experimental data is crucial to further develop the Probabilistic Structural Fire Engineering (PSFE) as these will bring more reliability and confidence. Although numerical models have been used widely and provide value to structural fire design, they contain limitations compared to experiments especially for the probabilistic-based assessments, where variation in properties play a significant role. If a numerical model was to be run for 'n' number of times, for a structural element under a same design fire with identical scenario, it will provide a result which is identical for every simulation run. On the other hand n' number of identical experiments will produce 'n' number of results. This is the value that experiments provide to further develop the probabilistic approach as they produce a distribution of different data within a range due to uncertainty in each fire characteristic. It has been identified in Chapter 2 that it is important to carry out as many tests as possible to obtain data since the confidence of the analysis increases with the data size. To the authour's knowledge, this study generates experimental data for the development of probabilistic structural fire engineering approaches. It is intended to be a stepping-stone for further experimental and numerical research in this regard.

There are different stages in the development of a fire and they can be divided into two main phases: Pre-flashover and post-flashover. Flashover is the point when the fire fully develops and starts burning all combustible materials in the room. In a structural fire, it is the point when the overall temperature of the compartment reaches a certain point where all of the fuel within the compartment is ignited. There is a lot of emphasis on post-flashover fires for structural design, as room temperatures are at their highest. However, pre-flashover fires may also significantly affect structures, depending on the specific fire scenario. The growth rate of the fire determines how long it will take for the fire to reach flashover. The flame spread at the initial stage of a fire can contribute to the overall fire affecting the structure. In terms of experiments, a pre-flashover fire can be generated in open air since it is in the initial stages of a fire whereas post-flashover

fires occur in compartment. There is value in data for both types of fires but in different ways. Post-flashover fires provide information on how compartment characteristics, fuel loads, ventilation conditions and linings affect fire development. This provides a holistic view on how the temperature of the compartment increases and the related structural response. On the other hand, pre-flashover fires provide information on how fire growth rates, peak heat release rates and non-uniform temperature distributions may affect structural behaviour. Although there are differences in the two, both pre and post-flashover fires contribute to overall behaviour of structures under fire conditions. For this study (where it provides a stepping stone for experimental studies) in PSFE, the aim is to experimentally investigate the fire-structure relationship. For a typical structural fire design, post-flashover fire is can be most beneficial. However, in attempting to develop a new research material, it is prudent to start with an easily manageable set up that can provide a large dataset. It is therefore decided to conduct a pre-flashover fire to study a single element in this study. One of the priorities in this study is to provide as much data as possible. It is clear that using a pre-flashover fire would provide more opportunity to obtain more data compared to a post-flashover fire. Once this study is completed, it can then lead on to studies that investigate on the similarities between the pre-flashover fire and post-flashover fire to further develop the findings in this study on to post-flashover fires.

There are a number of building materials that are used in the current building industry. Each material has their advantages and disadvantages. In order to select ideal material for the study, properties of typical construction materials are reviewed. Steel provides a good weight to strength ratio, concrete does not combust and wood is environment friendly. A structural experiment using any of these materials will certainly be valuable. For this study, steel is used. The main reason for using steel as the specimen is due to its quick reaction to heat. Steel has a high thermal conductivity compared to timber and concrete. Since thermal conductivity is the material's ability to transfer heat, steel responds quickest to fire. Steel has been used as it will be beneficial to use a material that can provide the broadest spectrum of data.

3.2 General Experimental Setup

Steel has been chosen to be used for the experiments due to its ability to quickly respond to heat. A single steel I-beam (150UB14.0) with a span of 2 m will be used. To reduce the complexity of the experimental procedure, the smallest section sized I-beam was chosen as it will be easier to handle a lighter beam for the experimental set up. The length of the beam is 2 m long to provide enough space to have loads placed on top and also to ensure the heat from the

gas burner is not affecting the frames that are set up to hold the beam in place. More complex structural element or combination of structural elements can be studied in the future.

There are a number of conditions to support a beam. It can be fully fixed, pin ended or simply supported. Fully fixed ends will mean that a beam will be permanently fixed at its ends to prevent it from moving in all directions. However, the study will involve multiple number of tests to be carried out which will mean the steel beam must be replaced for each test and the fixed supports will not be adequate to work with. A simply supported beam will be the simplest set up and easy to achieve. However, it will not be able to provide much data that will be of use for the study other than the temperature of the beam. For pin ended supports, the thermal expansion of the beam can be measured. As a pin ended support will have a degree of freedom to rotate, the beam will exert axial force as it is exposed to heat. Simply supported beams will not be able to measure the axial force of the beam but pin ended supports will be able to provide its reaction to fire. Since any structural response of the beam will be of value, pin-pin connection will be used.

There will always be a load on a structural beam due to factors such as self-weight, dead load and live load. In a lab environment the simplest way to imitate the scenario will be by using point loads. Therefore, a commonly used four point bending test configuration will be introduced to load a beam to investigate how the structural element behaves with loads applied while being exposed to fire. Four point bending test is beneficial in this study as it has a constant bending moment between the two loads. The purpose of the experiment is to have a fire underneath to observe how the beam behaves from different heat exposures. Hence, it will be more beneficial to have consistent stress under the area where there will be heat rather than having a setup which has varying stress along the length of the beam. The two point loads will be located at 0.5 m and 1.5 m away from one end of the beam.

The distance between the beam and the gas burner will be consistent throughout the study. By having a fixed set up, the flame height of the design fires can be varied to study the different scenarios such as below:

- When the flames are below the beam
- When the flames are touching the beam
- When the flames are fully engulfing the beam

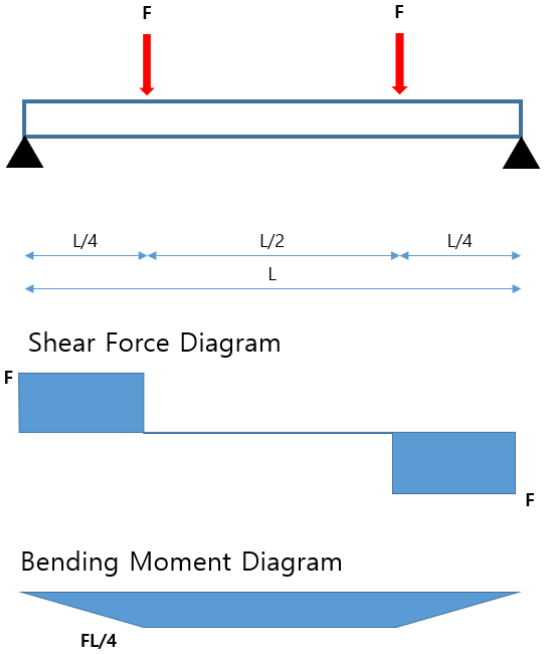

Figure 3.1: Layout of 4-point bending test

Throughout the planning of the experiment, the simplicity of the experiment has been emphasized since the acquisition of as much data as possible is crucial for the study. Through these experiments, the goal was to obtain a broad spectrum of structural response over a wide range of fire severity levels. The change in fire severity levels can be explained through a heat release rate (HRR) graph, as shown in Figure 3.2. It is a HRR of a typical wooden desk that has been tested. This single graph can be used to provide different information about pre-flashover fires. For example, the total time it took the desk to burn is the duration of the fire, the peak of the graph is the peak HRR of the desk fire. The initial changes in slope of the development of the fire describes growth rate of the fire. The area under the HRR graph is the Total Energy Released (TER) in the fire and lastly the average peak heat released is calculated as TER divided by the duration of the fire. All of these variables indicate the level of severity in a fire. Varying any of these properties with corresponding structural response will allow probabilistic analysis to be carried out to investigate the fire-structure relationship in a pre-flashover fire.

3.3 Possible FSMs

In structural fire, there are a number of variables involved that can be used to describe the fire characteristics as explained in Figure 3.2. The purpose of this study is to investigate different variables in a pre-flashover fire, called Fire Severity Measures (FSMs) through experiments and find different responses from a structural beam which will provide details on how different

structural responses, called Engineering Demand Parameters (EDPs) have behaved. It is important to find efficient FSMs as they are necessary to help accurately quantify structural response from various fire. This is done to gain better understanding of the FSM-EDP relationship. As FSMs are variables that provide information of different fires and their characteristics, EDPs are structural variables that provide information on how a structure responds to the fire with certain FSMs. Some possible EDPs can be the deflection of a column, a peak temperature of a connection or axial force of a beam. In simple terms, both FSM and EDP are a single variable of fire and structure that provides different kinds of information. The possible FSMs and EDPs to investigate in this study have been identified and discussed further below.

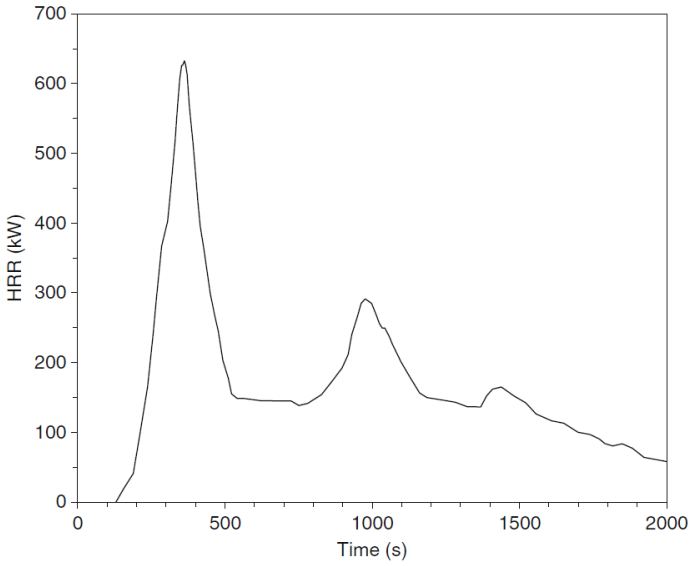

Figure 3.2: Typical HRR of a wooden desk tested (SFPE, 2016)

An idealised pre-flashover fire may be represented by the diagram in Figure 3.3. The possible FSMs are peak HRR, Total Energy Released (TER), average Heat Release Rate (HRR*), duration and growth rate. HRR is considered to be the single most important variable in fire hazard (SFPE, 2016). HRR is used to express how big or severe the fire is. TER also plays an important role in fire as it is how much heat energy is produced from the fire that may impact the structure. TER accounts for the overall heat that has affected the beam. The HRR* shows how much heat has released on average over the entire duration of the fire. It is obtained by dividing the sum of HRR by the total duration of the fire. Duration is the simplest factor that describes the fire characteristic, as it provides information on how long the fire went on for. The growth rate, expressed in alpha-time squared, is an important factor to consider in pre-flashover fire.

Alpha-time squared growth rate is a type of a growth rate used in fire engineering to describe how fast a fire initially develops by classifying into five categories (Ultra-slow, slow, medium, fast and ultra-fast). It determines how fast a fire will reach its peak heat release rate and may affect the temperature growth of the beam in the earlier stages. These FSMs are illustrated in Figure 3.3. The FSMs are varied severity levels to provide a wide range of fires starting from a short duration with high peak HRR to a long duration with low peak HRR. The variations will be made with different ranges of FSM values as shown in Table 3.1.

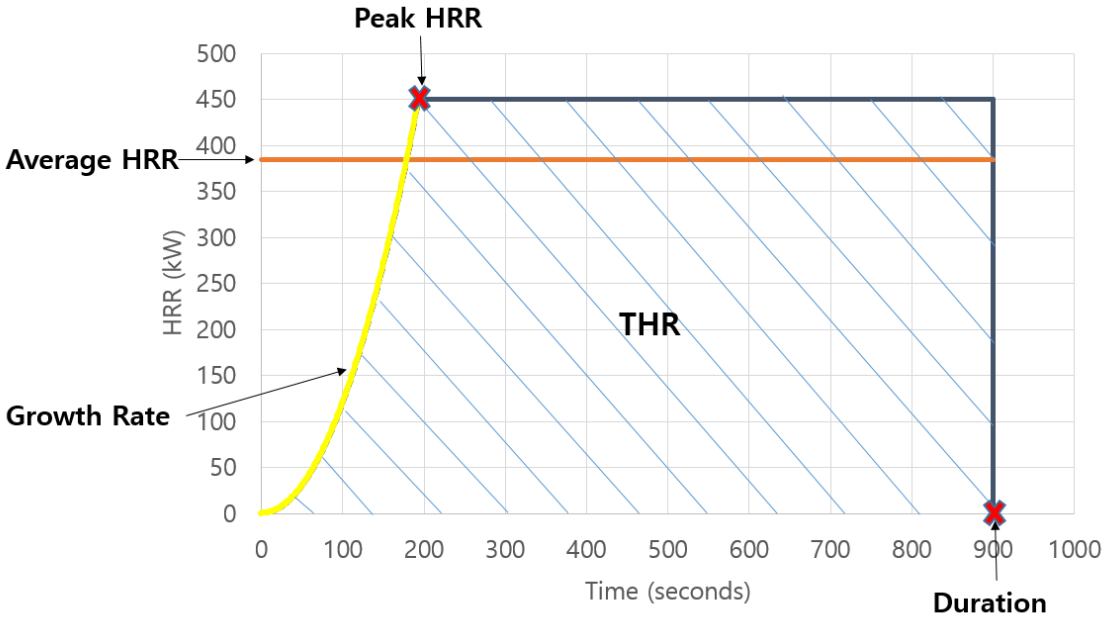

Figure 3.3: Example design fire with FSMs

By varying the FSMs, the design fires shown in Figure 3.4 are used in this study. The colours represent each of the growth rates from ultra-slow to fast. These design fires were developed in the early stages of the study before designing the experimental set up. They were checked with calculations for flame heights, temperature of the beam and deflection at the mid-point to determine the final experimental setup of the study. Chapter 6 compares the predictions with the actual experimental results.

Table 3.1: Fire Severity Measures and their ranges for the experimental testing

FIRE SEVERITY MEASURE	RANGE
Peak HRR	250 kW, 350 kW, 450 kW
Total Energy Released (TER)	125 MJ – 710 MJ
Duration	300 s, 600 s, 900 s
Growth Rate (kW/s²)	Ultra-Slow 1, 2, 3 - 0.0007, - 0.0014, - 0.0022 Slow 1, 2, 3 - 0.0029, - 0.0059, - 0.0089 Medium 1, 2, 3 - 0.012, - 0.0237, - 0.035 Fast 1 – 0.047
Average HRR (HRR*)	TER/Duration

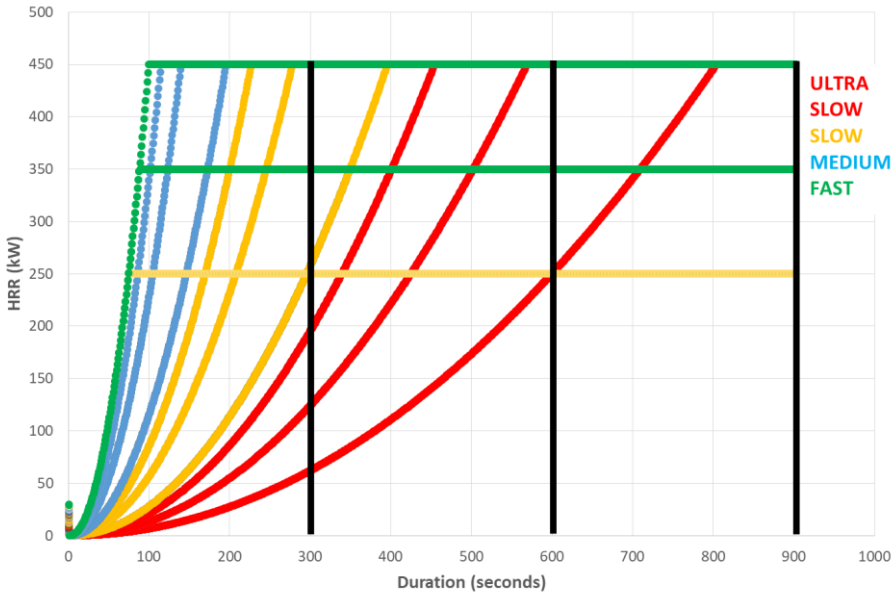

Figure 3.4: Design fires for experiment

There are three ways for fire to transfer heat to its surroundings: conduction, convection and radiation. Conduction is how heat is transferred through a solid, when one end of the rod is heated up and the temperature of the rod increases gradually from one end to the other. Convection is from a fluid to a solid surface. For example, activation of a sprinkler from the hot air around the sprinkler head is a form a convection as heat is transferred from hot air or smoke to the sprinkler. Lastly, radiation is the heat exchange between the two surfaces and an example of this would be the heat transferred from the surface of the flames on to a wall or furniture to ignite them.

The way the heat is transferred depends on the fire and the overall set up in a structural fire scenario. For a post-flashover compartment fire, heat is mainly through radiation where the heat waves travel from the burning object to nearby surfaces, whereas for localised fire, convection is the main source of heat transfer as the heat from the flame results in increase in the temperature of the air surrounding the steel beam which then heats the beam. The ratio of the convection heat is considered to be approximately 80% of the total heat released from the heat source (European Standard, 2002). In order to mimic different uniform beam temperatures in beams under pre-flashover fires, four different flame heights were explored above the burner. By having different flame heights, the distance between the flames and the beam will vary to affect the heat transfer. For example, if the beam is further away from the flames, it will take longer for the fire to heat up the air that is surrounding the beam. This will affect the temperature rise of the beam and its other responses related to its temperature. On the other hand, if the flame was touching the beam or engulfing the beam, the surrounding air will have a significantly higher temperature which will have more effect on the beam.

3.4 Simple Calculation

A number of simple calculations have been used to find various values such as the expected temperature of the beam and the expected flame height for different design fires. The purpose of carrying out simple calculations prior to the experiment was to ensure the defined design fires shown in Figure 3.4 provided a wide spectrum of results.

The following equations (European Standard, 2002; European Standard, 2005) were used to find the expected temperature of the beam,

$$h_{net} = \dot{h} - \alpha_c(\Theta_m - 20) - \Phi \dot{\varepsilon}_m \varepsilon_f \sigma [(\Theta_m + 273)^4 - (293)^4] \quad \text{Equation (1)}$$

$$\Delta\theta_{a,t} = k_{sh} \frac{A_m/V}{c_a \rho_a} h_{net} \Delta t \quad \text{Equation (2)}$$

The variables are explained in the nomenclature. The simple calculation assumes uniform temperature along the beam profile and that the entire beam is under the same amount of HRR along its entire length. This calculation method is used to design for structural elements in real buildings and therefore contains a number of conservative factors to ensure the designed structural elements have a factor of safety. The expected temperature profile of one design fire from simple calculation is shown as an example in Figure 3.5, showing a peak temperature of 359 ˚C at the end of the test. Appendix A shows an example spreadsheet of the calculation of temperature profile using simple calculation.

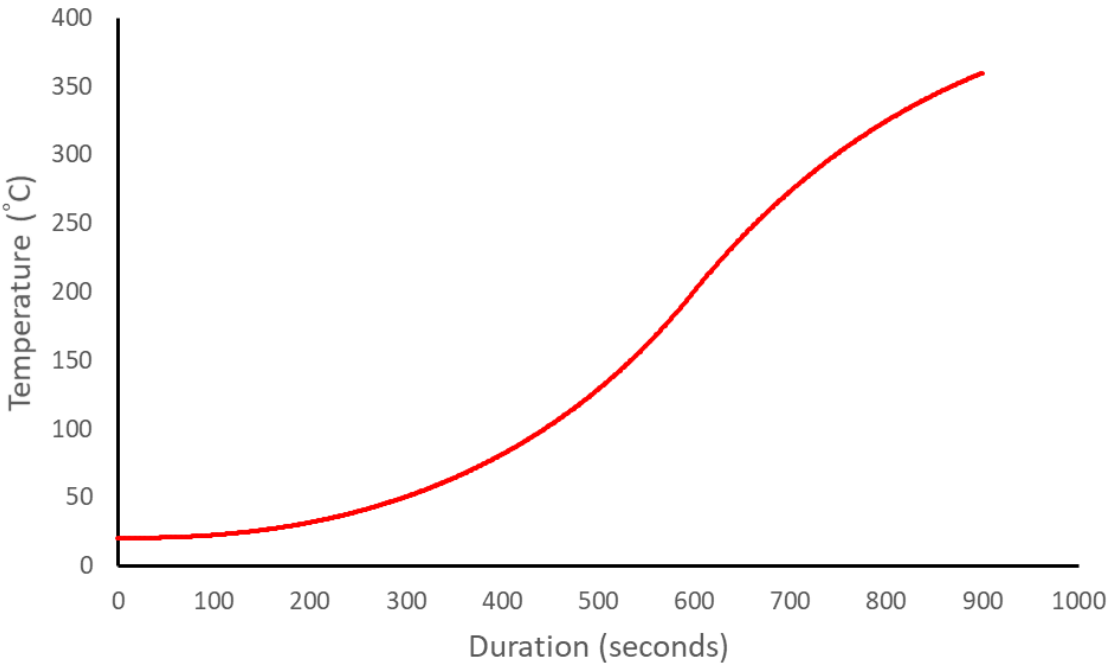

Figure 3.5: Expected temperature profile of the beam from Test 1 (Ultra-slow: 0.0007 kW/s2, 250 kW)

The distance from the gas burner to the beam was 1.5 m and flame heights were calculated using Heskestead's flame height calculation (SFPE, 2016) to provide different scenarios as explained in Section 3.2. The equation is shown as Equation 3,

$$L = -1.02D + \left(0.0148\dot{Q}^{\frac{2}{5}}\right) \qquad \text{Equation (3)}$$

The variables are explained in the nomenclature. The equivalent diameter was used as the equation is for liquid pool fires and the experiment will use a rectangular gas burner. The

expected different flame heights for peak HRR of 250 kW, 350 kW and 450 kW fires are shown in Figure 3.6. The blue dotted line represents the location of the beam above the fuel bed,

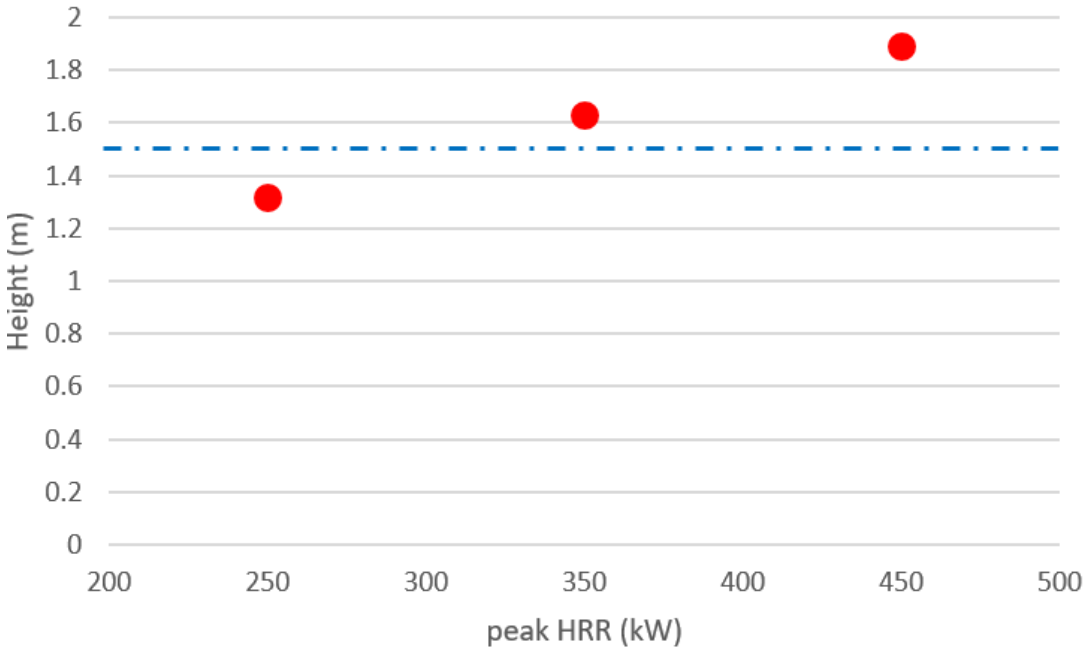

Figure 3.6: Expected flame heights at corresponding peak HRRs of 250 kW, 350 kW and 450 kW

The increase in temperature for an element will be dependent on the total amount of heat energy received from the fire. Assuming all other variables remain identical, the duration of a fire is an important factor that can vary the final outcome of the structure's response. The duration was in three different ranges, in 300 seconds intervals (300, 600 and 900 seconds). This resulted in obtaining three sets of data from one test since a test for 900 seconds would produce results for 300, 600 and 900 seconds. This provided a broader spectrum of different data to analyse.

Growth rate of a fire is an important variable in development of a fire especially in the early pre-flashover stages. The change in growth rate determines the time it takes for a fire to fully develop. The faster the growth rate, the faster the development of the fire. The growth rates were varied with different alpha time squared values as it is often used to describe design fires in fire engineering. The growth rate from ultra-slow (0.0007 kW/s^2) to fast (0.047 kW/s^2) were chosen in three increments to provide broad and spaced values. The total number of design fires were 102.

3.5 Possible EDPs

EDPs describe how a structure responds to a hazard. Following from the possible FSMs, possible EDPs that can be measured have to be identified. Two EDPs were chosen. They were the temperature profile of the beam and the axial force of the beam due to the restraint to thermal expansion. The temperature is an important EDP as it is directly related to the residual structural properties of steel elements. As the structural elements are always under some form of a load, the reduction in strength will be directly related to the deflection of the element. Axial force is an important factor in structural fire engineering since steel in particular tends to expand when it gets heated. Heated beams tend to expand in all directions. However, this is restrained by their supports that are colder than the heated beam and prevent the beam expansion, eventually resulting in buckling of the beam on prolonged exposure. Table 3.2 shows the EDPs.

Table 3.2: Engineering Demand Parameters recorded in the experiment

ENGINEERING DEMAND PARAMETER	REASONING
Axial Force on the beam (kN)	Indication of axial force build up in the beam
Beam Temperature Profile (˚C)	Temperature increase of steel affects structural characteristics such as yield strength and modulus of elasticity

3.6 Experimental set up – plan

There were 68 tests in total carried out for the study which consisted of 34 thermal tests and 34 structural tests. Thermal tests measured the temperature gradient of the beam and the structural test measured the axial force exerted due to restrained thermal expansion. These tests provided over 100 sets of data and provided a wide spectrum of results for later analysis. The initial concept of the experimental set up of the tests are as shown in Figure 3.7 and Figure 3.8, which illustrate the thermal test and the structural test respectively. The thermal test consisted of thermocouples along a steel I-beam to measure the temperature gradient from the bottom to top flanges at three different points along the beam. The structural test was a four-point bending test of the beam. The structural test had a load cell installed on one end of the frame to measure the axial load of the beam.

Recording both EDPs, in one experimental set up would have been ideal as this would have provided more time to carry out more experiments. In order to measure the temperature of the

beam along its length and depth throughout the entire experiment, thermocouples had to be drilled and embedded into the beam. A single beam was used to measure the temperature profile under different design fires with varying FSM levels. The use of a single beam for thermal tests meant that all the temperature data could be obtained from one setup of thermocouples in one beam, allowing for different beams to be used for the structural experiments, and not spending more time to drill in thermocouples for each beam. This setup also meant that for the structural tests, there were no holes in the beams to provide imperfections to initiate potential failures.

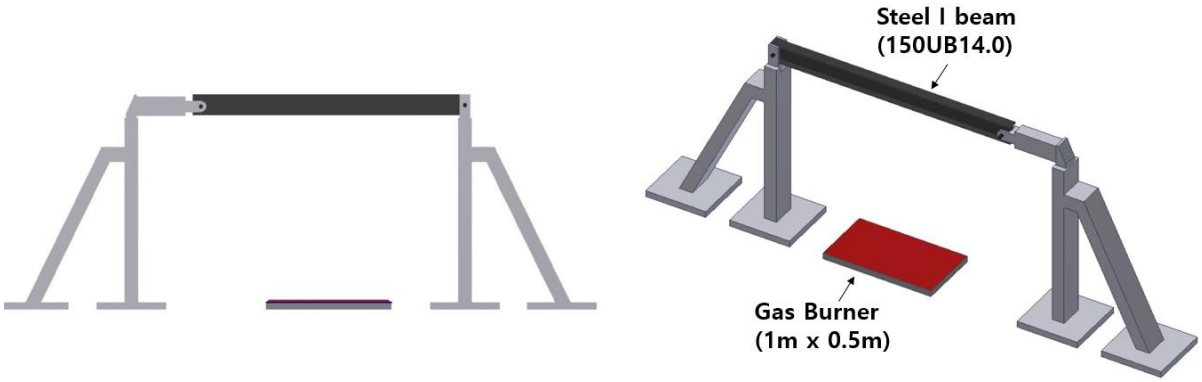

Figure 3.7: Thermal Experiment Setup

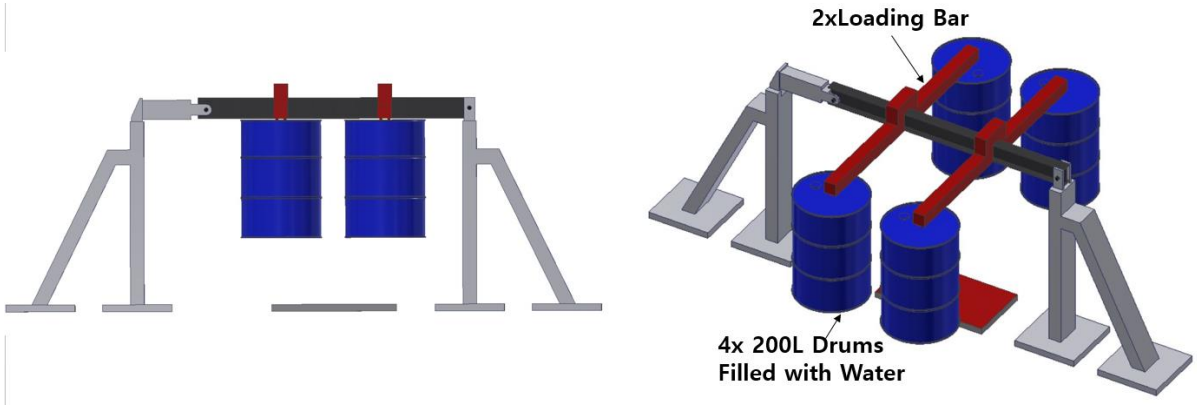

Figure 3.8: Structural Experiment Setup

3.7 Experiment set up – as built

The overall set up of the two experiments are as shown in Figure 3.10 and 3.11. They can be divided into three parts. Figure 3.10 shows only the beam, frame and the gas burner which is a set up for the thermal test. Figure 3.11 shows the experimental setup of a structural test with

the two point loads and the crane as well. The first is the beam and the frames. The beam had been placed on the main frames by using pins at each end. The main frames were bolted onto the strong floor to ensure they did not move during the test. It was important the main frames were firmly connected to the strong floor since the axial force will not be recorded accurately if the frames were to move during the test as beams go into compression due to thermal expansion. The second part is the loading bars and the water-filled drums. The loading bars were placed on top of the beam at two locations to act as the two point loads. The beam did not sway from side to side by using the rectangular blue frames to keep the loading bars in place as shown in Figure 3.11. These rectangular blue frames were also bolted onto the strong floor. The red loading bars were designed to fit on the beam but were made with enough space to prevent them acting as another constraint to the beam. Lastly, a crane was used to lift the beams when replacing the beam for the next experiment. It was made to lift up the loading bars and the water drums to remove the existing beam and to replace it with a new beam once the test was completed.

The beam was not replaced for every thermal test and only one identical beam was used over all of the thermal tests due to complexity. This was considered to be reasonable as the steel temperature did not exceed 600 ˚C in any of the tests and hence no metallurgical change of steel occurred. This meant that once the steel cools down, it could be tested under a different fire and would provide the same results as a new beam would. The beams had to be drilled in 21 locations to embed the thermocouples. Once one thermal test was done, the beam had to be cooled down before the next thermal test.

Figure 3.9: Thermal test set up showing the beam, frame and the gas burner

Figure 3.10: Overall set up for the structural test

3.8 Methodology

3.8.1 Thermal Experiment

The thermal test was conducted with no vertical loads. Once the beam was in place and the test was ready, the Universal Data Logger was started first with a computer programme (called LabView, discussed in Section 3.8.6) starting recording 60 seconds later. A computer programme was used to control the gas system to send a set amount of gas to the gas burner, and start the design fire. The design fires were created on a spreadsheet and uploaded to the programme. The gas valves were then turned on to send the equivalent amount of gas for each HRR. The gas burner was then ignited using a hand torch to ensure the flames were ignited evenly throughout the surface of the gas burner. Once a test reached its end, the gas valve was turned off automatically as LabView read 0 kW on its design fire input. The Universal Data Logger recorded the thermocouples for an additional 60 seconds after the test finished. The beam was then allowed to cool down from the heated temperature until it reached 40 ˚C to start the next thermal test.

3.8.2 Structural Experiment

The structural test was carried out with the two point loads using the loading bars and the water-filled drums. The first step was to ensure the beam was in place and the axial force reading from the load cell was between -1.0 kN to +1 kN. This was due to the manual handling involved in the experimental setup and was the tolerable sensitivity, of approximately 10% of the final outcome. As in the thermal test, the Universal Data Logger was started first and the LabView started 60 seconds later. Once the gas valves turned on, the gas burner was ignited with a torch and ensured the flame was spread evenly across the surface. Once the design fire ended, the gas valves turned off automatically and the Universal Data Logger recorded for an additional 60 seconds. Once the flame was completely out and the beam had cooled down to be removed safely, the loading bar was connected to the crane. The loading bar and the drums were lifted using the rig to provide space to remove the tested beam. Once the tested beam was removed, a new beam was placed into the frame and the rig placed the loading bar on top of the beams. The crane was then moved away from the set up to start the next structural test.

Every instrument that was used to carry out the experiment is explained in detail in the following sections.

3.9 Instrumentation

3.9.1 Specimen

Steel I-beams (150UB14.0) with a span of two metres was used as the test specimen. In total, 36 I-beams were prepared, two for the thermal tests and 34 for the structural tests. For the thermal test, the beam was drilled in 21 places with a depth of 0.5 mm to 1 mm to embed the thermocouples.

Figure 3.11: Specimen I-Beams 150UB14.0

3.9.2 Thermocouples

The beam for the thermal test had 21 k-thermocouples embedded throughout. The k-thermocouples have a ±5 ˚C variance. The thermocouples on the cross sectional area of the beam are as shown in Figure 3.12. This was done to find the temperature profile of the entire beam since there was also a temperature difference between the top and the bottom of the beam as well as along the beam. The thermocouples were positioned on three different points along the beam: A, B and C which were 0.5 m, 1.0 m and 1.5 m away from one end of the beam respectively. The 0.5 m and 1.5 m were where the vertical point loads were located and 1.0 m was the mid-point of the beam where the maximum deflection occurred. In Chapter 4, the temperature profiles of all the thermocouples from A1 to C7 will be illustrated through graphs and discussed in more detail.

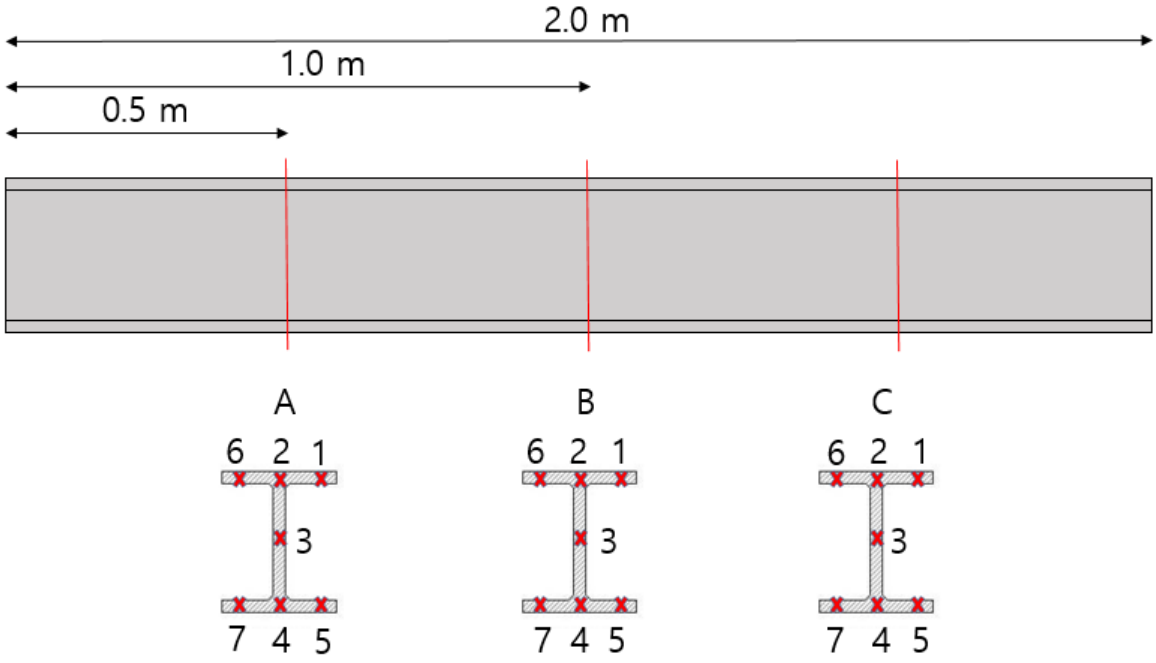

Figure 3.12: Lateral and cross sectional view of the beam where the thermocouples were embedded

3.9.3 Loading Bars

The two point loads that form the four point bending test for the structural tests were made using four drums each filled with 200 L of water. In total, they were 4 kN at each load point. The red loading bars were intentionally shaped like a hanger so they did not slide on to one side during the test.

Figure 3.13: Red loading bars for structural tests

Figure 3.14: Rectangular blue frames to stabilise the loading bars

3.9.4 Frames

Figure 3.16 and 3.17 show strong floor and the frames that were designed to hold the steel I-beam (150UB14.0) with a gas burner below the beam. The frame was made of 100 mm by 200 mm RHS steel. The height of the frame was 1.5 m with additional leg to support the main frame. The total distance from one end of the frame to the other was 2.4 m. Both ends of the

frame had a 50 mm pin connected to hold the beam. The frame was then connected to the strong floor. The strong floor had a connection grid of 400 mm by 400 mm. The frames were covered with fire resistant blankets to protect them from the flames.

Figure 3.15: Surface of the strong floor in laboratory with 400 mm by 400 mm connection grid

Figure 3.16: One side of the frame, with (left) and without (right) fire blanket

3.9.5 Gas Burner

The gas burner provided the pre-defined design fires for each of the experiment. It was connected to gas bottles at the back of the lab to send out a predetermined amount of gas on to the gas burner to provide the design fire for the chosen test. The dimension of the gas burner was 0.5 m by 1.0 m. There was a single pipe along the centre of the burner to supply gas for the fire. The burner was filled with pumice. Pumice is a light volcanic stone with large porosity. It allows gas to travel and spread throughout the surface of the burner easily which enables flames to be spread out evenly. The gas burner was connected with a computer program called LabView (explained in the next section). The program controlled how much volume of gas was required to provide the gas burner with the equivalent HRR as required by the pre-assigned design fire.

Figure 3.17: Gas burner (0.5 m by 1.0 m) filled with pumice

3.9.6 Lab View

LabView is a program used to control the amount of gas being extracted from the gas bottles to fuel the gas burner. It was connected to the gas bottles and the overall gas pipe system. Once the program starts, the valves automatically open. By specifying the right factor, feedback value and using a spreadsheet to input the desired design fire, the desired volume of gas in L/minute for the chosen design fire was sent on to the burner. The design fire was uploaded on to the program and the test was started as shown in Figure 3.19. A torch was used to ignite the fire.

3.9.7 Load cell

A load cell was installed on one end of the frame in order to measure the axial force due to the restrained thermal expansion of the beam. A Pancake load cell LPCH 2500 kg, made of alloy

steel shown in Figure 3.20 was chosen as it is used widely for its high accuracy for measurements of both tension and compression. It was calibrated with the computer to provide the correct readings. The load cell was then placed between the frame and the pin support as shown in Figure 3.21.

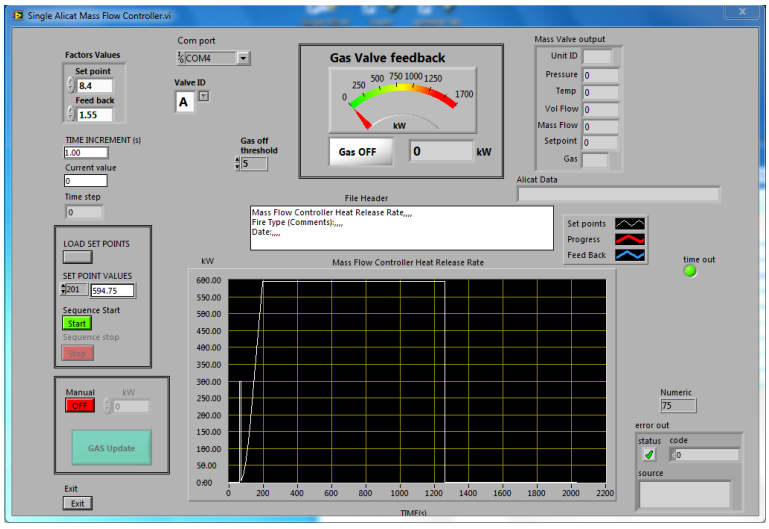

Figure 3.18: Lab View with an example design fire

Figure 3.19: Pancake load cell LPCH 2500kg

Figure 3.20: Load cell connected to the frames

3.9.8 Control Box

Both the thermocouples and the axial load cell were then connected to the control box. The Control box was then connected to the computer with the Universal Data Logger to interpret and record the data. The box was also protected with fire blankets to protect it from the radiant heat from the gas burner.

Figure 3.21: Thermocouples and Axial load connection to the control box

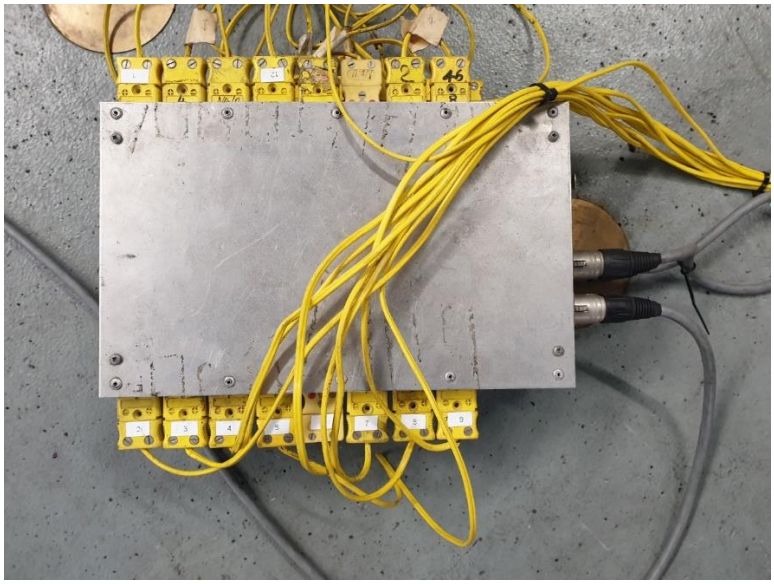

Figure 3.22: Main control box connected to the Computer – Universal Data Logger

3.9.9 Universal Data Logger

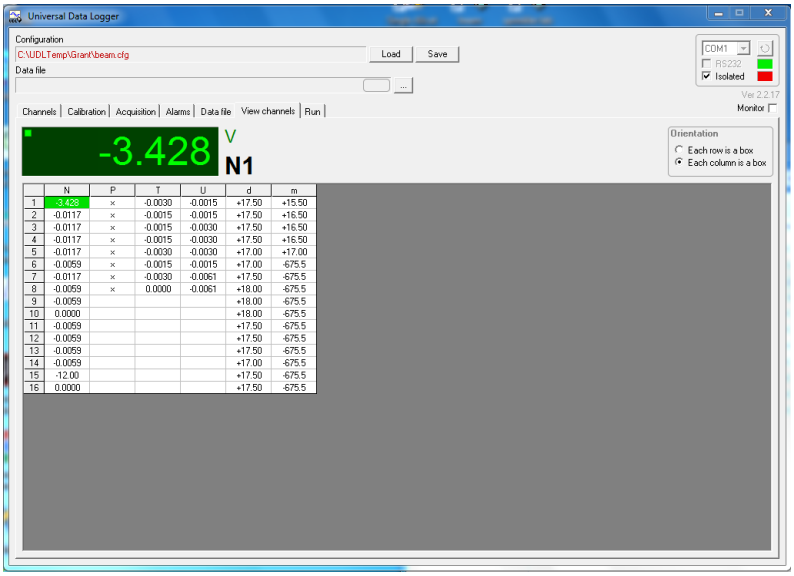

	N	P	T	U	d	m
1	-3.428	×	-0.0030	-0.0015	+17.50	+15.50
2	-0.0117	×	-0.0015	-0.0015	+17.50	+16.50
3	-0.0117	×	-0.0015	-0.0030	+17.50	+16.50
4	-0.0117	×	-0.0015	-0.0030	+17.50	+16.50
5	-0.0117	×	-0.0030	-0.0030	+17.00	+17.00
6	-0.0059	×	-0.0015	-0.0015	+17.00	-675.5
7	-0.0117	×	-0.0030	-0.0061	+17.50	-675.5
8	-0.0059	×	0.0000	-0.0061	+18.00	-675.5
9	-0.0059				+18.00	-675.5
10	0.0000				+18.00	-675.5
11	-0.0059				+17.50	-675.5
12	-0.0059				+17.50	-675.5
13	-0.0059				+17.50	-675.5
14	-0.0059				+17.00	-675.5
15	-12.00				+17.50	-675.5
16	0.0000				+17.50	-675.5

Figure 3.23: Universal Data Logger reading axial load

Universal Data Logger is a program which connects the computer to different instruments to record the measurements to time. As stated in Section 3.8h.8, the Universal Data Logger was connected to the control box which was connected to the load cell and the thermocouples installed on the frame and on the beam. Each of the thermocouples and load cell was assigned to a different recorder and measurement was recorded from the very beginning of the test to the

end. This was then automatically imported to a spreadsheet to be saved for further analysis to be carried out.

3.10 Conclusion

Chapter 3 has explained the process from the very early planning stage to the final experimental set up as well as the methodology of thermal and structural experiments. The variables in the fire and the structure, i.e. FSMs and EDPs, have been identified and the overall setup of both thermal and structural test have been explained including the background for separating the tests to remove bias. Each of the instruments used have been described individually and how they contribute to the experiment. Chapter 4 will report the results and the data obtained from each of these experiments.

4. EXPERIMENTAL RESULTS

Chapter 4 presents the results obtained from both thermal and structural experiments carried out following the experimental set up in Chapter 3. Since there were 68 tests total, not all of the results are individually covered in the chapter but are dealt in a comprehensive manner. The results of the growth rates (ultra-slow: 0.0007 kW/s^2, slow: 0.0029 kW/s^2, medium: 0.012 kW/s^2 and fast: 0.047 kW/s^2) as explained in Chapter 3, will be shown in a graph format to indicate how they developed with time. All of this data obtained from the tests are used for the analyses in Chapter 5.

4.1 Changes made to the experiment

As the experiments were being carried out, there were issues that were unexpected in the design stage of the experiments and this required improvisations to be made in order to produce more valuable data for the study.

4.1.1 Additional FSM levels

It was decided to have additional design fires with duration of 1200 seconds and include a 650 kW peak Heat Release Rate (HRR) fire. This was not planned at the initial stage of the study. However, when the first tests were carried out, it was found out that the temperature of the beams did not rise as high as expected with the simple calculations that were done pre-experiment. In order to obtain a wider spectrum of structural responses, it was decided to add additional Fire Severity Measure (FSM) levels of 1200 seconds for duration and 650 kW for the peak HRR of the fire. This allowed significantly higher maximum temperatures and axial force of the beam which were beneficial to the study.

4.1.2 Fire initialisation modification

During the first few tests, it was shown that the flames did not grow or spread across the burner evenly at the initial stage of the fire (approximately for the first 500 seconds of the fire). This was due to the size of the gas burner being too big compared to the low HRR at the initial growth stage of the design fires especially for the ultra-slow/slow growth rate fires. This meant that the equivalent volume of gas that was sent to the gas burner was simply not enough to spread across the entire surface of the gas burner quickly. From Test 9 (Ultra Slow: 0.0022 kW/s2, 450 kW fire), it was decided to give a HRR spike of 300 kW for 8 seconds at the beginning to provide sufficient amount of gas for the flames to spread evenly across the gas burner as shown in Figure 4.1.

Figure 4.1: Uneven flame spread in the gas burner, Test 1 (Ultra-slow: 0.0007 kW/s^2, 250 kW)

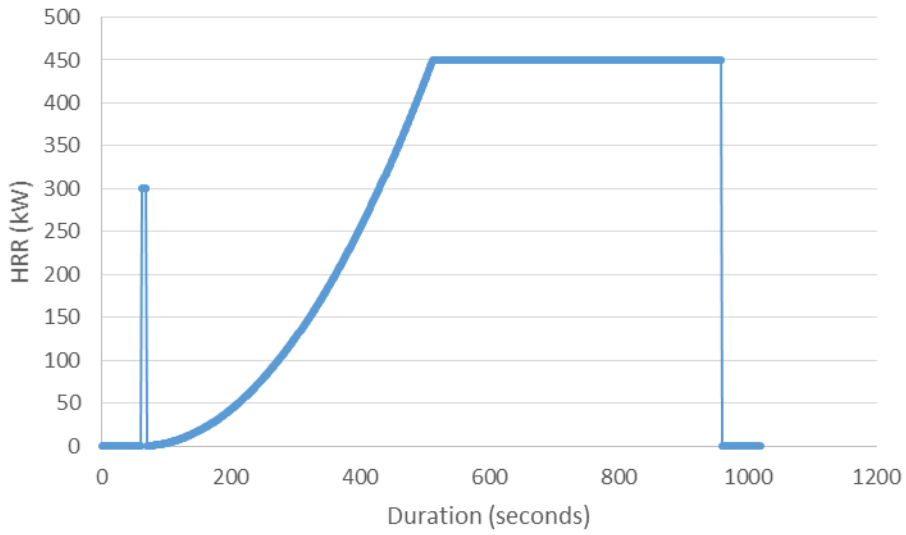

Figure 4.2: Test 9 (Ultra Slow: 0.0022 kW/s^2, 450 kW fire) with HRR spike for 8 seconds

Deflections were expected to be negligible. From simple calculation, 8 kN was not enough to significantly impact the beam. However, the mid span deflection was measured regardless, using a laser pointer. Although the deflections were not significant, this was later found to be valuable as it showed a correlation between the axial force and the temperature profile of the beam. It will be discussed further in Chapter 5.

4.2 Thermal Results

Thirty four thermal tests were carried out, providing 102 results. Thermocouple reading results are graphed below for all 21 thermocouples installed in the beam as shown in Figure 3.12. In total, eight thermal results over four different growth rates are shown in figures in this chapter. The overall thermal test result showing the FSMs and Engineering Demand Parameter (EDP) is shown in Appendix B due to its size. It shows the test numbers, duration for each tests divided into 300, 600, 900 seconds and also 1200 seconds if the test was run for 1200 seconds. The growth rates are fixed until the fire develops to its peak HRR or until the test ends. The target peak HRR, target Total Energy Released (TER), and target average HRR shows what the end value of each FSMs will be at the very end of the experiment. The maximum temperature is the maximum temperature of the beam recorded at the end of each duration within one test (300, 600, 900 seconds and some at 1200 seconds).

4.2.1 Ultra-slow (0.0007) design fires

Figure 4.3 and Figure 4.4 show the temperature profile of the beam at different locations under ultra-slow growth rate fire with a peak HRR of 250 kW and 350 kW over 900 seconds. The graphs show all 21 thermocouples as labelled in Figure 3.12 (all 21 thermocouples from A1 to C7). The rate of increase in the temperature was almost in a linear fashion from 500 seconds until the end of the experiment. It can be seen that the temperature does not change in the first 400 to 500 seconds. This is the time it takes for the fire to heat up the surrounding air around the beam. The ultra-slow growth rate resulted in only flickering flames during the early development stage and this meant the distance from the flame to the beam was greater and thus took longer for the air to heat up to transfer heat to the beam.

There were some common factors throughout the ultra-slow growth rate design fires with different peak HRRs ranging from 250 kW to 650 kW. Firstly, for the thermocouple at the midpoint of the beam, B was the region with highest temperatures. This was expected since the distance from the flames to A and C were further away compared to B. The flame height in the region of A and C was approximately 0.8 m whereas for B it is 1.3 m. This is shown in Figure 4.5, for the fully developed fire in Test 5 (Ultra-slow: 0.0014 kW/s^2, 350 kW).

It was also shown that the maximum temperature of the beam for each test occurred at B5 which is located on the bottom right flange. This was expected and was due to the shadow effect of the beam. A shadow effect is when the steel I-beam, due to its geometrical shape, has a difference in the amount of thermal radiation received in different area of the beam. The end of the flanges have greater exposure to heat compared to the centre of the flange which is

surrounded by both the flanges and the web which has more mass of steel to conduct the heat to reach the area. As the fires were all ultra-slow, it took considerable time for the fire to develop into a size to affect the temperature of the beams. This is shown in the temperature profiles of the tests where the temperature started to noticeably increase only after 500 seconds.

It was expected the temperature profile through the depth of A and C would have a similar growth rate and maximum temperatures for all of the tests as they were both located at 0.5 m away from the centre of the gas burner. However, this was not proven to be the case for all of the tests as there is a clear difference between A and C in both graphs presented in Figure 4.3. Test 1 (Ultra-slow: 0.0007 kW/s^2, 250 kW) only had an average temperature difference of 2 ˚C between thermocouples in A and B after 900 seconds of the test whereas the average temperature in C was almost 50 ˚C below B. The average temperature was obtained by adding the temperature of all seven thermocouples within each section at 900 seconds of the test. This may be due to a number of factors. The biggest reason will be due to the flame shape and its overall symmetry due to air current in the lab as shown in Figure 4.6 and this will be further discussed in Chapter 5.

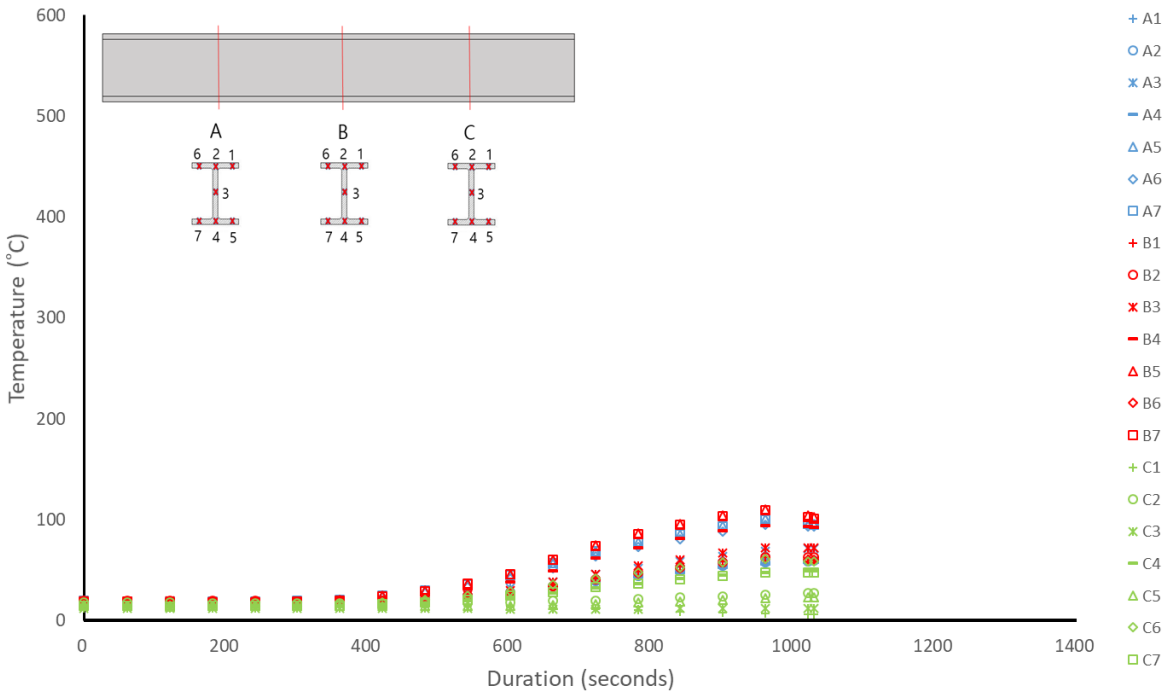

Figure 4.3: Test 1 (Ultra-slow: 0.0007 kW/s^2, 250 kW) thermal results

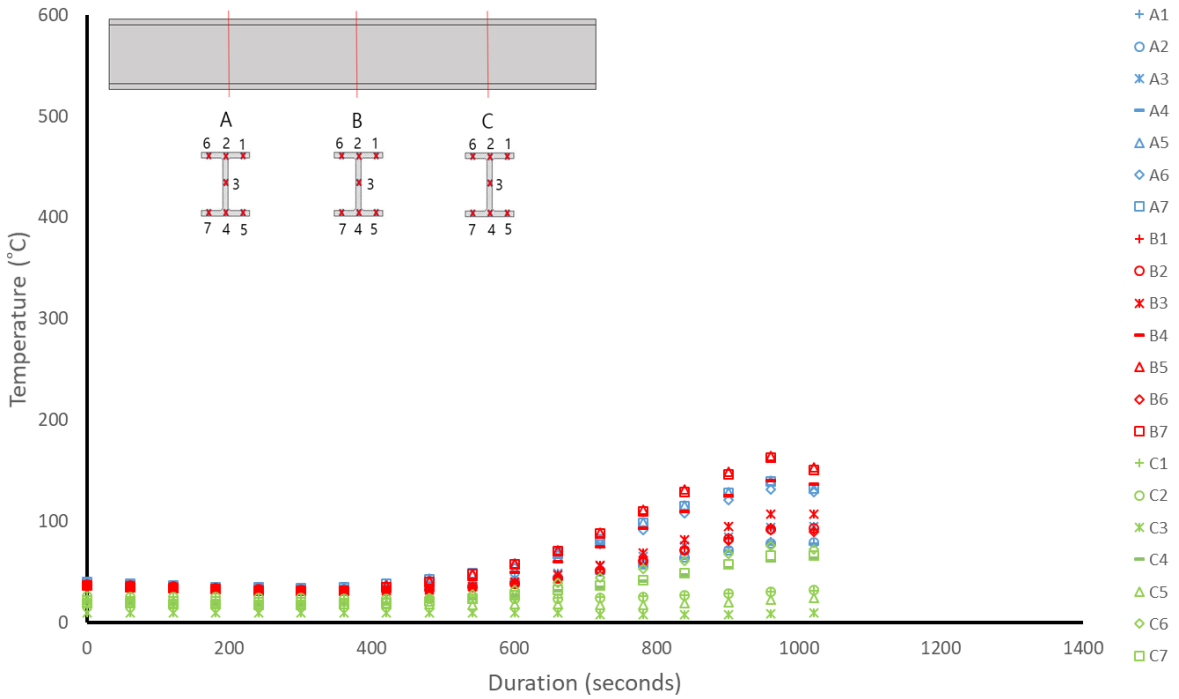

Figure 4.4: Test 2 (Ultra-slow: 0.0007 kW/s², 350 kW) thermal results

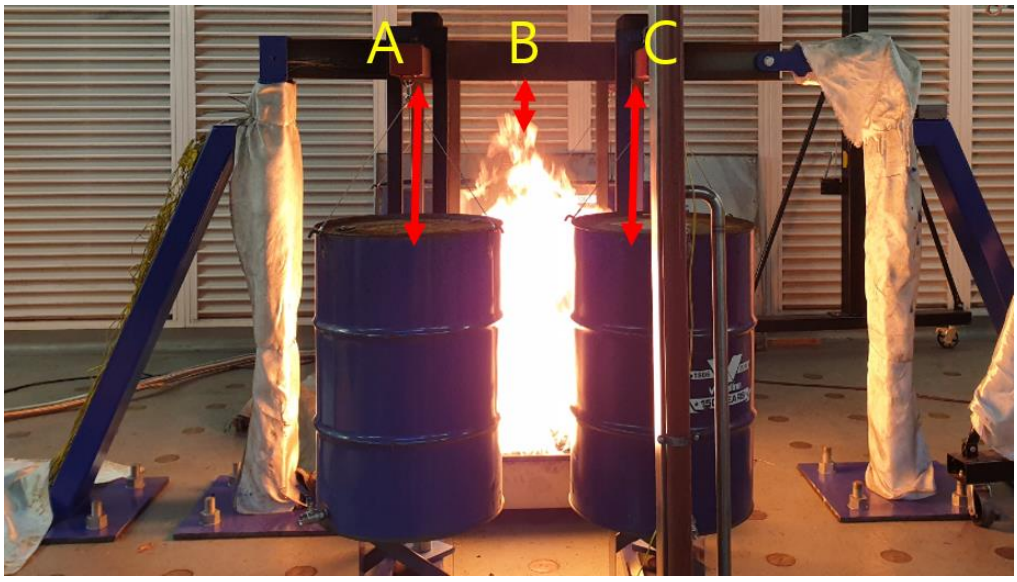

Figure 4.5: Difference in flame height at A, B and C in Test 5 (Ultra-slow: 0.0014 kW/s², 350 kW)

Another possibility is the uneven spread of gas on the gas burner resulting in flames to develop faster in some areas of the gas burner while other areas had a smaller fire and resulted in an uneven flame shape. This affected the C side of the beam more than the A side. This was not a significant issue once the fire was fully developed to reach its peak HRR, as the flames

developed enough to compensate and cover the area the flames had not spread within the gas burner. However, in the earlier stages some of the tests showed very uneven spread across the gas burner to have an impact on the initial thermal growth. The photos of the uneven flame spread in the gas burner in the early stages and at peak HRR of 250 kW stages of Test 1 (Ultra-slow: 0.0237 kW/s^2, 250 kW) are shown in Figure 4.7.

Figure 4.6: Examples of flame leaning towards one side in Test 24 (Medium: 0.0237 kW/s2, 450 kW) (left) and Test 34 (Fast: 0.047 kW/s^2, 650 kW) (right)

Figure 4.7: Flame spread across the gas burner at an initial stage and at 250 kW respectively in Test 1 (Ultra-slow: 0.0237 kW/s^2, 250 kW)

4.2.2 Slow (0.0029) design fires

Similar to ultra-slow fires, the slow growth rate fires showed that B5 had the highest temperature. These were all due to the same reason as stated earlier under ultra-slow fires. The temperature of the beam started to change from approximately 300 seconds after the test started. This was a lot faster compared to ultra-slow fires which took 500 seconds. The reason for this reduction in time was due to the HRR spike of 300 kW for 8 seconds at the beginning of the test to provide sufficient fire to be spread across the gas burner as well as having a higher growth rate.

As shown in Figure 4.8 and 4.9, unlike the Ultra-slow fires, the temperature profile through the depth of section A and C were a lot closer to each other with B being significantly greater than the two. As an example Figure 4.8, Test 12 (Slow: 0.0029 kW/s^2, 450 kW) at the end of the test at 900 seconds, the average temperature of all the thermocouples in A, B and C were 109 ˚C, 272 ˚C and 128 ˚C respectively. This was what was initially expected before the experiments as in an ideal situation, A and C will receive less amount of heat compared to B considering the cone-like shape of the flame.

In general, the fires showed a two phased temperature profile at cross-section B. The first phase showed a steeper increase in temperature and on the second phase the increase in temperature reduced until the end of the test. As an example, for Test 32 (Slow: 0.0029 kW/s^2, 650 kW) in Figure 4.9, the first phase was between 400 seconds to 800 seconds where the temperature increased from 70 ˚C to approximately 420 ˚C. On the second phase, from 800 seconds to the end of the test, the temperature reached approximately 550 ˚C with a temperature increase of only 130 ˚C. In all growth rates where such two phased growth was visible, it was clearly shown that the temperature of the beam increased faster during the first phase of the test compared to the second phase. This trend will be further discussed in Chapter 5.

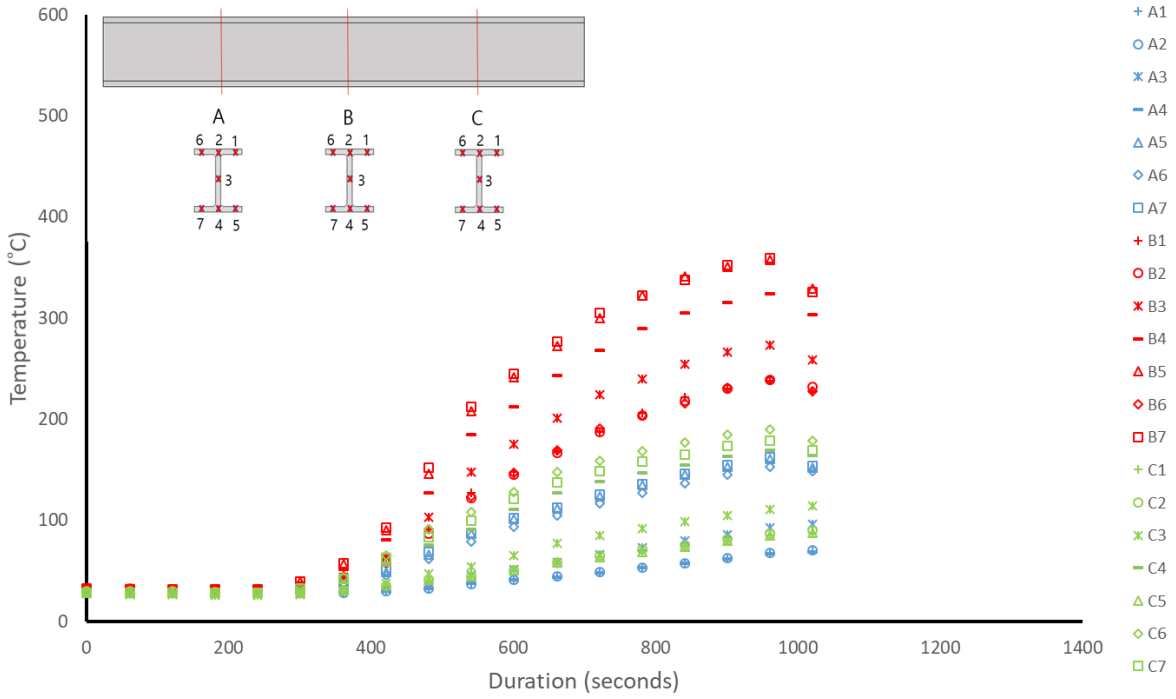

Figure 4.8: Test 12 (Slow: 0.0029 kW/s², 450 kW) thermal results

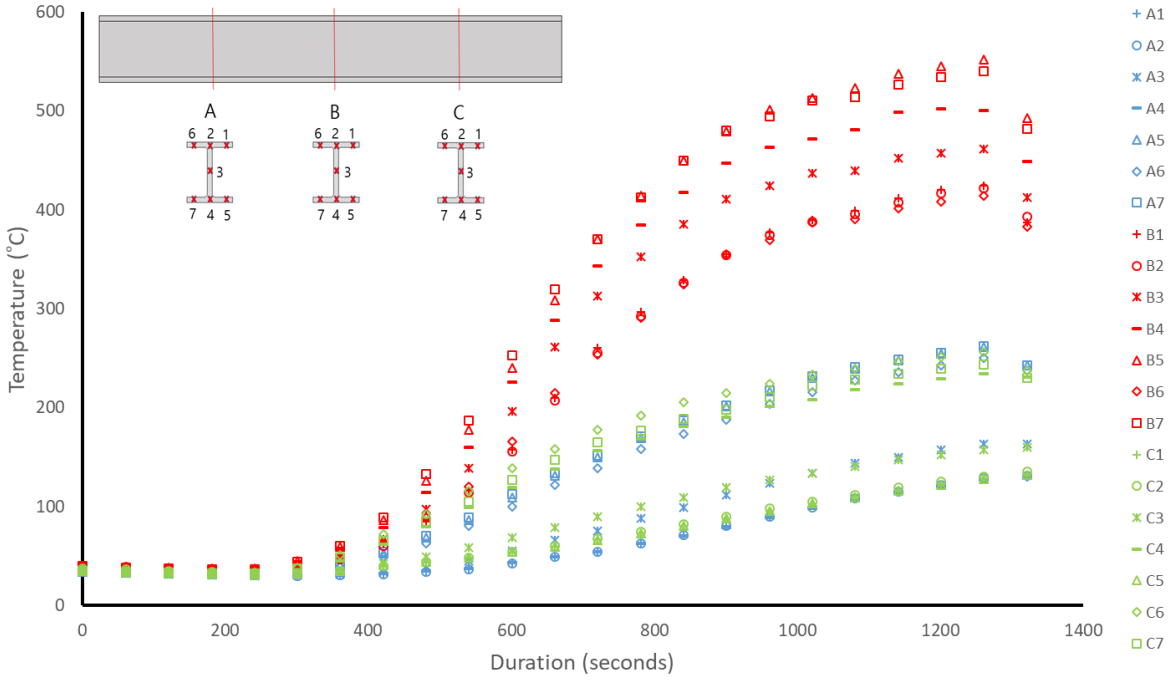

Figure 4.9: Test 32 (Slow: 0.0029 kW/s², 650 kW) thermal results

4.2.3 Medium (0.0012) design fires

Throughout the tests in medium fire, the temperature of C was clearly greater than A which is the opposite of what was observed in Ultra-Slow fires. The reason behind them have been stated in previous fires due to the leaning flame shape as shown in Figure 4.6 due to air current. This may be due to faster development of fire with flames being in closer proximity to the beam leaning towards C, the temperature of B was only slightly higher than C. It meant that A was considerably further away from the flames and resulted in even lower temperature than the tests with smaller fires. This is shown in Figure 4.12 as an example with the flame shape showing clear movement towards C moving away from A.

There were differences in the location of the maximum temperature of the beam. The 250 kW and 350 kW fires gave the maximum temperature at B5 which is the bottom right flange. On the other hand, 450 kW and 650 kW fires had their maximum temperature at B7 which was the bottom left flange. This was also affected by the flame shape and its movement but this was expected since both sides of the flange were equidistant from the gas burner. The flanges were expected to have a similar temperature profile and peak temperature. The shape of the flame shown in Figure 4.13 explains what has happened and why there was a difference in the final temperature between the two flanges in the same section, B5 and B7. The flame is clearly leaning towards B7 in this fire and would have resulted in higher temperature at B7.

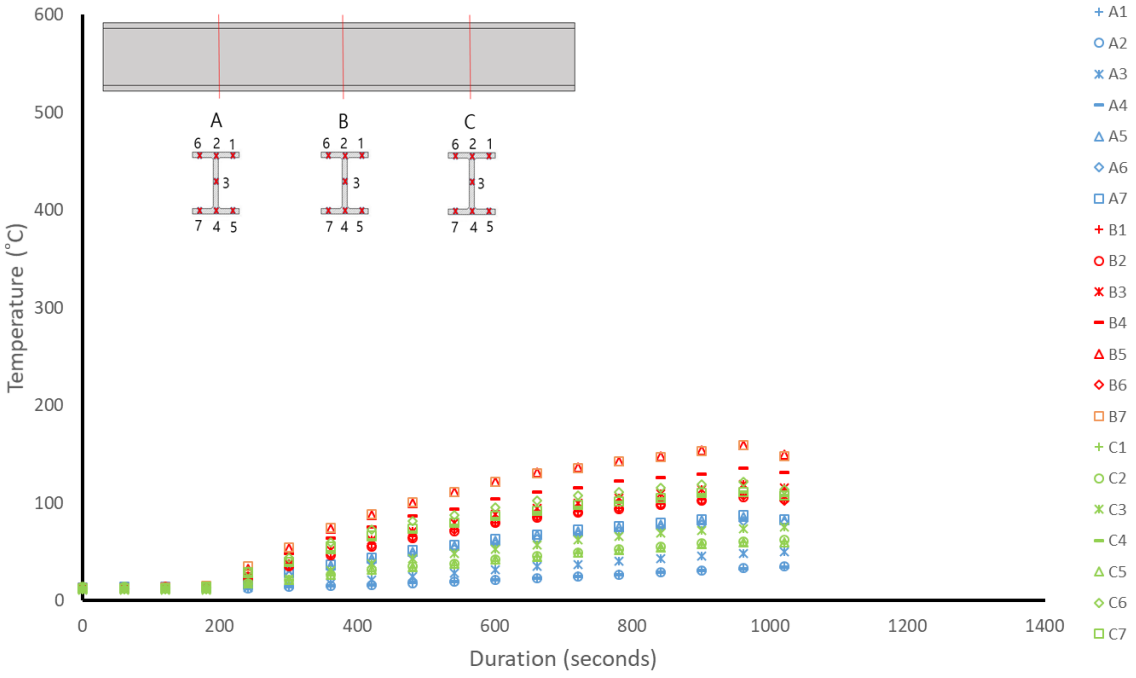

Figure 4.10: Test 19 (Medium: 0.0120 kW/s², 250 kW) thermal results

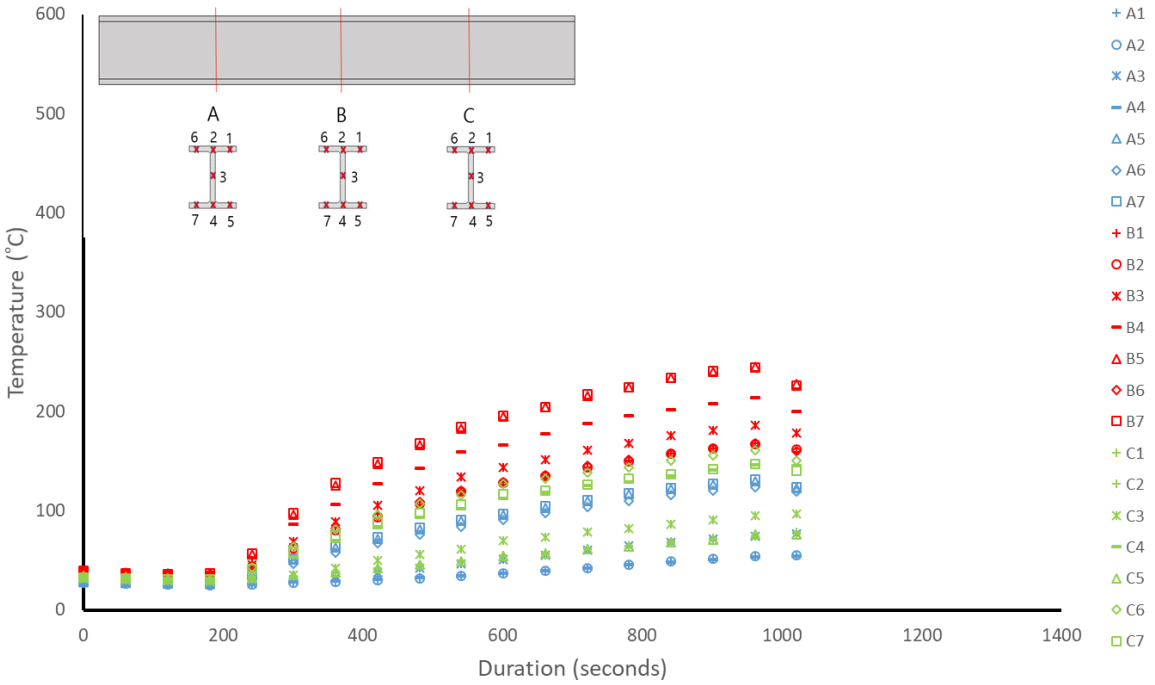

Figure 4.11: Test 20 (Medium: 0.0120 kW/s², 350 kW) thermal results

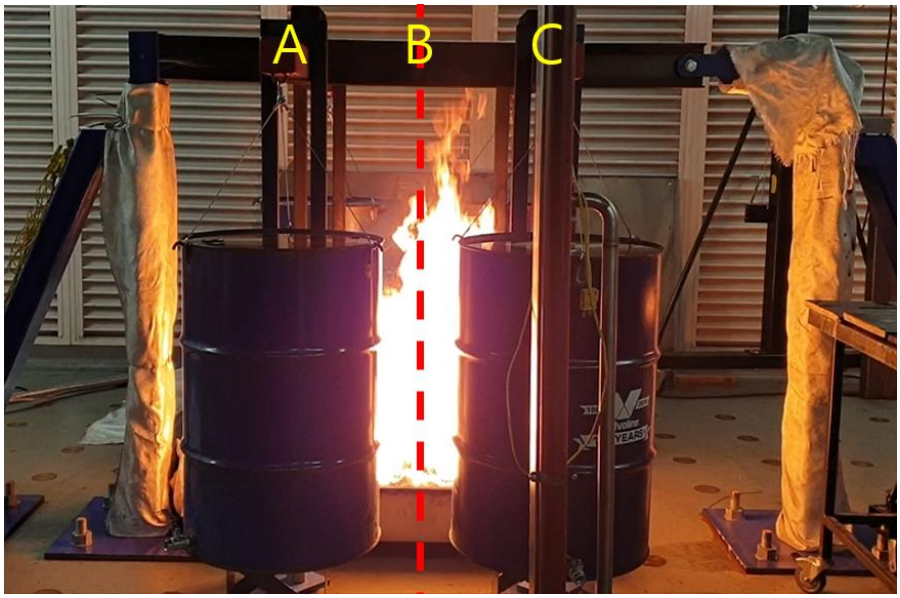

Figure 4.12: Flame shape in between Section B and C, Test 27 (Medium: 0.0353 kW/s², 450 kW)

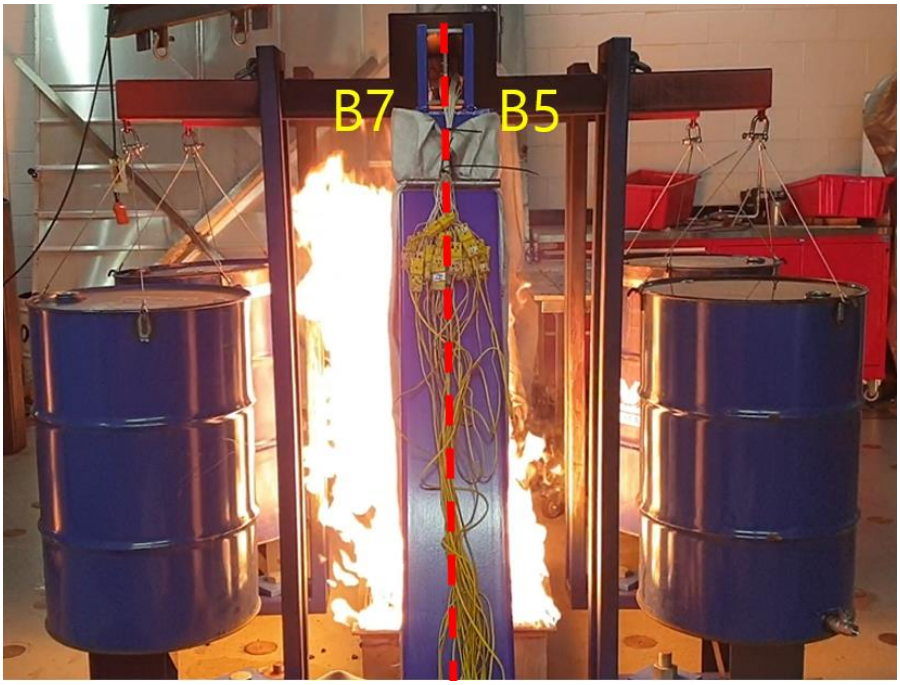

Figure 4.13: Test 27 (Medium: 0.0353 kW/s^2, 450 kW) fire leaning towards B7

4.2.4 Fast (0.047) design fires

For fast fires as shown in Figure 4.14 and 4.15, identical observations were made as the previous growth rate fires with B having the highest temperature in general but with differences seen between A and C. These have been discussed under previous growth rates in relation to the flame shape from air current and uneven spread of flames in the gas burner.

In the 650 kW fire test with 1200 seconds of duration, for the first time, the temperature of the beam dropped 1100 seconds after the test started. This will be from the flame shape changing during the test due to the air current in the lab. The change in the flame shape resulted in reduction in the heat energy to the mid-section of the beam resulting in a small temperature drop.

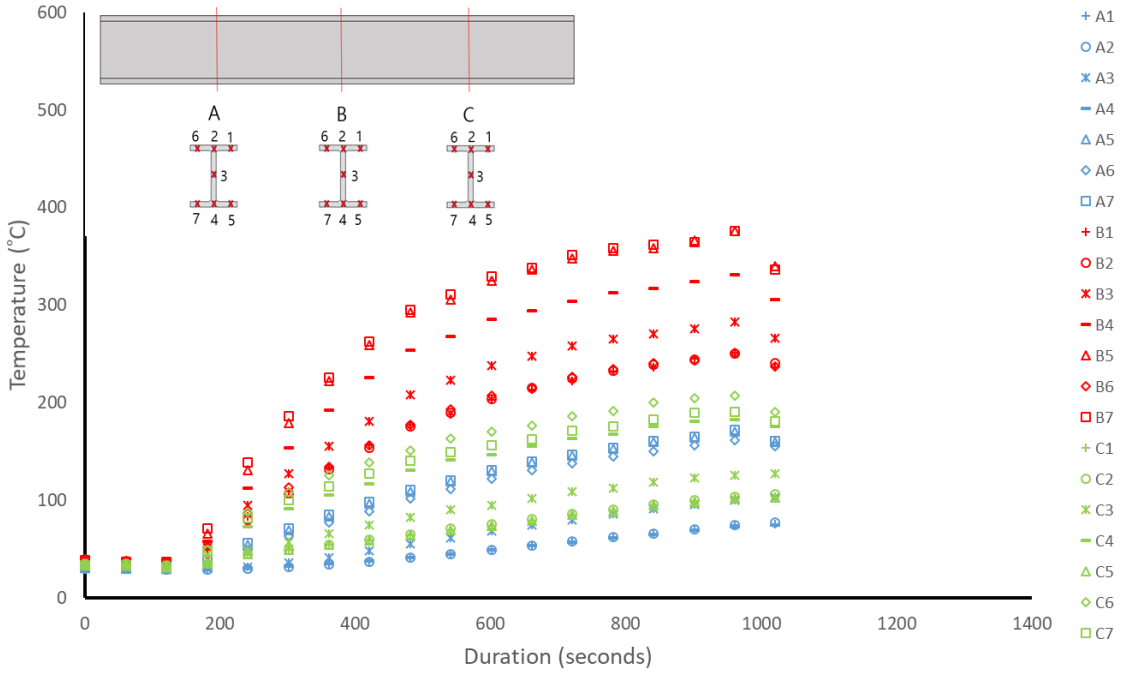

Figure 4.14: Test 30 (Fast: 0.0470 kW/s², 450 kW) thermal results

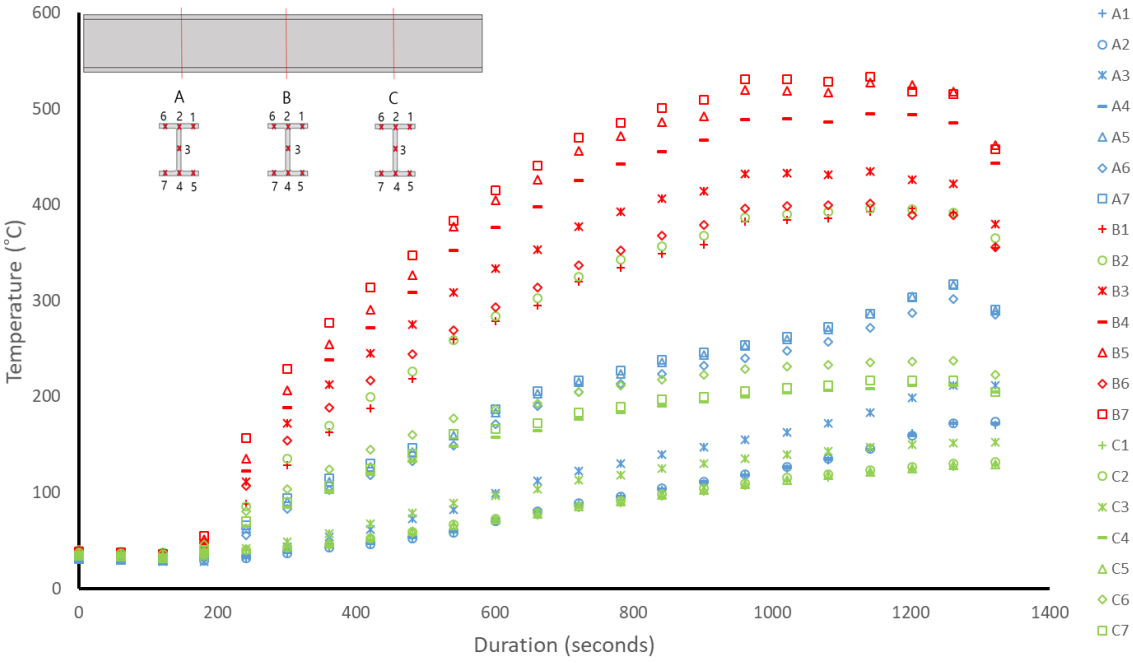

Figure 4.15: Test 34 (Fast: 0.0470 kW/s², 650 kW) thermal results

4.2.5 Thermal test overall result

Overall, the experimental results show significantly less temperature increase than what was expected from the results obtained through carrying out a simple calculation shown in Chapter 3, Experimental Setup, and this will be discussed in more detail in Chapter 5. One of the reasons for that is due to the gas burner not igniting or spreading out evenly across the gas burner as soon as the design fire started. After ignition of the fire, it had to be over approximately 30 kW to have a fire that was evenly spread throughout the gas burner. Until then, it was only a small flickering fire on the edges of the gas burner which would not have impacted the beam 1.5 m above. The time it took for different design fires to reach 30 kW dependent on the growth rate of each of the design fires and this was a factor that may have affected the fires with slower growth rates even more. A decision was made to reduce this issue by providing a HRR spike for 8 seconds with 300 kW at the very beginning of the test to spread the gas evenly throughout the gas burner from Test 9 (Ultra-slow, 450 kW). After the HRR spike, the flames developed across the surface more evenly when HRR dropped back to 30 kW. This made a clear difference and enabled the flames to develop from the beginning of the test.

As shown in a number of results, there was a temperature difference between sections A and C. This was due to the asymmetry of the flames. This was as a result of air current changes in the lab. It is an environmental factor that cannot be controlled in fire and the photos from the test and the test results show the varying flame shape and the final temperature of the beam. It was seen throughout the tests as the maximum temperature in Section B was alternating between B5 and B7 which were the two bottom left and right flanges.

It is important to note that a test was started when the temperature of the beam dropped down to 40 ˚C and not to ambient temperature. This was done as a result of time constraints in the lab. The time required for the beam to cool down from 40 ˚C to 25 ˚C was estimated to be over 500 seconds and significantly longer for it to reach 20 ˚C from simple calculation (see Figure 4.16). It was decided that it will not affect the overall results significantly by starting the test at 40 ˚C considering the time required to wait for the beam to reach ambient temperature.

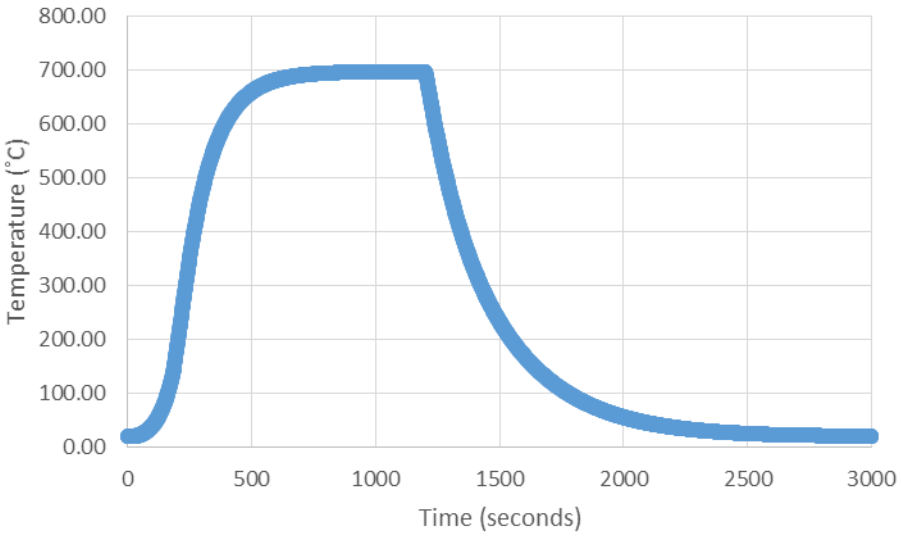

Figure 4.16: Example temperature profile of a beam to show its cool down

Lastly, the maximum temperature reached during the entire thermal test was 552 ˚C at B7. This was for a slow (0.0029 kW/s^2) growth rate fire with peak HRR of 650 kW. The maximum temperature of all the tests was expected to occur with the fast (0.047 kW/s^2) fire with peak HRR of 650 kW. This was supposed to be 735 ˚C from simple calculations. This is a good example of how fire is unpredictable as there are a countless number of variables and factors that may affect the results. This result may be due to a number of reasons. It may be due to the ambient temperature of the surroundings, the air flow and wind flow within the laboratory and also the uncertainty within the gas burner and human factors involved. This will be discussed in Chapter 5.

4.3 Structural Results

The procedure described in Chapter 3 was followed and in total 34 structural tests were carried out, yielding 102 results. Load cell readings of the beams axial force results are graphed below. The results for each of the growth rate fires are collated into one graph. The deflections were recorded at the end of each test using a digital laser measure. The deflection measurements are provided on the top left of Figure 4.17 to Figure 4.20. All of the structural results are shown after Section 4.3.4.

4.3.1 Ultra-slow (0.0007) design fires

From the tests of ultra-slow fire with a peak HRR of 250 kW, 350 kW, 450 kW and 650 kW, it showed that as the peak HRR increased, the growth rate of the axial force became non-linear

and carried on increasing until the end of the test at 900 seconds or 1200 seconds. For 250 kW and 350 kW fire, the increase of the axial force was close to linear, whereas for 450 kW and 650 kW fire, the axial force carried on increasing until or near the end of the test. The reduction of the axial force shown in all of the tests are what is recorded after the gas burner has turned off which shows 60 seconds after the experiment has finished.

4.3.2 Slow (0.0029) design fires

The 650 kW fire showed the steepest growth rate in axial force out of all of the slow fires with the maximum axial force of 20.56 kN at 1200 seconds. The other tests with smaller peak HRRs showed highest increase of axial force at the beginning and decayed until the end of the test but for 650 kW, the maximum axial force was in the middle phase of the growth from 500 seconds to 800 seconds.

4.3.3 Medium (0.0012) design fires

The maximum axial force in medium fire was 17.54 kN in the 650 kW fire. It showed that the 650 kW fire's axial force plateaued and started to decrease at 1100 seconds before the fire stopped at 1200 seconds. This was due to the interaction between thermal expansion of the beam from temperature increase, curvature of the beam from bending from temperature gradient and the point loads acting on the beam. This was an overall trend that was observed in structural tests with slow, medium and fast growth rate fires although the medium fire was the only one with a decrease in axial force during the experiment. This is further discussed in detail in Chapter 5.

4.3.4 Fast (0.047) design fires

The maximum axial force exerted in the fast fire with peak HRR of 650 kW was 16.58 kN at 1200 seconds. The axial force of the beam started to increase from around 150 seconds of the test which was clearly faster than the other growth rates. The maximum axial force in the 650 kW fire was the smallest out of all the 650 kW fires and this shows a clear trend in larger fires resulting in lower axial force as well as plateau of axial force. This is due to curvature of the beam due to temperature increase of the beam and this is explained further in Chapter 5.

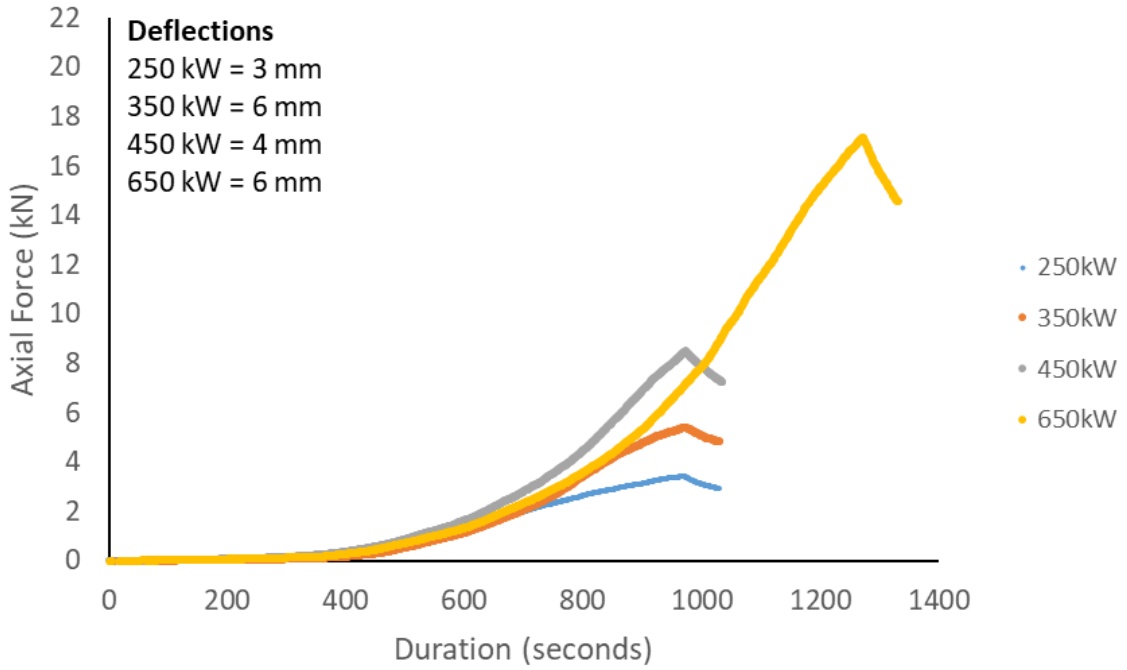

Figure 4.17: Axial load of Ultra slow fire with varying peak HRR

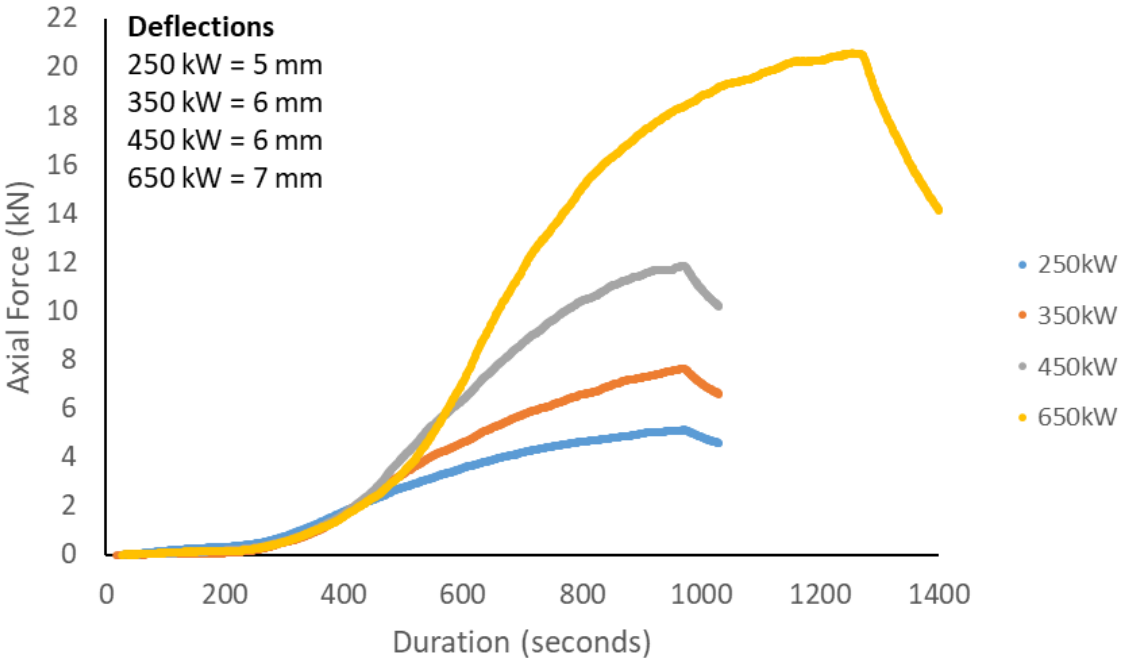

Figure 4.18: Axial load of Slow fire with varying peak HRR

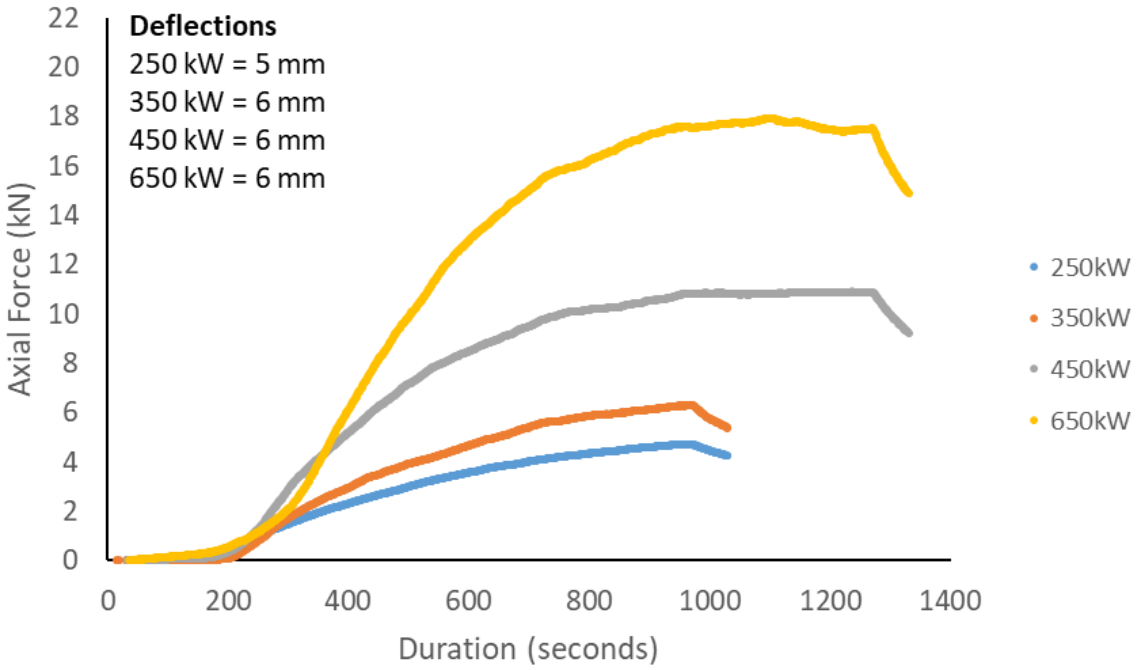

Figure 4.19: Axial load of Medium fire with varying peak HRR

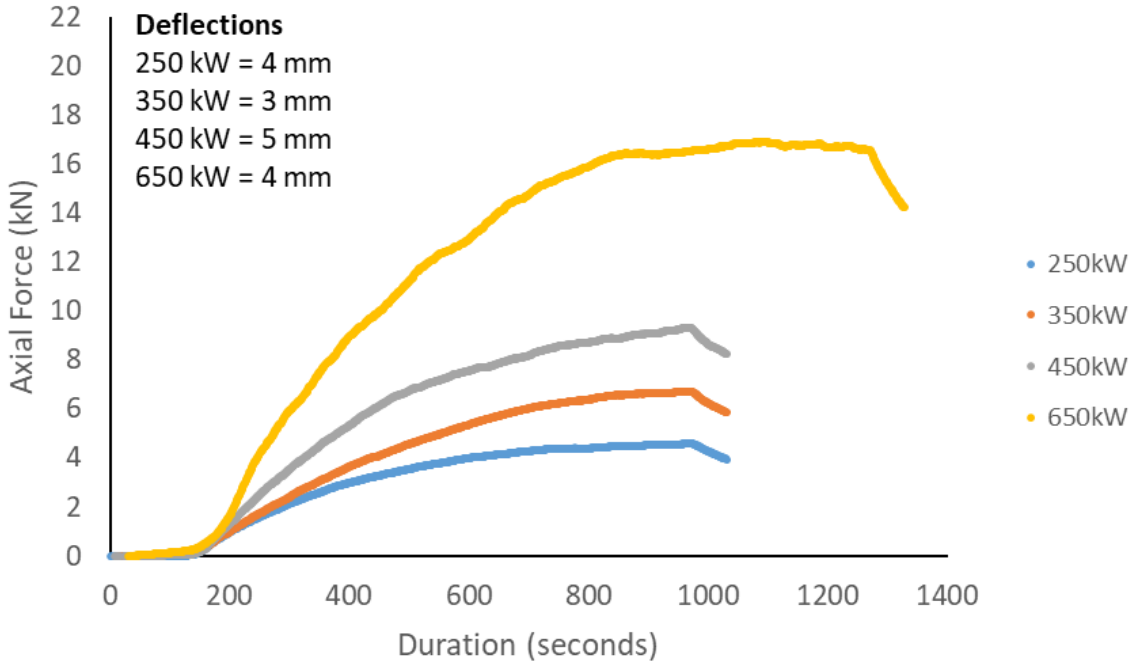

Figure 4.20: Axial load of Fast fire with varying peak HRR

4.3.5 Structural test overall result

In general, the structural results showed some clear trends throughout the tests. The maximum axial force of 20.56 kN obtained from the entire test was from a slow growth rate fire with peak HRR of 650 kW. Most of the axial force growth profiles followed a similar pattern where it had the greatest growth rate at the beginning when the axial force started to increase and the rate started to decrease until the test ended. Another characteristic was for high peak HRR fires, the axial force started to plateau and the axial force no longer increased after it reached a certain point. As stated before, the reason for having these results are due to combination of thermal expansion, curvature from temperature growth in the beam and the load applied on the beam.

The axial force due to thermal expansion is significantly lower than the theoretical axial force using simple calculation. There are many reasons that may have caused this. The beam had to be replaced once each test was completed and for every replacement, one frame had to be unbolted from the strong floor and once the new beam was placed, the frame was bolted back firmly to the strong floor. Due to this, the load cell had a different reading at the beginning of the test. The frame had to be screwed to ensure the load cell was reading between -1 kN to +1 kN before the test was started. This may have resulted from having maximum possible difference of 2 kN of axial force where one test starts from -1 kN and the other starts from +1 kN.

4.4 Conclusion

Chapter 4 has provided an overview of what results were obtained through thermal and structural experiments. In total, 68 tests were carried out to obtain over 200 sets of data. Due to excessive amount of data from the experimental results, only ultra-slow (0.0007 kW/s^2), slow (0.0029 kW/s^2), medium (0.012 kW/s^2) and fast (0.047 kW/s^2) growth rate fires in different peak HRRs (250 kW, 350 kW, 450 kW and 650 kW) are presented in this chapter. There were clear trends observed during the tests and also a number of limitations and improvements identified. One of the trends observed was the two phased growth rate of temperature of beams in thermal tests. It had two phases with the rate being greater in the first phase. One of the observations made in structural test was the plateau of axial force in the latter stages of the test for high peak HRR fires. Another observation was the uncontrollable air current in the lab that resulted in a flame shape leaning on to one side of the beam rather than keeping an ideal cone-like shape. There were also some ad-hoc changes that had to be made as the experiment was carried out to provide more valuable data for the study. An example of this would be extending fire duration to 1200 seconds. The trends in the results, comparison of theoretical numbers and real test results, unexpected results or behaviour during the test and future improvements identified are further discussed in the subsequent chapters.

In summary, the thermal test was done to find the temperature profile and the maximum temperature of the steel beam for each of the design fires. The structural test was done to find the growth of axial force due to thermal expansion under different design fires. A wide spectrum of thermal and structural results was obtained. The maximum temperature of the beam ranged from 19.5 ˚C to 552 ˚C. The maximum axial force of the beam ranged from 0.06 kN to 20.56 kN. These data have been analysed to find the best relationship between FSM and EDP in Chapter 5. All of the thermal and structural test results are shown in Appendix C and Appendix D.

5. ANALYSIS AND DISCUSSION

This chapter uses different analytical methods and the experimental data obtained from Chapter 4 to determine the most efficient Fire Severity Measure (FSM) using Cloud Analysis (CA) to investigate the relationship between the fire hazard and structural response. It uses each of the FSMs (duration, growth rate, peak HRR, Total Energy Released and average HRR) against the Engineering Demand Parameters (EDP) that were recorded during the experiments, which are maximum beam temperature and the axial force of the beam. Furthermore, the chapter compares predictions of simple calculations, experimental results and the observations made during experiments.

5.1 Introduction

One of the aims of the study was to provide real experimental data that could be used for a probabilistic study. No experiment has been specifically setup to provide this information for Probabilistic Structure Fire Engineering (PSFE) until now due to a number of reasons. This includes reasons such as excessive cost and resources required in order to produce multiple number of experiments to obtain data. The results of a loaded I-beam heated to a number of pre-flashover fires has been presented in Chapter 4. As experimental data has been obtained through a multiple number of tests, they are analysed to find the best relationship between fire and structural response. Past studies on PSFE have developed analytical methods, and Chapter 2 has identified what methods could be used on the obtained data.

Each of the analytical methods has advantages and disadvantages, in terms of computational effort and their level of accuracy. In this study, the CA method developed by the Pacific Earthquake Engineering Research (PEER) Centre (Jayaler, 2003) was used to analyse the data to find relationship, between FSMs and EDPs. CA is done by plotting all of the data that has been obtained using one fire severity measure against the chosen structural response. This is then analysed through linear regression and the correlation is expressed in terms of the R^2 value. R^2 value of 1 shows that the regression prediction perfectly fits the data, meaning that the FSM-EDP has a perfect correlation. A perfect correlation will mean that once a value of FSM is chosen, the corresponding EDP response will be able to be obtained. An R^2 value of 0 means that the regression cannot explain the relationship meaning that the FSM-EDP has no correlation and the FSM does not explain the structural response at all. Hence for CA, a FSM that achieves the highest R^2 value will be the FSM that best describes the corresponding EDP as higher R^2 will be able to predict the expected structural response more accurately. CA is used over other analytical methods as it does not require scaling of the data, and it helps visualise results

quickly. All other analytical methods require scaling whereas CA uses the raw data itself. The CA approach assumes a linear relationship between the lognormal EDP and lognormal FSM as shown in the equation below.

$$\ln(\text{FSM}) = a + b\ ln(EDP) \qquad \text{Equation (4)}$$

where a and b are regression coefficients that can be obtained through a linear least squares regression technique. The relationship expressed as Equation 4 is investigated for each FSM-EDP plot with the R^2 value to show the correlation between FSM and EDP.

The data points in the negative region for the analysis shown in Figure 5.1 to 5.10 represent the data points with a true value of less than 1. This is for both ln(FSM) axis and ln(EDP) axis.

5.2 Thermal Tests

5.2.1 Thermal test Duration-Maximum Temperature

Figure 5.1 is linear regression plot of the FSM-EDP relationship. The FSM is duration and the EDP is the maximum temperature of the beam. The lowest duration and temperature were 300 seconds and 20.5 ˚C. The longest duration was 1200 seconds and the highest temperature was 540 ˚C. There are no clear trends in the plot. The R^2 value is 0.4713 which shows the relationship between the two variables is not strong. It is clear that the plot for each fire severity level is very widely spread out across the maximum temperature range.

5.2.2 Thermal test Growth Rate-Maximum Temperature

Figure 5.2 shows the CA of growth rate and maximum temperature of the beam. The slowest growth rate was 0.0007 kW/s^2 and the fastest growth rate was 0.047 kW/s^2. The growth rate was separated into ten different levels, covering ultra-slow to fast growth rate. Again, there are no clear trends in the plot. The R^2 value is 0.2026 which is the lowest value out of all the FSMs in the thermal test.

5.2.3 Thermal test Peak HRR-Maximum Temperature

Figure 5.3 shows the CA of peak HRR and the maximum temperature of the beam. The lowest peak HRR was 63 kW and the highest peak HRR was 650 kW. The peak HRR produced a range of flames that were below the beam to flames that engulfed the heated 1 m length of the beam. Compared to the last two FSMs, there is a clear trend in the plot and also few outliers. The R^2 value is 0.7554 which shows that the peak HRR has a stronger relationship with the maximum temperature compared to the previous two FSMs (duration and growth rate).

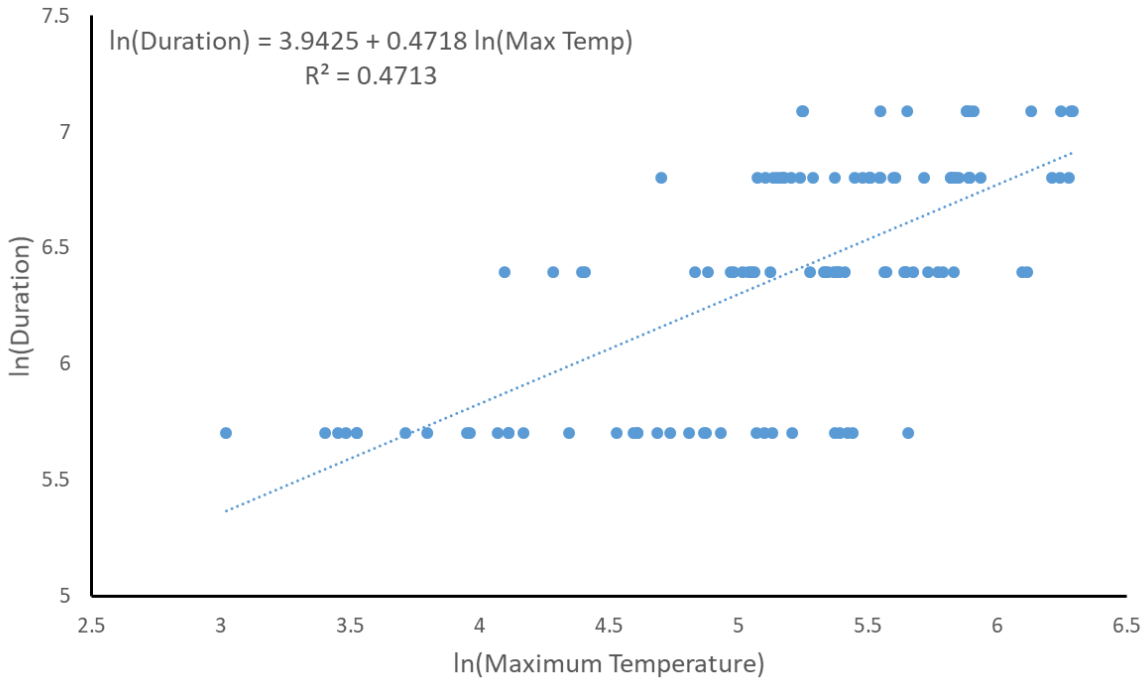

Figure 5.1: Cloud analysis of duration and maximum temperature

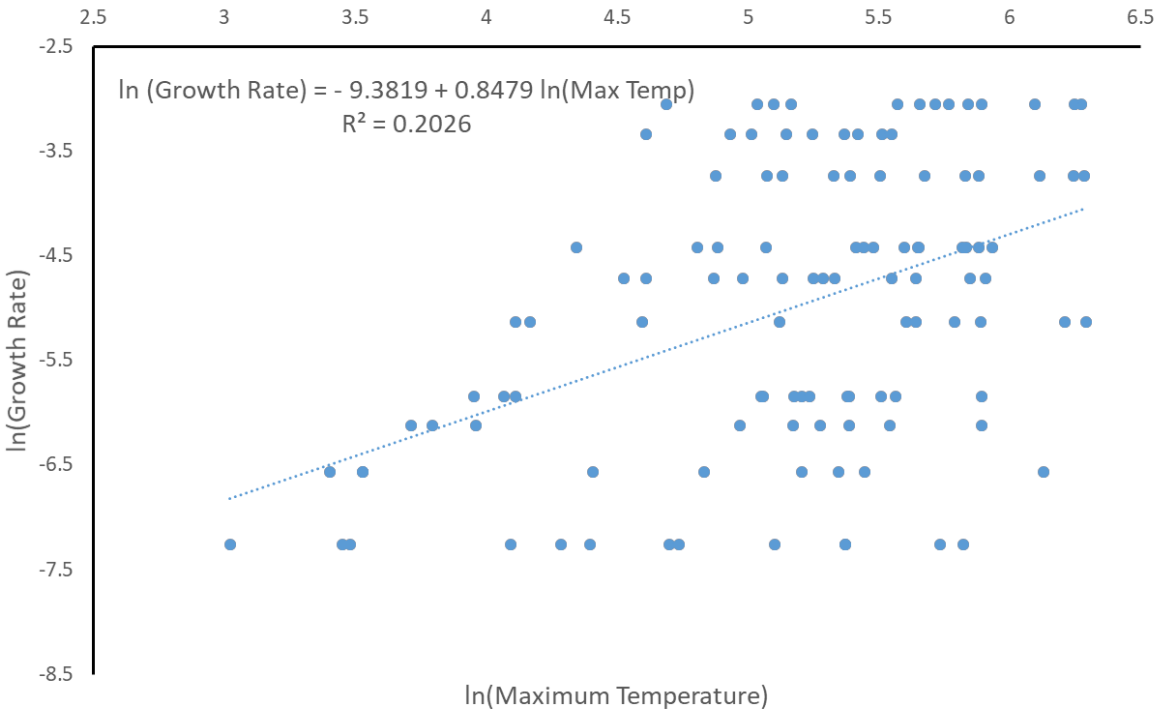

Figure 5.2: Cloud analysis of growth rate and maximum temperature

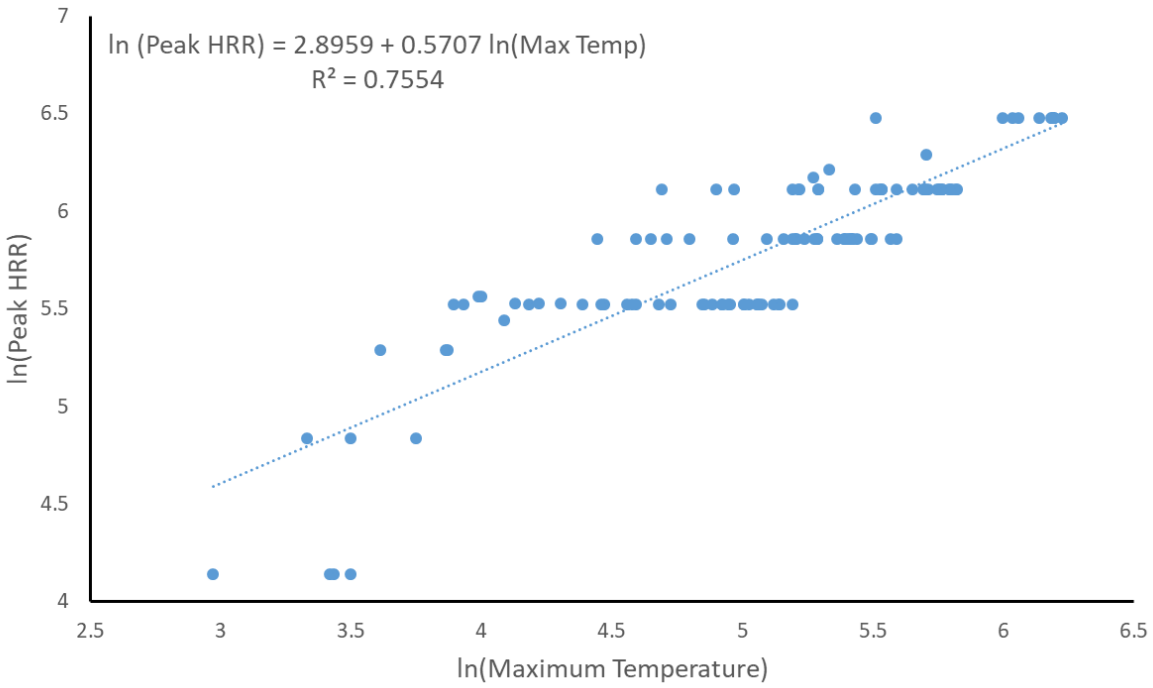

Figure 5.3: Cloud analysis of peak HRR and maximum temperature

5.2.4 Thermal test Total Energy Released-Maximum Temperature

Figure 5.4 shows the Cloud Analysis of Total Energy Released (TER) and the maximum temperature of the beam. The lowest TER was 6.3 MJ and the highest TER was 711 MJ. There exists a clear trend for this FSM-EDP graph. As the TER increases, the maximum temperature increases as well. The data tends to be stronger with lower TER and as TER increases, the results spread out more. The spread in the higher region is visible with the highest TER not producing the maximum beam temperature. The highest temperature of 540 ˚C resulted from a fire with TER of 526 MJ and not 711 MJ. This is due to the flame fluctuation and uneven flame shape resulting in the flame leaning towards one side away from section B. However, it still shows a high R^2 value of 0.8908 showing that there is a strong relationship between the two variables. TER had the strongest correlation with the EDP: Maximum beam temperature, out of all the FSMs in the thermal test.

5.2.5 Thermal test Average HRR-Maximum Temperature

Figure 5.5 shows the Cloud Analysis of average HRR and the maximum temperature of the beam. The lowest average HRR was 20.9 kW and the highest average HRR was 592.6 kW. There exists a clear trend in this FSM-EDP plot as most of the data points are around or well near the R^2 regression line. As the average HRR increases, the maximum temperature increases as well.

The relationship is similar to TER, but with less dispersion throughout the graph. The relationship tends to get weaker as the average HRR increases but this may be due to not having as many data points in the higher average HRR levels. The R^2 value is 0.8785 which is the second highest after the TER.

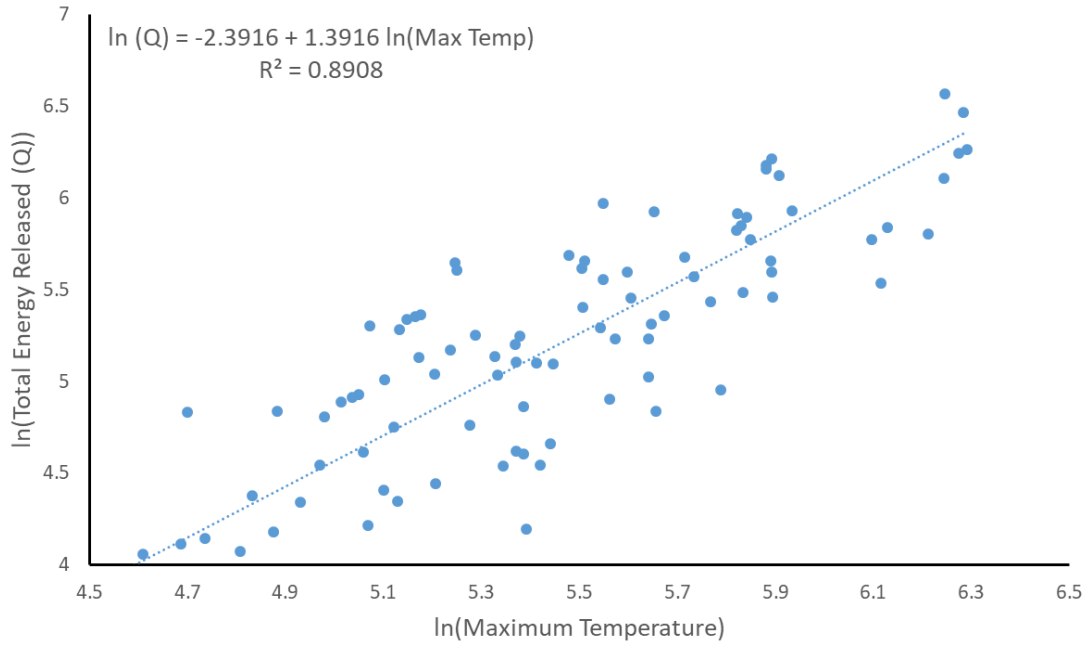

Figure 5.4: Cloud analysis of TER and maximum temperature

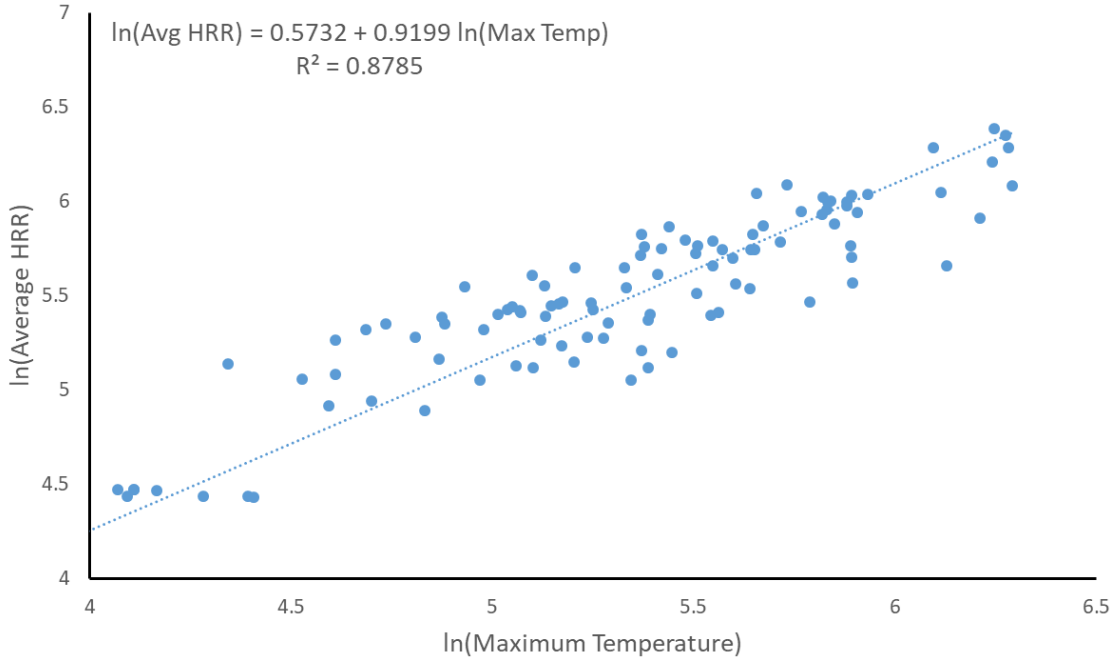

Figure 5.5: Cloud analysis of average HRR and maximum temperature

5.3 Structural Tests

5.3.1 Structural test Duration-Axial Force

Figure 5.6 shows the Cloud Analysis for the duration of the test against the axial force of the beam. The duration ranges from 300 seconds to 1200 seconds and the graph shows the result tends to spread wider as the duration increases. It is also important to note that 1200 seconds duration had the least number of results compared to 300, 600 and 900 seconds. The R^2 value is 0.4650 which shows that the relationship between the two variables is not strong.

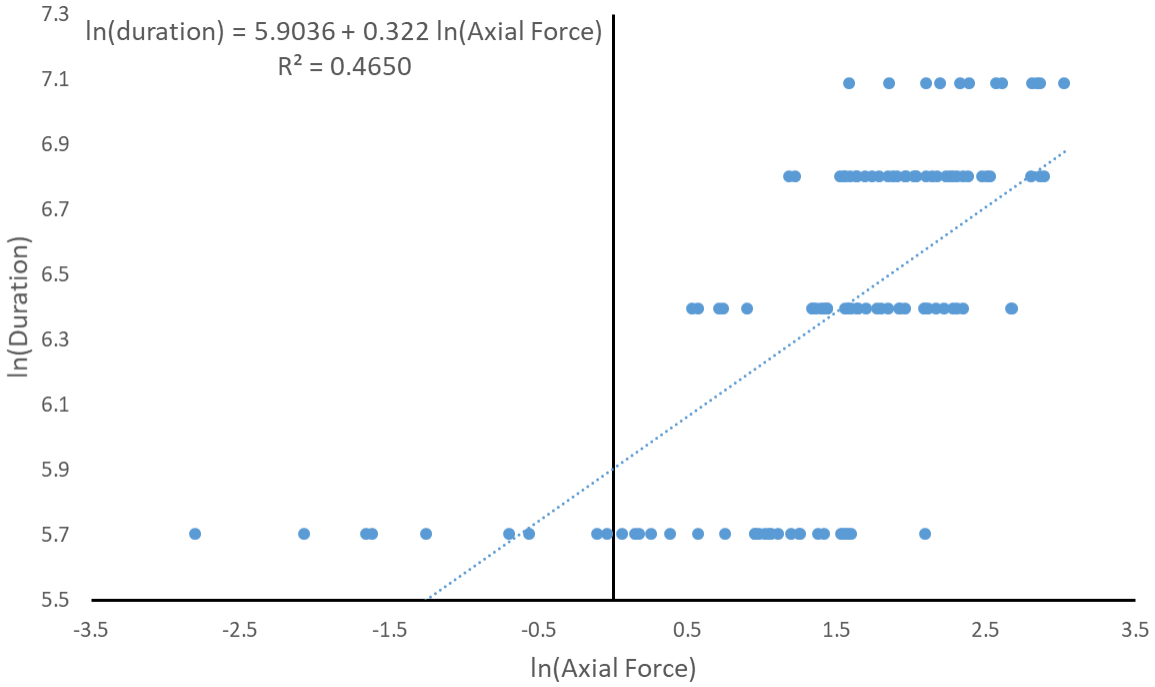

Figure 5.6: Cloud analysis of duration and axial force

5.3.2 Structural test Growth Rate-Axial Force

Figure 5.7 shows the Cloud Analysis of growth rate and axial force of the beam. There were ten growth rates from ultra-slow to fast growth rates. The R^2 value is 0.1872 and as the value shows, there is almost no correlation between the two variables as the results are simply spread all across the graph. As in the thermal test, the growth rate was the FSM that had the weakest relationship with the axial force.

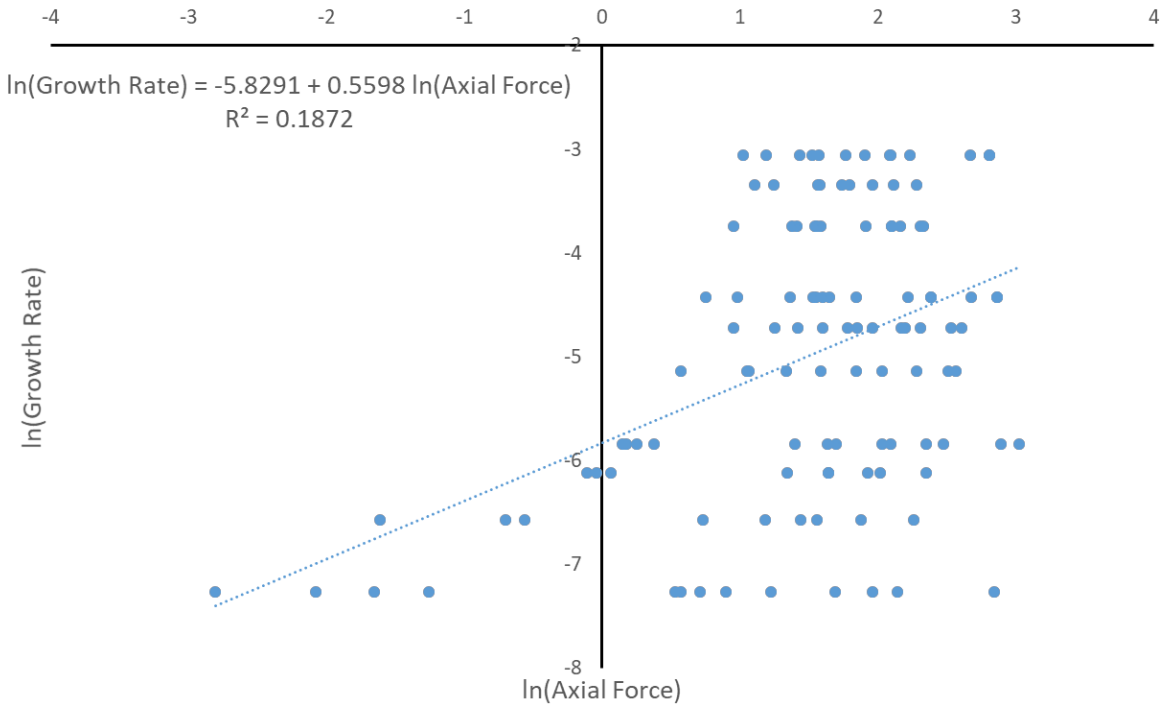

Figure 5.7: Cloud analysis of growth rate and axial force

5.3.3 Structural test Peak HRR- Axial Force

Figure 5.8 shows the Cloud Analysis of peak HRR and the axial force of the beam. The peak HRR ranged from 63 kW to 650 kW. The structural test shows a similar trend as the thermal test where there exists a clear relationship between the two variables with a few outliers. The R^2 value is 0.8167 which shows that the peak HRR has a clear correlation with the axial force. The data points in general are more spread out in the negative ln(axial force) region and get closer as peak HRR and axial force increase.

5.3.4 Structural test Total Energy Released- Axial Force

Figure 5.9 shows the Cloud Analysis of TER and the axial force of the beam. The TER ranged between 6.3 MJ and 711 MJ. The results of the structural test shows an obvious relationship between the two variables with a clear trend. It scatters around the trend line in a band-like fashion. The R^2 value is 0.8959 which was the highest R^2 value out of all of FSMs in the structural test. This was identical to the thermal test.

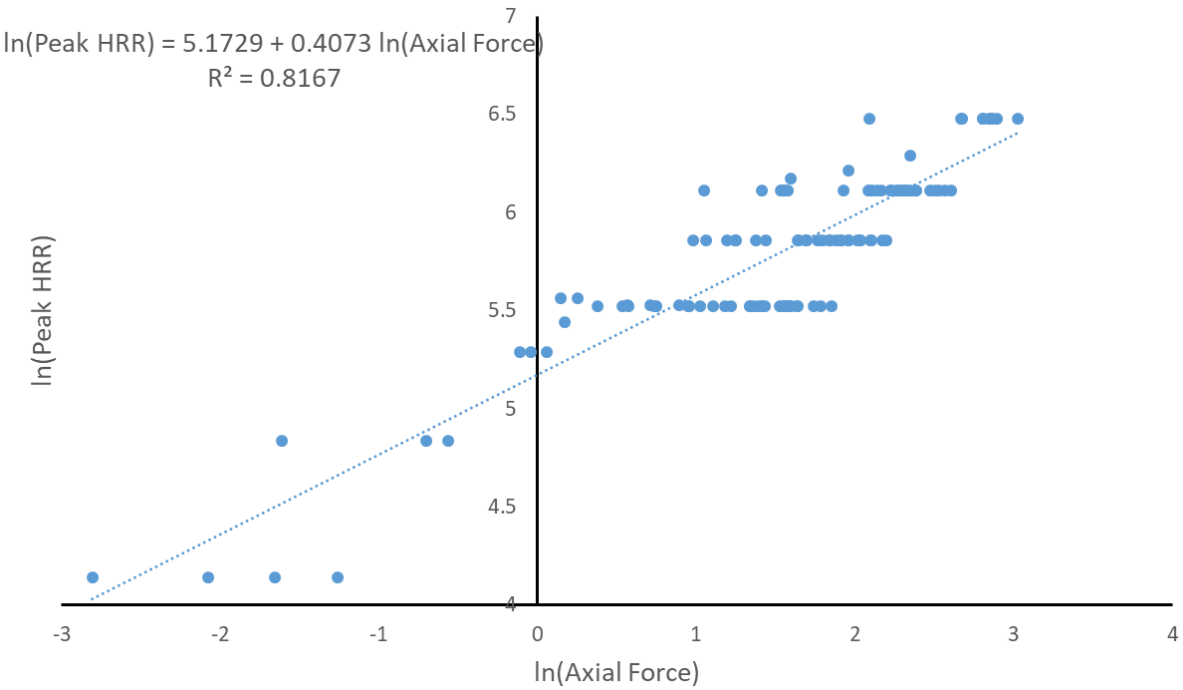

Figure 5.8: Cloud analysis of peak HRR and axial force

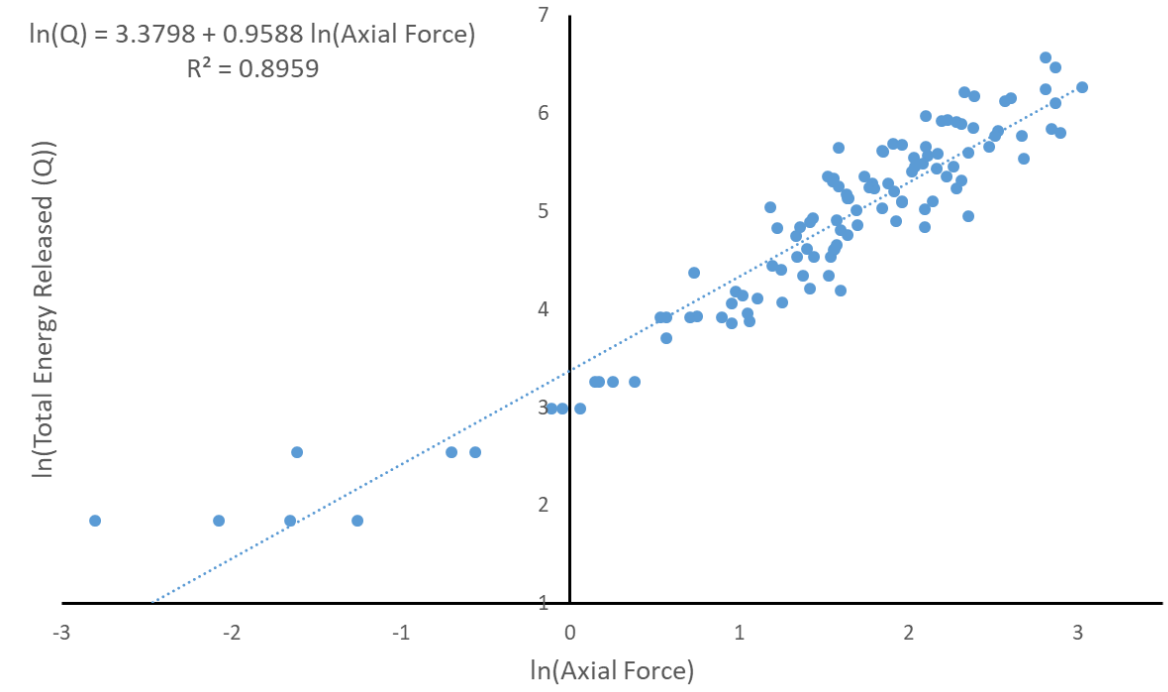

Figure 5.9: Cloud analysis of TER and axial force

5.3.5 Structural test Average HRR- Axial Force

Figure 5.10 shows the Cloud Analysis of average HRR and the axial force of the beam. The average HRR was between 20.9 kW to 592.6 kW. There exists a clear trend. The majority of the data points are between axial forces of 2 kN to 10 kN. The relationship is similar to TER, but with more dispersion. The R^2 value is 0.8922 which was slightly lower than the R^2 value of TER-axial force.

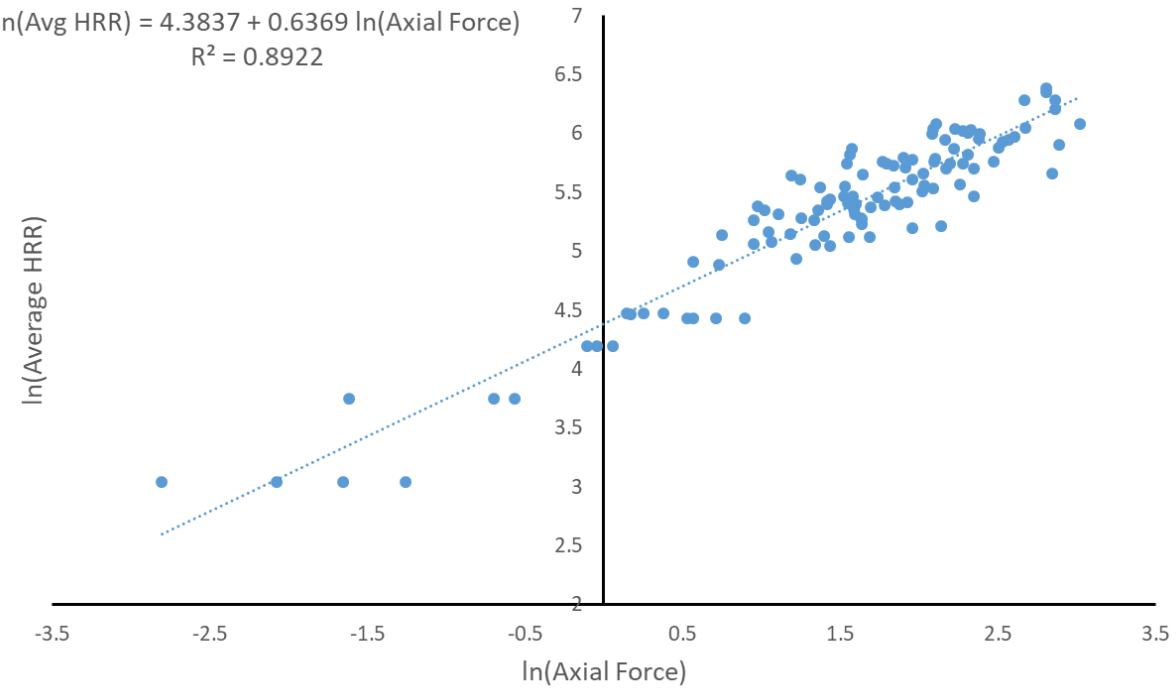

Figure 5.10: Cloud analysis of average HRR and axial force

5.4 Summary of CA

102 data points were obtained for each thermal and structural experiments and used for analysis. As stated before, the possible FSMs analysed were duration, growth rate, peak HRR, TER and average HRR. The EDPs were axial force and maximum temperature of the beam

Cloud Analysis uses linear regression to analyse all of the data and this means that the R^2 value shows the correlation of the FSM and EDP. The closer the R^2 is to 1, the stronger the relationship between the two variables. TER was the FSM with the highest R^2 for both thermal and structural tests as shown in Figure 5.11. The growth rate had the weakest correlation with the thermal and structural EDPs (maximum beam temperature and maximum axial force of the beam). Both

peak HRR and average HRR also showed a high correlation with the EDPs and may be valuable for further investigation.

It was shown that the R^2 was quite similar for thermal and structural results for each of the FSMs which is to be expected since the temperature of the beam is related to the axial force of the beam due to restrained thermal expansion.

In general, the thermal and structural test showed very similar trends. It is very clear to see that there exists a relationship between fire properties and their corresponding structural response. In total, five FSMs and two EDPs were investigated in this study. This demonstrates the potential of PSFE and suggests further studies are necessary to continue this development.

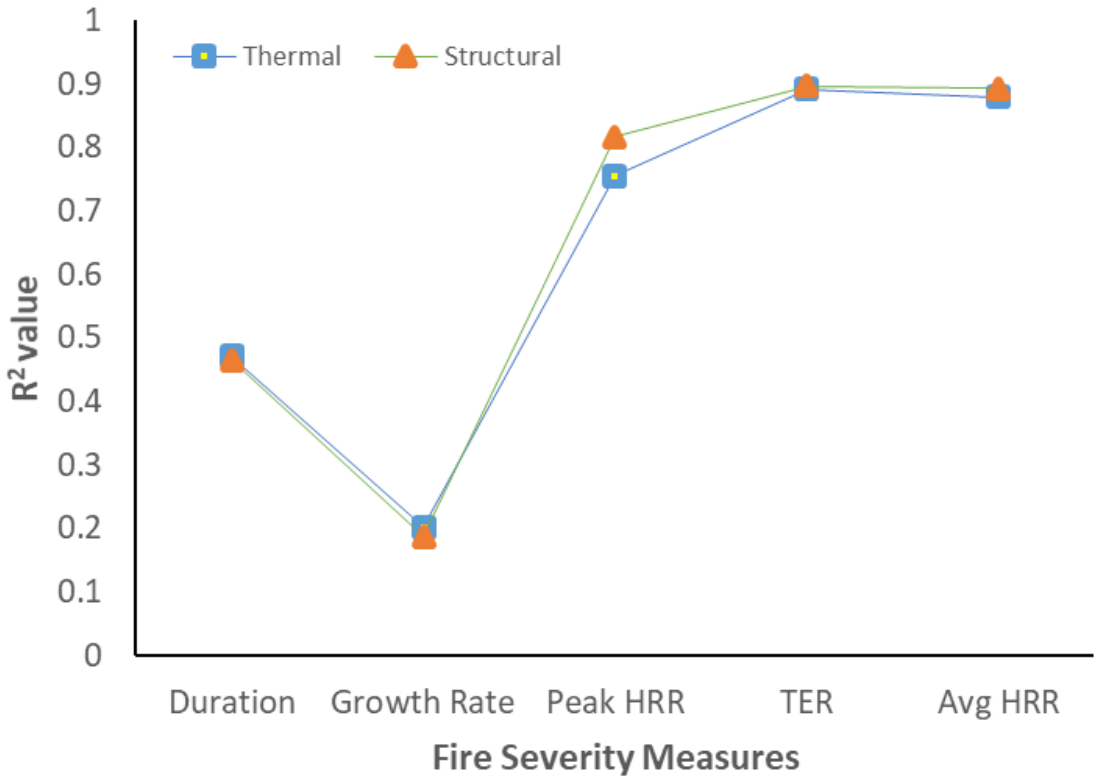

Figure 5.11: Comparison of Cloud Analysis results for both thermal and structural data

5.5 Discussion

5.5.1 Temperature profile using Simple Calculation and Experimental results

During the early stages of the study, simple calculations were carried out which are shown in Figure 3.6 and the comparison of simple calculation and experimental results are shown from Figure 5.12 to 5.15. This was to determine the range of a number of variables for the

experiment. This allowed the design fires to provide structural responses over a broad spectrum to enable further analysis. The temperature profile of the beam and Heskestad's flame height calculations were done and created in a spreadsheet for each of the design fires to find the expected temperature profile. The spreadsheet for Test 1 can be found in Appendix A. The calculation also assisted in determining the overall dimension of the experimental set up such as frame height and the distance between the gas burner to the beam. This gave an outline of how big the fires should be and also the dimension of the gas burner to provide adequate flame height.

The following figures illustrate the comparison of temperature profiles of the beam using simple calculation (blue) and from the experiment (orange). Test 31 (Ultra-slow: 0.0007 kW/s^2, 650 kW) in Figure 5.12, Test 32 (Slow: 0.0029 kW/s^2, 650 kW) in Figure 5.13, Test 33 (Medium: 0.0120 kW/s^2, 650 kW) in Figure 5.14 and Test 34 (Fast: 0.0470 kW/s^2, 650 kW) in Figure 5.15 are shown.

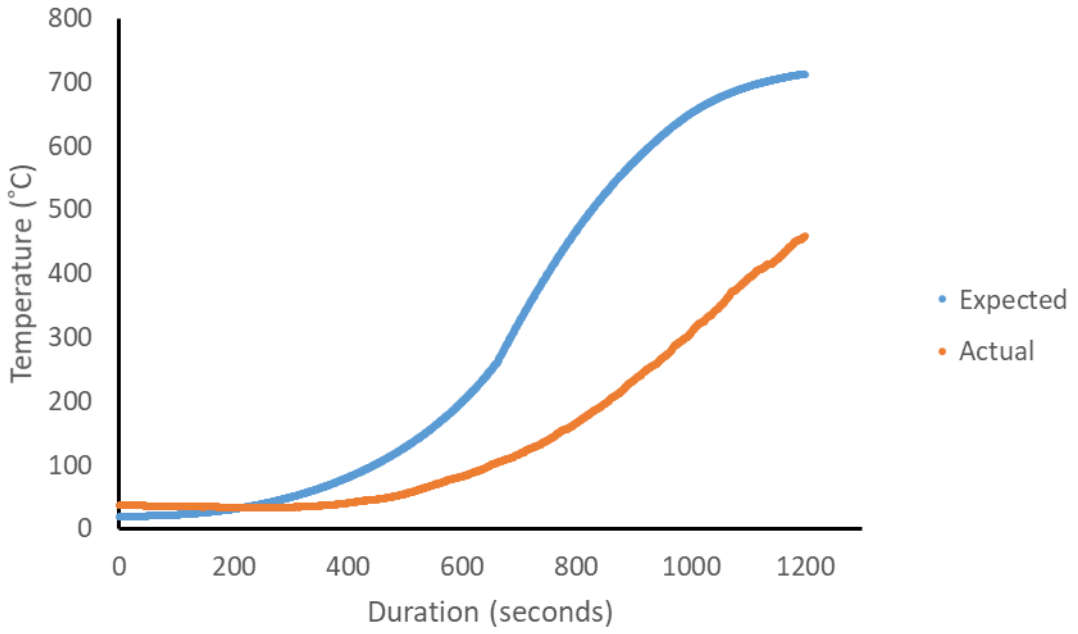

Figure 5.12: Test 31 (Ultra-slow: 0.0007 kW/s^2, 650 kW) temperature profile of expected and experimental results

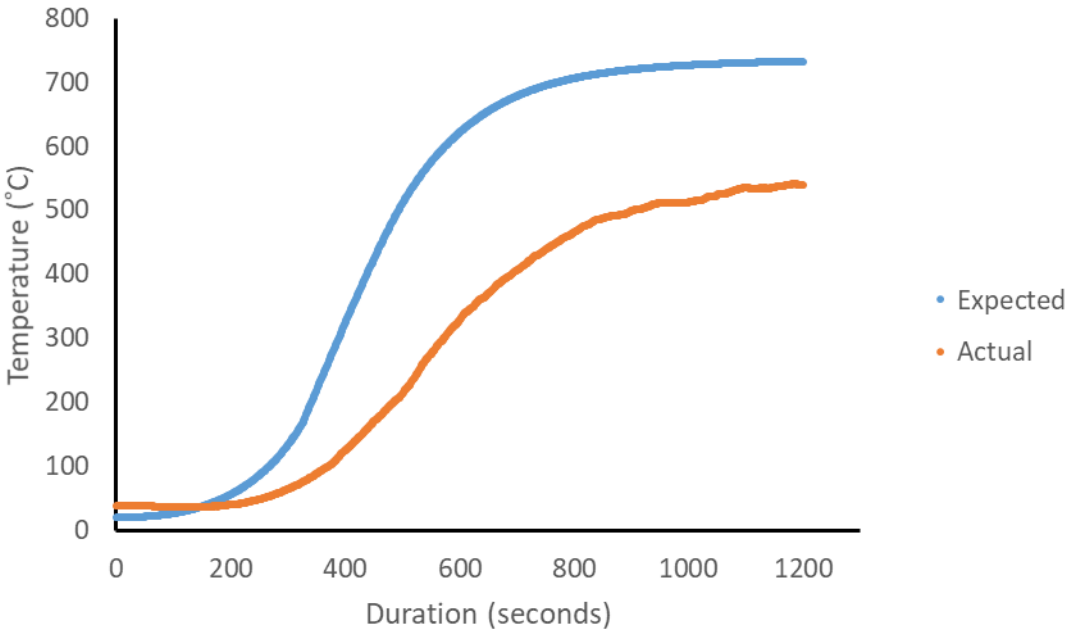

Figure 5.13: Test 32 (Slow: 0.0029 kW/s², 650 kW) temperature profile of expected and experimental results

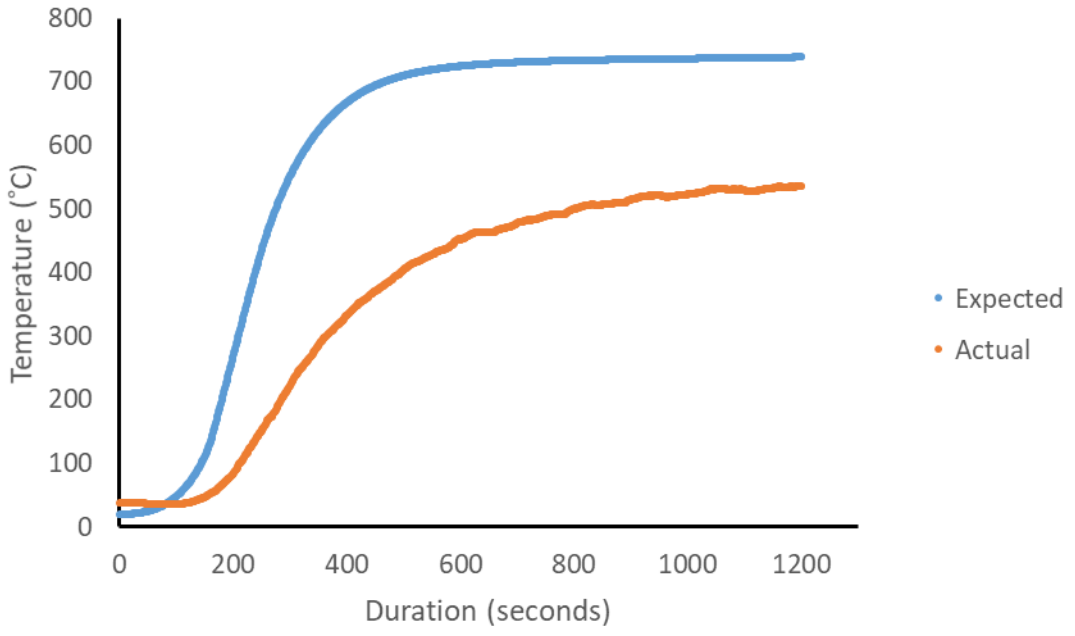

Figure 5.14: Test 33 (Medium: 0.0120 kW/s², 650 kW) temperature profile of expected and experimental results

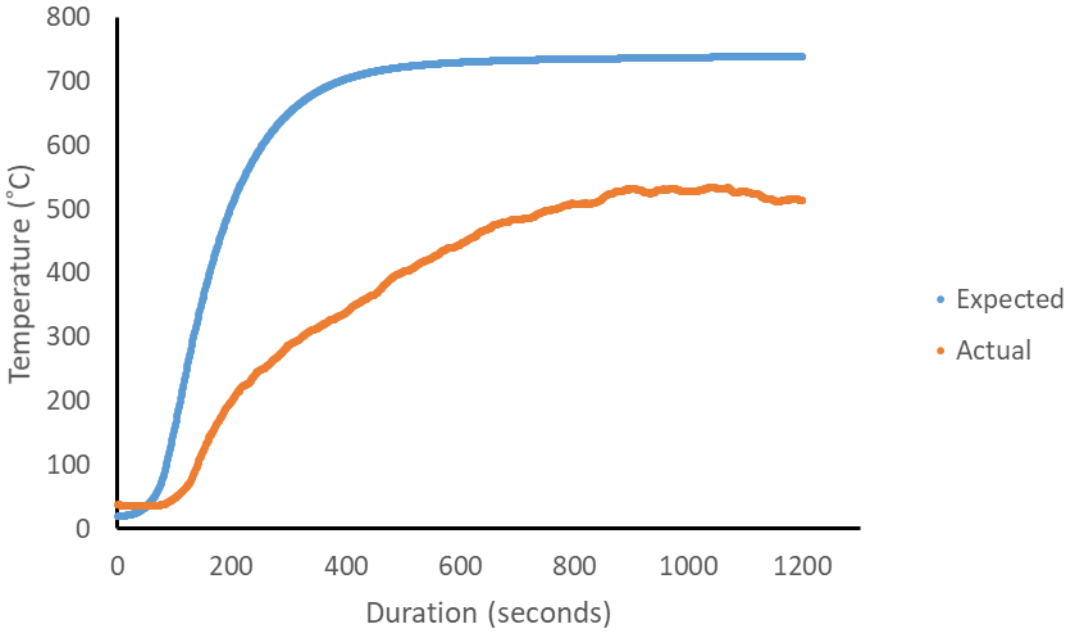

Figure 5.15: Test 34 (Fast: 0.0470 kW/s^2, 650 kW) temperature profile of expected and experimental results

For all simple calculations, the temperature of the beams reached 700 ˚C. There is a clear trend in the profile as well when the temperature slowly increases at the beginning then reaches a peak rate of temperature increase and once it reaches 700 ˚C, it starts to plateau. The time it takes to reach 700 ˚C varies depending on the growth rate of the design fire but this was the general trend using simple calculation. The maximum expected temperature through simple calculation was 739.5 ˚C and the maximum temperature reached in the thermal experiment was only 540 ˚C. This may be due to a number of assumptions in the simple calculation. The calculation involves a number of factors that have been chosen conservatively. The emissivity of 1.0 and 0.7 was used for flame and steel surface respectively. As stated from SFPE handbook (2016), emissivity is the ratio of the amount of radiation emitted by a surface to the maximum amount of radiation that can be emitted by that surface if it was a blackbody. The emissivity of a surface of a material may vary depending on its temperature and different steel materials can have different emissivity. As an example, rolled sheet steel has an emissivity of 0.66 and oxidised steel has an emissivity of 0.79 (SFPE, 2016). Another factor that was used is a configuration factor. Configuration factor is the fraction of radiated energy that is radiated from surface A on to surface B. In this study, surface A would be the flame and B would be the steel I-beam. As the configuration factor of 1.0 was used, it assumed that all of the radiated energy

from the flames has transferred to the beam. However, this is only in an ideal world and in reality, there are surrounding environment in the experiment such as water tanks, surrounding walls and other objects in the lab that would have received of radiation energy from the flames.

It is also important to note that the simple calculation assumes a uniform profile over the depth of the beam. Uniform profile is when the temperature over the depth of a beam in this case is identical which is not the case in real life since the bottom of the beam which has heat exposure first will have higher temperature than the top of the beam which will still have an ambient temperature. There is a gradual increase from the point closest to the heat which would be the bottom of the beam to the point furthest away from the heat which would be the top of the beam. Another important difference is that the simple calculation that was used is for structural fire design which means that the method including the factors are made conservative to design with a safety factor. Nevertheless, in each of the comparisons, it is evident that the general trend: the point of rapid temperature increase, the point where the temperature increase starts to plateau, are very similar to each other, it is just the degree of the rate of increase that is different in each case.

The common theme that is evident in both simple calculations and experimental results is that they both have a maximum temperature range that they have reached. For simple calculation the maximum temperature ranges from 700 ˚C to 740 ˚C. For experimental results, the maximum temperature ranges from 500 ˚C to 530 ˚C. This shows that there is a consistency between the two types of results which can be due to the factors used in the simple calculation. The key difference is that the simple calculation is what is expected in an ideal situation whereas the experiments had a number of variables changing every time.

5.5.2 Flame height calculation and experimental results

As observed in Chapter 4, the pre-defined design fires did not produce as high temperature in the beam as expected. One factor was due to the flame heights at their peak HRR (250 kW, 350 kW and 450 kW) not being as high as the calculated values which required an introduction of a 650 kW peak HRR fire as a new FSM level. Figure 5.16 shows the flame shape in Test 34 (Fast: 0.0470 kW/s^2, 650 kW). The expected flame height from the simple calculation is 2.32 m. The flame height observed in the experiment ranged between 1.5 m to 2.0 m. It is clearly less than the expected flame height and this was observed throughout the experiments. The calculated flame height was potentially the peak flame height that could be observed from intermittent flames in experiments. This is in line with the study done by Madrzykowski et al (2010). The study involves experiments with three different fuels to compare theoretical flame height and the mean flame height of the experiments. Photos were taken and video was

recorded during these experiments to find the mean flame height and the range of natural gas flame, polyurethane foam fueled fire and gasoline fueled fire. By using the Heskestad's flame height equation, it showed that the calculated flame heights were closer to the maximum observed flame height from the experiments for all three fuels. A 650 kW peak HRR fire had to be added as another FSM level as the 450 kW peak HRR fire did not fully engulf the beam and it was only intermittent flames in the plume zone that were hitting the beam from time to time. It is also important to note that the top of the flame has a very small diameter since a flame is a cone-like shape not a cylinder-like shape. This meant that only a limited part of the beam at the mid span was covered in flames even for a 650 kW fire. It would require the beam to be in the continuous flame zone for it to be constantly engulfed in fire.

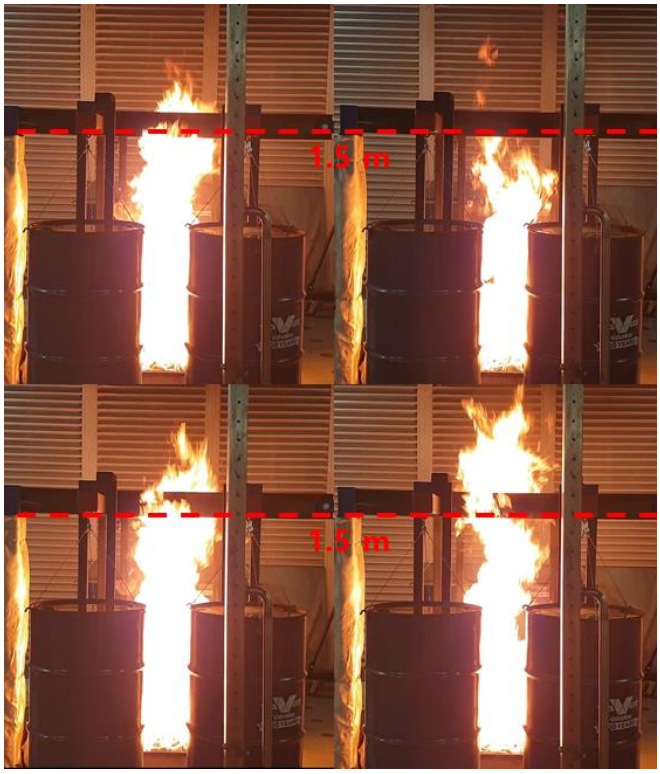

Figure 5.16: Flame height in Test 34 (Fast: 0.0470 kW/s^2, 650 kW)

5.5.3 Phase of temperature profile in thermal tests

There were clear differences between thermal test results as the fire severity for the design fire increased. In fires with slow growth rates and small peak HRR, the temperature growth was in a linear fashion. As the severity of the design fires increased, a clear two phased temperature growth was visible especially with 650 kW peak HRR fires. This is shown in Figure 5.17. Test 20 (Medium: 0.0120 kW/s^2, 350 kW) in Figure 4.11 shows almost a linear growth rate whereas

Test 32 (Slow: 0.0029 kW/s^2, 650 kW) in Figure 4.9 shows a clear two phased growth rate with a fast growth in the first phase and then a second phase with a reduction in the growth rate.

The different trends shown in thermal tests are a result of the material behaviour. The slow growth at the initial stage was due to high thermal inertia of steel. Thermal inertia is a measure of how a material gains heat from its surroundings. The higher the thermal inertia, the longer it takes for a material to change its temperature. When the fire started, the surrounding temperature increased but since steel tries to keep its initial temperature, it resisted temperature rise in the first stage until sufficient amount of heat had been provided. Once the steel temperature started to increase, it showed different phases with varying growth rates. This was again due to the thermal properties of steel. Firstly, it is the specific heat of steel increasing as the temperature of the beam increased. The specific heat is the amount of heat energy required to increase the material by 1 ˚C. As the temperature of the steel beam increased, it required more heat for the beam to heat up and since there was only a limited amount of heat, the rate of temperature rise reduced. Secondly, it was due to thermal conductivity. It is a measure of the material's ability to conduct heat. For steel, the thermal conductivity increased as the temperature increased which again meant that as the temperature of the beam increased, the beam required more energy to conduct heat. These thermal behaviour of steel resulted in reduction of the growth rate in the temperature of the beam.

5.5.4 Curvature of the beam with axial force structural tests

In structural tests, the maximum axial force was recorded in Test 32 (Slow: 0.0029 kW/s^2, 650 kW) as 20.56 kN. On the other hand, Test 34 which had the highest FSMs involved had an axial force of 16.57 kN which was clearly less than the maximum axial force recorded. It showed that the axial force from the beam does not occur in the largest fires and is dependent on a number of variables involved. As the temperature of the beam increases, the bottom of the beam is affected first since it is closest to the fire. This results in the temperature difference between the bottom and the top of the beam which leads to curvature as shown in Figure 5.18. Curvature is the result of such temperature difference where the beam starts to bend. This effect is further worsened by the two point loads that are directed downwards causing the beam to bend even more. As a result of this curvature, even though the beam is expanding due to thermal expansion, it does not exert as much axial force as it would in a condition without curvature. This proves why Test 34 did not produce the highest axial force even though it was the biggest fire out of all the tests. The axial force of the beam will depend on the design fire, dimension of the beam, loading condition and many other factors. The curvature of the beam due to sudden increase in the temperature of the beam not being uniform counteracts the thermal expansion

which also explains the general plateau of axial forces in structural tests with high FSMs. This would not occur as much in tests with low FSMs as they will have more uniform temperature through the depth of the beam as it is heated up slowly. This is further supported by the mid span deflection of the beams that were measured from structural tests. Although the deflections were very small ranging between 3 mm to 7 mm, it shows that the beams were deflected as well having a thermal gradient through the depth of the beam leading to curvature. To further investigate the curvature and its relationship with deflection and thermal gradient, more studies will be required with greater point loads to have significant deflection of a beam.

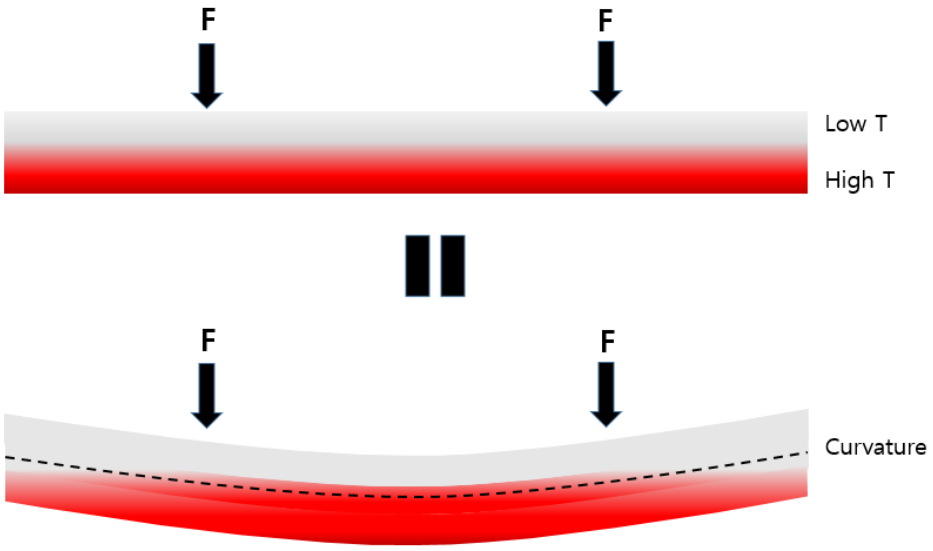

Figure 5.17: Curvature of a beam due to temperature difference through its depth

5.5.5 Correlation between thermal and structural results

After the experiments were completed, the results were combined to find out the correlation between the thermal and structural responses. This showed that out of 102 tests, 14 tests had identical results when ordered from highest to lowest thermal and structural results. Test 32 produced both the greatest maximum temperature of 552 ˚C and the highest axial force of 20.56 kN. The design fire was a 1200 second slow growth rate (0.0029 kW/s^2) fire with a peak HRR of 650 kW and the results are shown in Figure 5.19. It is important to note that the thermal tests and structural tests were done separately. Both thermal and structural results were ordered from highest to lowest shown in Appendix E. It was shown that out of 102 results, only 14 results had identical order. This shows that there are many variables and factors that affect the fire.

5.6 Issues identified from the study

Throughout the study from the initial calculations using theoretical formulae to carrying out the experiments, a number of issues were raised and found. This included human errors, experimental issues and environmental factors as well. In order to minimize the uncertainty and the errors from the identified issues, some adaptions had to be made throughout the study. These can also be learnt and improved on for future experimental studies in PSFE and in structural fire engineering in general. They are:

- Human error in preparing specimens for testing
- Test environment
- Instruments used in the test

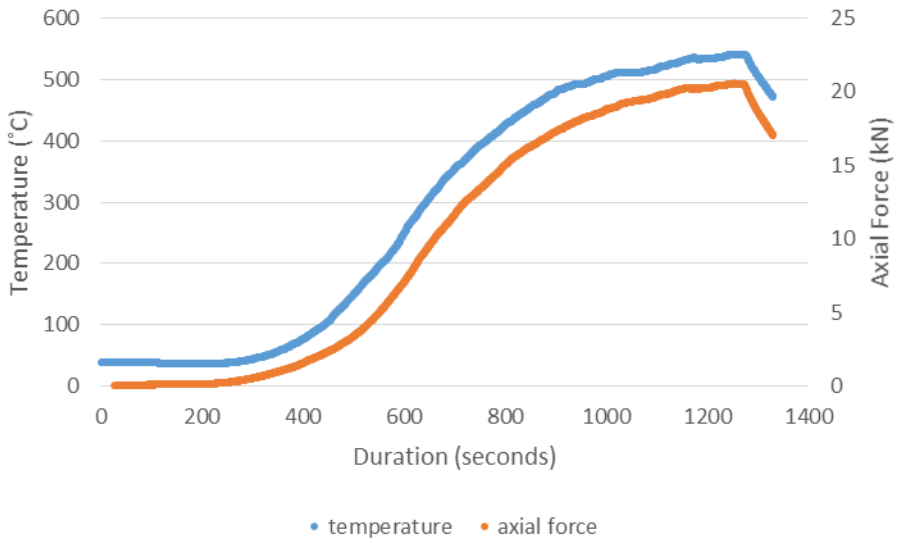

Figure 5.18: Test 32 (Slow: 0.0029 kW/s², 650 kW), thermal and structural results

5.6.1 Human Errors

One possible human error is related to preparing the steel I-beams. All steel beams came in 6 m lengths which meant that the beams had to be cut into three pieces for the tests with a length of 2 m. The beams were drilled for pin ended supports. It had instances where it had to be hammered through or the hole was too big compared to the pin. This would have resulted in different results for the initial axial force reading. Another part of human error in the beam was the thermal test. In total 21 holes were drilled to embed thermocouples up to 0.5 mm to 1 mm inside the beam to measure the temperature. The depth could be inconsistent for each of the

holes since the lab technician drilled the holes and this means that some of the thermocouples could have been exposed to heat earlier than other thermocouples in different part of the beam.

5.6.2 Test environment

As shown in Chapter 4, there were clear differences in thermal results for section A and C of the beam throughout the tests. This may be due to a number of factors but the biggest reason will be due to the flame shape and its overall symmetry. In an ideal world, a fire has a cone shape with the centre of the flame having a biggest height and the edges decreasing in size. It was shown through the experiments that the flame does not keep the symmetric shape at all as the flames are constantly fluctuating. It was also evidently clear from observation that during certain tests, the flames swayed on to one side. This is due to the air current within the lab that moves and affects the movement of the flame. In Chapter 4, figures such as Figure 4.6 showed an indication of how the flames clearly leaned to one side in two different tests. This is one of the factors that cannot be controlled and this was observed throughout both thermal and structural tests. The flames were often fluctuating and did not keep their symmetrical shape and the heat transfer to A and C was affected accordingly.

As shown in Figure 5.20, the ambient conditions in the laboratory where the tests were carried out varied each day. This would have been dependent on the weather and time of the day. Four to eight tests were carried out each day and as the tests were carried out the ambient temperature of the laboratory varied. The change in the ambient condition of the surroundings of the test could have affected the entire test result even though it may not have played a significant role in temperature changes of the beam. Future study can be carried out to further investigate the impact of ambient condition by carrying out an identical test on multiple number of days at different times.

5.6.1 Instruments used in the test

One of the most crucial part of the test was to ensure the gas burner provided the required design fire for each of the tests for it to affect the beam. When the test began, it was clearly shown that the gas burner did not ignite or fully develop around the surface until the HRR reached at least 30 kW. Even after the fire reached 30 kW, it would often have an uneven flame spread across the burner. This was since the surface area and the pipe of the gas were too big compared to the HRR. This was an issue especially for the fires with ultra-slow to slow growth rates as it took up to 4.5 minutes to reach 30 kW. The chosen ignition source was a hand torch as shown in Figure 5.21 and even if the torch ignited the surface at the beginning, the flame died until it reached around 30 kW. In order to solve this issue, a HRR spike of 300 kW for 8 seconds was provided at the initial phase of the test to provide enough gas to spread around the surface

of the gas burner to maintain the fire until it reached 30 kW. This meant that the TER was affected since there was a variation in the amount of time the torch was used for each test.

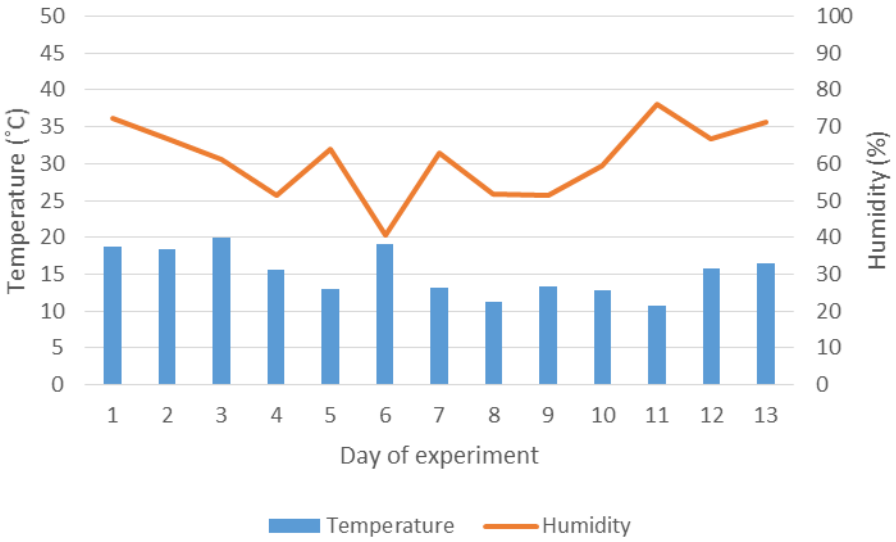

Figure 5.19: The ambient temperature and humidity for every day

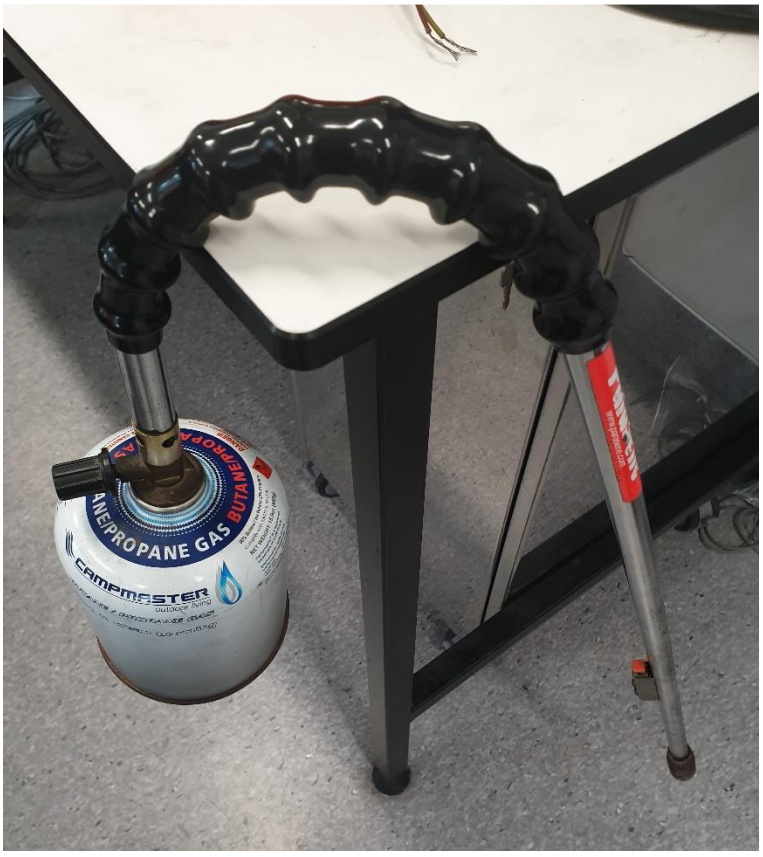

Figure 5.20: Hand torch used as the ignition source

As stated before, it was also noticeable to see that fire did not spread evenly across the surface. This was a concern as this would mean that certain areas of the beam had less exposure to radiation than the other parts of the beam. The gas burner had a large pipeline underneath to provide gas and the surface was pumice as explained in Chapter 3. It was quite clear as shown in Figure 5.22, that the edges of the gas burner did not have flames and this would have affected radiation on to the beam and the thermal behaviour of the beam. In order to spread the flame throughout the pumice across the gas burner, the hand torch was used a number of times to achieve a more well developed fire. This again would have affected the TER of the design fire which could result in a biased result. However, this is not considered to have significantly affected the overall results of the test as the TER of each tests are far greater than the HRR provided from the blowtorch. However, to mitigate such issue in future studies, it is recommended to start the design fire with a minimum of 30 kW as the initial HRR to ensure enough gas is provided to develop a well spread fire.

Figure 5.21: Uneven spread of the flame across the gas burner

5.7 Conclusion

The chapter has explained how the experimental data has been analysed to find the most efficient FSM. By using Cloud Analysis developed by the PEER Centre's PBEE method, the most efficient FSMs were obtained. Other analytical methods were not used in this study. The best FSM was Total Energy Released (TER) with R^2 of 0.8908 and 0.8959 for thermal and structural tests respectively. It was the FSM with the highest R^2 value for both of the tests.

In addition, this chapter reports discussion about the results obtained and the justifications behind what was observed from the experimental results. The thermal tests showed different phases of temperature growth in the beam depending on the range of FSMs with design fires with low FSMs showing a single linear phase whereas design fires with high fire severity levels over all FSMs showed two different phases with the first phase being a steep rapid increase and the second phase with a reduction in the growth rate. Structural tests showed the effect of curvature for design fires with high FSM values as they had a more rapid temperature increase compared to smaller fires. Comparisons between simple calculation and the experiment results showed that the theoretical values overestimate the expected outcome and this is due to the safety factors embedded within these formulae.

6. SUMMARY

6.1 Study objective

This experimental study was conducted to further develop Probabilistic Structural Fire Engineering (PSFE) using the Pacific Earthquake Engineering Research (PEER) Centre's Performance Based Earthquake Engineering (PBEE) methodology. The first two stages were investigated by identifying relationships between pre-flashover fires (as hazard) and structural response.

In current structural fire design, there is a concern of assuming worst case scenario fire which may not be the actual worst fire. This can lead to structural failure as a more realistic account of the potential damage may not have been considered. In order to eliminate this issue, there has been a number of studies on PSFE. Majority of these studies focus on using numerical models as they are cost and time efficient. However, since fire has great number of variables, using models are not considered to be 100% reliable as the models cannot accurately predict the response due to the uncertainties within each of the variables. To fill this gap in PSFE, this study has focused on experiments to provide over 100 results to study the relationship between fires and structures. The experimental data can be used to further support or improve the existing models by implementing the uncertainties obtained from the test results in future studies. This study is considered to be a step to set a foundation on experimental research on probabilistic approaches.

6.2 Steel I-beam experiment

Experiments were carried out on 150 UB 14.0 steel I-beam on pin-pin ended supports to produce over 100 data points. The experiment was done in a four point bending test configuration to record both maximum temperature of the beam and the axial force of the beam due to thermal expansion. Pre-flashover fires were used and this was the first known experimental based PSFE study to obtain multiple data point to analyse the different range of FSMs to find the best relationship between Fire Severity Measure (FSMs) and Engineering Demand Parameters (EDPs).

6.3 Experimental results

The experiments were done in two parts, thermal and structural. In total 34 tests were carried out for each part, totalling 68 experiments. This produced 102 results each for the thermal and structural experiments. After the first few thermal experiments were carried out, it showed that

the temperature of the beam was significantly lower than the expected results obtained prior to the tests from the simple calculations.

In the thermal tests, it showed that the highest temperature of the beam reached 552 ˚C in Test 32. Test 32 was a slow growth rate (0.0029 kW/s^2) fire with a duration of 1200 seconds and 650 kW peak HRR. The area of the highest temperature within the beam was at the right bottom flange at the centre of the beam. This was expected as each side of the bottom flange had the most heat exposure from the flames. In the structural tests, it also showed that Test 32 resulted in the highest axial force of 20.56 kN.

6.4 Analysis of the results

The main purpose of carrying out large number of experiments on wide range of design fire was to obtain a spectrum of results for thermal and structural response of the beam. This provided enough data investigate the relationship between different FSMs and EDPs to find the most efficient FSM that could quantify fire. Cloud Analysis (CA) was used for this study as it does not involve any scaling of the data.

CA was carried out on both thermal and axial test results. As it uses linear regression, R^2 is obtained for each FSM-EDPs to show the strength of relationship between the chosen FSM and EDP. The most efficient FSM was found to be Total Energy Released (TER) for both the thermal test and structural test with R^2 values of 0.8908 and 0.8959 respectively. The FSM with the lowest R^2 was the growth rate and showed that there was almost no relationship between the fire growth rate and structural response with a R^2 values of 0.2026 and 0.1872 for thermal and structural tests respectively.

6.5 Future Recommendations

The objective of this study was to provide a foundation to further develop a method to quantify the effects of fire. By quantifying the fire, the structural response of the fire can also be obtained and hence structures can be designed for the most likely worse-case fire. There are currently a number of areas where PSFE needs developing in order to use this approach in real practice like earthquake engineering. Further studies are required to achieve this.

This study focused on pre-flashover fire and a single element experiment. In future studies, a post-flashover test on the same element can be carried out to compare pre-flashover and post-flashover fire. Although many FSM variables will be different, there may be opportunities to compare similar variables for pre-flashover and post-flashover fires. An example of this would be the comparison between pre-flashover FSMs such as total energy released, average HRR to

post-flashover FSMs such as compartment temperature and Cumulative Incident Radiation (CIR) which has been studied in a PSFE study (Shrivastava, 2019). This can allow better understanding of the overall fire behaviour instead of pre and post-flashover fires in two separate parts. Another possible study may be the comparison of experimental results against the simulation results obtained from numerical models to further develop advanced models.

A study on a structural frame and carrying out tests on this would provide valuable information for PSFE. The ultimate objective of PSFE is to use the method of quantifying fire for the design of structures. This means that the goal is to be able to quantify fire and predict how a structure will respond to such fire. This study involved a single element but this should be further developed and studied to carry out an experiment on a full scale structure to develop a probabilistic methodologies to design full structures.

Another study that could be done would be to carry out tests on different structural materials such as timber and concrete. As steel was used as the specimen in this study, timber, concrete and composite beams can be used to carry out the same study either for pre-flashover or post-flashover fires to find the relationship between fire variables and structural response. This will provide a wider spectrum for PSFE.

REFERENCES

Bailey, C. (1995). Simulation of the structural behaviour of steel-framed buildings in fire, PhD Thesis, University of Sheffield. Sheffield, UK.

Barbarto, M., Petrini, F., Ciampolie, M. (2011). "A preliminary proposal for a probabilistic performance based hurricane engineering framework", *Structure Congress,* pp. 1618-1629.

Buchanan, AH & Abu, AK. (2017). *Structural design for fire safety,* John Wiley & Sons.

Buchanan, AH. (1994). 'Fire Engineering for a Performance based code', *Fire Safety Journal,* vol.23, pp. 1-16.

Cornell, C.A., Krawinkler, H. (2000). "Progress and challenges in seismic performance assessment", *Peer Centre News,* Vol.3 No.2, pp.1-3.

Devaney, S. (2014). *Development of software for reliability based design of steel framed structures in fire,* Ph.D. Dissertation Thesis, University of Edinburgh, Edinburgh.

European Standard. (2002). Actions on structures – Part 1-2: General actions – Actions on structures exposed to fire. European Standard, European Committee for Standardization.

European Standard. (2005). Design of steel structures – Part 1-2: General rules – Structural fire design. European Standard, European Committee for Standardization.

FENZ. (2019). Annual report for the year ended 30 June 2018. Fire and Emergency NZ.

Franssen, J. (2005), "SAFIR: A thermal/structural program for modelling structures under fire". *Engineering Journal-American Institute of Steel Construction Inc,* 42(3), 143-158

Gernay, T., Van Coile, R., Khorasani, N. E., Hopkin, D. (2019). "Efficient uncertainty quantification method applied to structural fire engineering computations." *Engineering Structures*, pp. 1-17

Giovenale, P., Cornell, CA., Esteva, L. (2004). 'Comparing the adequacy of alternative ground motion intensity measures for the estimation of structural responses', *Earthquake engineering & structural dynamics,* vol. 33, no. 8, pp. 951-979

Hadjisophocleous, GV., Benichou, N., Tamim, AS. (1998). 'Literature Review of Performance-Based Fire Codes and Design Environment', *Journal of Fire Protection Engineering,* vol. 9, no. 1, p. 12-40, doi:10.1177/104239159800900102

Hamilton, SR. (2011). *Performance-based fire engineering for steel framed structures: a probabilistic methodology,* Ph.D. Dissertation Thesis, Stanford University, California, USA.

Home office. (2019). Fire and rescue incident statistics, England: year ending September 2018. National Statistics.

Jayaler, F. (2003). *Direct Probabilistic Seismic Analysis: Implementing Non-Linear Dynamic Assessments*. Stanford University, Stanford.

Johnstone, E.D., Sofe, C.V., Shrivastava, M., Abu. A., Moss. P., (2019). Comparative evaluation of analysis methods for probabilistic structural fire engineering. Nanyang Technological University, Singapore: Applications of Structural Fire Engineering, 12-14 Jun 2019. In proceedings of applications of structural fire engineering Conference 2019: 370-375

Lange, D., Devaney, S., Usmani, A., (2014). *An application of the PEER performance based earthquake engineering framework to structures in fire.* BRE Centre for Fire Safety Engineering, Edinburgh.

Lennon, T., Moore, D. (2003). *The natural fire safety concept – test at Cardington.* Centre for Steel Construction, Garston.

Luco, N., Cornell, CA. (2007). 'Structure-specific scalar intensity measures for near-source and ordinary earthquake ground motion', *Earthquake Spectra,* vol. 23, no. 2, pp. 357-392.

Madrzykowski, D.M., Fleischmann, C., Harris, G. L. (2010). Flame height and heat transfer from gaseous, liquid and solid fuels for burn pattern repeatability research. In *Interflam 2010.*

Moehle, J., Deierlein, GG. (2004). 'A framework methodology for performance-based earthquake engineering', *13th world conference on earthquake engineering,* Canadian Association for Earthquake Engineering under the auspices of International Association for Earthquake Engineering, Vancouver, British Columbia, Canada, pp. 3812-3814.

Moss, P.J., Abu, A.K., Dhakal, R.P. (2014). *Intensity Measures for Probabilistic Structural Fire Engineering.* University of Canterbury, Canterbury.

Petrini, F., Ciampoli, M. (2012), "Performance based wind design of tall buildings", *Structure and Infrastructure Engineering,* Vol. 8 No. 10, pp. 954-966.

Pope, ND., Bailey, CG. (2006). 'Quantitative comparison of FDS and parametric fire curves with poth-flashover compartment fire test data', *Fire Safety Journal,* vol. 41, no. 2, pp. 99-110.

Porter, KA. (2003). 'An overview of PEER's performance-based earthquake engineering methodology', *Ninth International Conference on Applications of Statistics and Probability in Civil Engineering,* edited by Armen Der Kiureghian, Samer Madanat, and Juan M. Pestana, San Francisco, California, USA.

Ribeiro, FL,. Rosario, RP., Barbosa, AR., Neves, LC. (2016). 'Sensitivity analysis of steel moment frames subjected to structural fire using the OpenSees framework', in *10th National Conference on Seismology and Earthquake Engineering,* Azores, Portugal.

Riggs, H., Robertson, I.N., Cheung, K.F., Pawlak, G., H. Young, Y.L., Yim, S.C. (2008), "Experimental simulation of tsunami hazards to buildings and bridges", in *Proceedings of 2008 NSG Engineering Research and Innovation Conference,* pp. 1056-1064

Sanad, AM., Rotter, JM., Usmani, AS., O'Connor, MA. (2000). 'Composite beams in large buildings under fire – Numerical modelling and structural behaviour', *Fire Saf. J., 35(3), 165-188.*

SFPE. (2016). SFPE handbook of Fire Protection Engineering. SFPE, Springer.

Shrivastava, M., Abu, A.K., Dhakal, R.P., Moss, P.J. (2018). Severity Measures and Stripe Analysis for Probabilistic Structural Fire Engineering. Fire Technology. Reprinted with Permission.

Shrivastava, M., Abu, A.K., Dhakal, R.P., Moss, P.J. (2019). State-of-the-art of probabilistic performance based structural fire engineering. Journal of Structural Fire Engineering.

Tothong, P., Luco, N. (2007). 'Probabilistic seismic demand analysis using advanced ground motion intensity measures', *Earthquake Engineering & Structural Dynamics,* vol. 36, no. 13, pp. 1837-1860.

Van Coile, R., Hopkin, D., Lange, D., Jomaas, G. and Bisby, L. (2018), "The need for hierarchies of acceptance criteria for probabilistic risk assessments in fire engineering", *Fire Technology,* pp.1-36.

Wang, YC,. Lennon, T., Moore, DB. (1995). 'The behaviour of steel frames subject to fire' *J. Constr. Steel Res., 35(3), 291-322.*

APPENDIX A. TEMPERATURE PROFILE OF TEST 1 USING SIMPLE CALCULATION

Scenario 1 Ultra Slow	Ultra Slow Fire Growth rate, Peak HRR 250kW, THR 126 MJ, Duration 900 seconds, Flame not touching the beam			
				unit
Height	H		1.5	m
Horizontal distance	r		0	m
Flame Diameter	D		0.798086884	m
Gas burner dimension	0.5m x 0.5m			
Steel beam	150 UB 14.0			
Flame Emissivity	εf		1	
Configuration Factor	Φ		1	
Stefan Boltzmann constant	σ		5.67E-08	W/m2K4
Coefficient of Heat Transfer	α		35	W/m2K4
Section Factor	Am/V		330.8214286	/m
Surface Area	SA		0.59	m2
Volume(box)	Vb		0.01125	m3
Volume	V		0.001783439	m3
Surface Area (box)	Am(box)		4.725	m2
Section Factor(box)	Am/V(box)		252.8089888	m2
Unit Mass	ρ		7850	kg/m3
Surface Emissivity	εm		0.7	
	Ksh		0.687767086	
Total Heat Released	125.5225865	MJ		
THR 600	50.5225865	MJ		
THR 300	6.331535	MJ		

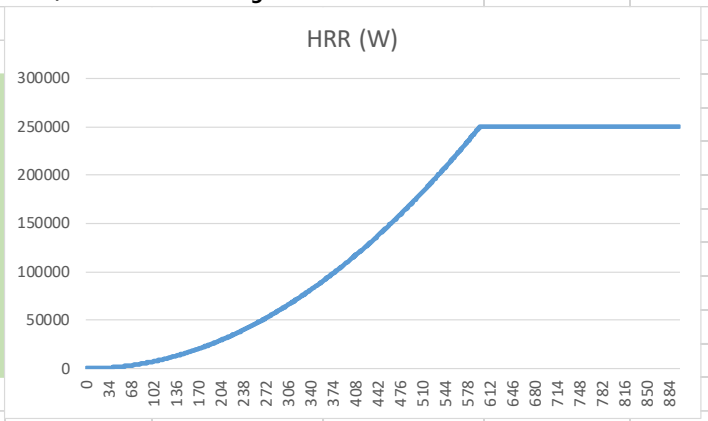

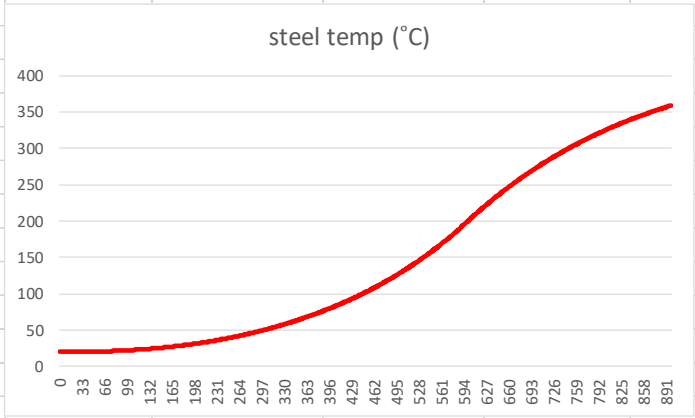

Exemplar spreadsheet of simple calculation

Time (sec)	HRR (W)	Flame Height (m)	Model A/B	Z (m)	Z0 (m)	Gas Temp (C)	QD	Z'	QH	Lh	y	steel tem	h_dot	hc	hr	hnet	ca	theta delta
869	250000	1.32	A	1.50	-0.06	429.97	-	-	-	-	-	350	0.00	2808.79	3723.97	6532.76	583.59	0.32
870	250000	1.32	A	1.50	-0.06	429.97	-	-	-	-	-	350	0.00	2797.43	3711.52	6508.96	583.72	0.32
871	250000	1.32	A	1.50	-0.06	429.97	-	-	-	-	-	350	0.00	2786.12	3699.10	6485.22	583.85	0.32
872	250000	1.32	A	1.50	-0.06	429.97	-	-	-	-	-	351	0.00	2774.85	3686.71	6461.57	583.99	0.32
873	250000	1.32	A	1.50	-0.06	429.97	-	-	-	-	-	351	0.00	2763.63	3674.35	6437.98	584.12	0.32
874	250000	1.32	A	1.50	-0.06	429.97	-	-	-	-	-	351	0.00	2752.45	3662.02	6414.47	584.25	0.32
875	250000	1.32	A	1.50	-0.06	429.97	-	-	-	-	-	352	0.00	2741.31	3649.71	6391.02	584.38	0.32
876	250000	1.32	A	1.50	-0.06	429.97	-	-	-	-	-	352	0.00	2730.22	3637.44	6367.66	584.51	0.32
877	250000	1.32	A	1.50	-0.06	429.97	-	-	-	-	-	352	0.00	2719.16	3625.19	6344.36	584.63	0.31
878	250000	1.32	A	1.50	-0.06	429.97	-	-	-	-	-	353	0.00	2708.16	3612.98	6321.13	584.76	0.31
879	250000	1.32	A	1.50	-0.06	429.97	-	-	-	-	-	353	0.00	2697.19	3600.79	6297.98	584.89	0.31
880	250000	1.32	A	1.50	-0.06	429.97	-	-	-	-	-	353	0.00	2686.27	3588.63	6274.90	585.02	0.31
881	250000	1.32	A	1.50	-0.06	429.97	-	-	-	-	-	354	0.00	2675.38	3576.50	6251.89	585.15	0.31
882	250000	1.32	A	1.50	-0.06	429.97	-	-	-	-	-	354	0.00	2664.55	3564.40	6228.95	585.27	0.31
883	250000	1.32	A	1.50	-0.06	429.97	-	-	-	-	-	354	0.00	2653.75	3552.33	6206.08	585.40	0.31
884	250000	1.32	A	1.50	-0.06	429.97	-	-	-	-	-	354	0.00	2642.99	3540.29	6183.28	585.53	0.31
885	250000	1.32	A	1.50	-0.06	429.97	-	-	-	-	-	355	0.00	2632.28	3528.28	6160.56	585.65	0.30
886	250000	1.32	A	1.50	-0.06	429.97	-	-	-	-	-	355	0.00	2621.61	3516.29	6137.90	585.78	0.30
887	250000	1.32	A	1.50	-0.06	429.97	-	-	-	-	-	355	0.00	2610.98	3504.34	6115.32	585.90	0.30
888	250000	1.32	A	1.50	-0.06	429.97	-	-	-	-	-	356	0.00	2600.39	3492.41	6092.81	586.03	0.30
889	250000	1.32	A	1.50	-0.06	429.97	-	-	-	-	-	356	0.00	2589.85	3480.52	6070.36	586.15	0.30
890	250000	1.32	A	1.50	-0.06	429.97	-	-	-	-	-	356	0.00	2579.34	3468.65	6047.99	586.28	0.30
891	250000	1.32	A	1.50	-0.06	429.97	-	-	-	-	-	357	0.00	2568.87	3456.82	6025.69	586.40	0.30
892	250000	1.32	A	1.50	-0.06	429.97	-	-	-	-	-	357	0.00	2558.45	3445.01	6003.46	586.53	0.30
893	250000	1.32	A	1.50	-0.06	429.97	-	-	-	-	-	357	0.00	2548.07	3433.23	5981.30	586.65	0.30
894	250000	1.32	A	1.50	-0.06	429.97	-	-	-	-	-	357	0.00	2537.72	3421.48	5959.21	586.77	0.29
895	250000	1.32	A	1.50	-0.06	429.97	-	-	-	-	-	358	0.00	2527.42	3409.76	5937.18	586.89	0.29
896	250000	1.32	A	1.50	-0.06	429.97	-	-	-	-	-	358	0.00	2517.16	3398.07	5915.23	587.02	0.29
897	250000	1.32	A	1.50	-0.06	429.97	-	-	-	-	-	358	0.00	2506.94	3386.41	5893.35	587.14	0.29
898	250000	1.32	A	1.50	-0.06	429.97	-	-	-	-	-	359	0.00	2496.75	3374.78	5871.53	587.26	0.29
899	250000	1.32	A	1.50	-0.06	429.97	-	-	-	-	-	359	0.00	2486.61	3363.18	5849.79	587.38	0.29
900	250000	1.32	A	1.50	-0.06	429.97	-	-	-	-	-	359	0.00	2476.51	3351.61	5828.12	587.50	0.29

The following steps for followed to produce the Simple calculation spreadsheet for the thermal response of the beam exposed in a designated design fire,

1. Determine if the flame height is greater than the height of the beam

$$-1.02\mathrm{D} + \left(0.0148\dot{Q}^{0.4}\right) = Flame\ height$$

2. Find Virtual origin, Z_0

$$-1.02\mathrm{D} + \left(0.00524\left(\dot{Q}^{0.4}\right)\right) = Virtual\ Origin$$

3. The temperature of the plume is

$$\Theta_z = 20 + 0.25 Q_c^{\frac{2}{3}} (z - z_o)^{\frac{-5}{3}} \leq 900$$

If the flame height is not impacting the beam (when the flame height is less than the frame height (1.5m): Case A,

A1) The net convective heat flux component is

$$\dot{h}_{net,c} = \alpha_c(\Theta_g - \Theta_m)$$

A2) The net radiative heat flux per unit surface area is

$$\dot{h}_{net,r} = \emptyset \varepsilon_m \varepsilon_f \sigma[(\Theta_r + 273)^4 - (\Theta_m + 273)^4]$$

A3) To determine Specific heat of steel, c_a (J/kgK)

For 20 ˚C ≤ θ_a ≤ 600 ˚C,

$$c_a = 425 + 7.73 \times 10^{-1}\theta_a - 1.69 \times 10^{-3}{\theta_a}^2 + 2.22 \times 10^{-6}{\theta_a}^3$$

For 600 ˚C ≤ θ_a ≤ 735 ˚C,

$$c_a = 666 + \frac{13002}{738 - \theta_a}$$

For 735 ˚C ≤ θ_a < 900 ˚C,

$$c_a = 545 + \frac{17820}{\theta_a - 731}$$

For 900 ˚C ≤ θ_a ≤ 1200 ˚C,

$$c_a = 650$$

A4) Hence the change in temperature of the beam per second is,

$$\Delta\theta_{a,t} = k_{sh}\frac{A_m/V}{c_a\rho_a}\dot{h}_{net,d}\Delta t$$

If the flame height is impacting the beam (when the flame is equal to or greater than the frame height (1.5m): Case B

B1) Find non-dimensional rate of heat release, Q_H^*

$${Q_H}^* = Q/(1.11 \times 10^6 H^{2.5})$$

B2) Find the vertical position of the virtual heat source, z'

$$z' = 2.4D\left({Q_D}^{*\frac{2}{5}} - {Q_D}^{*\frac{2}{3}}\right) when\ {Q_D}^{*} < 1.0$$

Or

$$z' = 2.4D\left(1.0 - {Q_D}^{*\frac{2}{5}}\right) when\ {Q_D}^{*} \geq 1.0$$

Where Q_D is,

$${Q_H}^{*} = Q/(1.11 \times 10^6 D^{2.5})$$

B3) Find the horizontal flame length, L_h

$$L_h = (2.9\ H\ ({Q_H}^{*})^{0.33}) - H$$

B4) To obtain the parameter y given by,

$$y = \frac{r + H + z'}{L_h + H' + z'}$$

B5) Find the heat flux, h, received by the beam

$$\dot{h} = 100{,}000 \quad if\ y \leq 0.30$$

$$\dot{h} = 136{,}300\ to\ 121{,}000y \quad if\ 0.30 < y < 1.0$$

$$\dot{h} = 15{,}000y^{-3.7}\ if\ y \leq 0.30$$

B6) The net radiative heat flux per unit surface area is

$$\dot{h}_{net,c} = \alpha_c(\Theta_m - 20)$$

B7) The net radiative heat flux per unit surface area is

$$\dot{h}_{net,r} = \emptyset\varepsilon_m\varepsilon_f\sigma[(\Theta_m + 273)^4 - (293)^4$$

APPENDIX B. RESULTS OF FSMS AND EDP FROM THERMAL TEST

TEST	Durations	Growth Rate	Target Peak HRR	Target TER	Target Avg HRR	Max Temp
1	300, 600, 900	0.0007	250	125.5	139.4	21.5, 60.0, 111.0
2	300, 600, 900	0.0007	350	150.2	166.9	35.0, 73.5, 166.5
3	300, 600, 900	0.0007	450	164.7	183.0	35.0, 81.0, 217.5
4	300, 600, 900	0.0014	250	154.7	171.9	30.0, 125.5, 182.0
5	300, 600, 900	0.0014	350	198.5	220.6	34.0, 210.0, 255.5
6	300, 600, 900	0.0014	450	235.1	261.2	45.5, 218.5, 363.0
7	300, 600, 900	0.0022	250	168.9	187.7	52.5, 144.0, 176.5
8	300, 600, 900	0.0022	350	222.1	246.8	41.0, 195.5, 247.0
9	300, 600, 900	0.0022	450	269.5	299.4	52.0, 260.5, 366.0
10	300, 600, 900	0.0029	250	176.2	195.8	58.5, 157.5, 188.0
11	300, 600, 900	0.0029	350	234.1	260.1	61.0, 220.0, 272.5
12	300, 600, 900	0.0029	450	287.0	318.9	61.0, 281.5, 361.5
13	300, 600, 900	0.0059	250	190.8	212.0	99.0, 167.5, 199.0
14	300, 600, 900	0.0059	350	258.3	287.0	100.5, 207.0, 257.5
15	300, 600, 900, 1200	0.0059	450	457.0	380.9	130.0, 282.0, 347.0 367.5
16	300, 600, 900, 1200	0.0089	250	272.2	226.7	92.5, 145.5, 169.5 191.0
17	300, 600, 900, 1200	0.0089	350	374.0	311.4	122.5, 224.0, 270.0, 286.0
18	300, 600, 900, 1200	0.0089	450	472.8	393.7	159.0, 284.5, 337.0, 359.0
19	300, 600, 900	0.0120	250	201.1	223.4	77.0, 132.0, 160.0
20	300, 600, 900	0.0120	350	275.3	305.9	131.0, 206.0, 246.0
21	300, 600, 900, 1200	0.0120	450	482.2	401.5	169.0, 291.0, 340.5, 358.0
22	300, 600, 900, 1200	0.0237	250	283.1	235.7	100.5, 150.5, 172.0, 190.0
23	300, 600, 900, 1200	0.0237	350	391.9	326.3	138.5, 214.5, 247.5, 257.0

24	300, 600, 900, 1200	0.0237	450	498.9	415.4	226.5, 320.0, 347.0, 369.0
25	300, 600, 900	0.0353	250	211.1	234.6	108.5, 154.0, 175.5
26	300, 600, 900	0.0353	350	291.9	324.3	164.0, 263.0, 303.5
27	300, 600, 900	0.0353	450	371.4	412.7	215.0, 309.0, 337.5
28	300, 600, 900	0.0470	250	213.0	236.7	114.0, 157.0, 177.5
29	300, 600, 900	0.0470	350	295.0	327.8	182.5, 216.5, 239.5
30	300, 600, 900	0.0470	450	375.9	417.7	230.5, 341.5, 377.5
31	300, 600, 900, 1200	0.0007	650	344.3	286.9	34.5, 82.0, 232.0, 459.0
32	300, 600, 900, 1200	0.0029	650	526.1	438.4	64.5, 326.5, 503.0, 552.0
33	300, 600, 900, 1200	0.0120	650	643.3	536.1	219.5, 463.5, 523.0, 535.5
34	300, 600, 900, 1200	0.0470	650	711.2	592.6	286.0, 444.5, 531.0, 519.5

APPENDIX C. THERMAL TEST RESULTS

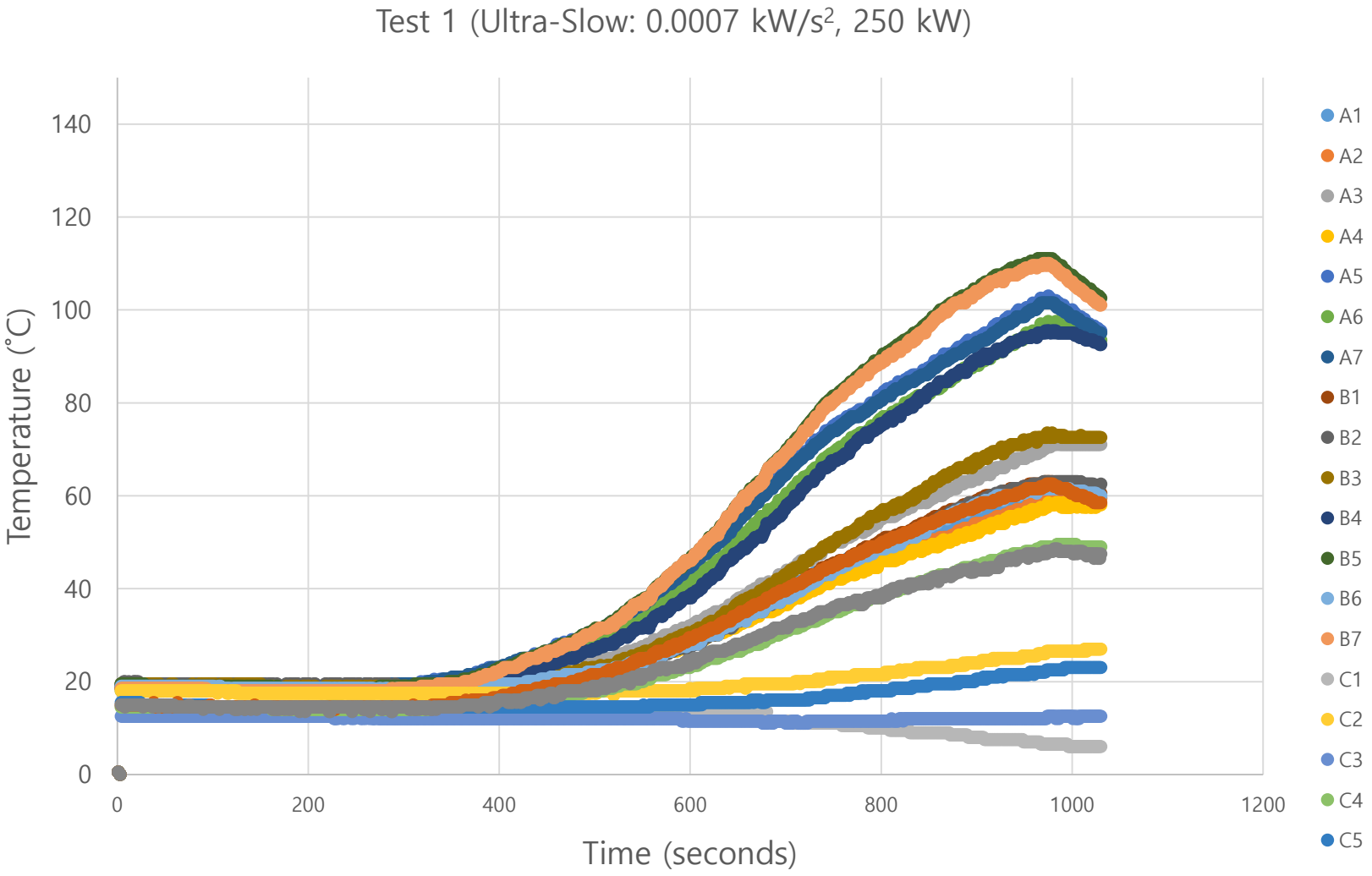

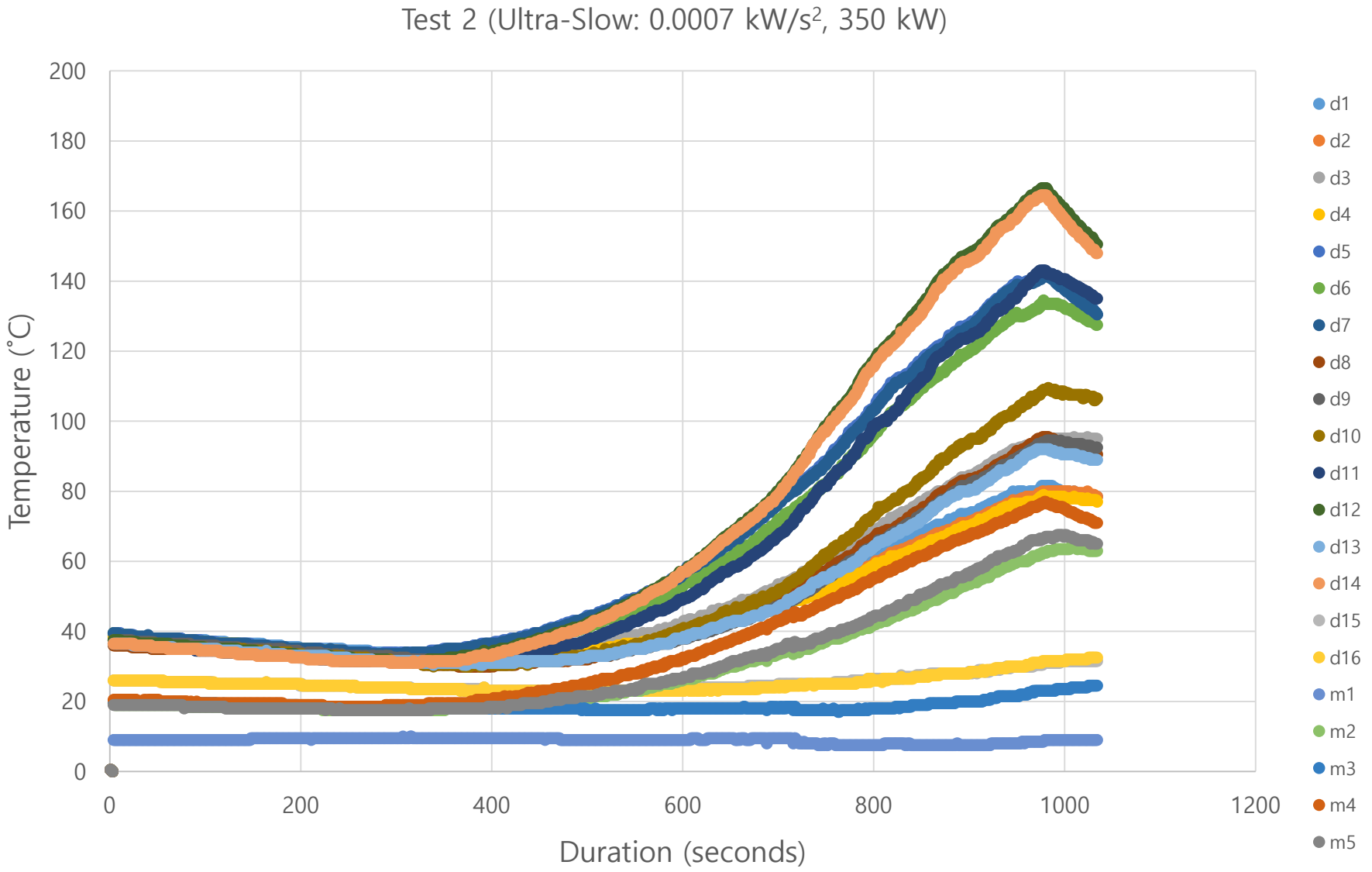
Test 2 (Ultra-Slow: 0.0007 kW/s², 350 kW)
Temperature (°C)
200
180
160
140
120
100
80
60
40
20
0
0
200
400
600
800
1000
1200
Duration (seconds)
d1
d2
d3
d4
d5
d6
d7
d8
d9
d10
d11
d12
d13
d14
d15
d16
m1
m2
m3
m4
m5

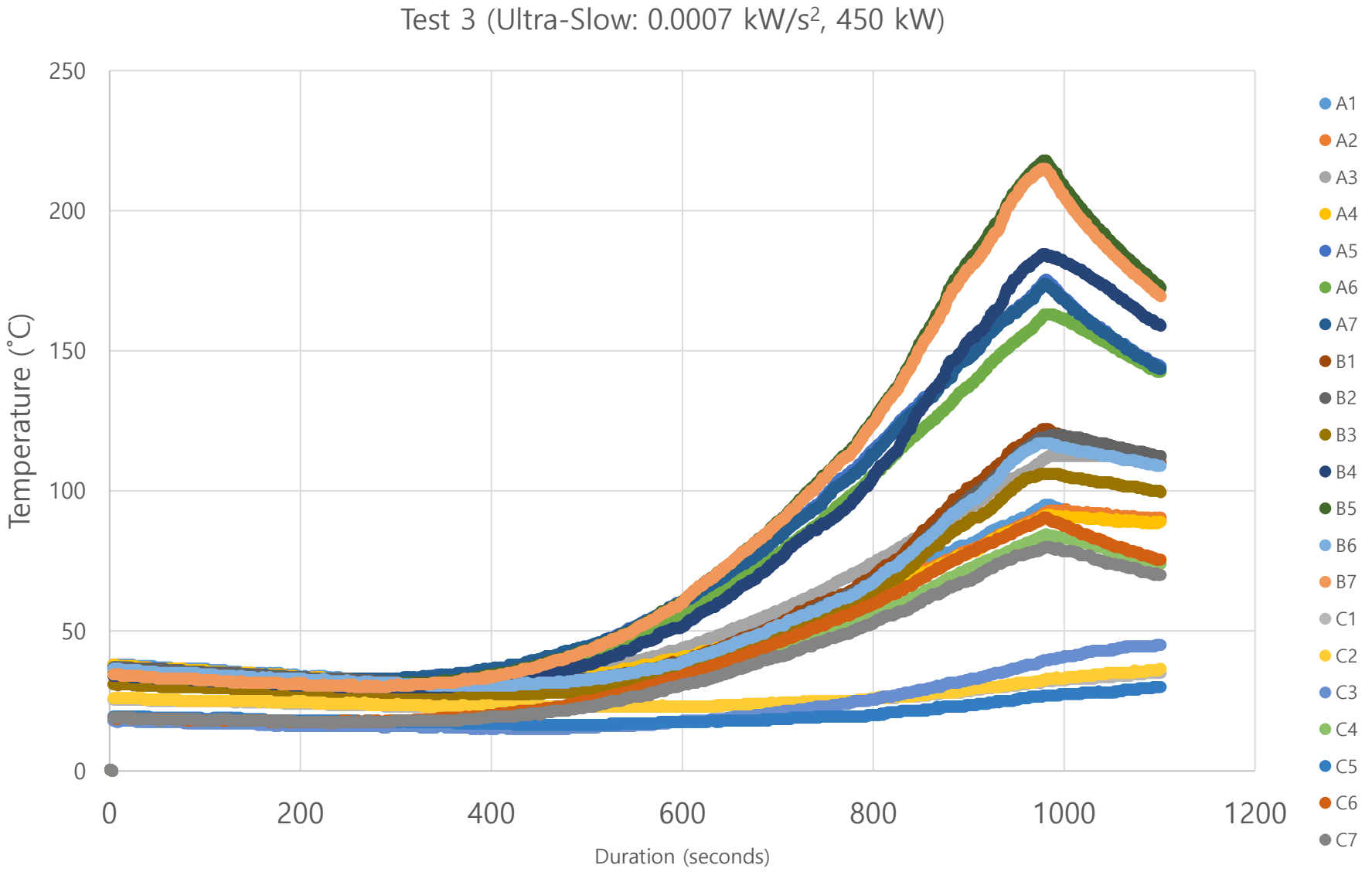
Test 3 (Ultra-Slow: 0.0007 kW/s², 450 kW)
Temperature (°C)
250
200
150
100
50
0
0
200
400
600
800
1000
1200
Duration (seconds)
A1
A2
A3
A4
A5
A6
A7
B1
B2
B3
B4
B5
B6
B7
C1
C2
C3
C4
C5
C6
C7

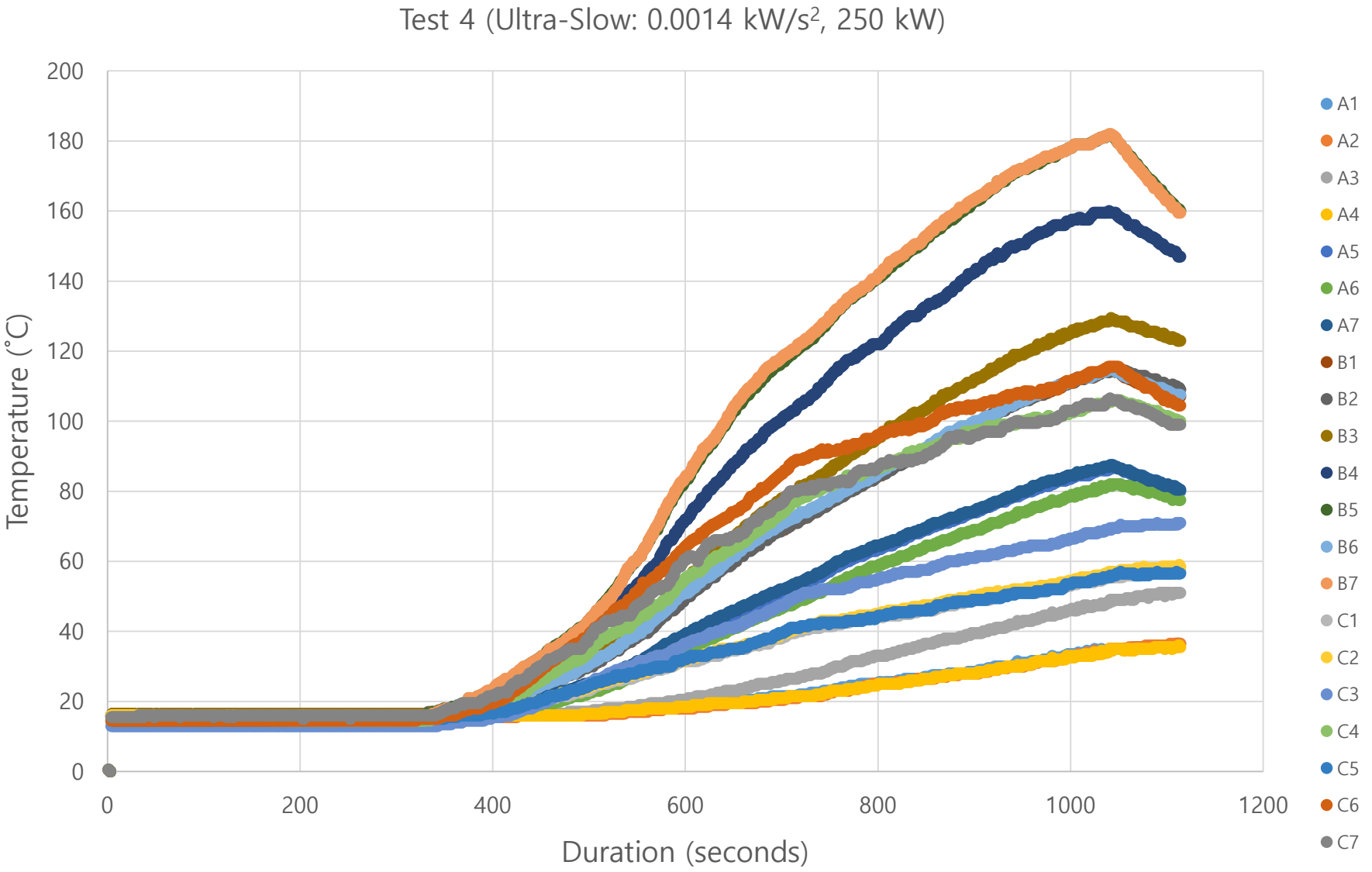
Test 4 (Ultra-Slow: 0.0014 kW/s², 250 kW)
Temperature (°C)
200
180
160
140
120
100
80
60
40
20
0
0
200
400
600
800
1000
1200
Duration (seconds)
A1
A2
A3
A4
A5
A6
A7
B1
B2
B3
B4
B5
B6
B7
C1
C2
C3
C4
C5
C6
C7

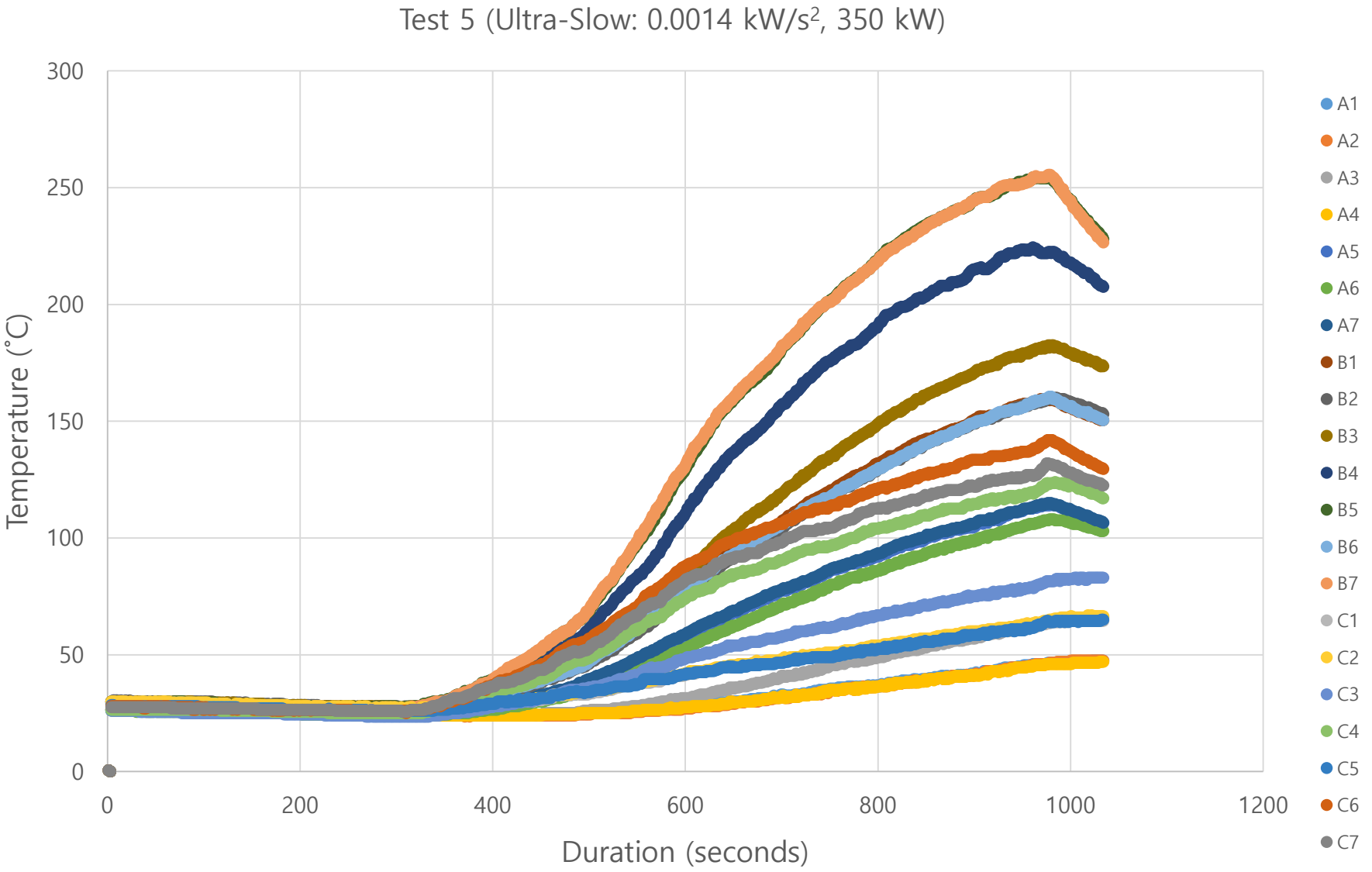
Test 5 (Ultra-Slow: 0.0014 kW/s², 350 kW)
Temperature (°C)
300
250
200
150
100
50
0
0
200
400
600
800
1000
1200
Duration (seconds)
A1
A2
A3
A4
A5
A6
A7
B1
B2
B3
B4
B5
B6
B7
C1
C2
C3
C4
C5
C6
C7

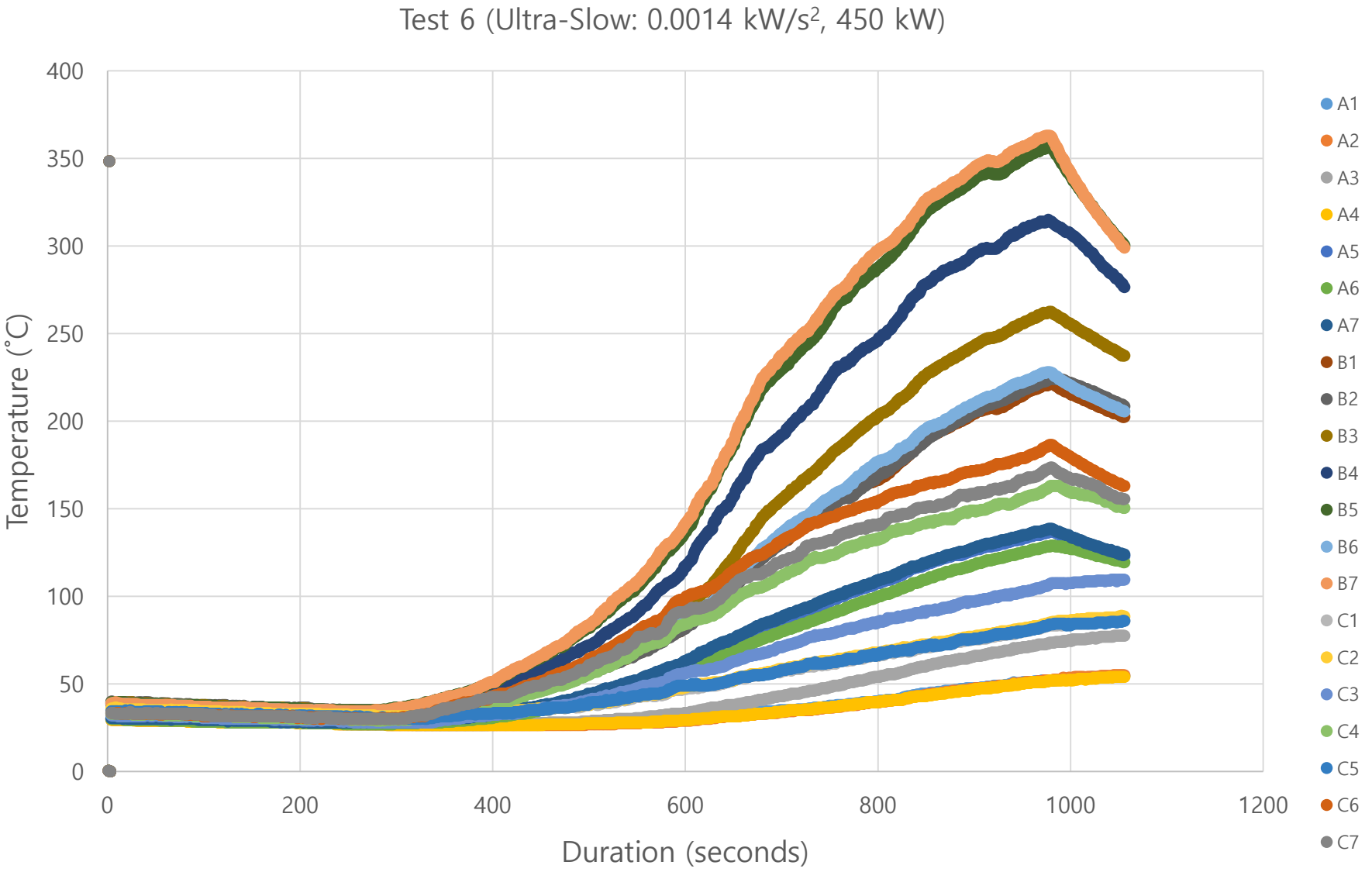
Test 6 (Ultra-Slow: 0.0014 kW/s², 450 kW)
Temperature (°C)
400
350
300
250
200
150
100
50
0
0
200
400
600
800
1000
1200
Duration (seconds)
A1
A2
A3
A4
A5
A6
A7
B1
B2
B3
B4
B5
B6
B7
C1
C2
C3
C4
C5
C6
C7

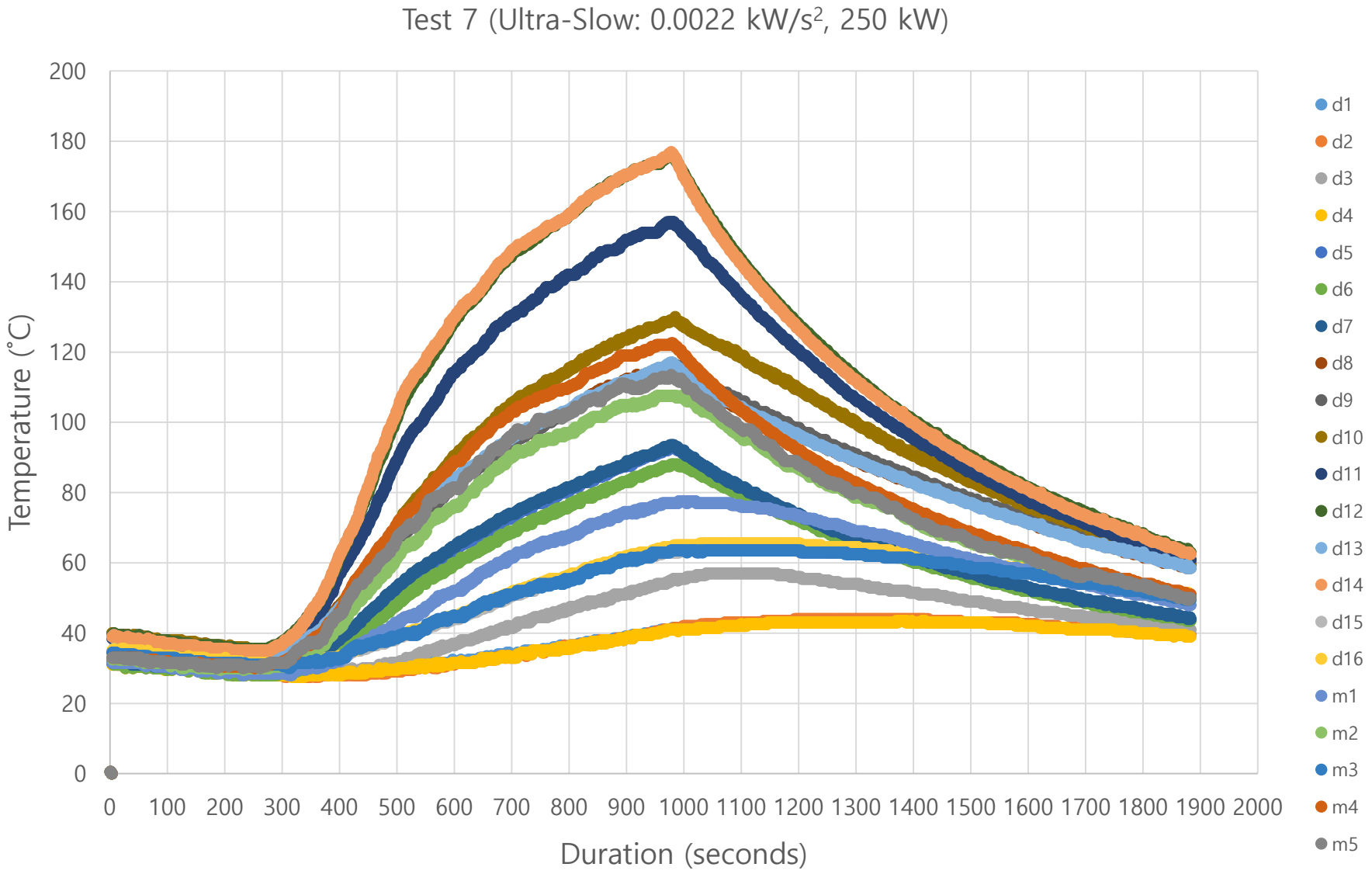
Test 7 (Ultra-Slow: 0.0022 kW/s², 250 kW)
Temperature (°C)
200
180
160
140
120
100
80
60
40
20
0
0 100 200 300 400 500 600 700 800 900 1000 1100 1200 1300 1400 1500 1600 1700 1800 1900 2000
Duration (seconds)
d1
d2
d3
d4
d5
d6
d7
d8
d9
d10
d11
d12
d13
d14
d15
d16
m1
m2
m3
m4
m5

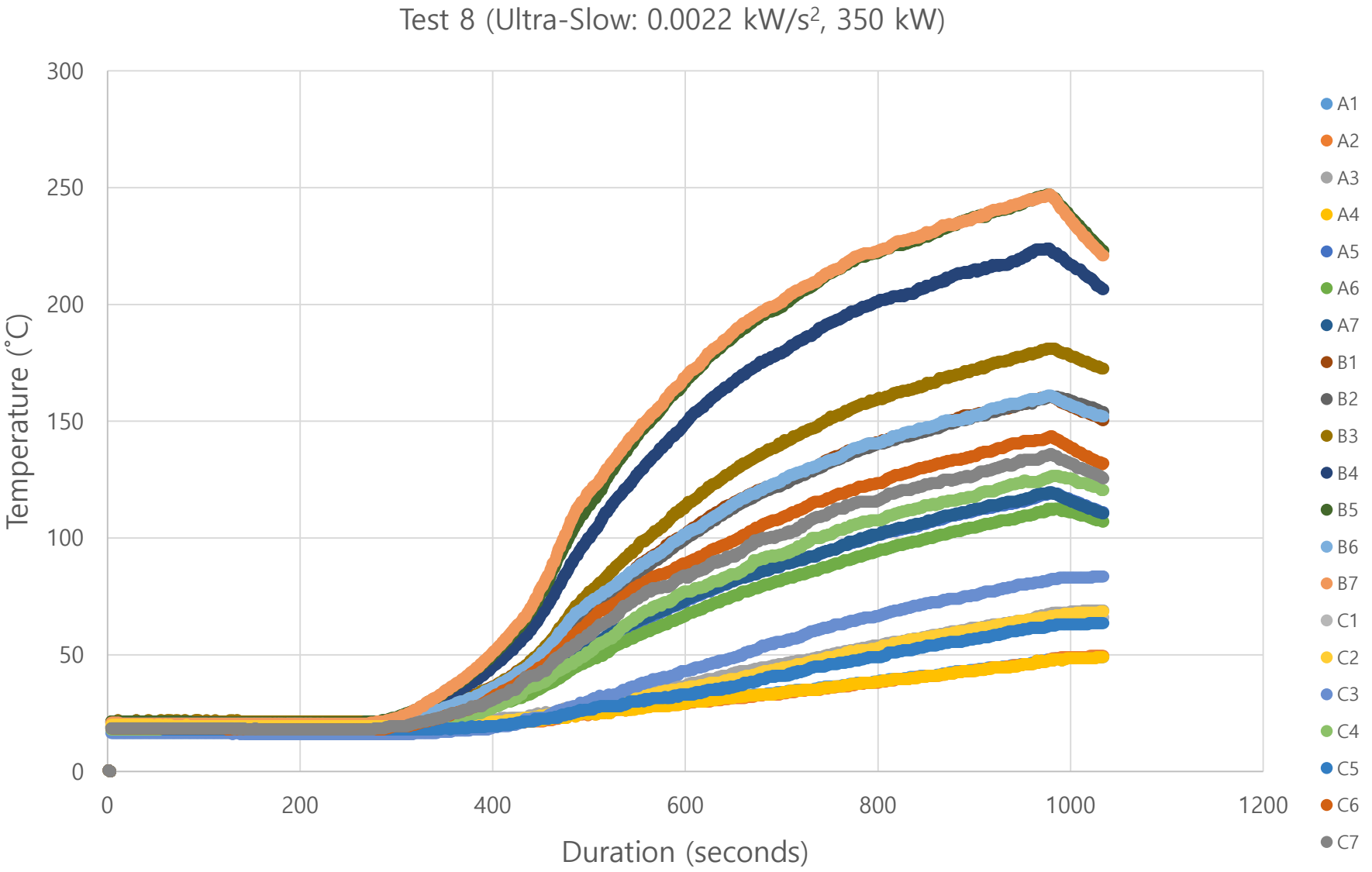
Test 8 (Ultra-Slow: 0.0022 kW/s², 350 kW)
Temperature (°C)
300
250
200
150
100
50
0
0
200
400
600
800
1000
1200
Duration (seconds)
A1
A2
A3
A4
A5
A6
A7
B1
B2
B3
B4
B5
B6
B7
C1
C2
C3
C4
C5
C6
C7

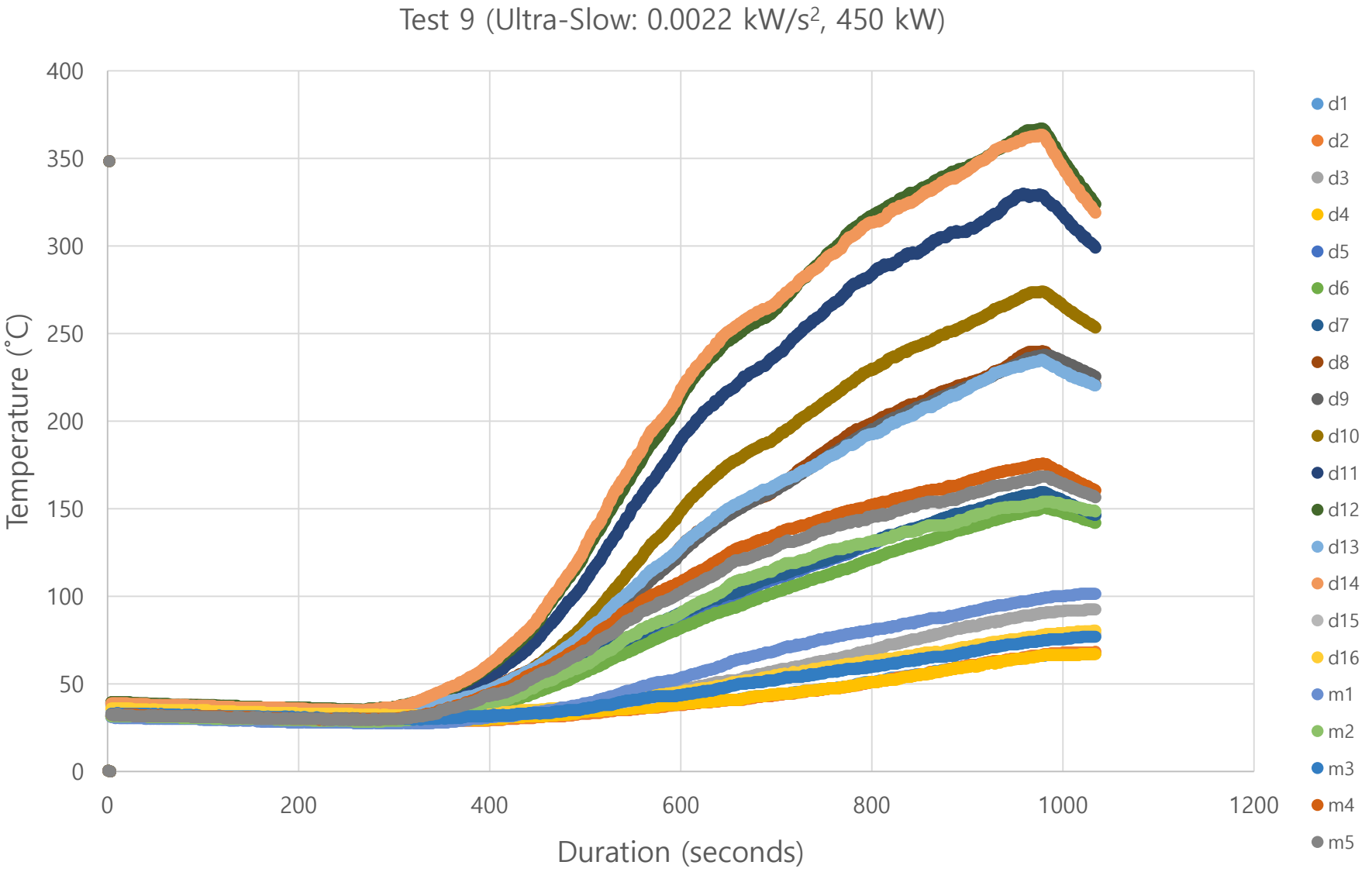
Test 9 (Ultra-Slow: 0.0022 kW/s², 450 kW)
Temperature (°C)
400
350
300
250
200
150
100
50
0
0
200
400
600
800
1000
1200
Duration (seconds)
d1
d2
d3
d4
d5
d6
d7
d8
d9
d10
d11
d12
d13
d14
d15
d16
m1
m2
m3
m4
m5

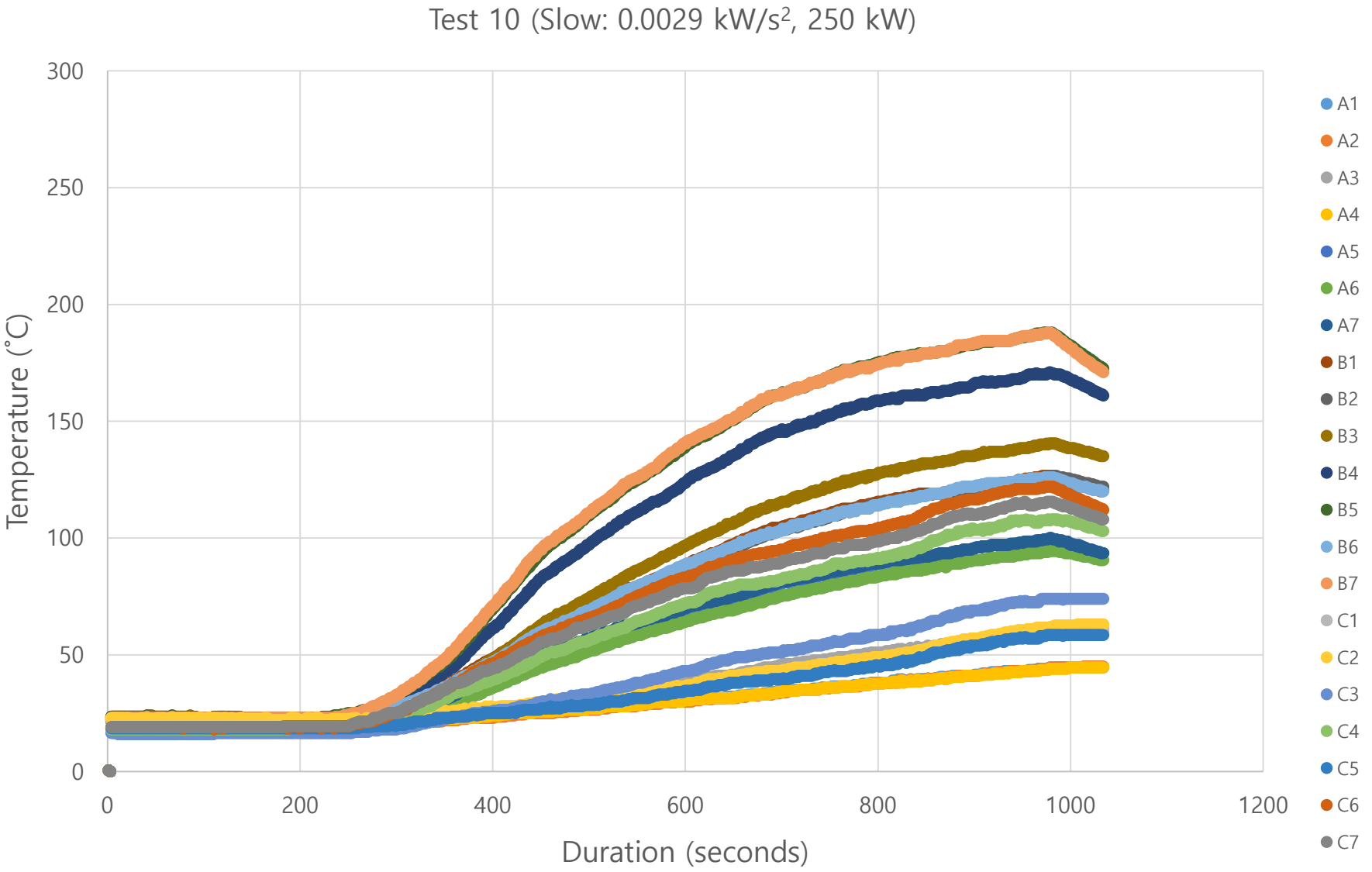
Test 10 (Slow: 0.0029 kW/s², 250 kW)
Temperature (°C)
300
250
200
150
100
50
0
0
200
400
600
800
1000
1200
Duration (seconds)
A1
A2
A3
A4
A5
A6
A7
B1
B2
B3
B4
B5
B6
B7
C1
C2
C3
C4
C5
C6
C7

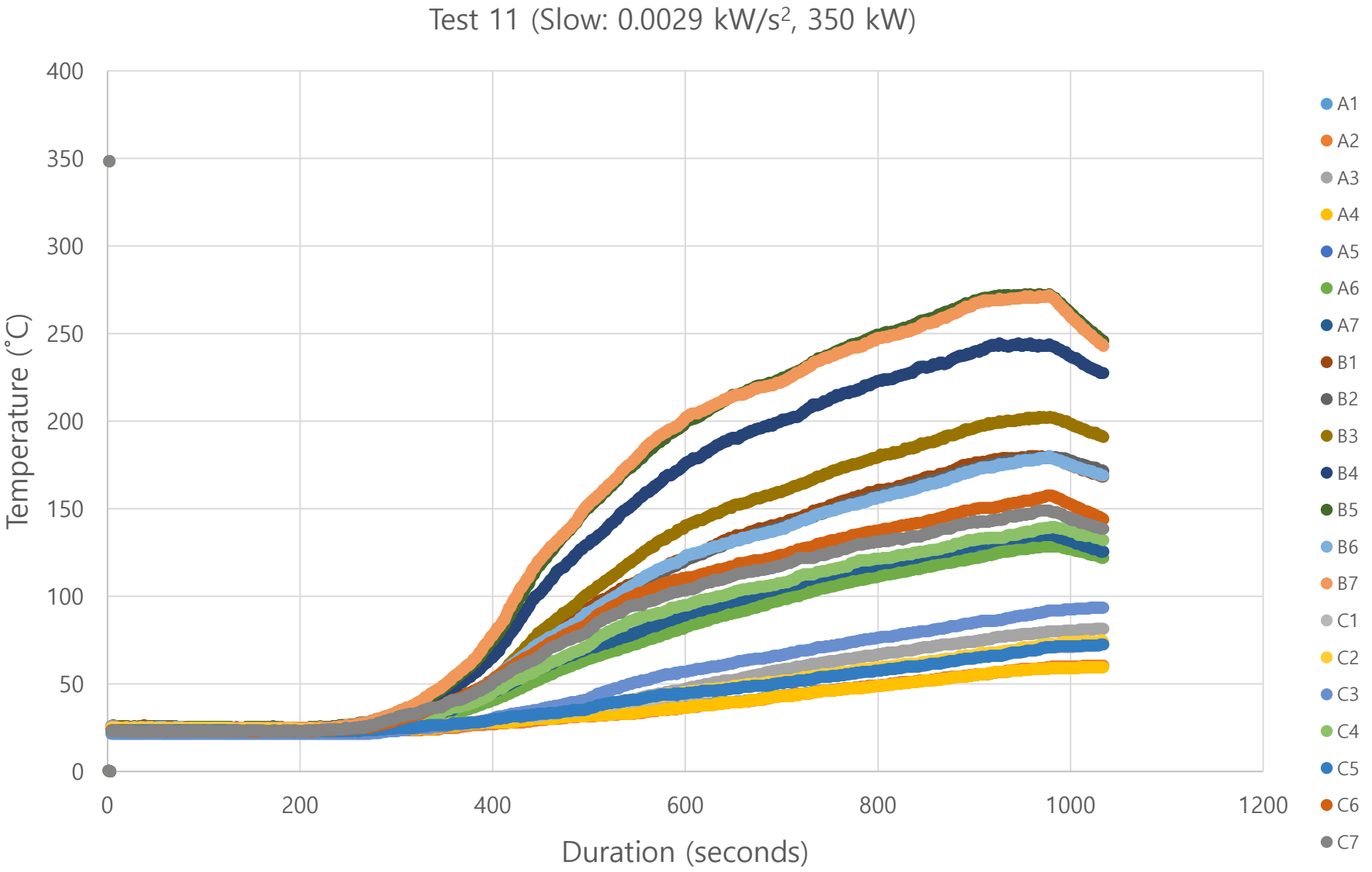
Test 11 (Slow: 0.0029 kW/s², 350 kW)
Temperature (°C)
400
350
300
250
200
150
100
50
0
0
200
400
600
800
1000
1200
Duration (seconds)
A1
A2
A3
A4
A5
A6
A7
B1
B2
B3
B4
B5
B6
B7
C1
C2
C3
C4
C5
C6
C7

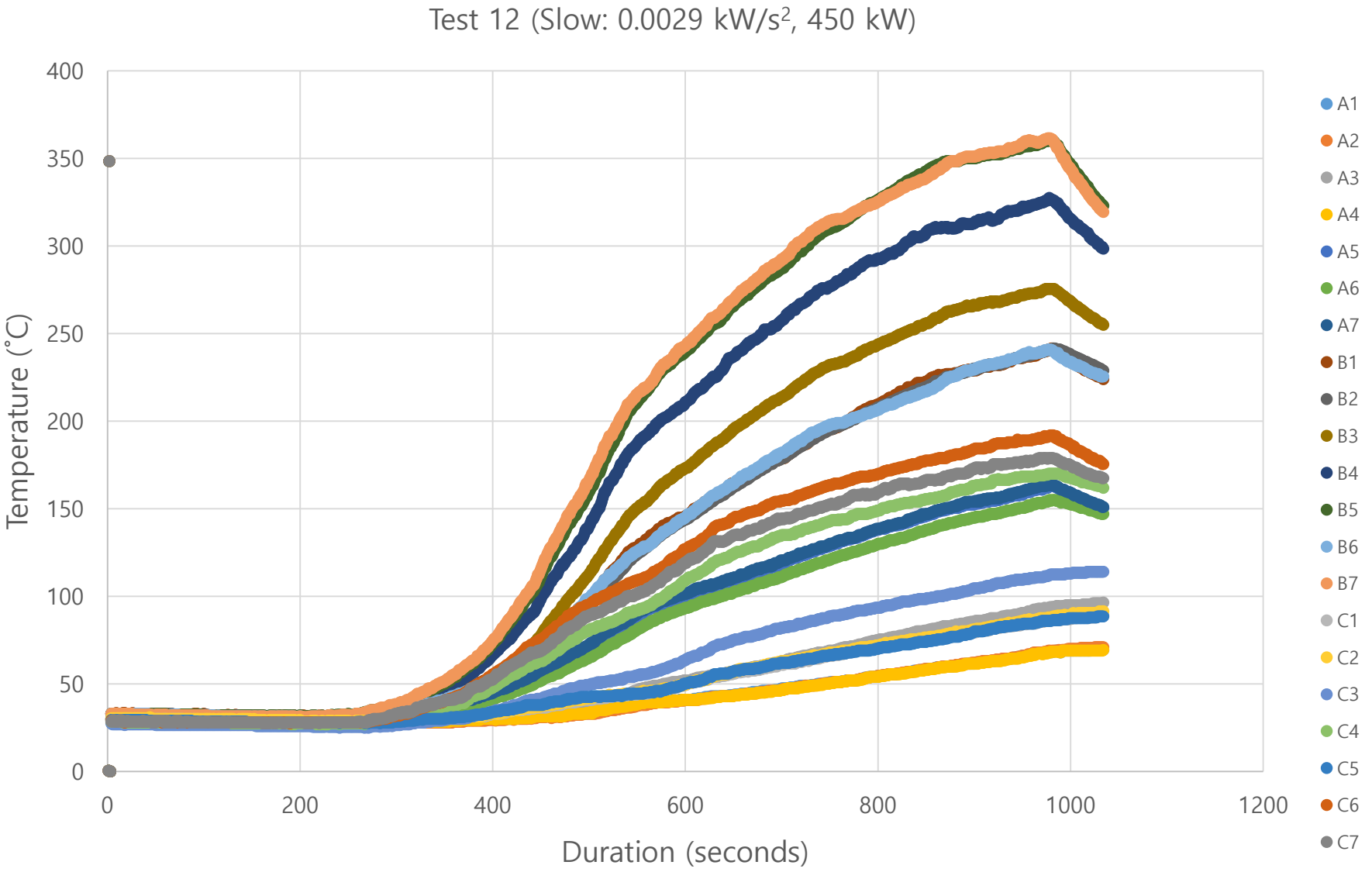
Test 12 (Slow: 0.0029 kW/s², 450 kW)
Temperature (°C)
400
350
300
250
200
150
100
50
0
0
200
400
600
800
1000
1200
Duration (seconds)
A1
A2
A3
A4
A5
A6
A7
B1
B2
B3
B4
B5
B6
B7
C1
C2
C3
C4
C5
C6
C7

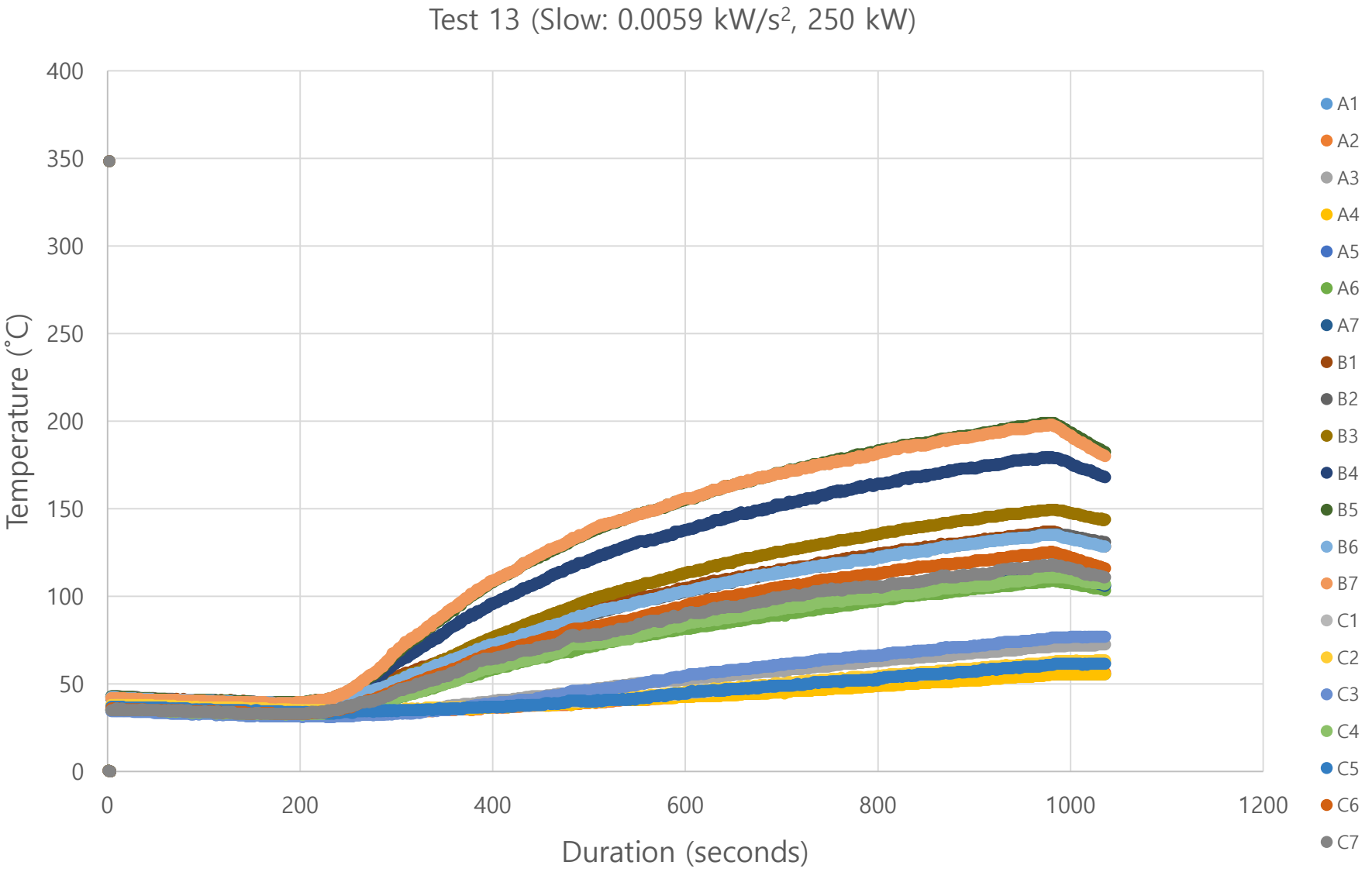
Test 13 (Slow: 0.0059 kW/s², 250 kW)
Temperature (°C)
400
350
300
250
200
150
100
50
0
0
200
400
600
800
1000
1200
Duration (seconds)
A1
A2
A3
A4
A5
A6
A7
B1
B2
B3
B4
B5
B6
B7
C1
C2
C3
C4
C5
C6
C7

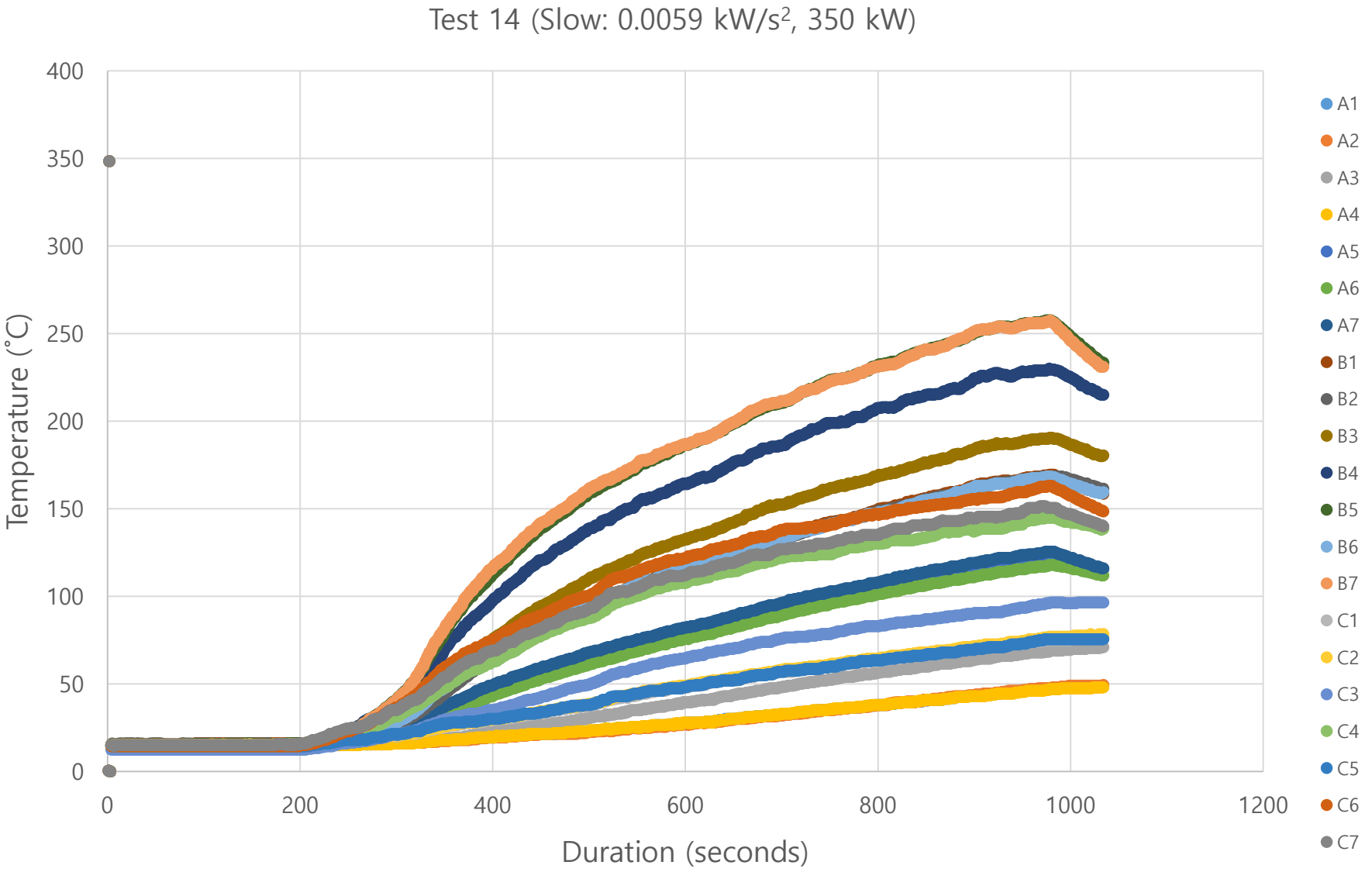
Test 14 (Slow: 0.0059 kW/s², 350 kW)
Temperature (°C)
400
350
300
250
200
150
100
50
0
0
200
400
600
800
1000
1200
Duration (seconds)
A1
A2
A3
A4
A5
A6
A7
B1
B2
B3
B4
B5
B6
B7
C1
C2
C3
C4
C5
C6
C7

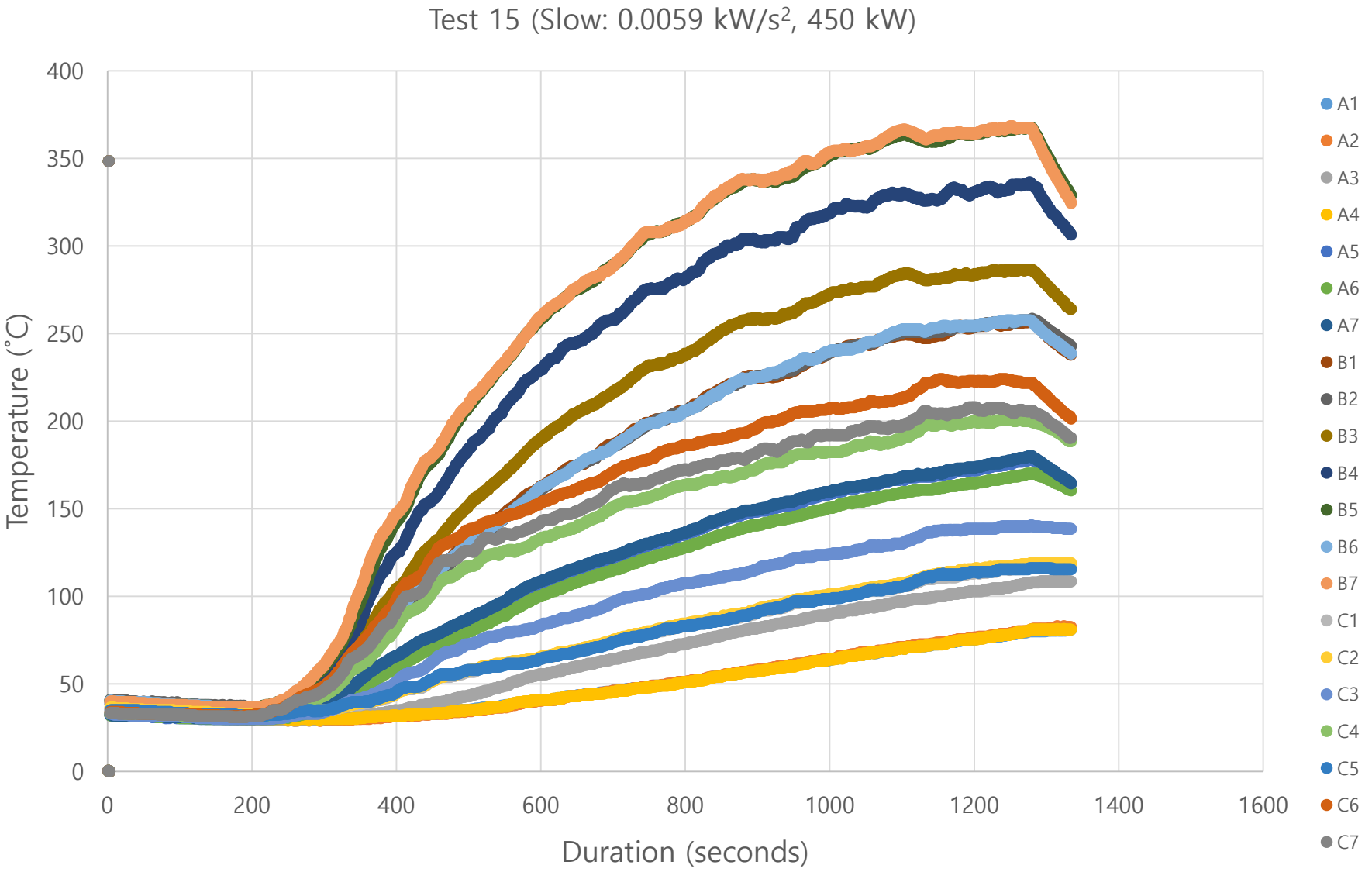
Test 15 (Slow: 0.0059 kW/s², 450 kW)
Temperature (°C)
400
350
300
250
200
150
100
50
0
0
200
400
600
800
1000
1200
1400
1600
Duration (seconds)
A1
A2
A3
A4
A5
A6
A7
B1
B2
B3
B4
B5
B6
B7
C1
C2
C3
C4
C5
C6
C7

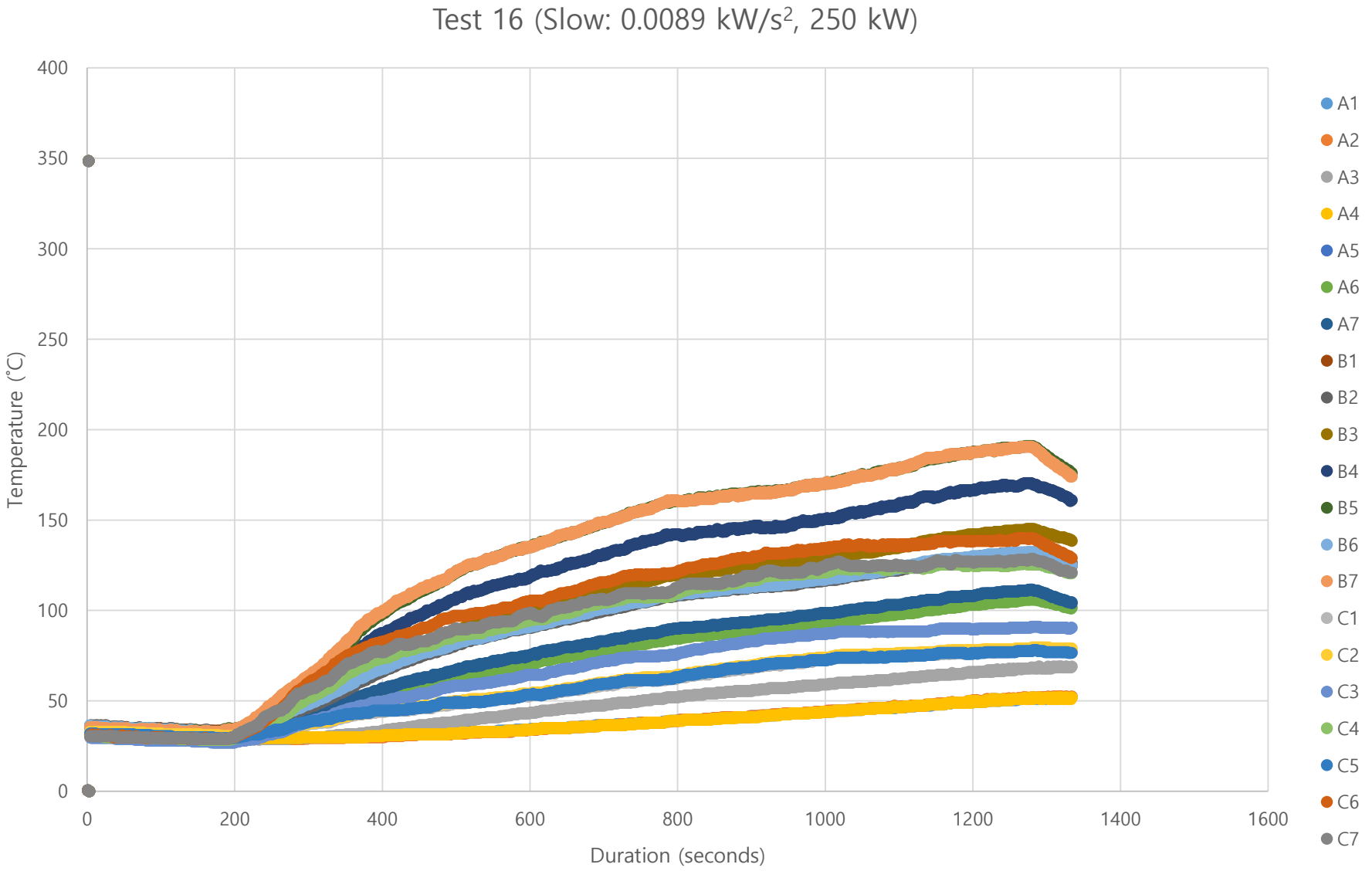
Test 16 (Slow: 0.0089 kW/s², 250 kW)
Temperature (°C)
400
350
300
250
200
150
100
50
0
0
200
400
600
800
1000
1200
1400
1600
Duration (seconds)
A1
A2
A3
A4
A5
A6
A7
B1
B2
B3
B4
B5
B6
B7
C1
C2
C3
C4
C5
C6
C7

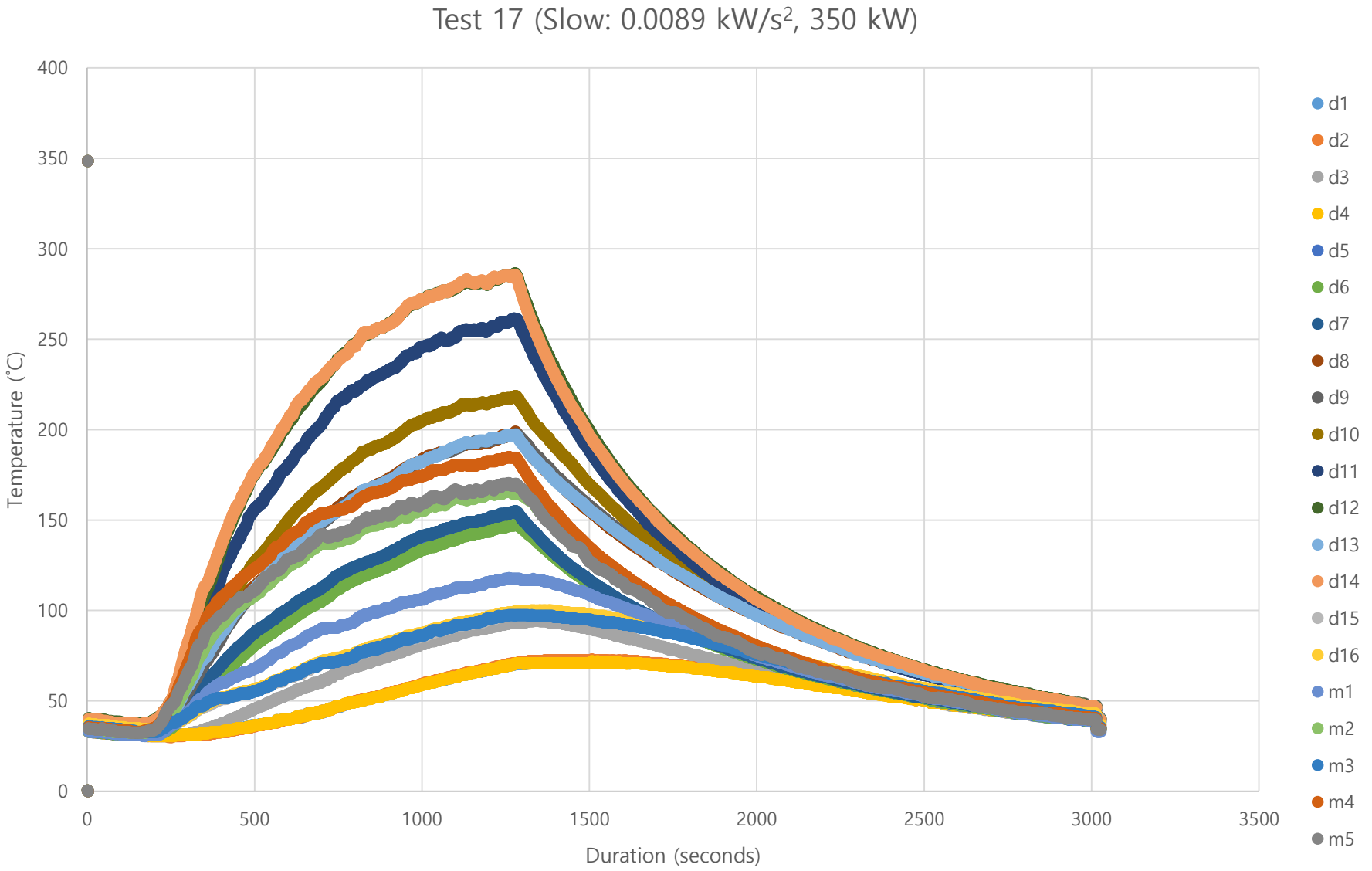
Test 17 (Slow: 0.0089 kW/s², 350 kW)
Temperature (°C)
400
350
300
250
200
150
100
50
0
0
500
1000
1500
2000
2500
3000
3500
Duration (seconds)
d1
d2
d3
d4
d5
d6
d7
d8
d9
d10
d11
d12
d13
d14
d15
d16
m1
m2
m3
m4
m5

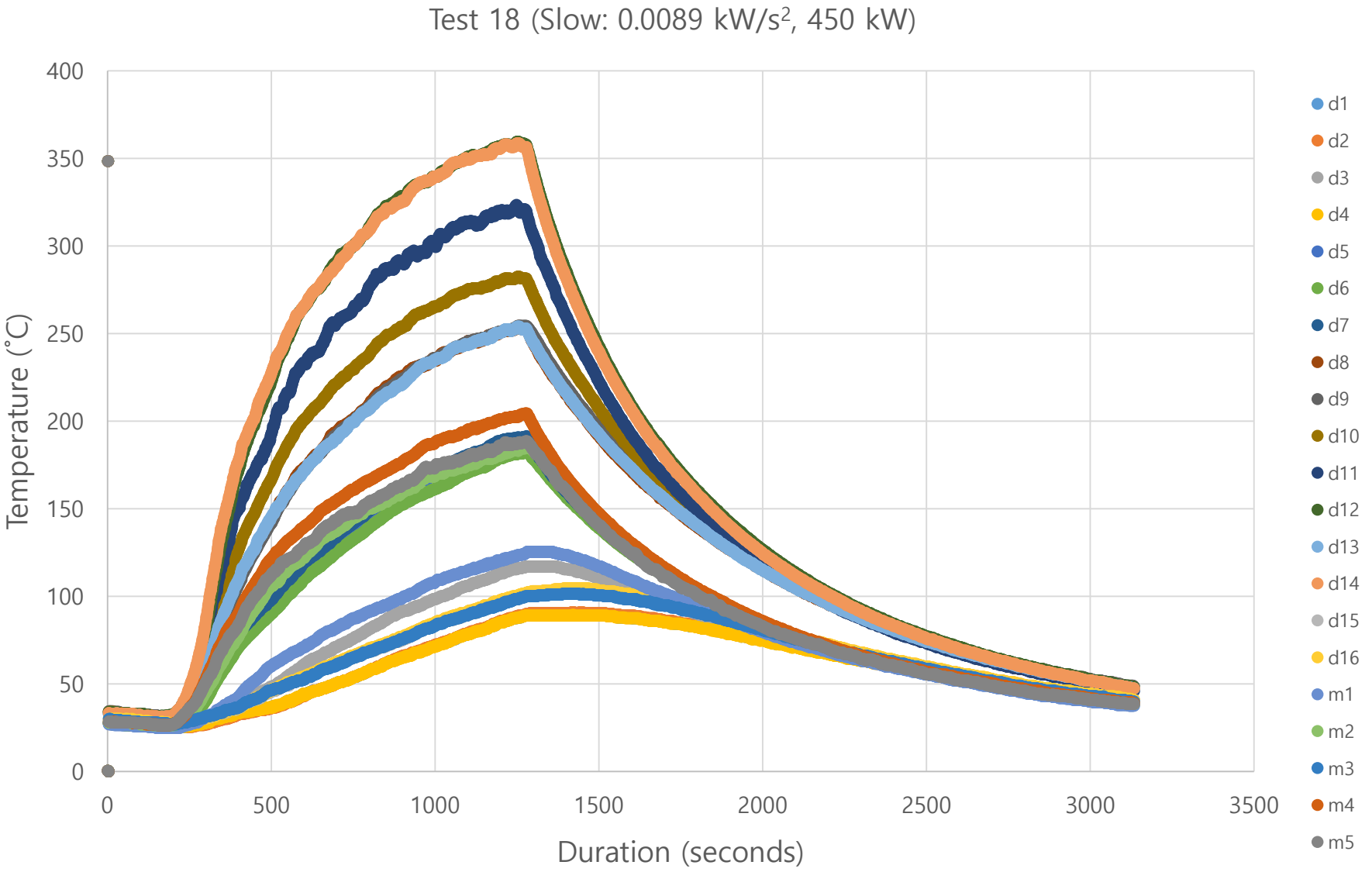
Test 18 (Slow: 0.0089 kW/s², 450 kW)
Temperature (˚C)
400
350
300
250
200
150
100
50
0
0
500
1000
1500
2000
2500
3000
3500
Duration (seconds)
d1
d2
d3
d4
d5
d6
d7
d8
d9
d10
d11
d12
d13
d14
d15
d16
m1
m2
m3
m4
m5

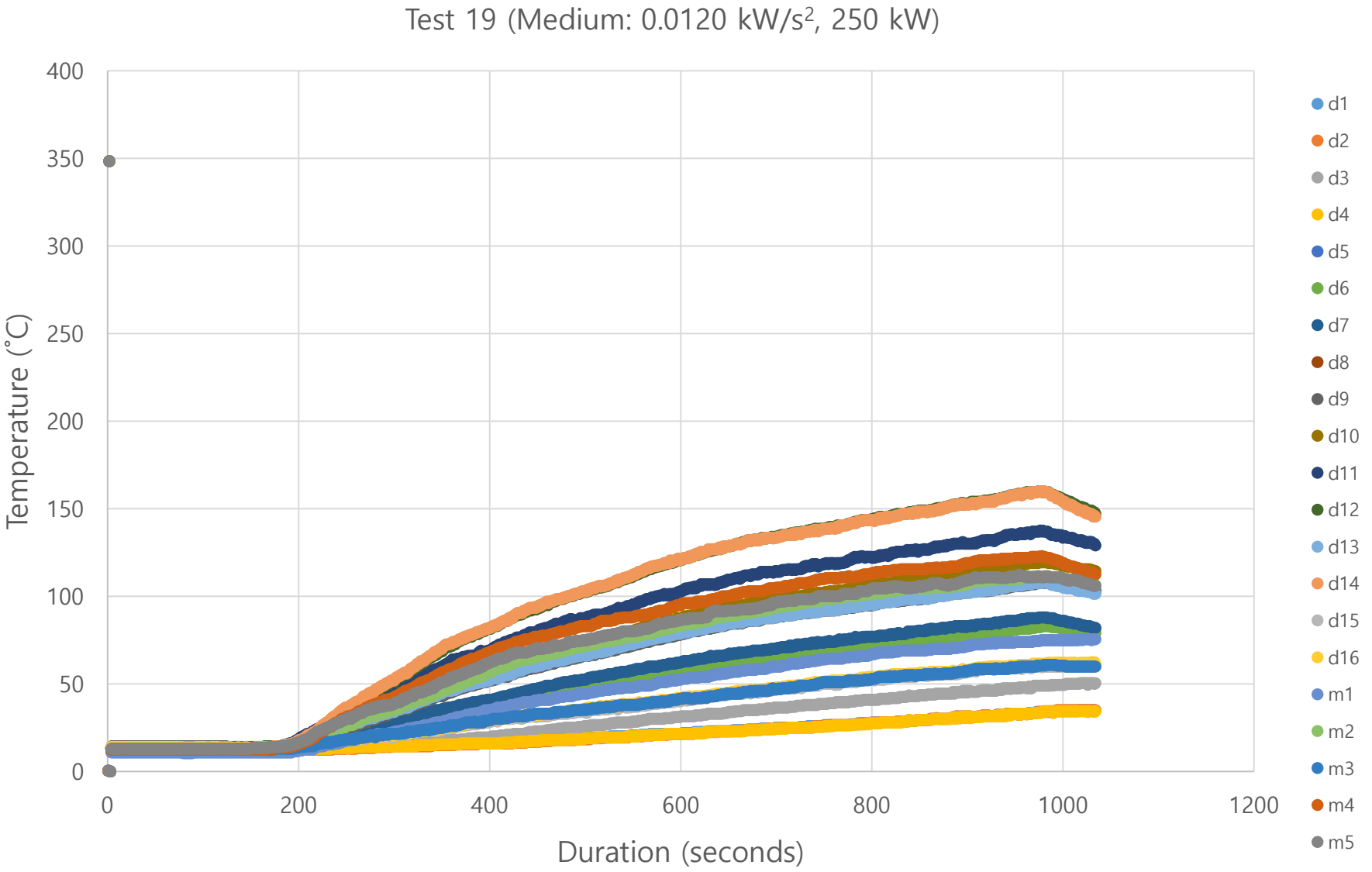
Test 19 (Medium: 0.0120 kW/s², 250 kW)
Temperature (°C)
400
350
300
250
200
150
100
50
0
0
200
400
600
800
1000
1200
Duration (seconds)
d1
d2
d3
d4
d5
d6
d7
d8
d9
d10
d11
d12
d13
d14
d15
d16
m1
m2
m3
m4
m5

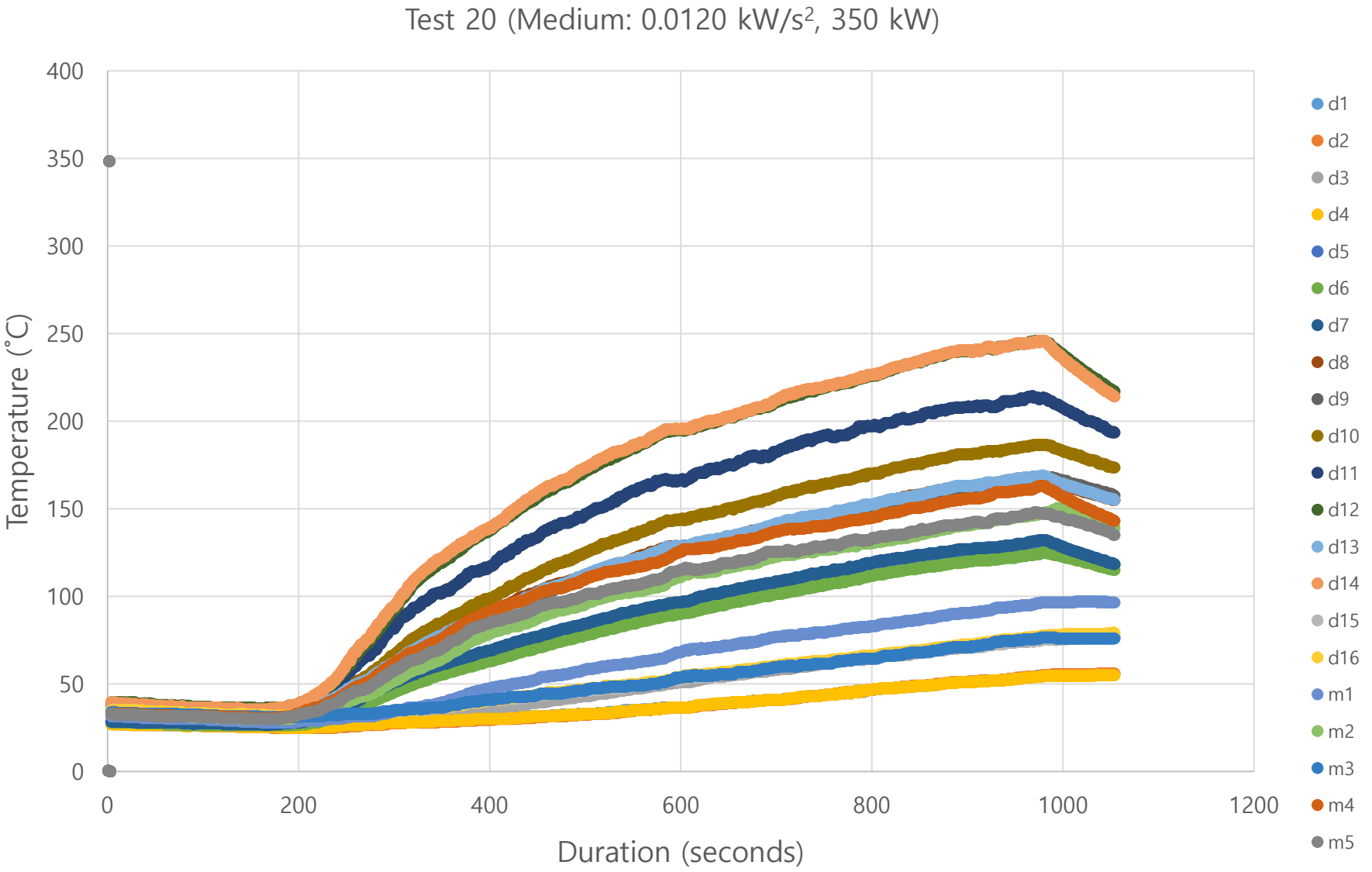
Test 20 (Medium: 0.0120 kW/s², 350 kW)
Temperature (°C)
400
350
300
250
200
150
100
50
0
0
200
400
600
800
1000
1200
Duration (seconds)
d1
d2
d3
d4
d5
d6
d7
d8
d9
d10
d11
d12
d13
d14
d15
d16
m1
m2
m3
m4
m5

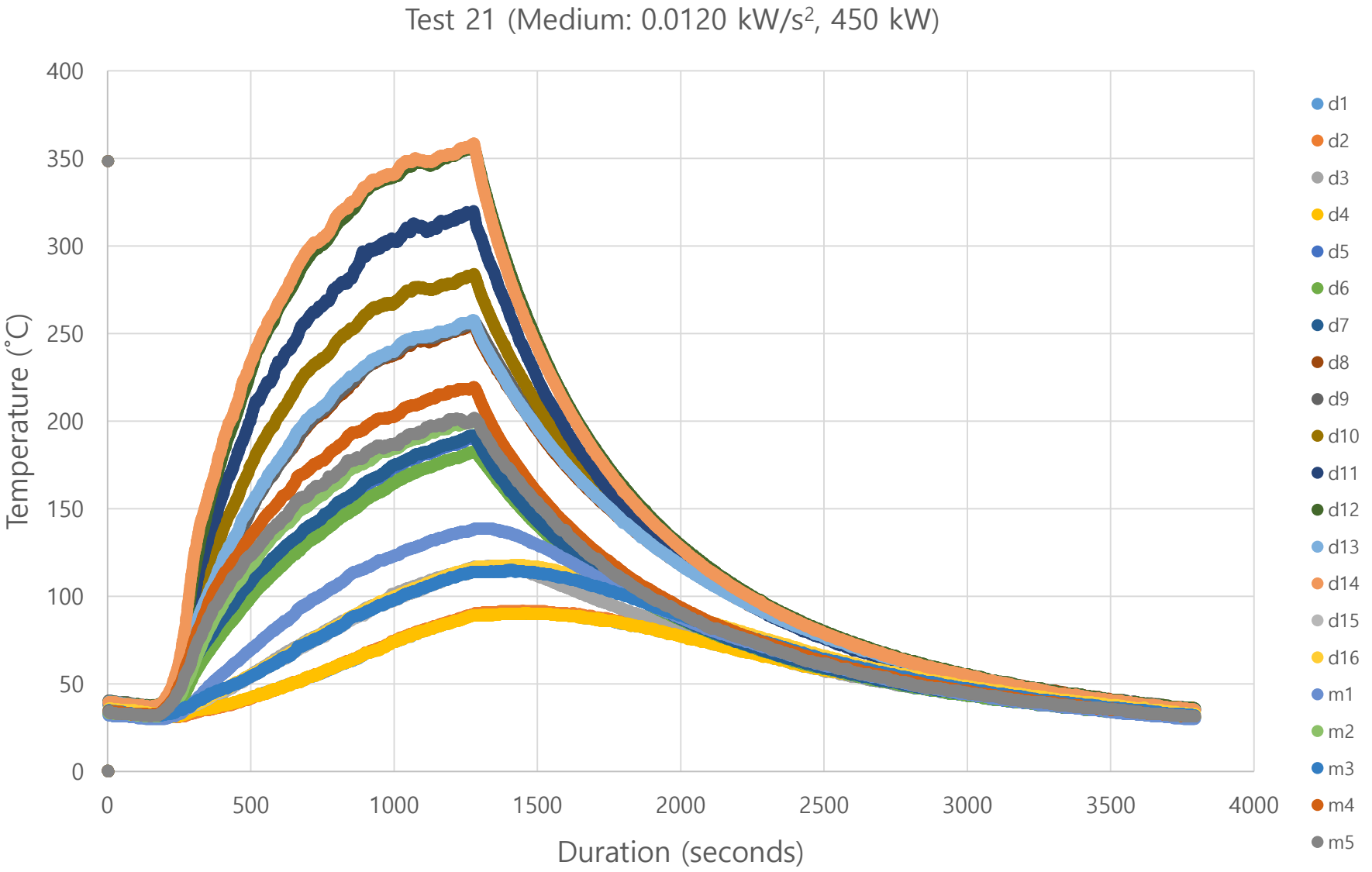
Test 21 (Medium: 0.0120 kW/s², 450 kW)
Temperature (°C)
400
350
300
250
200
150
100
50
0
0
500
1000
1500
2000
2500
3000
3500
4000
Duration (seconds)
d1
d2
d3
d4
d5
d6
d7
d8
d9
d10
d11
d12
d13
d14
d15
d16
m1
m2
m3
m4
m5

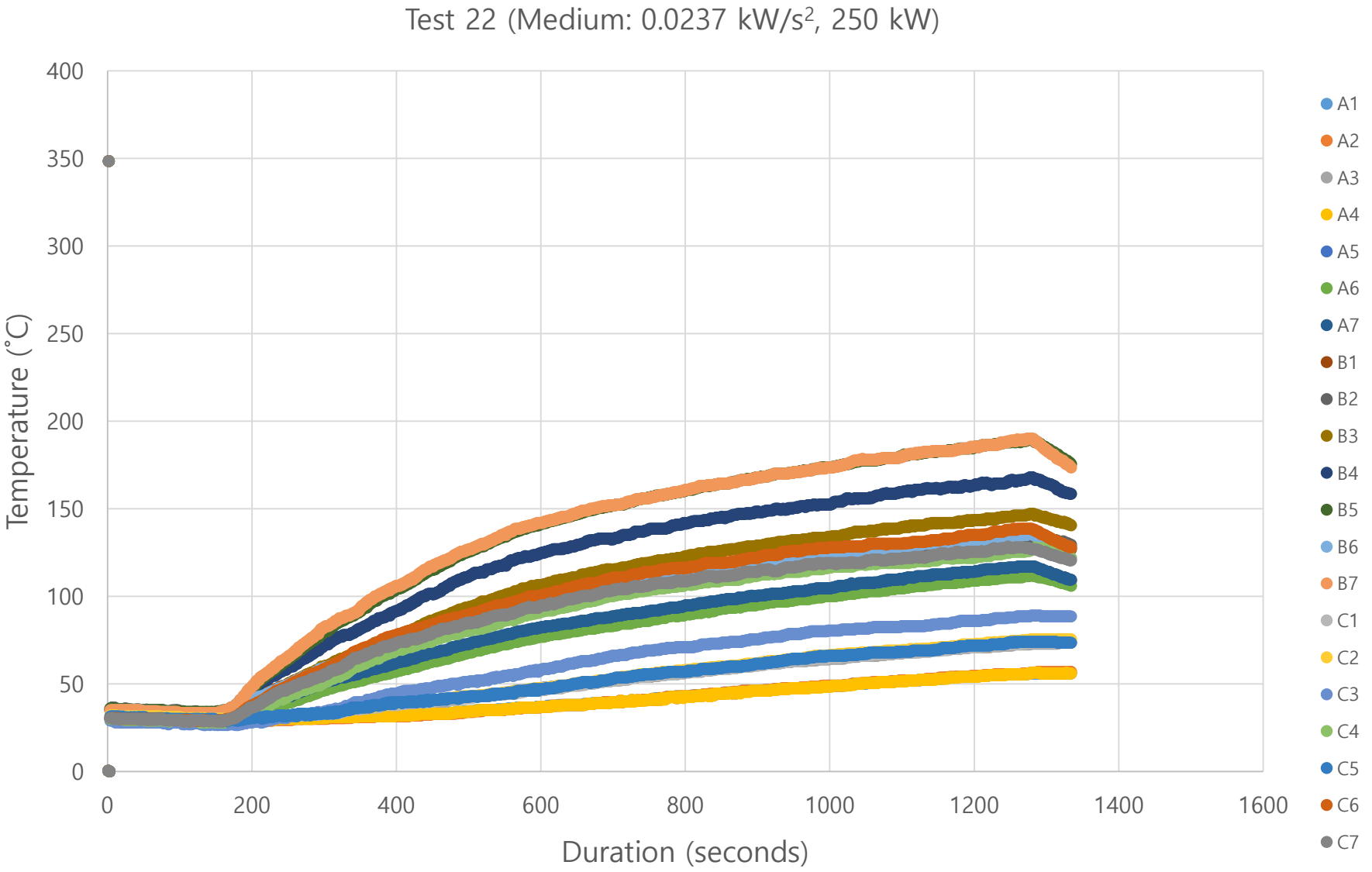
Test 22 (Medium: 0.0237 kW/s², 250 kW)
Temperature (°C)
400
350
300
250
200
150
100
50
0
0
200
400
600
800
1000
1200
1400
1600
Duration (seconds)
A1
A2
A3
A4
A5
A6
A7
B1
B2
B3
B4
B5
B6
B7
C1
C2
C3
C4
C5
C6
C7

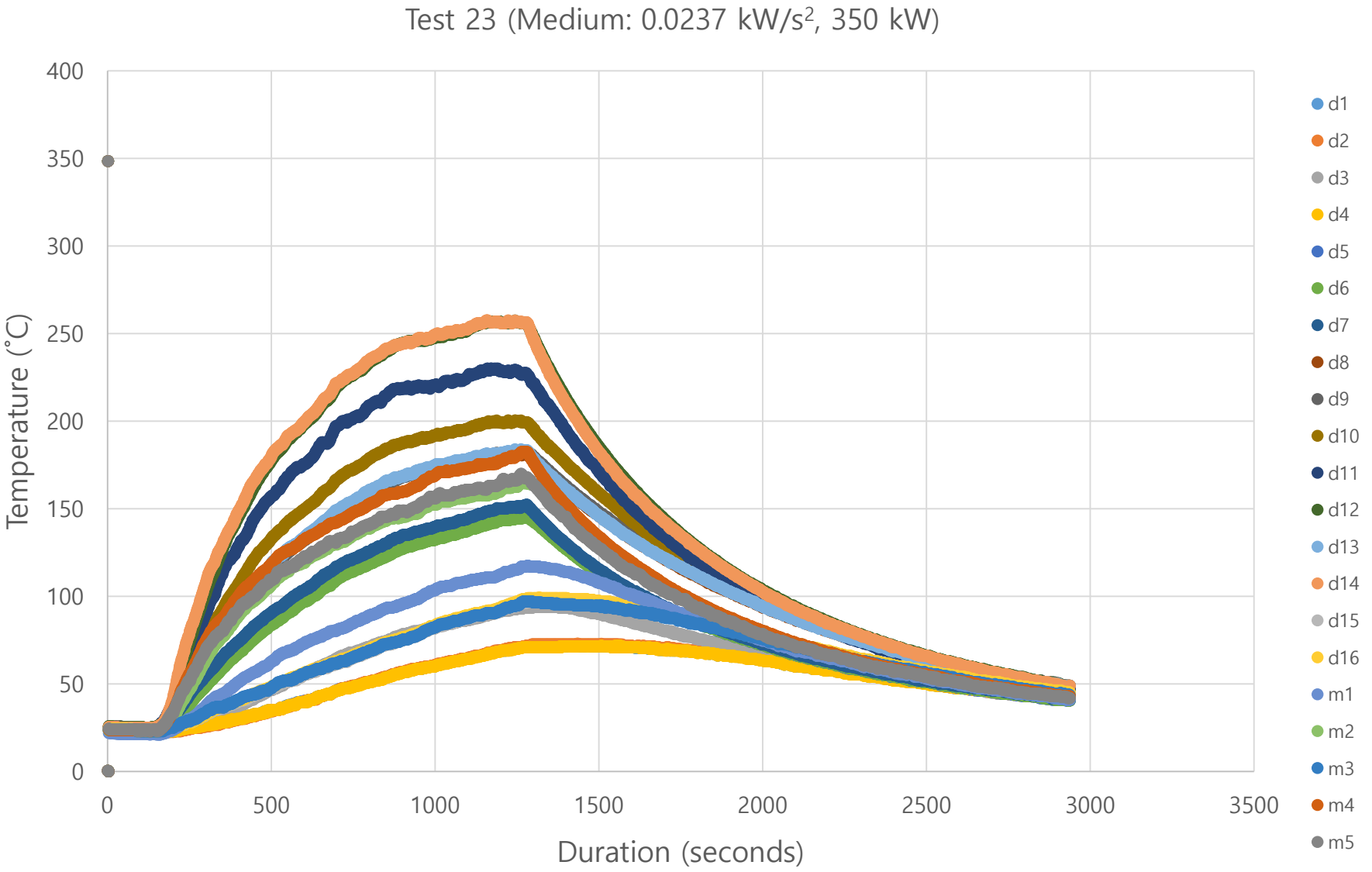
Test 23 (Medium: 0.0237 kW/s², 350 kW)
Temperature (˚C)
400
350
300
250
200
150
100
50
0
0
500
1000
1500
2000
2500
3000
3500
Duration (seconds)
d1
d2
d3
d4
d5
d6
d7
d8
d9
d10
d11
d12
d13
d14
d15
d16
m1
m2
m3
m4
m5

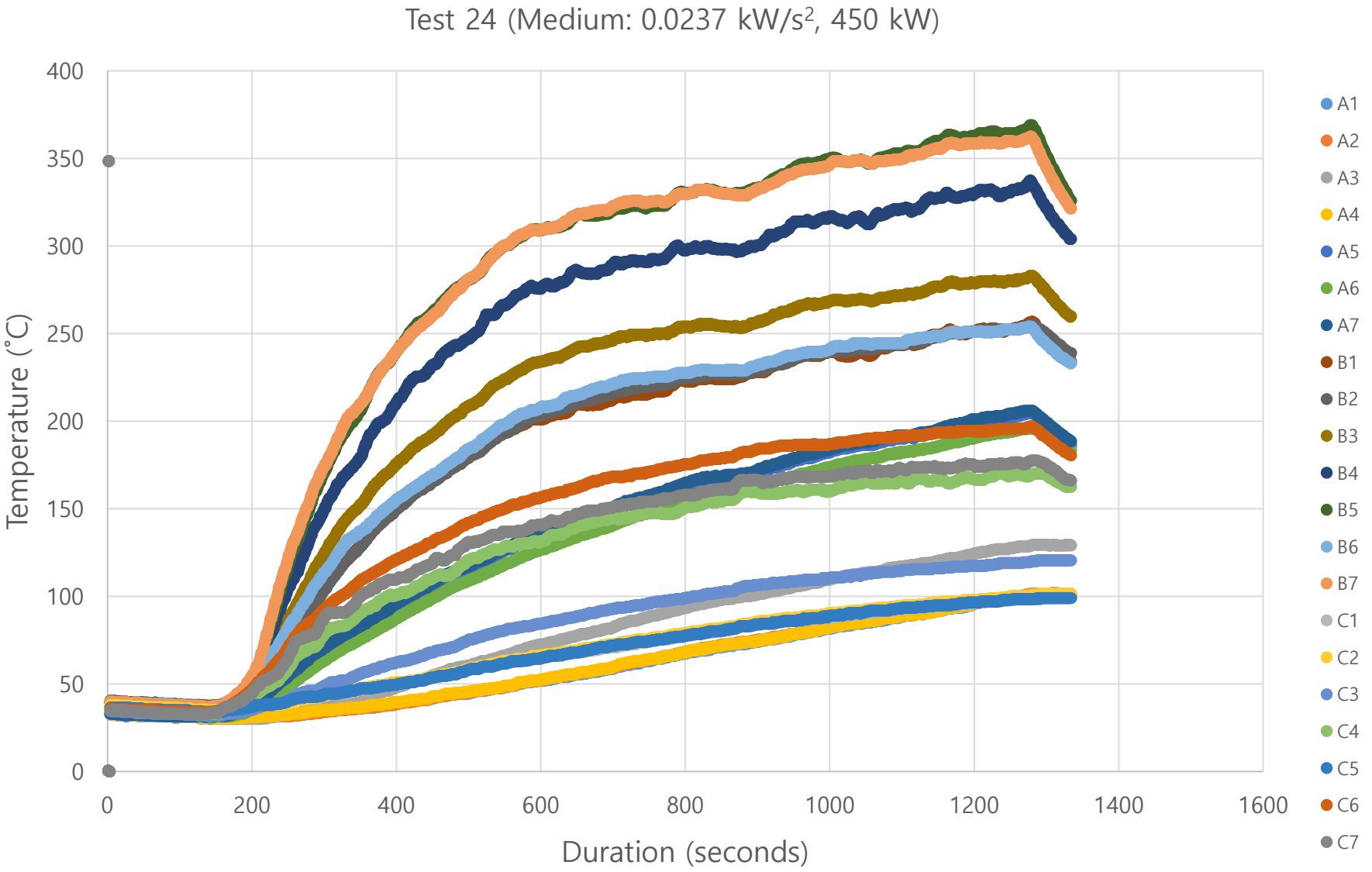
Test 24 (Medium: 0.0237 kW/s², 450 kW)
Temperature (°C)
400
350
300
250
200
150
100
50
0
0
200
400
600
800
1000
1200
1400
1600
Duration (seconds)
A1
A2
A3
A4
A5
A6
A7
B1
B2
B3
B4
B5
B6
B7
C1
C2
C3
C4
C5
C6
C7

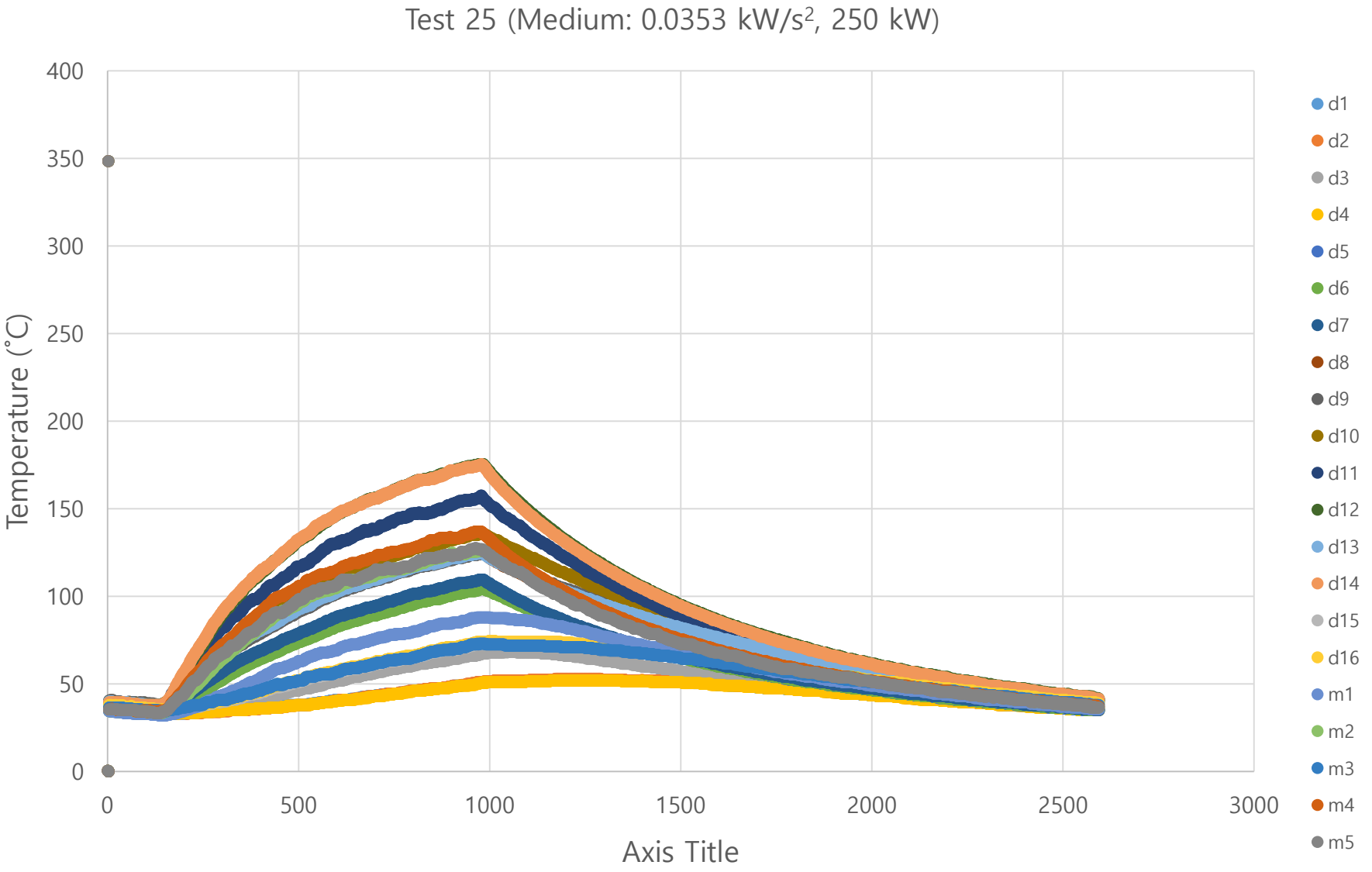
Test 25 (Medium: 0.0353 kW/s², 250 kW)
Temperature (°C)
400
350
300
250
200
150
100
50
0
0
500
1000
1500
2000
2500
3000
Axis Title
d1
d2
d3
d4
d5
d6
d7
d8
d9
d10
d11
d12
d13
d14
d15
d16
m1
m2
m3
m4
m5

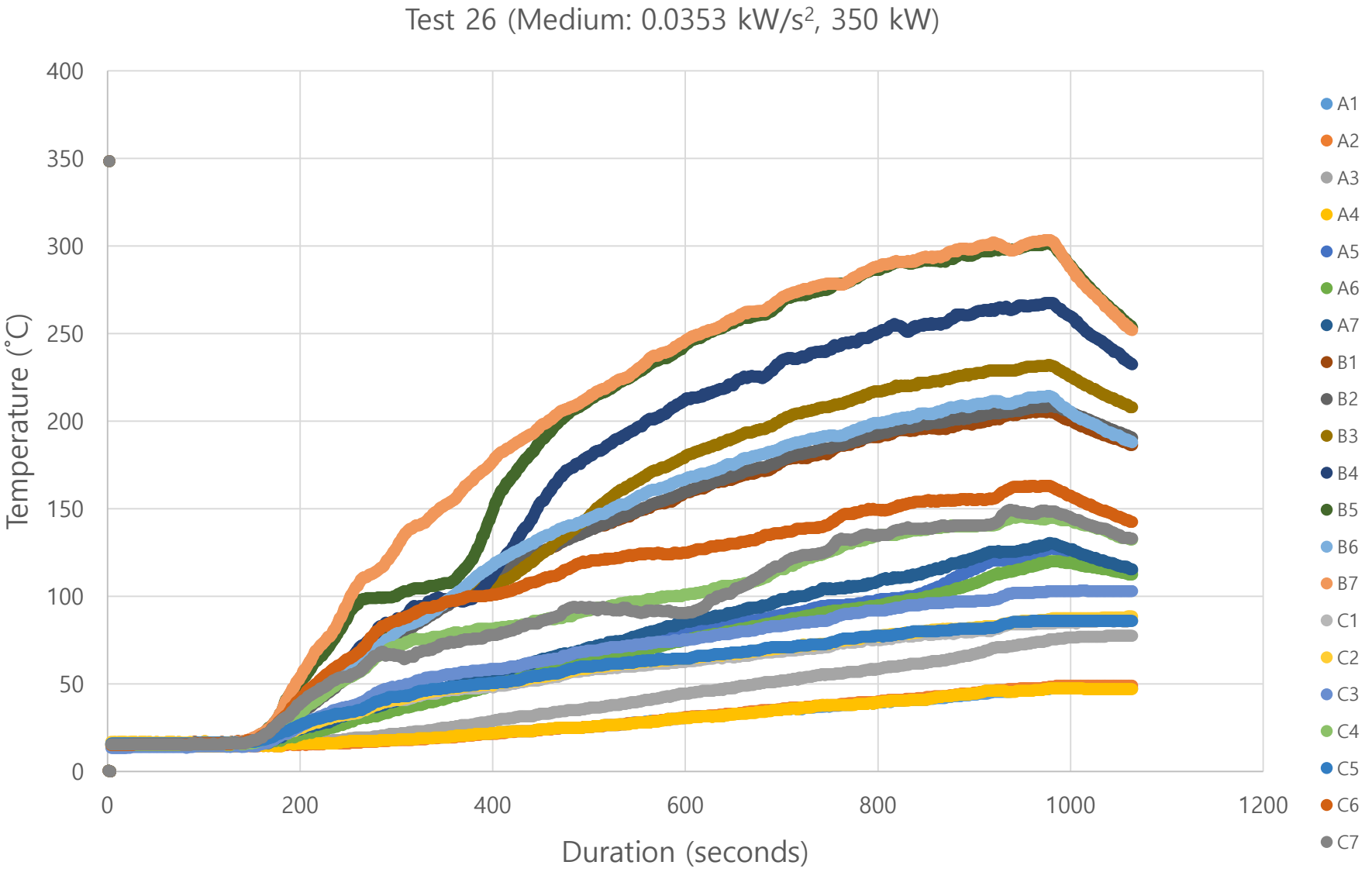
Test 26 (Medium: 0.0353 kW/s², 350 kW)
Temperature (°C)
400
350
300
250
200
150
100
50
0
0
200
400
600
800
1000
1200
Duration (seconds)
A1
A2
A3
A4
A5
A6
A7
B1
B2
B3
B4
B5
B6
B7
C1
C2
C3
C4
C5
C6
C7

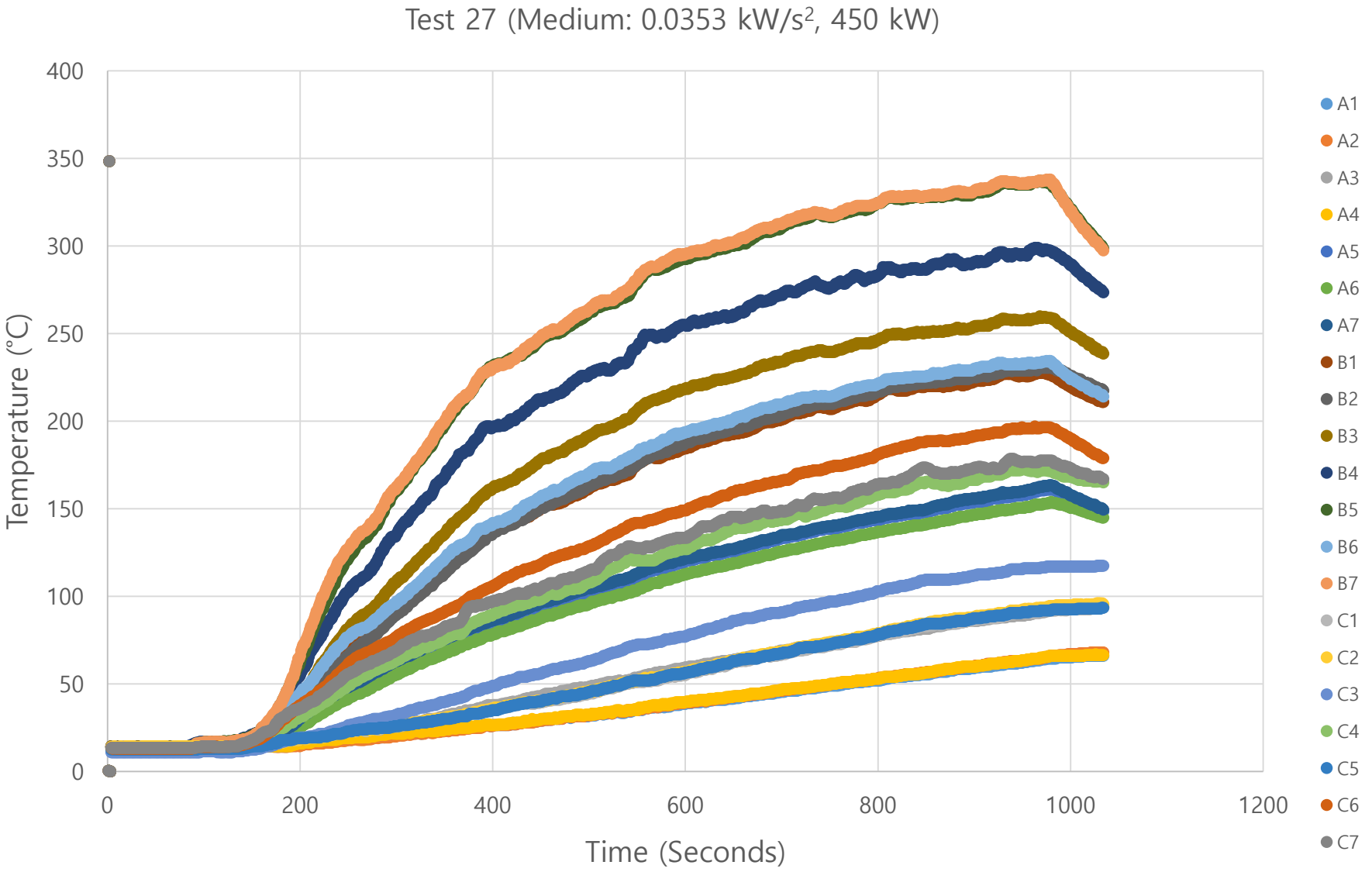
Test 27 (Medium: 0.0353 kW/s², 450 kW)
Temperature (°C)
400
350
300
250
200
150
100
50
0
0
200
400
600
800
1000
1200
Time (Seconds)
A1
A2
A3
A4
A5
A6
A7
B1
B2
B3
B4
B5
B6
B7
C1
C2
C3
C4
C5
C6
C7

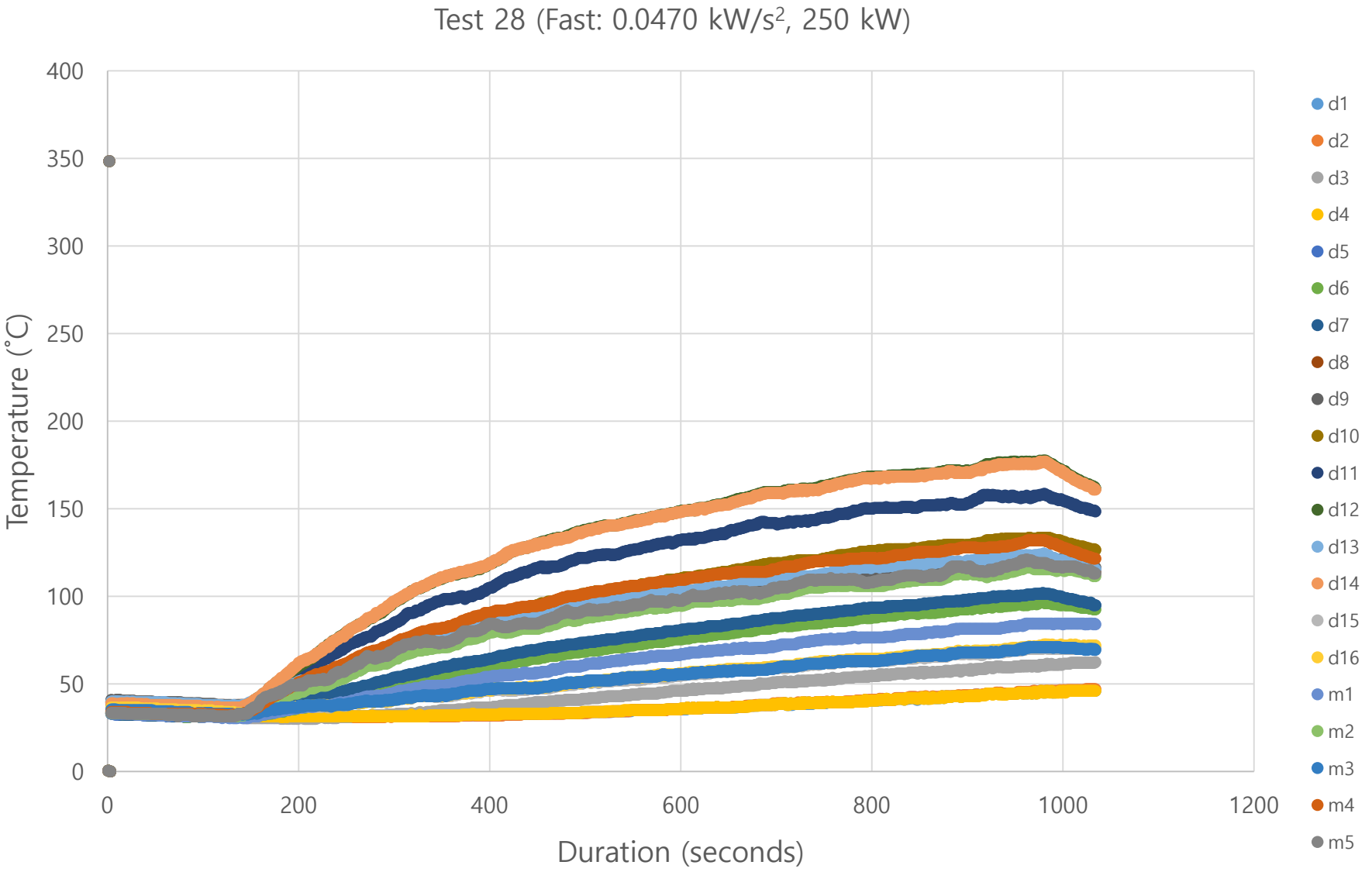
Test 28 (Fast: 0.0470 kW/s², 250 kW)
Temperature (°C)
400
350
300
250
200
150
100
50
0
0
200
400
600
800
1000
1200
Duration (seconds)
d1
d2
d3
d4
d5
d6
d7
d8
d9
d10
d11
d12
d13
d14
d15
d16
m1
m2
m3
m4
m5

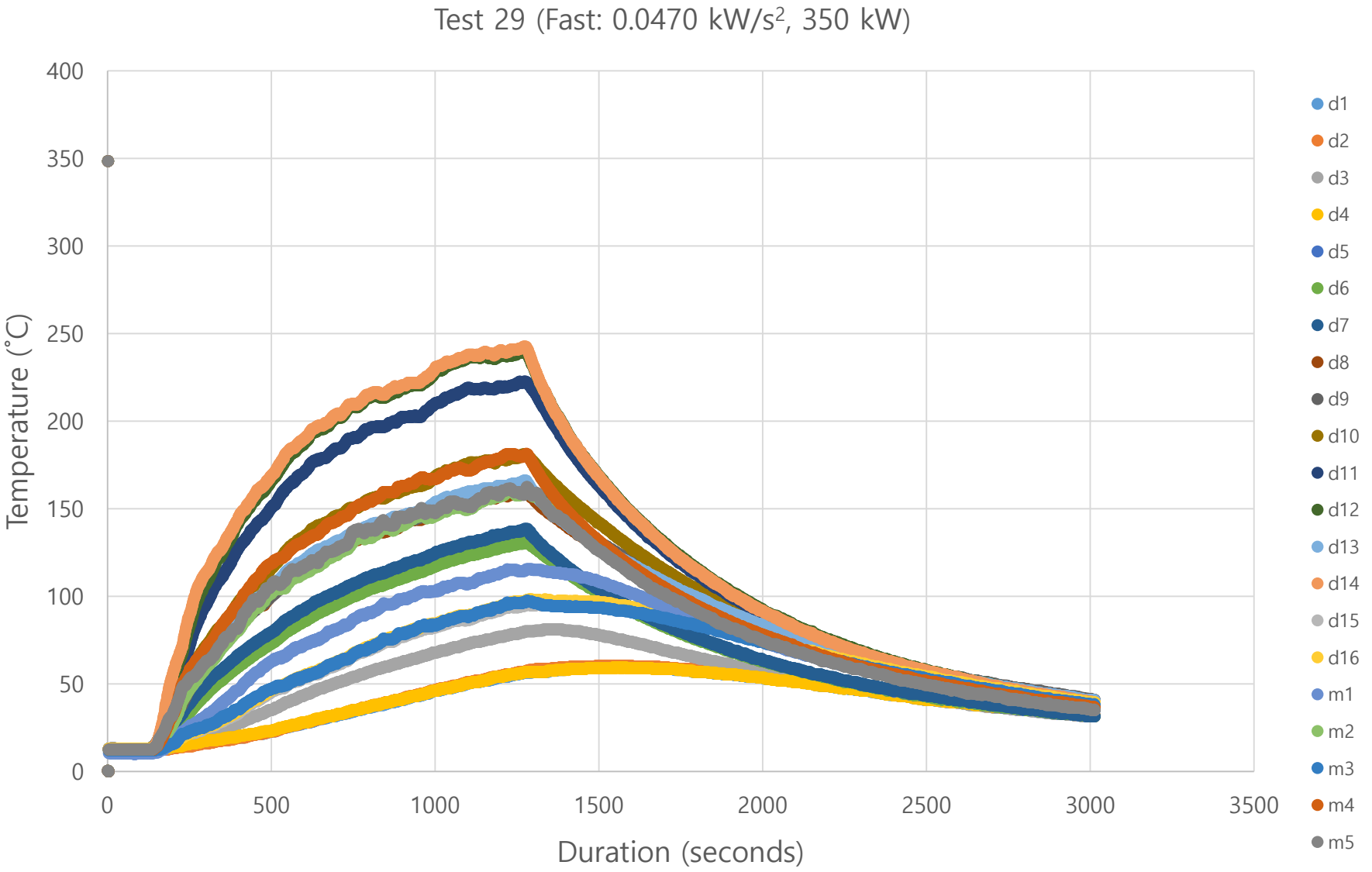
Test 29 (Fast: 0.0470 kW/s², 350 kW)
Temperature (°C)
400
350
300
250
200
150
100
50
0
0
500
1000
1500
2000
2500
3000
3500
Duration (seconds)
d1
d2
d3
d4
d5
d6
d7
d8
d9
d10
d11
d12
d13
d14
d15
d16
m1
m2
m3
m4
m5

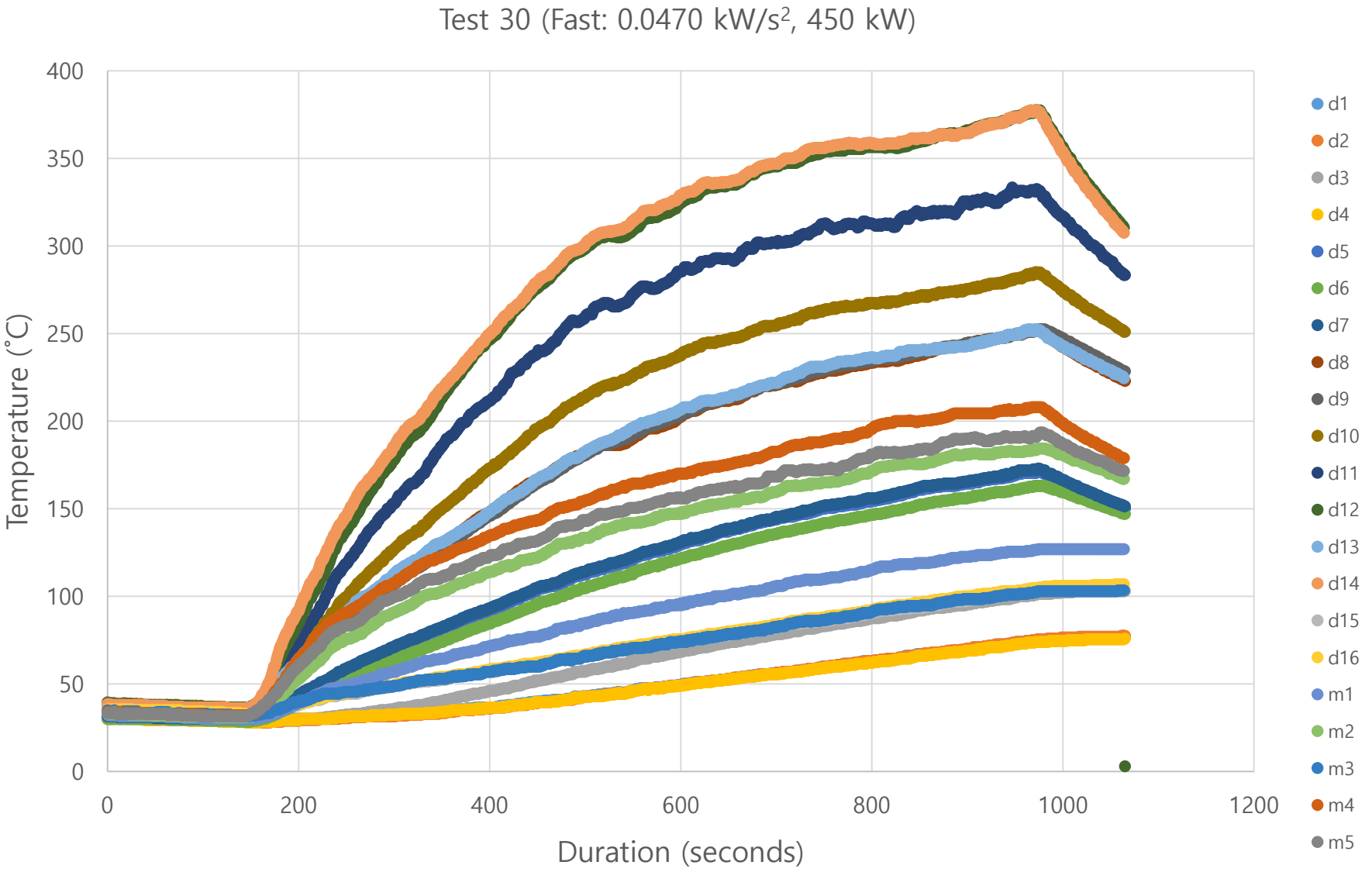
Test 30 (Fast: 0.0470 kW/s², 450 kW)
Temperature (°C)
400
350
300
250
200
150
100
50
0
0
200
400
600
800
1000
1200
Duration (seconds)
d1
d2
d3
d4
d5
d6
d7
d8
d9
d10
d11
d12
d13
d14
d15
d16
m1
m2
m3
m4
m5

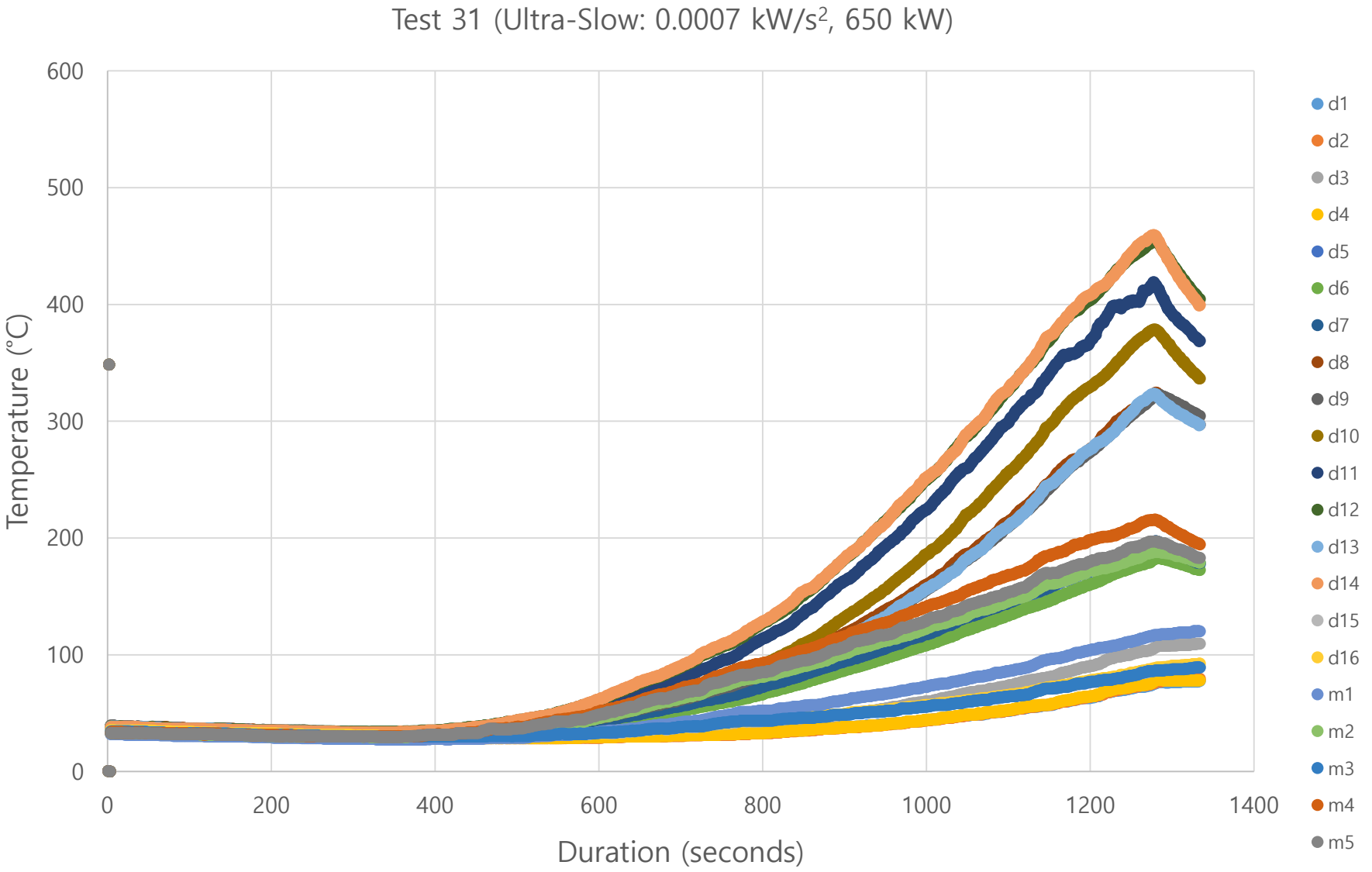
Test 31 (Ultra-Slow: 0.0007 kW/s², 650 kW)
Temperature (°C)
600
500
400
300
200
100
0
0
200
400
600
800
1000
1200
1400
Duration (seconds)
d1
d2
d3
d4
d5
d6
d7
d8
d9
d10
d11
d12
d13
d14
d15
d16
m1
m2
m3
m4
m5

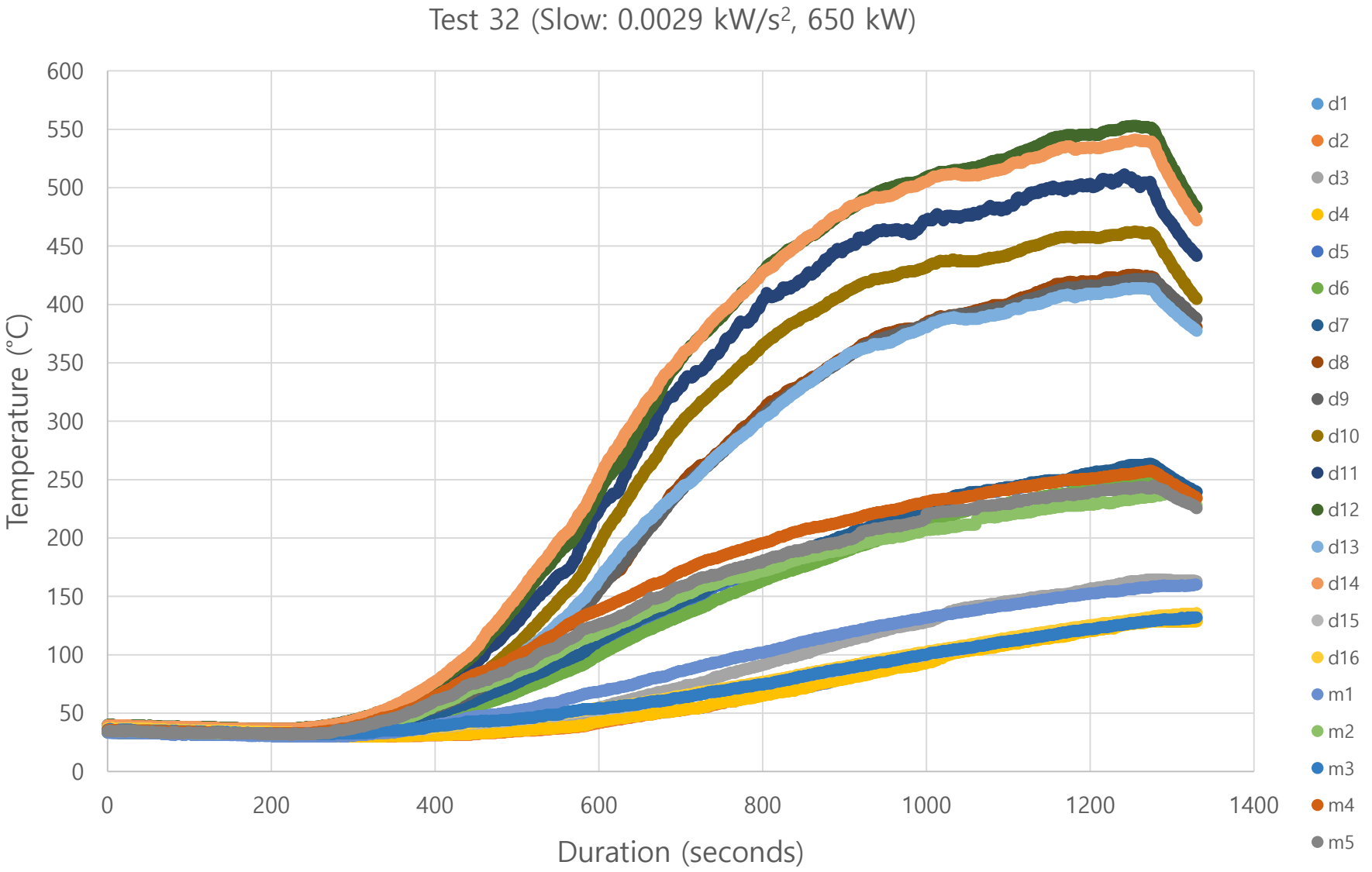
Test 32 (Slow: 0.0029 kW/s², 650 kW)
Temperature (°C)
600
550
500
450
400
350
300
250
200
150
100
50
0
0
200
400
600
800
1000
1200
1400
Duration (seconds)
d1
d2
d3
d4
d5
d6
d7
d8
d9
d10
d11
d12
d13
d14
d15
d16
m1
m2
m3
m4
m5

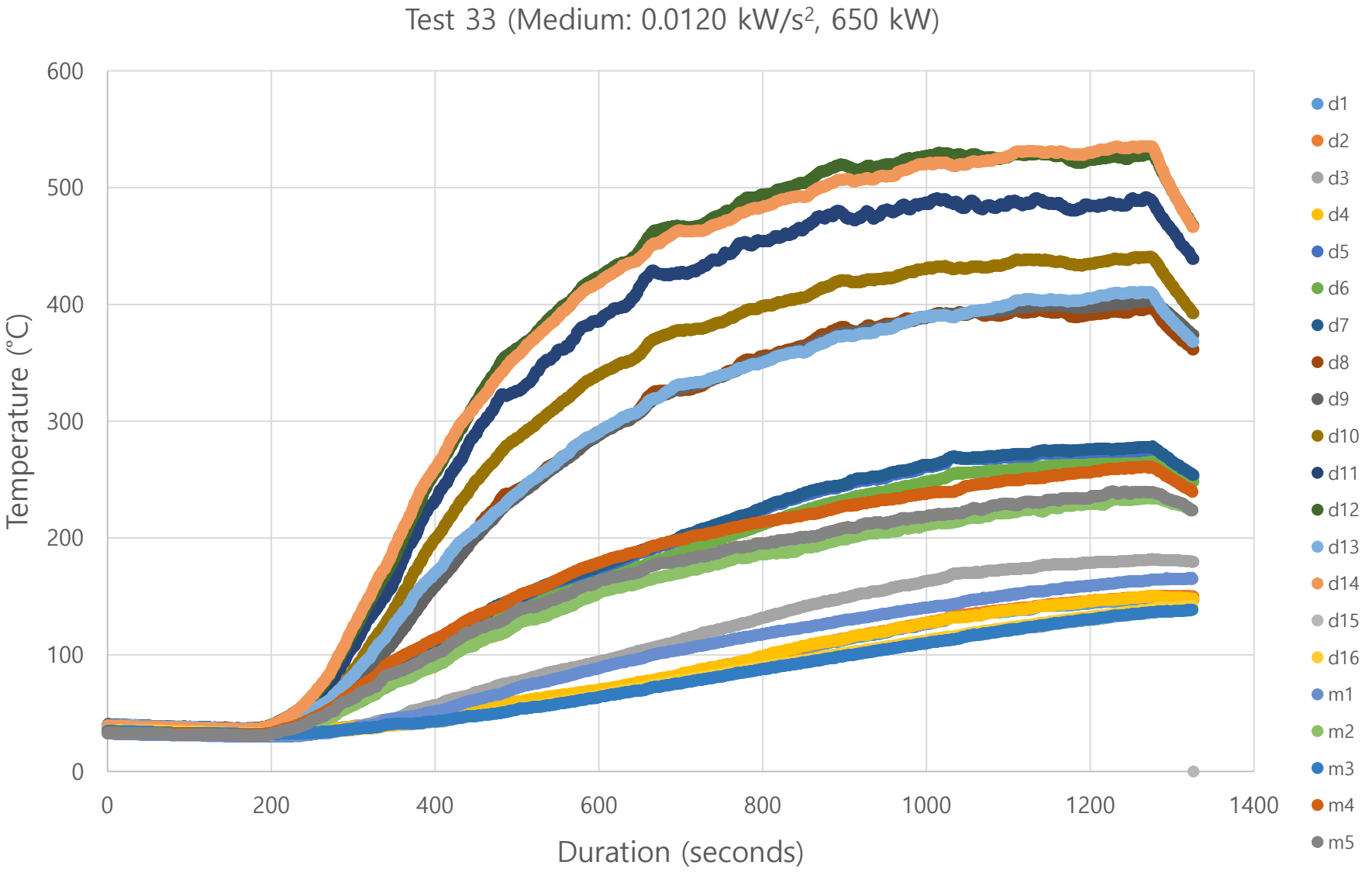
Test 33 (Medium: 0.0120 kW/s², 650 kW)
Temperature (°C)
600
500
400
300
200
100
0
0
200
400
600
800
1000
1200
1400
Duration (seconds)
d1
d2
d3
d4
d5
d6
d7
d8
d9
d10
d11
d12
d13
d14
d15
d16
m1
m2
m3
m4
m5

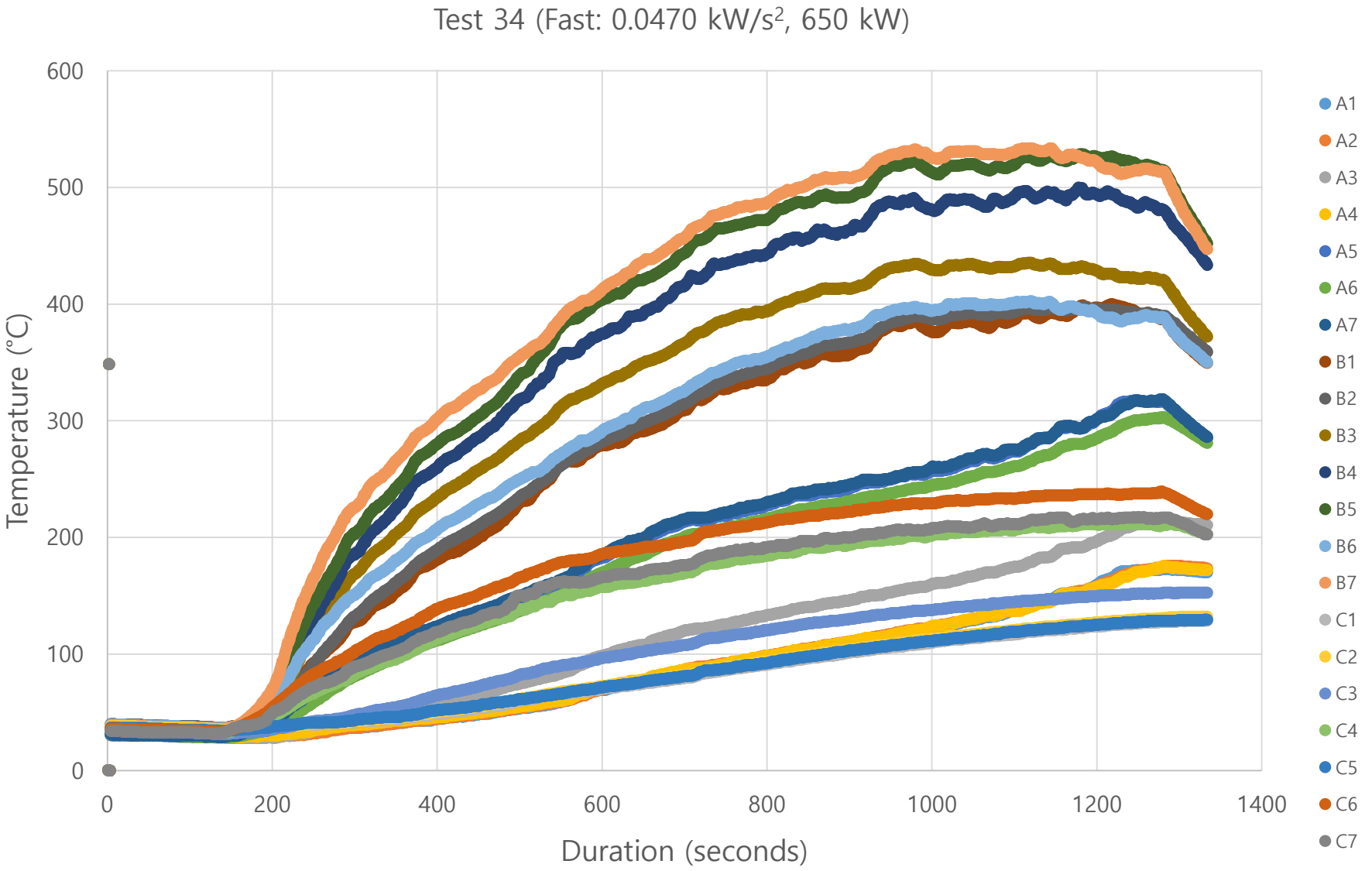
Test 34 (Fast: 0.0470 kW/s², 650 kW)
Temperature (°C)
600
500
400
300
200
100
0
0
200
400
600
800
1000
1200
1400
Duration (seconds)
A1
A2
A3
A4
A5
A6
A7
B1
B2
B3
B4
B5
B6
B7
C1
C2
C3
C4
C5
C6
C7

APPENDIX D. STRUCTURAL TEST RESULTS

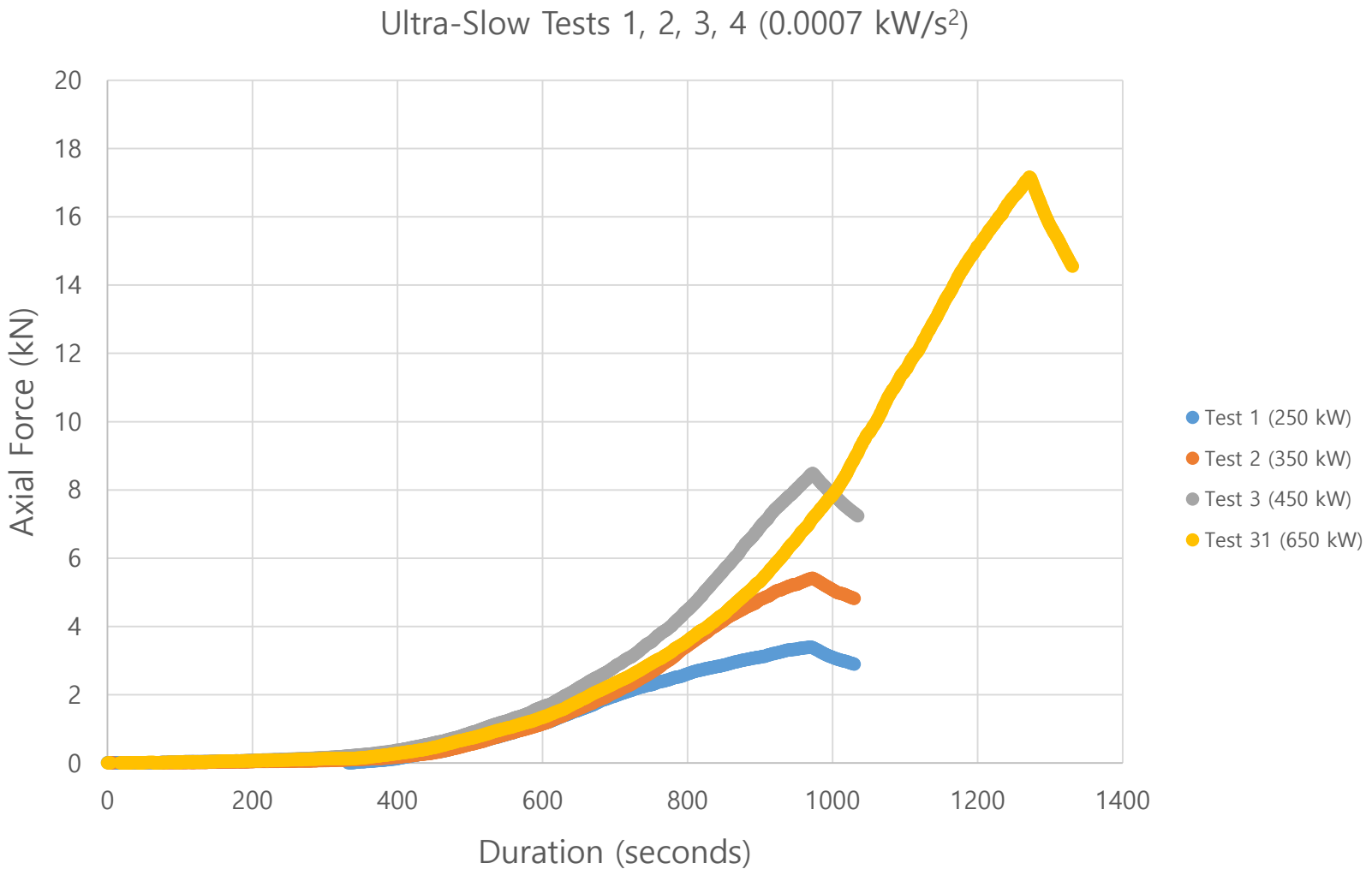

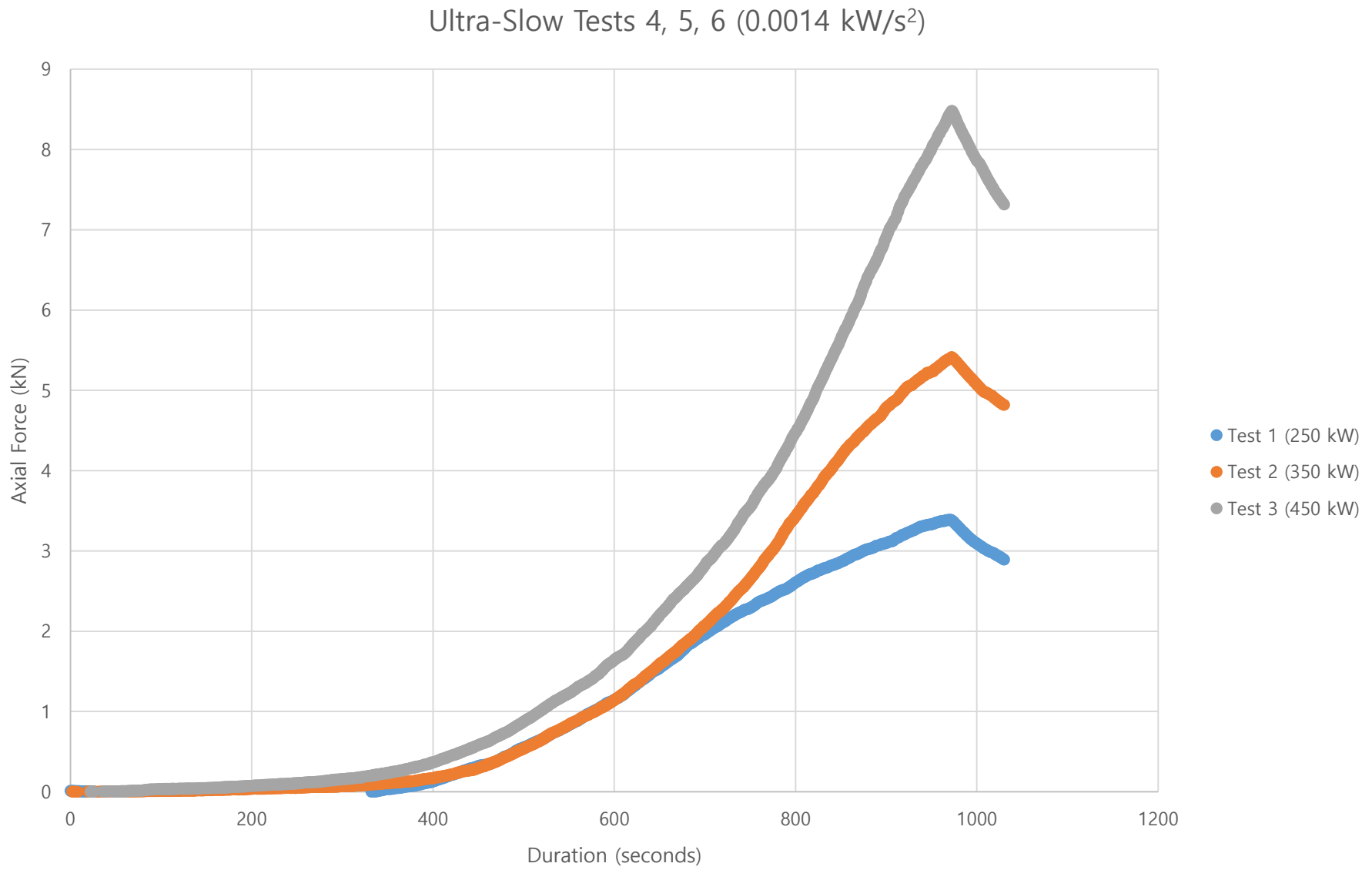
Ultra-Slow Tests 4, 5, 6 (0.0014 kW/s²)
Axial Force (kN)
0
1
2
3
4
5
6
7
8
9
0
200
400
600
800
1000
1200
Duration (seconds)
Test 1 (250 kW)
Test 2 (350 kW)
Test 3 (450 kW)

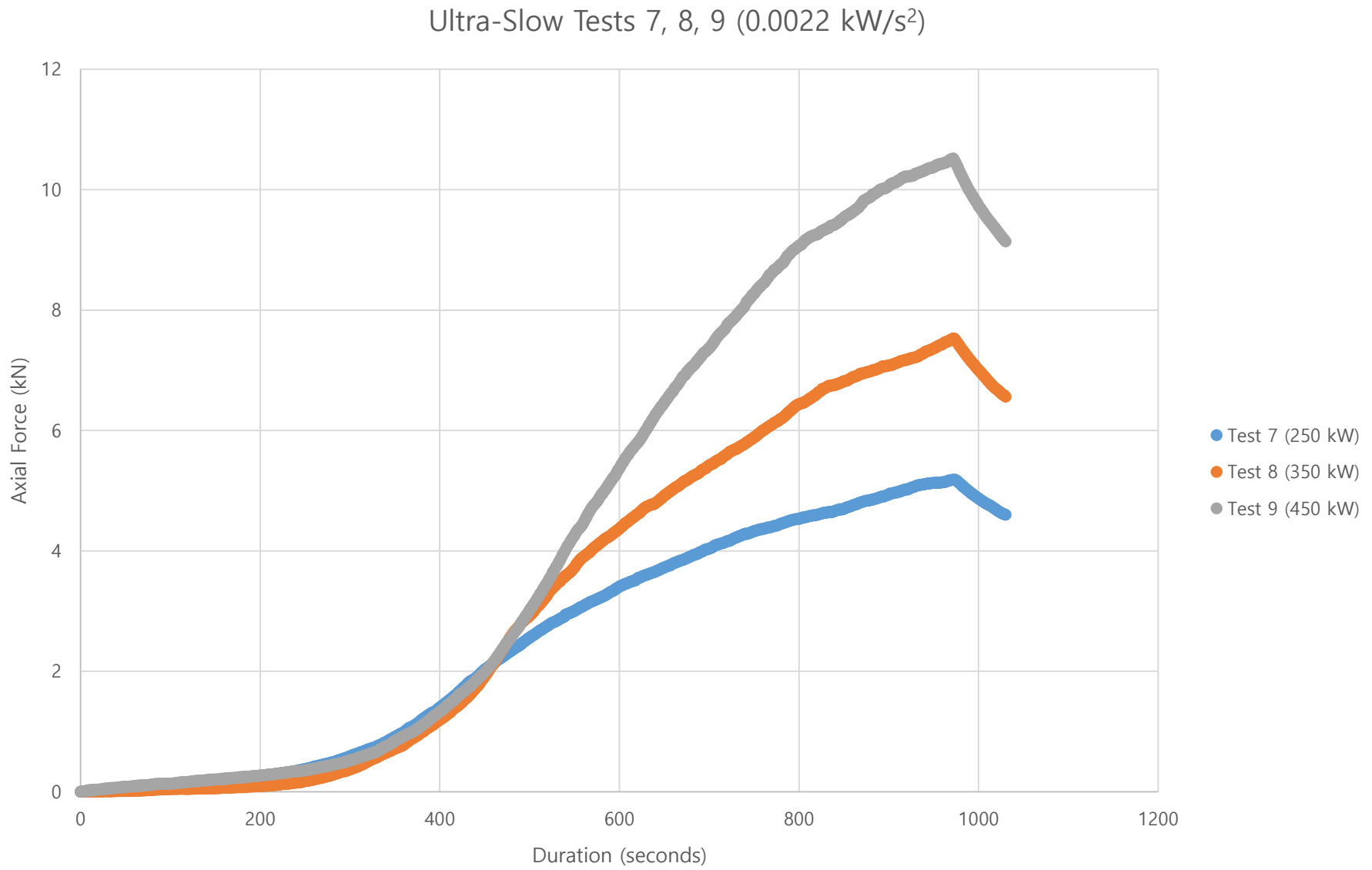
Ultra-Slow Tests 7, 8, 9 (0.0022 kW/s²)
Axial Force (kN)
0
2
4
6
8
10
12
0
200
400
600
800
1000
1200
Duration (seconds)
Test 7 (250 kW)
Test 8 (350 kW)
Test 9 (450 kW)

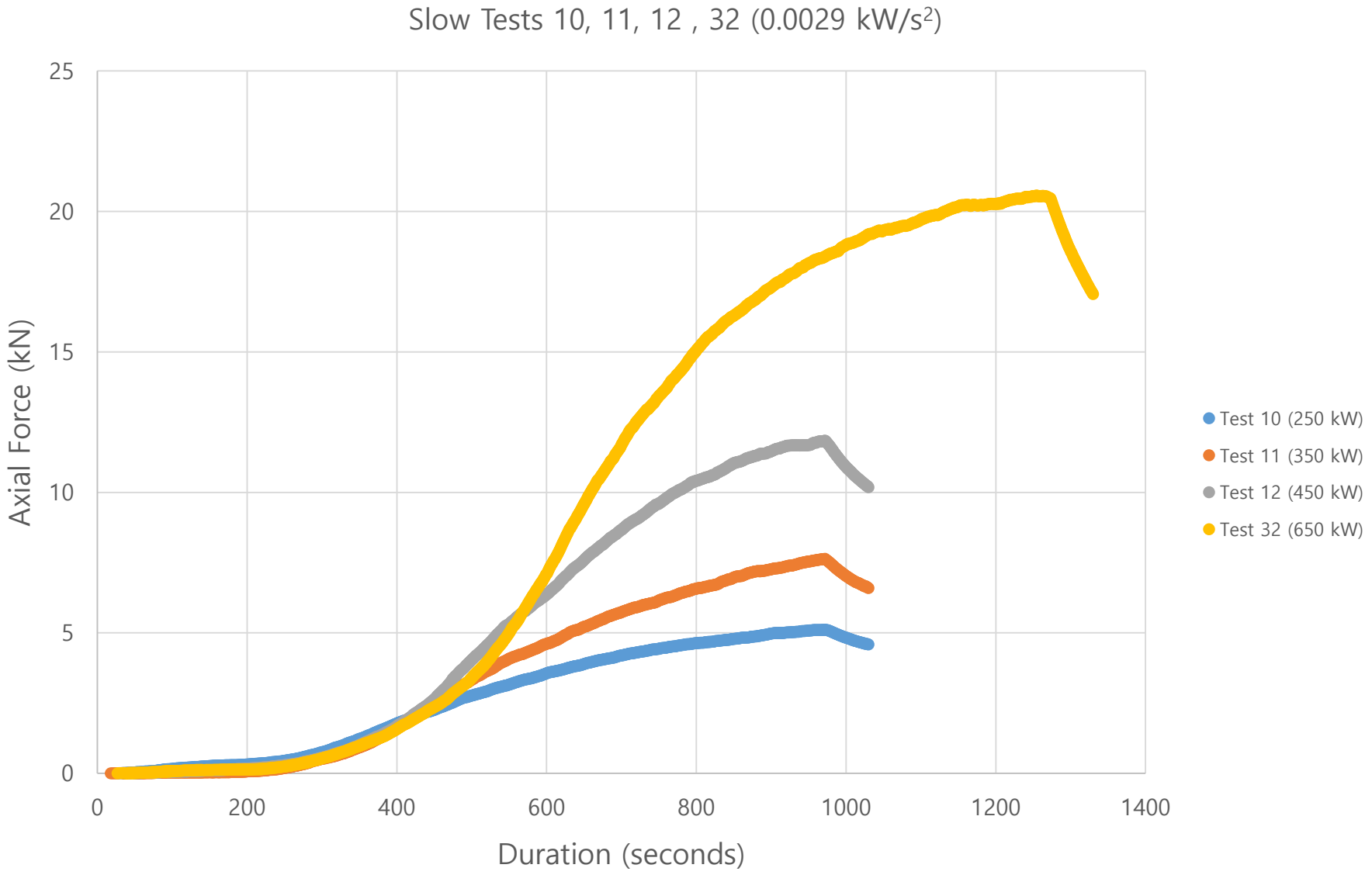
Slow Tests 10, 11, 12 , 32 (0.0029 kW/s²)
Axial Force (kN)
25
20
15
10
5
0
0
200
400
600
800
1000
1200
1400
Duration (seconds)
Test 10 (250 kW)
Test 11 (350 kW)
Test 12 (450 kW)
Test 32 (650 kW)

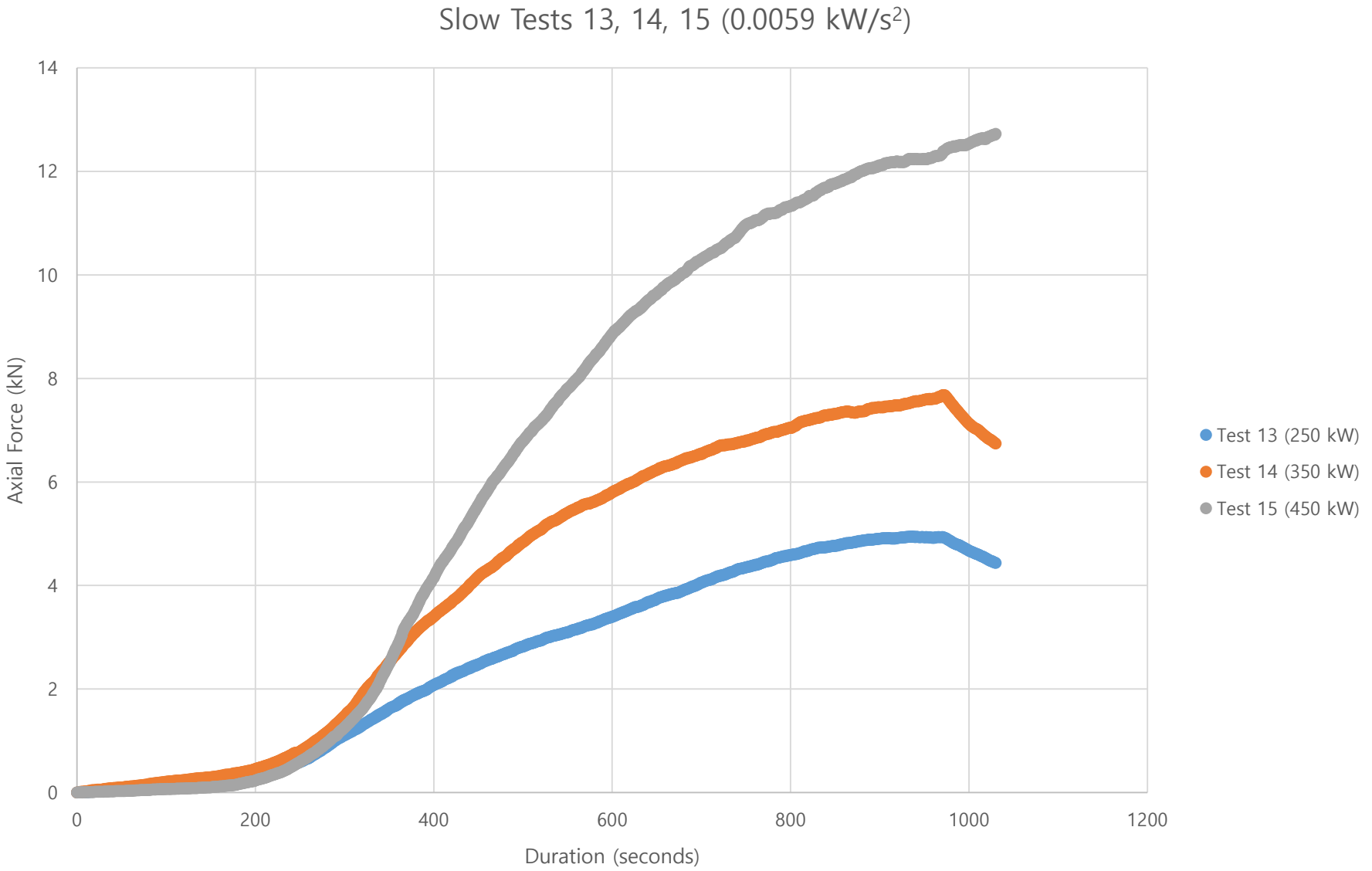
Slow Tests 13, 14, 15 (0.0059 kW/s²)
Axial Force (kN)
0
2
4
6
8
10
12
14
0
200
400
600
800
1000
1200
Duration (seconds)
Test 13 (250 kW)
Test 14 (350 kW)
Test 15 (450 kW)

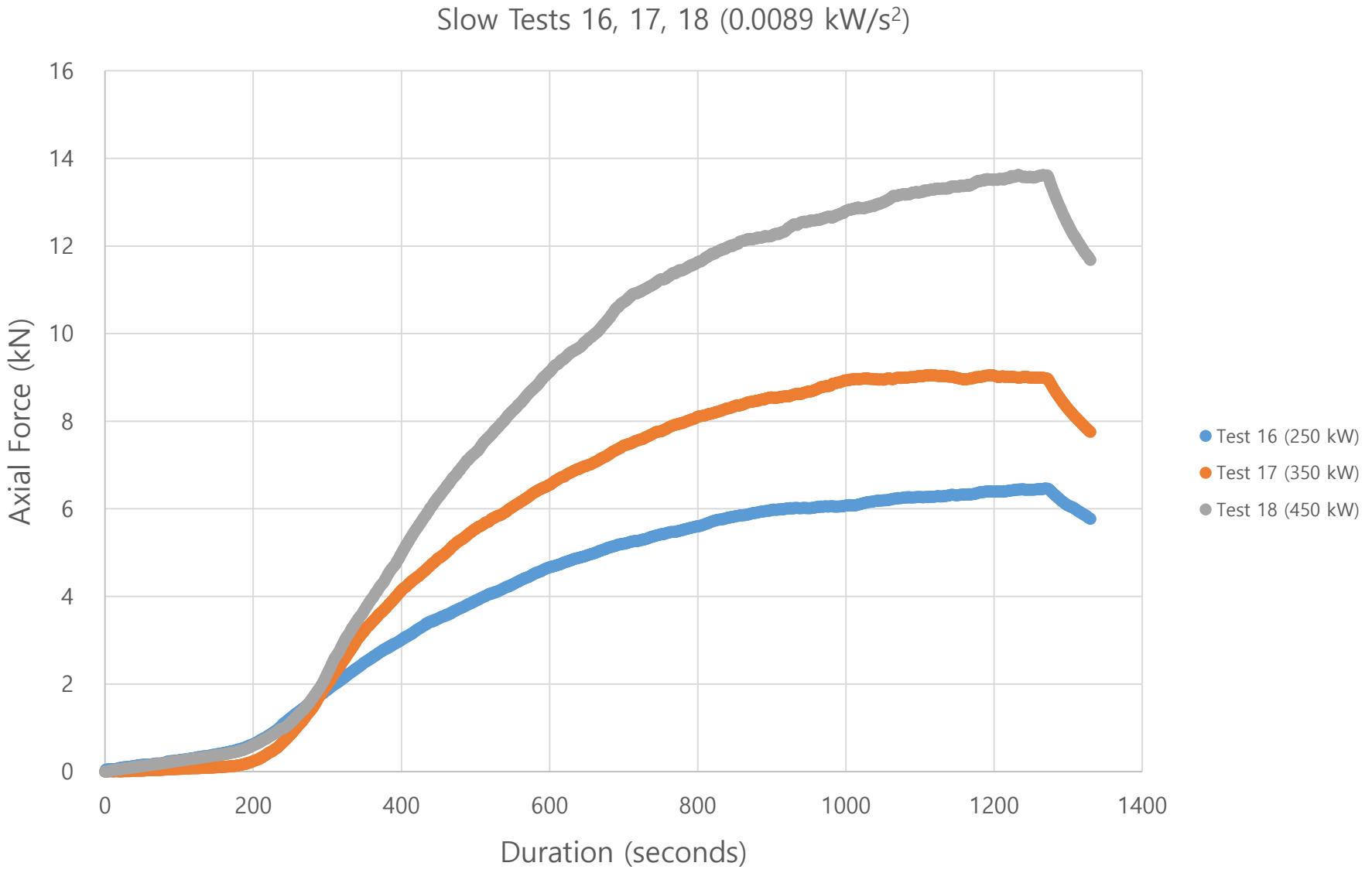
Slow Tests 16, 17, 18 (0.0089 kW/s²)
Axial Force (kN)
16
14
12
10
8
6
4
2
0
0
200
400
600
800
1000
1200
1400
Duration (seconds)
Test 16 (250 kW)
Test 17 (350 kW)
Test 18 (450 kW)

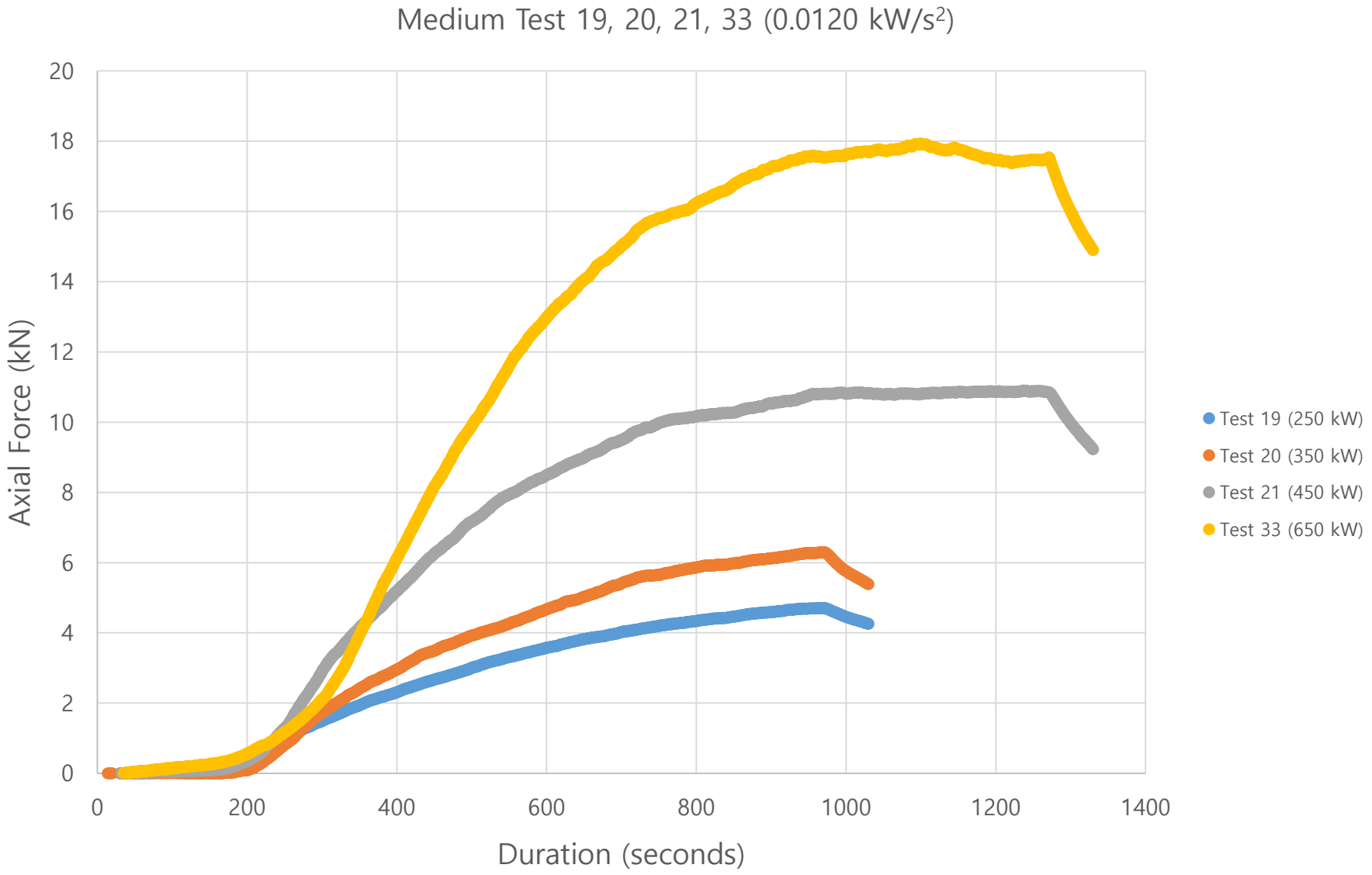
Medium Test 19, 20, 21, 33 (0.0120 kW/s²)
Axial Force (kN)
0
2
4
6
8
10
12
14
16
18
20
0
200
400
600
800
1000
1200
1400
Duration (seconds)
Test 19 (250 kW)
Test 20 (350 kW)
Test 21 (450 kW)
Test 33 (650 kW)

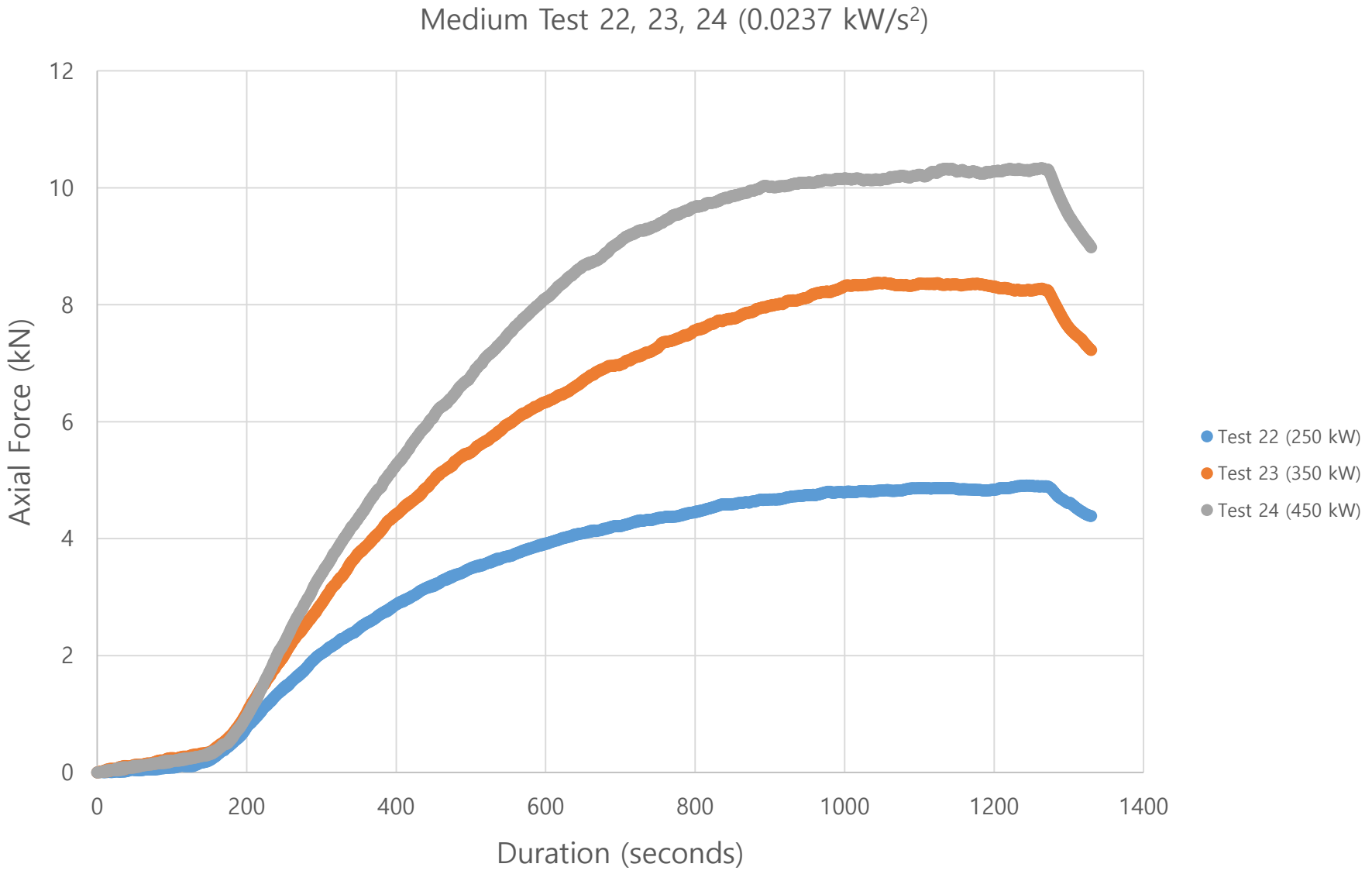
Medium Test 22, 23, 24 (0.0237 kW/s²)
Axial Force (kN)
0
2
4
6
8
10
12
0
200
400
600
800
1000
1200
1400
Duration (seconds)
Test 22 (250 kW)
Test 23 (350 kW)
Test 24 (450 kW)

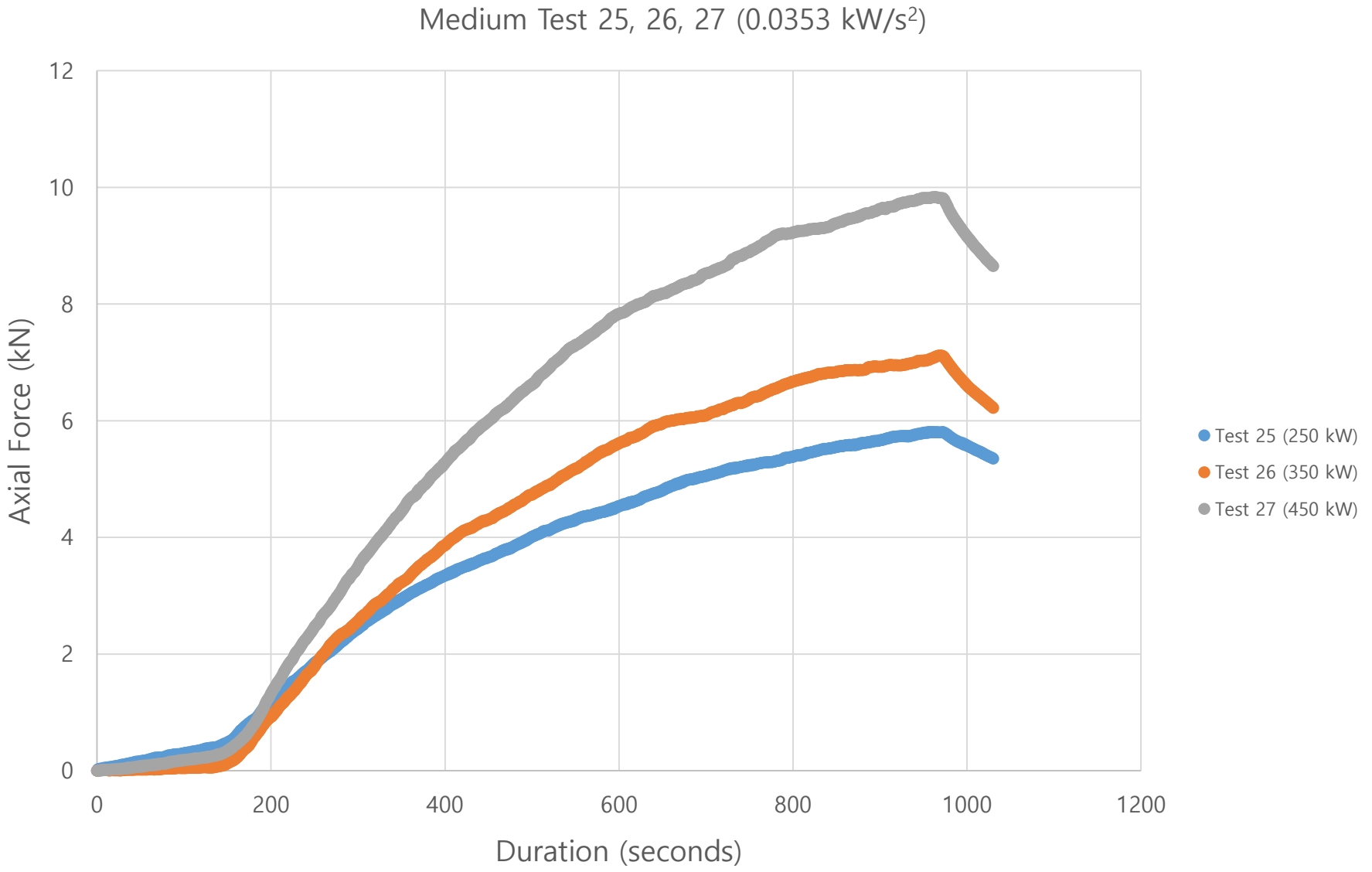
Medium Test 25, 26, 27 (0.0353 kW/s²)
Axial Force (kN)
12
10
8
6
4
2
0
0
200
400
600
800
1000
1200
Duration (seconds)
Test 25 (250 kW)
Test 26 (350 kW)
Test 27 (450 kW)

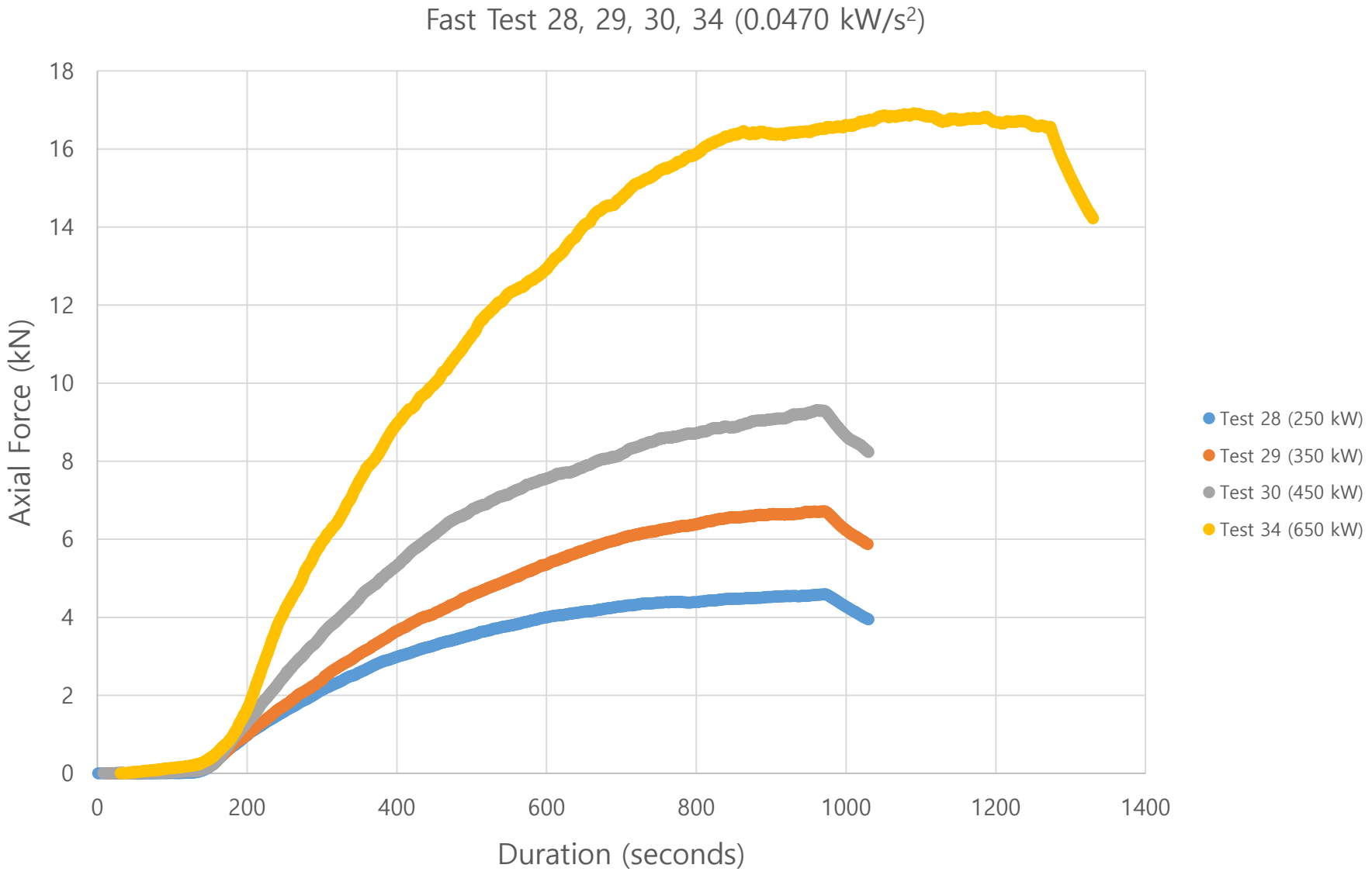
Fast Test 28, 29, 30, 34 (0.0470 kW/s²)
Axial Force (kN)
18
16
14
12
10
8
6
4
2
0
0
200
400
600
800
1000
1200
1400
Duration (seconds)
Test 28 (250 kW)
Test 29 (350 kW)
Test 30 (450 kW)
Test 34 (650 kW)

APPENDIX E. THERMAL AND STRUCTURAL TEST RESULTS IN ORDER

Thermal Test	peak Temperature (˚C)	Structural Test	Axial Force (kN)
32-4	552.0	**32-4**	20.56
33-4	535.5	**32-3**	18.04
34-3	531.0	**33-4**	17.54
33-3	523.0	**33-3**	17.53
34-4	519.5	**31-4**	17.16
32-3	503.0	**34-4**	16.57
33-2	463.5	**34-3**	16.52
31-4	459.0	**33-2**	14.52
34-2	444.5	**34-2**	14.42
30-3	377.5	**18-4**	13.52
24-4	369.0	**15-4**	13.01
15-4	367.5	**18-3**	12.54
9-3	366.0	**15-3**	12.26
6-3	363.0	**12-3**	11.84
12-3	361.5	**21-4**	10.84
18-4	359.0	**21-3**	10.81
21-4	358.0	**32-2**	10.47
15-3	347.0	**9-3**	10.46
24-3	347.0	**24-4**	10.25
30-2	341.5	**18-2**	10.05
21-3	340.5	**24-3**	10.05
27-3	337.5	**27-3**	9.77
18-3	337.0	**15-2**	9.77
32-2	326.5	**6-3**	9.59
24-2	320.0	**30-3**	9.29
27-2	309.0	**21-2**	9.22
26-3	303.5	**17-4**	8.98
21-2	291.0	**17-3**	8.76
17-4	286.0	**24-2**	8.70
34-1	286.0	**3-3**	8.48
18-2	284.5	**27-2**	8.26
15-2	282.0	**23-4**	8.17

12-2	281.5	**23-3**	8.14
11-3	272.5	**12-2**	8.10
17-3	270.0	**34-1**	8.09
26-2	263.0	**30-2**	8.03
9-2	260.5	**11-3**	7.63
14-3	257.5	**14-3**	7.61
23-4	257.0	**8-3**	7.52
5-3	255.5	**26-3**	7.10
23-3	247.5	**17-2**	7.10
8-3	247.0	**31-3**	7.09
20-3	246.0	**9-2**	6.86
29-3	239.5	**23-2**	6.78
31-3	232.0	**29-3**	6.71
30-1	230.5	**5-3**	6.54
24-1	226.5	**16-4**	6.35
17-2	224.0	**14-2**	6.31
11-2	220.0	**20-3**	6.30
33-1	219.5	**26-2**	6.01
6-2	218.5	**16-3**	5.94
3-3	217.5	**29-2**	5.85
29-2	216.5	**25-3**	5.69
27-1	215.0	**11-2**	5.44
23-2	214.5	**2-3**	5.41
5-2	210.0	**20-2**	5.18
14-2	207.0	**8-2**	5.14
20-2	206.0	**7-3**	5.14
13-3	199.0	**10-3**	5.11
8-2	195.5	**33-1**	4.94
16-4	191.0	**16-2**	4.93
22-4	190.0	**13-3**	4.89
10-3	188.0	**22-4**	4.86
29-1	182.5	**25-2**	4.84
4-3	182.0	**30-1**	4.82
28-3	177.5	**27-1**	4.77

7-3	176.5	**22-3**	4.74
25-3	175.5	**6-2**	4.74
22-3	172.0	**19-3**	4.71
16-3	169.5	**24-1**	4.66
21-1	169.0	**21-1**	4.61
13-2	167.5	**28-3**	4.59
2-3	166.5	**5-2**	4.21
26-1	164.0	**28-2**	4.19
19-3	160.0	**18-1**	4.11
18-1	159.0	**22-2**	4.11
10-2	157.5	**10-2**	4.04
28-2	157.0	**23-1**	3.95
25-2	154.0	**19-2**	3.89
22-2	150.5	**7-2**	3.81
16-2	145.5	**13-2**	3.80
7-2	144.0	**17-1**	3.50
23-1	138.5	**26-1**	3.47
19-2	132.0	**1-3**	3.39
20-1	131.0	**29-1**	3.29
15-1	130.0	**4-3**	3.26
4-2	125.5	**25-1**	3.02
17-1	122.5	**14-1**	2.89
28-1	114.0	**15-1**	2.85
1-3	111.0	**28-1**	2.77
25-1	108.5	**20-1**	2.66
14-1	100.5	**22-1**	2.59
22-1	100.5	**16-1**	2.59
13-1	99.0	**3-2**	2.45
16-1	92.5	**19-1**	2.11
31-2	82.0	**4-2**	2.08
3-2	81.0	**31-2**	2.03
19-1	77.0	**13-1**	1.77
2-2	73.5	**2-2**	1.76
32-1	64.5	**1-2**	1.70

11-1	61.0	**10-1**	1.46
12-1	61.0	**12-1**	1.29
1-2	60.0	**32-1**	1.19
10-1	58.5	**11-1**	1.16
7-1	52.5	**7-1**	1.06
9-1	52.0	**9-1**	0.96
6-1	45.5	**8-1**	0.90
8-1	41.0	**5-1**	0.57
2-1	35.0	**6-1**	0.50
3-1	35.0	**3-1**	0.28
31-1	34.5	**4-1**	0.20
5-1	34.0	**31-1**	0.19
4-1	30.0	**2-1**	0.13
1-1	21.5	**1-1**	0.06